T.R.
ONDOKUZ MAYIS UNIVERSITY
INSTITUTE OF GRADUATE STUDIES
DEPARTMENT OF CIVIL ENGINEERING

THE EFFECT OF GLOBAL CLIMATE CHANGE ON HYDROELECTRIC POWER PLANTS AND ENERGY PRODUCTION IN THE CENTRAL BLACK SEA BASIN

PhD Thesis

Hesham ALRAYESS

Supervisor

Assoc. Prof. Dr. Asli ULKE KESKIN

SAMSUN
2021

ACCEPTANCE AND APPROVAL OF THE THESIS

The study entitled **"The Effect Of Global Clımate Change On Hydroelectric Power Plants And Energy Production In The Central Black Sea Area Basin"** prepared by **Hesham ALRAYESS** and supervised by **Assoc. Prof. Dr. Aslı ULKE KESKIN** was found successful and unanimously accepted by committee members as PhD thesis of the Department of Civil Engineering, following the examination on the date 23/12/2021.

	Title Name Surname **University** **Department**	**Signature**	**Final decision**
Chairman **(Supervisor)**	Assoc. Prof. Dr. Asli ULKE KESKIN Ondokuz Mayis University Department of Civil Engineering		☐ Acceptant ☐ Rejection
Member:	Prof. Dr. Turgay PARTAL Ondokuz Mayis University Department of Civil Engineering		☐ Acceptant ☐ Rejection
Member:	Assoc. Prof. Dr. Meral DEMIRTAS Samsun University Department of Meteorological Engineering		☐ Acceptant ☐ Rejection
Member:	Assoc. Prof. Dr. Serife Yurdagul KUMCU Necmettin Erbakan University Department of Civil Engineering		☐ Acceptant ☐ Rejection
Member:	Assoc. Prof. Dr. Salem GHARBIA Institute of Technology - Sligo Department of Environmental Science		☐ Acceptant ☐ Rejection

This thesis has been approved by the committee members that already stated above and determined by the Institute Executive Board.

CONFIRMATION
… /12/2021
Prof. Dr. Ali BOLAT
Head of Institute of Graduate Studies

DECLARATION OF COMPLIANCE WITH SCIENTIFIC ETHIC

I hereby declare and undertake that I complied with scientific ethics and academic rules in all stages of my PhD thesis, that I have referred to each quotation that I use directly or indirectly in the study and that the works I have used consist of those shown in the sources, that it was written in accordance with the institute writing guide and that the situations stated in the article 3, section 9 of the Regulation for TÜBİTAK Research and Publication Ethics Board were not violated

İmza
23 /12 / 2021
Hesham ALRAYESS

DECLARATION OF THE THESIS STUDY ORIGINAL REPORT

Thesis Title: The Effect Of Global Climate Change on Hydroelectric Power Plants and Energy Production in The Central Black Sea Basin

As a result of the originality report taken by me from the plagiarism detection program on 18.11.2021 for the thesis titled above;

Similarity Ratio : % 13

Single Source Rate : % 1 Has been reached.

İmza
23 /12/ 2021
Assoc. Prof. Dr. Asli ULKE KESKIN

ÖZET

KÜRESEL İKLİM DEĞİŞİKLİĞİNİN ORTA KARADENİZ HAVZASINDA HİDROELEKTRİK SANTRALLER VE ENERJİ ÜRETİMİ ÜZERİNE OLAN ETKİSİ

Hesham ALRAYESS
Ondokuz Mayıs Üniversitesi
Lisansüstü Eğitim Enstitüsü
İNŞAAT MÜHENDİSLİĞİ ANA BİLİM DALI
Doktora, Aralık/2021
Danışman: Doç. Dr. Aslı ULKE KESKIN

İklim değişikliği tüm dünya için önemli problemlerden biri haline gelmektedir. Yenilenebilir enerji esas olarak yağış, sıcaklık ve yağış-akış oranları gibi yerel çevresel koşullara bağlıdır. Hidroelektrik enerji, temiz enerji sağlamak için birincil yenilenebilir kaynaktır ve gelecekteki katkısının önemli ölçüde artması beklenmektedir.
İklim değişikliği tüm dünyada kritik zorluklardan biri haline gelmektedir. Yenilenebilir enerji esas olarak yağış, sıcaklık ve yağış-akış oranları gibi yerel çevresel koşullara bağlıdır. Hidroelektrik enerji, temiz enerji sağlamak için birincil yenilenebilir kaynaktır ve gelecekteki katkısının önemli ölçüde artması beklenmektedir.

Gerekli yağış, debi, göl seviyesi, debi ve enerji üretim verileri Meteoroloji Genel Müdürlüğü (MGM), Devlet Su İşleri (DSİ), Türkiye Elektrik Üretim İletim A.Ş. (TEİAŞ) kurumlarından elde edilmiştir. Hidroelektrik üretiminin iki önemli senaryosu kullanılmış ve çok kullanılan iki iklim değişikliği senaryosu; RCP 8.5 ve RCP 4.5 temel alınmıştır. Küresel Sirkülasyon Modelleri (GCM'ler) yağış ve ortalama sıcaklık verileri, hidroelektrik santrallerin (HES'ler) enerji üretimini tahmin etmek için kullanılmıştır.

Tez, çalışma alanı olarak Yeşilırmak ve Kızılırmak Havzalarına odaklanmıştır. Bölgede yer alan altı adet Hidroelektrik Santral üzerinde çalışılmıştır. Tahmin değerleri, Makine Öğrenimi (ML) teknikleri arasındaki bağıl hata ve korelasyon değerlerine dayalı olarak hesaplanmıştır. 1971'den 2018'e kadar aylık hidroelektrik enerji üretim verileri kullanılarak enerji üretimini tahmin etmek için beş model (Derin Öğrenme, Karar Ağacı, Genelleştirilmiş Doğrusal, Rastgele Orman ve Gradyan destekli ağaçlar (GBT)) kullanılmıştır.

Tahmin ve değerlendirme çalışmaları için Makine Öğrenme teknikleri ve GCM kullanılmaya başlanmıştır. Çalışmada, GCM'lerin sıcaklık ve yağış değerlerine göre, 2018'den 2080'e kadar HES'lerin üreteceği enerji miktarının tahmininde her model için ML Teknikleri ile elde edilen sonuçlar sunulmuştur. Korelasyon ve bağıl hata değerleri, GBT modelinin altı ana HES için daha doğru sonuçlar verdiğini doğrulamıştır. Göreceli Hata için GBT yüzdeleri Almus, Hasan Uğurlu, Suat Uğurlu, Hirfanlı, Kesikköprü ve Kapulukaya için sırasıyla %31, %29, %15, %22, %28,6 ve %23 olarak bulunmuştur. GBT'nin korelasyonu ise Almus, Hasan Uğurlu, Suat Uğurlu, Hirfanlı, Kesikköprü ve Kapulukaya için sırasıyla 0.717, 0.602, 0.729, 0.76, 0.623 ve 0.801 olarak bulunmuştur. Bu sonuçlara göre, elektrik üretimini tahmin etmek için GBT modeli seçilmiştir. Sonuçlar, modeller arasında küçük farklılıklar

olduğunu göstermekte, bu da tüm bu modellerde tahminlerin benzer olduğu ifade etmektedir.

Anahtar Sözcükler: İklim değişikliği, Hidroelektrik enerji, Küresel Dolaşım Modeli, Makine Öğrenimi, Enerji Üretimi, Temsili Konsantrasyon Rotaları, Türkiye.

ABSTRACT

THE EFFECT OF GLOBAL CLIMATE CHANGE ON HYDROELECTRIC POWER PLANTS AND ENERGY PRODUCTION IN THE CENTRAL BLACK SEA BASIN

Hesham ALRAYESS
Ondokuz Mayıs University
Institute of Graduate Studies
Department of Civil Engineering
PhD, December/2021
Supervisor: Assoc. Prof. Dr. Asli ULKE KESKIN

Climate change becomes one of the critical challenges all over the world. Renewable energy mainly depends on many criteria, like precipitation, temperature, and rainfall-runoff ratios. Hydropower is the primary renewable source for supplying clean energy, and its future contribution is anticipated to increase significantly.

Necessary rainfall, flow, lake level, flow and energy production data have been provided from relevant institutions such as Turkish State of Meteorological Services (TSMS), Turkish State of State Hydraulic Works (TSHW), Turkish Electricity Generation Company (TEGC) and Turkish Electricity Transmission Corporation (TETC). Two scenarios of hydropower generation were used and developed based on two climate change scenarios of climate change (namely RCP 8.5 and RCP 4.5). The Global Circulation Models (GCMs) data of precipitation and average temperature are used for predicting the energy production of the hydroelectrical power plants (HEPPs).

The thesis focused on Yesilirmak and Kizilirmak Basins as study area. It included six main HEPPs. The prediction step was calculated based on relative error and correlation values between the Machine Learning (ML) techniques. Five techniques were used to predict the energy production (Deep Learning, Decision Tree, Generalized Linear, Random Forest and Gradient boosted trees (GBT)) using monthly hydroelectric power generation data from 1971 to 2018.

Using Machine Learning techniques and GCM have started for predicting and evaluation studies. According to the temperature and precipitation values of the GCMs, the study presented the results of deploying ML Techniques in predicting the energy production which will be produced by HEPPs from 2018 to 2080. The performance criteria showed the differences between the five models and the quality of results in each model. The correlation and relative error values verified that GBT model gives more accurate results to the six main HEPPs. For Relative Error, the percantages of GBT were 31%, 29%, 15%, 22%, 28.6% and 23% for Almus, Hasan Ugurlu, Suat Ugurlu, Hirfanli, Kesikkopru and Kapulukaya, respectively. On the other hand, the results of corelation of GBT were 0.717, 0.602, 0.729, 0.76, 0.623 and 0.801 for Almus, Hasan Ugurlu, Suat Ugurlu, Hirfanli, Kesikkopru and Kapulukaya, respectively. According to that, the GBT model was used for predicting the production of electricity. The results show that there are small differences between the models which means that the predictions are going in similar directions at all these models.

Keywords: Climate change, Hydropower, Global Circulation Model, Machine Learning, Energy Production, Representative Concentration Pathways, Turkey.

ACKNOWLEDGEMENT

I would like to deeply appreciate the efforts of my supervisor (Dr. Asli Ulke Keskin) for the endless support through my PhD journey.

I would like to also thank My thesis committee and Dr. Mesut Demircan for there valuable advises.

My Family, who taught me aspire, dream and gain knowledge without limits, who didn't spare any time or effort to support me in all of my life. All people supported me in this long trip through hard days.

Hesham ALRAYESS

CONTENTS

ABBREVIATION OF TERMS

AE : Absolute Error

AEP : Annual Energy Production

AI : Artificial Intelligence

AIMF : Annual Instantaneous Maximum Flows

AR5 : Fifth Assessment Report

ANN : Artificial Neural Network

CMIP5 : The Coupled Model Intercomparison Project Phase 5

DL : Deep Learning

DT : Decision Tree

GBT : Gradient Boosted Tree

GCM : General Circulation Model

GL : Generalized Linear

GW : Gigawatt

HEPP : Hydro-Electricitcal Power Plant

IPCC : the Intergovernmental Panel on Climate Change

kWh : Kilowatt-hour

MENR : Ministry of Energy and Natural Resources

MK : Mann-Kendall test

MW : Megawatt

ML : Machine Learning

R : Correlation

RCP : Representative Concentration Pathways

RE : Relative Error

RF : Random Forest

RMSE : Root Mean Squared Error

SNHT : Standard Normal Homogeneity Test

SRES : Special Report on Emissions Scenarios

TEGC : Turkish Electricity Generation Corporation

TETC : Turkish Electricity Transmission Corporation

TSMS : Turkish State of Meteorological Services

TSHW : Turkish State of Hydraulic Works

FIGURES LEGENDS

TABLES LEGENDS

1. INTRODUCTION

In recent years, many countries have started to consider about using cleaner renewable energy for various reasons. Authorities preferred using Hydroelectricity power stations because they are eco-friendly and carry low potential risk of the environment and climate. Beside of that, there are environmental and economic impacts associated with harnessing hydropower (Chiang et al., 2013). Recently, hydropower became very important contributing energy source which supply in the worldwide. Hydropower is supplying 71% of all renewable electricity which represents 1,064 GW of the installed capacity in 2016. This value is highly predicted to significantly rise in the future (World Energy Council, 2018).

As a result of the climate change, all regions will face a variety challenge which can effect on many life fields. Changing droughts, amounts of flood, increasing temperatures and precipitation decreasing are all indications of climate change that will make side effect for hydroelectric generation by increasing water resources and hydropower potential (Blackshear et al., 2011).

According to Intergovernmental Panel on Climate Change (IPCC) 5th report, temperature is projected to increase over the 21st century base on all assessed emission scenarios (IPCC, 2012).

In Turkey, Hydropower generation relies widely on water resources and the availability of these resources. Turkey is classified as one of the most rapidly growing countries with constant growth of population and economy. That means there is an increase in Turkey's Energy demand. Turkey has many renewable energy resources that can supply all the country is energy demand (Yuksel, 2008). To examine the interdependence of energy and water in the electricity context, the assessment of the impacts of climate change on electricity generation within the Yesilirmak and Kizilirmak Basins are examined in this thesis.

According to the Ministry of Energy and Natural Resources (MENR), the renewable energy potential of Turkey possesses a hydropower potential of 433 billion kWh. Moreover, the economic hydropower potential is 140 billion kWh/year. Turkey has an ambitious target of having 34 GW of installed hydropower capacity by 2023. According to energy sources, the number of current plants consist of 653 hydraulic, 320 natural gas, 48 geothermal, 5868 solar, 42 coal, 249 wind and 243 other power plants (The Turkish Ministry of Energy and Natural Resources, 2019a).

By the end of June 2018, there were 636 (six-hundred thirty-six) hydropower plants, with a total capacity of 27,912 MW (The Turkish Ministry of Energy and Natural Resources, 2019a). Hydroelectricity production has reached about 33 billion kWh and 22.4% of Turkey's energy production was estimated from hydropower production (The Turkish Ministry of Energy and Natural Resources, 2019a).

The Turkish government vision aims to use local energy resources (renewable) effectively, efficiently and in a way that has a minimum impact on the environment (The Turkish Ministry of Energy and Natural Resources, 2019b). The global climate change caused by global warming has made a big change in the hydrological cycle of the earth (Kang et al., 2015). Climate change has several effects on some sides of the hydrology, like the pattern and magnitude of water level in the rivers and lakes and the water quality which affects the operation of dam and hydropower production. The assessment of how climate change impacts water resources, would, therefore, be crucial for sustainability of any long-term hydroelectric generation stations (Pokhrel et. al, 2018; Sharma and Shakya, 2006).

Since 2008, the number of studies of regional climate simulation have been increased on Turkey. The simulations of regional climate change based on the Special Report on Emissions Scenarios (SRES) have been performed by Gao and Giorgi (2008), Onol and Semazzi (2009), Onol and Unal (2012), Onol et al. (2013), Black et al. (2010), Sen et al. (2011), Demir (2011), Ozdogan (2011), Bozkurt and Sen (2011), Onol (2012), Bozkurt et al. (2012) and Bozkurt and Sen (2013). In these studies, the researchers found a decrease in annual precipitation with time for the entire region and a temperature increase. These changes might effect on Hydroelectric power plants (HEPPs).

1.1. Dams and Hydropower

Dams are considered as one of the most important water saving way as they help communities have domestic water and provide water for industry, navigation in rivers, recreation, irrigation, hydroelectric power production, and other important needs. During times of excess flow, dams store water in reservoir that can release water during the times when water availability is inadequate to meet water needs (Yildiz and Ozguler, 2017).

The process of flowing water which creates energy to be captured and turned into electricity is called Hydroelectric power. It is a sort of renewable energy because

the water on the earth is continuously renewed by the hydrologic cycle. Any typical hydro plant consists of a dam, a reservoir and a power plant. The dam is for controlling the water flow by opening and closing the gates. The reservoir is to store the water and the power plant is to produce the electricity. The first attempt to generate electricity from water power was in England in 1870 (Viollet, 2017). Hydropower is mainly generating energy from water that is collected behind dams. Any changes of the hydrological cycle caused by the climate change had and will have impacts on the amount of electricity produced from the hydropower. The change of precipitation and water amounts in the basins are the main climate change influencing factors on Hydropower (Blackshear et al., 2011).

HEPPs depend on the potential energy converted into kinetic energy from water falling from specific heights. This energy is then converted tomechanical energy by turbines and electrical energy by generators. HEPP projects are the basic structures of electricity generation by using the energy of water (Akpinar, 2005; Sekkeli and Kececioglu, 2011).

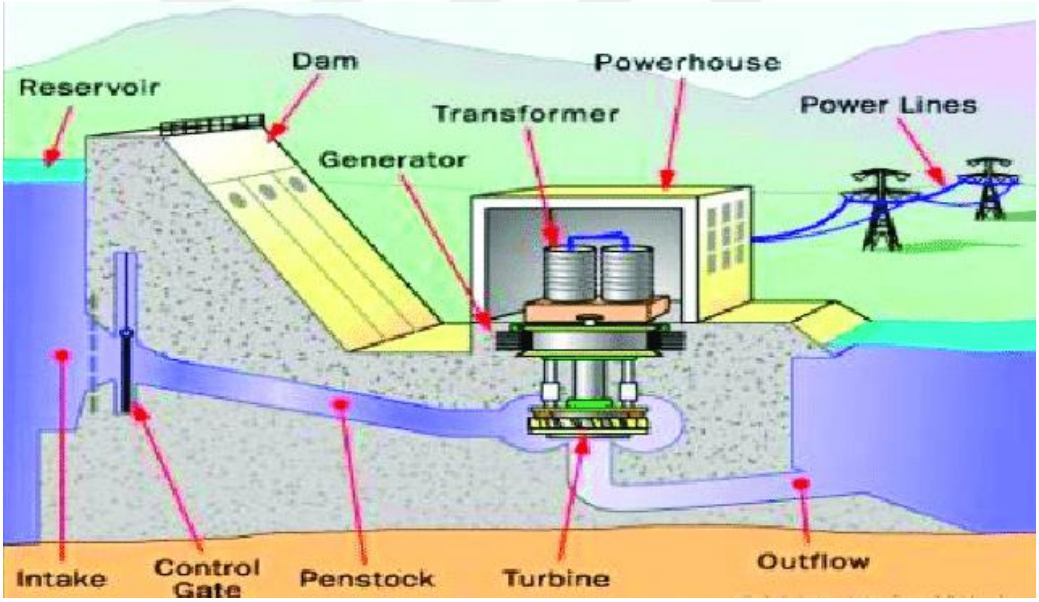

Figure 1.1. Main parts of hydropower plants (Bonsor, 2019).

Hydropower production has become a very important renewable energy source for people. In addition to that, climate change is considered as part of the biggest obstacles on a global scale. The increasing of average global temperature has been observed by local authorities. Precipitation and temperature variations have a direct relation on the energy production with time. The hydrological cycle is considered the main core for the availability of water resources which is it in Hydropower generation.

As a result of that, hydropower sources are a result of the extra water that is converted into runoff. Many of the hydrological models applied to estimate and evaluate the climate change impacts which may have on runoff using temperature and precipitation projections from hypothetical scenarios or General Circulation Models (GCM) (Schaeffer et al., 2012).

Hydroelectric power's near-zero pollution emissions, low cost and ability to fast respond to peak loads make it important renewable energy source (Madani and Lund, 2009; Gokgoz and Filiz, 2018). However, many countries are prefering hydroelectric power for its economic, technical and environmental benefits (Huang and Yan, 2009). In HEPP, the main concept of turbines is based on converting water pressure into mechanical power. The produced power is proportional to the product of pressure head and water discharge (Yuksek et al., 2006).

The generated amount of electricity from hydropower plants depends on many factors like the variation in water inflows to the power plants' reservoirs and the installed generation capacity. Natural climate change already has a huge influence on the planning, estimation and operations of hydropower systems. These systems are made based on old historical records of climatic patterns which estimate the variability and amount of energy produced over daily or seasonal fluctuations (Schaeffer et al., 2012).

In Turkey, dams are very important infrastructures for providing domestic water, water for industry, irrigation and recreation, hydroelectric power production, navigation in rivers. Beside of that, dams represent a critical point for flood protection and water conservation. Most HEPPs are located in the east side of Turkey as shown in Figure 1.2.

Figure 1.2. HEPPs distribution map in Turkey (Cografyaharita, 2017).

In Turkey, the number of HEPP is increased with time to cover the increasing population and the increasing energy demand. For example, more than nine HEPPs cover the energy production in Yesilirmak and Kizilirmak Basins. Dams and HEPP with over 14-MW capacity have been installed in Yesilırmak Basin: Almus Dam, Kokluce Dam, Hasan Ugurlu Dam, Suat Ugurlu Dam. Dams and HEPPs with over 11-MW capacity have been installed in Kizilirmak Basin: Hirfanlı Dam, Kesikkopru Dam, Kapulukaya Dam, Obruk Dam, Altinkaya Dam and Derbent Dam. (Enerji Atlas, 2020)

1.2. Aims and Objectives

This study examines how energy production is affected by climate change. The study also examines the efficiency of energy structures which are fed by water.

In streams and reservoirs where the flow is getting smaller, it will probably be required to build a new HEPP, which requires large costs, and should be designed to work efficiently for generating electricity. This thesis is examining the Yesilirmak and Kizilirmak Basins, but, because of this study, the need for a detailed study of the whole basins in Turkey will increase.

The focus of this thesis is on this potential impact of climate change on hydropower production using GCMs projection data for Representative Concentration Pathways (RCP) 4.5 and 8.5 scenarios. The climate change and impact of it on hydropower hasn't received a big attention in the academic literature in Turkey and it isn't also clear to which extent climate change-induced variations in temperature and

rainfall are incorporated into the decision-making process during the planning stages of dams. Both Iimi (2007) and Pottinger (2009) claim that climate change impacts are rarely explicitly considered at the step of planning hydropower projects.

This study will model the decrease or increase in efficiency of energy structures in recent years as a consequence of global climate change with various parameters. The aim of this work is to investigate the direct effect of climate change on the efficiency of energy production using Machine Learning models for power production. In this thesis study, rainfall and current stations that have long-term measurements in the basins are examined. Necessary rainfall, lake level, flow and energy production data have been provided from relevant institutions such as Turkish State of Meteorological Services (TSMS), Turkish State of State Hydraulic Works (TSHW), Turkish Electricity Generation Company (TEGC) and Turkish Electricity Transmission Corporation (TETC). Two important scenarios of hydropower generation were used and developed based on two scenarios of climate change, namely RCP 8.5 and RCP 4.5, which are formulated by IPCC in Fifth Assessment Report (AR5). The GCMs (HadGEM ES, MPI ESM MR and GFDL ESM 2M) projections of precipitation and average temperature are used for forecasting the energy production of the HEPPs of the study area.

The main objectives of this thesis include in the following points. Firstly, to perform an extensive review of the literature and understand more clearly the relations between climate change and hydropower generation according to previous studies. Secondly, to analysis positive or negative trends from the GCMs of the selected basins (Yesilirmak and Kizilirmak basins) and to make a link to the climate change analysis. Thirdly, to specify the best GCM that will provide the most accurate future atmospheric projections for the selected basins. Fourthly, to perform the results of downscaling steps and to explain the reason of using multi global climate model. Fifthly, to analyze the impacts of climate change on the dynamic water balance of the selected basins (Yesilirmak and Kizilirmak basins). Finally, to predict the energy production using machine learning and to execute the machine learning model. Figure 1.3 shows a step-by-step flow chart of this study. Starting from the introduction and literature review of previous studies.

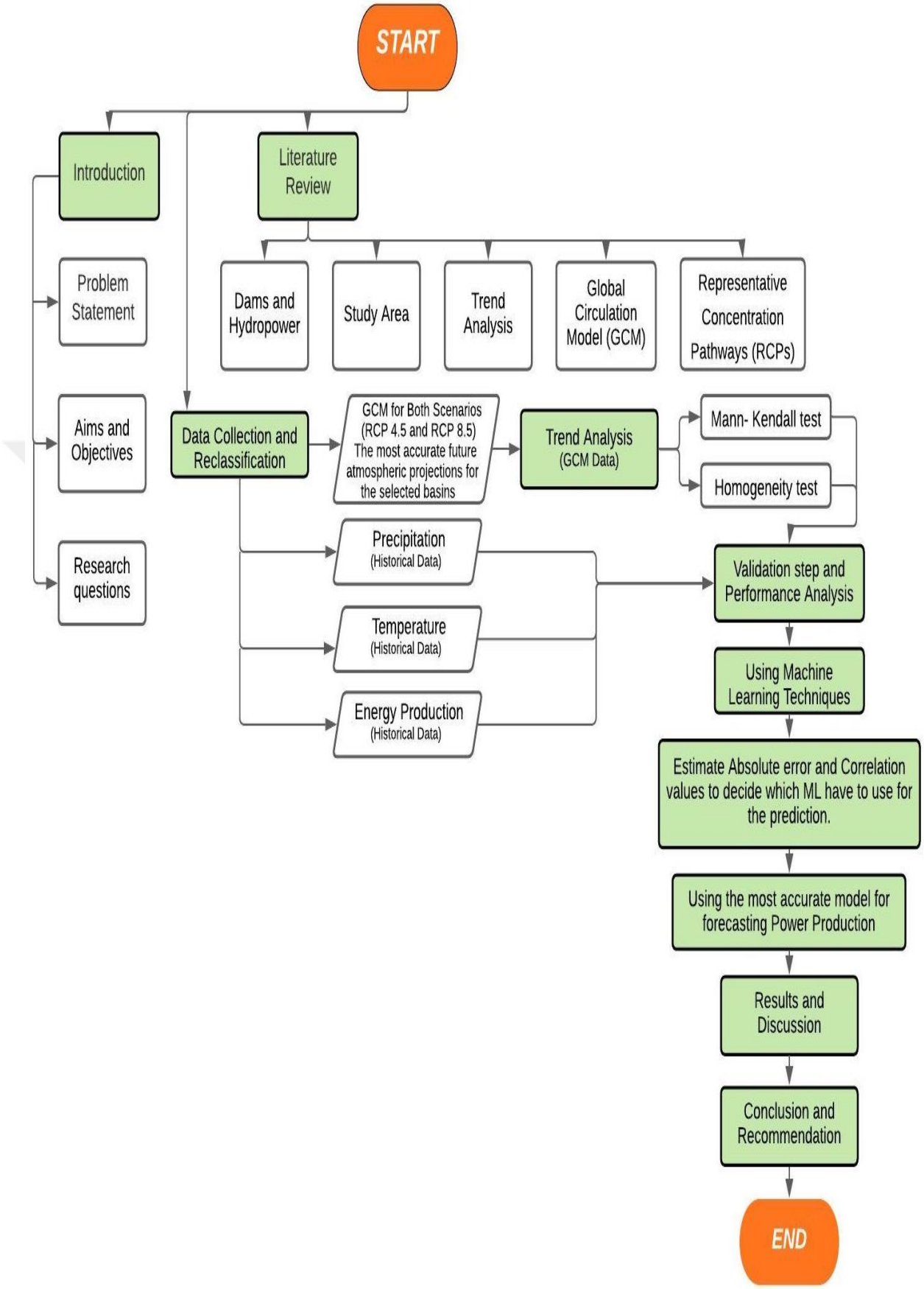

Figure 1.3. Flow chart of the thesis.

This research study presents the use of machine learning techniques for power production, for which, there is clearly a gap in the literature. There is already lack in the studies that estimate the effect of climate change on hydropower plants in Turkey in general and especially in the Black Sea Basin. Furthermore, the hydropower studies in Turkey do not use the latest machine learning techniques. These techniques produce more accurate results for forecasting the hydropower's production. This research also evaluates the impact of climate change on hydropower production in the Yesilirmak and Kizilirmak Basins. This evaluation can be used to analyse the climate situation in the next years and the possibilities of droughts and floods.

1.3. Research Questions

Five questions have to be answered by the end of this study.

1. What is the historical trend situation (Mean temperature and Precipitation) of Black Sea Region?
2. Would the trend analysis for the GCM of the selected basins provide positive or negative trend?
3. Which GCM would provide the most accurate future atmospheric projections for the selected basins?
4. Which ML technique can provide most accurate results? What is the validation steps that used to perform the technique?
5. What are the impacts of the climate change on the hydroelectricity of the selected basins? What is the needed data to support the future studies?

1.4. Chapters Summary

Chapter one presents the aims and objectives of this study. Moreover, it provides some details for dams and hydropower. Chapter two focuses on literature review and summarizing previous studies of related topics. Chapter three represents the study area properties including climate, topography, basins and HEPP data. The fourth chapter explains the used simulation methods in this thesis. The data collection and reclassification have been applied for historical data and GCMs data. The historical data are the energy production of HEPPs and the total incoming water. The GCMs data are the precipitation and temperature of each scenario, RCP 8.5 and RCP 4.5. Trend analysis is a very important step to check the homogeneity and Man Kendall test using the GCMs data. The trend estimated using each GCMs and RCP scenarios (RCP 4.5

and RCP 8.5) which applied for the trend analysis. The trend interval is between 2018 to 2080. Before the modeling step, a validation of performance analysis is very necessary to be applied.

After that, applying the model using machine learning techniques of Gradient boosted trees (GBT), Decision Tree (DT), Generalized Linear (GL), Deep Learning (DL) and Random Forest (RF) models takes place. The performance metrics played the criteria role of choosing the most accurate model of forecasting. It includes many parameters to test the performance like the root mean square error (RMSE), relative error (RE), Absolute error (AE) and correlation values (R) to decide which model will be used to predict the energy production.

Chapter five represents the applications and results of homogeneity test, Mann-Kendall test and applying Machine Learning techniques for forecasting engergy production. Chapter six focuses on analyzing and discussing the results from Chapter 5. The most accurate model is used for analyzing the effect of climate change on energy production for each HEPP. At the end of the study, Chapter 7 represents the conclusion and recommendations for the whole thesis based on the results of the predicted energy production.

2. LITERATURE REVIEW

This chapter will show the previous studies related to the topic of this thesis. Several studies tried to focus on Trend analysis and predicting using ML techniques. Some of these studies were in Turkey and the remainder were form other countries.

2.1. Trend analysis studies

Trend analysis have gotten a lot of attention from researchers in the past years, especially in Turkey. In the literature, numerous methods were used for estimating and testing the meteorological variables homogeneity. This section shows the newest studies which focused on this study.

Turkes (1996) tested homogeneity of annual precipitation data of ninety-one stations in Turkey for interval between 1930 to 1993 in Turkey using the Kruskal-Wallis test and Mann Kendall test before studying their spatial and temporal characteristics. The results showed the variation of the annual precipitation like decreasing trends in Black Sea and Mediterranean regions at that time.

Busuioc and Storch (1996) studied the variability of mean precipitation for winter at fourteen Romanian gauge stations between 1901 to 1988. Pettitt's statistics used to detect changes of systems in the time series. Almost all stations exhibited a downward shift -systemic decrease- at about 1960. An upward shift at about 1919 for the Bucharest station was likely determined by the urbanization effect. Furthermore, a downward shift in the mid of 1920's in the northwest and an upward shifts were identified for the southwestern stations at 1933. The authors found that Pettitt's statistic was sensitive to the presence of trend and serial correlation.

Tarhule and Woo (1998) examined changes in various rainfall characteristics in northern Nigeria. The records at twenty-five locations were analyzed for the occurrence of abrupt changes using the Pettitt test (Further information about Pettitt test theory can be found at Pettitt (1979)). Many of the analyzed variables included the number of rain days and the annual total rainfall. The results showed a decreased in the frequency of many variables based on rainy season during August and September.

Kahya and Kalaycı (2004) tested homogeneity of trends in monthly streamflow for 31 years period in Turkey using a procedure developed and tested by Van Belle and Hughes (1984). The methods showed a downward trend of the western basins of Turkey. However, the eastern part of Turkey showed no trend. The first four tests

resulted with the same trend situation. Some southern basins showed a trend implying the homogeneity of trends based on Van Belle and Hughes'basin trend test.

Partal and Kahya (2006) estimated the long-term trend for monthly total and annual mean precipitation serises. All these estimations were made using non parametric methods like Mann kendall test and Sen's T test. Beside of that, the authors analyzed temporal trends of 13 climate variables recorded at 96 stations across Turkey for the interval from 1929 to 1993. The reuslts of applying the trend's methods showed some significant trends in January, February and september. Furthurmore, the results showed a decrease in the annual mean precipitation in western and southern Turkey.

Karabork et al. (2007) studied the homogeneity of two hundred and twelve precipitation records of data in Turkey for the period between 1973 to 2002. They reviewed and checked the homogeneity of precipitation records in Turkey by the Pettitt Test and Standard Normal Homogeneity Test (SNHT). Stations were classified as inhomogeneous if one of the tests rejects the homogeneity at least. The authors found that Fourty-three out of two hundred and twelve stations were found to be as inhomogeneous. The results confirmed the wet respones condition of Turkish precipitation to El Nino events.

Machina and Sharma (2017) have assesed the impacts of climate change on the water resources of Kainji Hydropower Station, Nigeria as a case study using the statistical analysis of hydro-meteorological data for the interval between 1961 and 2011. The non-parametric Man-Kendall test was used to detect monotonic trends. Also, regression analysis was used to develop models for the variables.

Yilmaz and Tosunoglu (2019) have fully evaluated the trend in annual instantaneous maximum flows (AIMF) for 26 basins (153 Gauge stations) in Turkey by using non-parametric trend tests like Spearman's rho and Mann Kendall tests. The tests result showed statistically decreasing trends in most of the stations and increasing trends in the rest of the stations. The sample results of this study supported the development of a more accurate evaluation for the trends.

Guclu (2020) compared Mann-Kendall (MK) test and Şen-innovative trend analysis methods by suggesting a new methodology of trend analysis with a special graphical representation. The total rainfall data of Turkey (8 stations) from 1966 to 2015 were used in this study. The results showed the importance of using the graphical comparison for the trends. Moreover, The results showed an increase with time for the selected stations which covered Turkey like Ordu, Zongukda, Canakkale and Siirt.

Yacoub and Tayfur (2020) studied the trend analysis using a monthly data set for precipitation for a 100-year interval, from 1919 to 2016 in Mauritania. The results of Mann Kendall test showed many intervals of droughts throughout the study period.

Tokgoz and Partal (2020) estimated the trend analyses of temperature and precipitation of Black Sea region. They used a precipitation and temperature data of 16 stations spanning from 1960 to 2015. The results showed generally increasing trend.

For Turkey, many regional climate simulation studies have been conducted using scenarios since 2010. Demircan et al. (2017) used three GCMs (HadGEM2-ES, GFDL-ESM2M and MPI-ESM-MR) for RCP 8.5 and RCP 4.5 scenarios to study the climate change projections for Turkey. The GCMs were used after a 20-km resolution Dynamic Downscaling that covered the period of the study, from 2016 to 2099. The study showed an increase in mean temperature between 1 to 6 degrees. On the other hand, the results showed a decreasing in precipitation with time. Also, no regular increasing or decreasing trend was observed throughout the projection period. Although Demircan studies focused on GCMs prediction the results supported for showing the increase and decrease of temperature.

2.2. Energy production predicition studies

Several studies have examined and checked the climate change impacts on HEPPs all over the world.

Harrison and Whittington (2002) studied the energy production in Batoka Gorge hydro project and predicted that a 35% fall in the flow of water over the Victoria Falls would cut annual power production by 21% and dry season production by 32%. They argue that such a fall would make the Batoka Gorge uneconomic. The climate data used in the study are for the 1901-1996 interval.

In 2009, a study conducted by scientists from Peribonka River stated that the climate change has affected the plant's efficiency and reliability (Minville et al., 2009). Minville et al. (2009), have used the Canadian regional climate model (CRCM). The study uses Hydrotel program to simulate the distributed hydrological model. The impacts are estimated for the interval between 1961 and 2099. The study interval is divided into four periods (a control period from 1961 to 1990, Horizon-2020 from 2010 to2039, Horizon-2050 from 2040 to 2069 and Horizon-2080 from 2070 to 2099). The results indicate that the annual mean hydropower might decrease in Horizon-2020 and back to increase in the other horizons. In general the trend is increasing

statistically.

Beyene, Lettenmaier, and Kabat (2010) estimated the potential impact of climate change using downscaled precipitation and temperature data from running eleven GCMs based on IPCC report. The results showed that the Nile basin will experience increases in precipitation the early years of the period 2010-2039. The basin however will experience decreases for the periods 2040-2069 and 2070-2099 with exception of some ethiopian highlands which expected icreasing by 2080-2100. All these changes in temperature and percipitation results streamflows at the nearest dam (Aswan Dam).

For the Zambezi River Basin, Yamba et al. (2011) studied the effects of different factors, including climate change on HEPP potential. The evaluation process uses the power potential historical data 1970-2009. The effect of climate change on the HEPP were estimated to predicte future production, GCMs were used also to generate projected temperature and percipitation. The study predicted a gradual reduction in hydropower generation in the next 60 years although a large variability is expected.

Hamududu and Killingtveit (2012) assessed the climate change impact on Global hydropower. The study used 12 models with GCMs simulations to estimate the hydropower generation using the runoff changes with time. IPCC AR4 represented the base structure of this study (IPCC, 2007a). The results showed different indicates which may be decreases or increases in some times for the targeted areas.

Shrestha et al. (2014) studied the impact of climate change on hydropower production and river flow in Kulekhani Hydropower of Nepal by downscaling the outputs of B2 and A2 scenarios of the HadCM3 GCM for three different periods (2010-2039, 2040-2069 and 2070-2099). HEC-HMS hydrological model is used to estimate and simulate the river discharges during baseline and future periods in the watershed. The results showed a decrease in the energy production during the dry months and an increase during the rest of the year which means that the energy production had been affected by the climate change only seasonally.

Solaun and Cerda (2017) studied the climate change impact on Hydropower generation in Southern Spain for operation with various scenarios. A special model has been prepared and designed for HEPP operations scenarios. The results predicted a decrease in the production from 10 to 49 % of the total production in the study area depending on the scenario and the HEPP.

Forrest et al. (2018) used projections from four climate models under RCP 8.5 and RCP 4.5 for future period from 2046 to 2055 to evaluate the impact of climate

change situations on California hydropower generation to the baseline 2000 to 2009. The study showed the drought effect on the HEPP during the period of the study.

Jong et al. (2018) studied the climate change effects as a long term on the Brazilian Northeast's hydropower production. The study used average rainfull criteria to show the climate change effects based on the emissions scenario using different IPCC models. The reserchers take the last 57 years to analyze the historical rainfall data. The study forecasted a rainfall decrease, higher temperatures and drought-frequency increase by the end of 2100 which may cease the production of energy.

Mishra et al. (2018) investigated the climate change impact on the hydroelectricity in the Trishuli River in Nepal. RCP 4.5 and RCP 8.5 data were used to project the future discharges in the streams of the HEPP. The results estimated the energy production until 2080 for both RCPs. The forecasted climate change showed increasing in the basin flow and the effects on the hydropower productions.

Elias and Miegel (2018) evaluated the climate change effect on the energy production of HEPP in Upper Awash River Basin, Ethiopia. Two scenarios were used, RCP 4.5 and RCP 8.5, formulated by IPCC 5th assessment report. RCP 4.5 was used for the normal case and RCP 8.5 was used for the usual scenario with bad condition for the climate change effects. The study period was divided into three intervals 2019–2040, 2041–2070, and 2071–2100. The period from 2006 to 2014 was used as a reference period which included monthly and annually energy production data. RCP 4.5 scenario has showed an increase in energy production for the three periods with variable percentages. The differences between these values were very small which indicates that the trend may sometimes decrease.

Alrayess et al. (2018) predicted the energy production of Almus HEPP using Deep learning, Artifical neural network and Support vector machine. The results showed that using Deep Learning model was the most accurate model based on the performance validation criteria.

Beheshti et al. (2019) studied the effect of climate change on annual average of power generation in Karun 3 Dam by using HadGEM data after the statistical downscaling process for the period from 2020 to 2099. An artificial neural network (ANN) model respectively simulated the rainfall–runoff process and hydropower generation. This period is divided for two periods a near from2020 to 2049 and a far from 2070 to 2099. The results showed a gradual increasing of the annual average power generation with time for both scenarios, A2 and B2.

Li et al. (2020) evaluated the impact of climate change on hydropowers of the Peral River basins, China. Three RCP scenarios (RCP 2.6, RCP 4.5 and RCP 8.5) were used in this evaluation. The results showed that the dry years could become drier and the wet years could become wetter with time, but this does not mean that the energy production from HEPP will be significantly affected during the same time interval. This study supported an insight into the response of HEPP to climate change.

Huangpeng et al. (2021) forecasted the hydropower generation under the effect of climate change based on Developed Crow Search Optimization Algorithm (DCSA) which is a new innovation from ANN. With this algorithm, more accurate results were accomplished. For instance, the maximum R^2 correlation recorded using the algorithem is 0.88 for the studied dam, Jinanqiao Dam. The study was applied for the interval between 2021 to 2050. The results showed a gradual decrease in the power generation of all RCP scenarios that were used in the prediction process.

Many studies have focused on the hydropower situation in the future which would decrease by using the climate change scenarios. This decrease came as a normal result of rising temperatures and decreasing the amount of precipitation. The impacts of climate change may cause serious problems and negative effects on HEPP projects from the functional and economical sides. These studies could be helpful during the useful life of the HEPP and the results could be necessary for the long-term dam's susceptibility and feasibility of hydropower generation.

Turkey faces a very significant climate change related challenge. It is very important to study and estimate the prediction of the effect of the climate change on hydropower production (Iseri and Guney, 2017). From the revision of previous studies related to this topic, it has been determined that there is no such a study in the Central Black Sea Basin. This study will model the change in efficiency of energy structures in recent years as a consequence of global climate change with various parameters.

Climate change projections for Yesilirmak and Kizilirmak Basins in Turkey will be studied for several climate variables from GCM ensembles for two future time intervals between 2018 to 2080 (From 2018 to 2050 and from 2051 to 2080) using different RCP.

3. MATERIALS

The characteristics of the study area considers as one of the important points to understand the input data and results of the study. Topography, climate characteristics, basin's details and location represent the properties of the study area. Dataset and the characteristics of each HEPP for both basins are represented in this chapter to give background about the differences between each HEPP and the base of them.

3.1. Topography

Turkey is located in the southeast of Europe between the longitudes 26° and 45° E and latitudes 36° and 42° N. This proper location gave Turkey a diversified climate. Turkey is hydrologically divided into Twenty-six drainage basins as shown in Figure 3.1.

Figure 3.1. The drainage basins in Turkey.

Twenty-six basins are covering all the area of Turkey. Kizilirmak and Yesilirmak Basins are two of the largest basins in Turkey. Yesilirmak and Kizilirmak are affected by the global climate change which is concluted from TSMS reports (SNCT, 2016).

3.2. Climate Characteristics

This section will focus on the climate characteristics of the study area. It has two sub sections, Temperature and Precipitation.

3.2.1. Temperature

The average temperature is a very important factor in the Black Sea Area. In

Turkey as general, the average temperature was 14 ^{o}C in 2020. This value is slightly above the normal value for the interval between 1981 to 2010 (13.5 ^{o}C). The year 2020 had been the third most warm year since 1971. In September and October, temperature values have increased between 3.2 and 3.4, respectively (The Turkish State of Meteorological Services, 2020). The seasonal temperature has also increased based on the average of the interval from 1981 to 2010, especially in the Autumn season.

3.2.2. Precipitation

Precipitation is one of the most affected factors by climate change, especially in the Black Sea Area. The Black Sea coast receives the highest amount of precipitation throughout the year in comparison with other areas of Turkey. In 2020, the average precipitation was 500 mm in Turkey. This value is 13% below the average precipitation in the interval between 1981 to 2010 (574 mm). The monthly precipitation data has increased for the first period of the year till April (The Turkish State of Meteorological Services, 2020).

3.3. Yesilirmak and Kizilirmak Basins

The study area of this thesis is in the central Black Sea Basin. There are two main rivers which cover the whole basin. These rivers are called Kizilirmak River and Yesilirmak River.

3.3.1. Kizilirmak Basin

Kizilirmak Basin is located between 41°- 44' and 38°-25' north latitudes and 32°-48' and 38°-25' east longitudes. Kizilirmak Basin constitutes 10.49% of Turkey's surface area and it's the 15th basin of Turkey. Kizilirmak Basin is considered as the second-longest basin in Turkey after the Euphrates, is located in the eastern side of Central Anatolia. While the large part of the basin, that covers near 11% of the country's territory, is hilly, only the eastern and northern parts are mountainous. Kizilirmak River is considered as Turkey's longest river. It starts from Mount Kizil in Sivas province. It flows over 1,355 kilometers across the Central Anatolia into the Black Sea near the town of Samsun. While the humid and semi-humid climate type is dominant in the coastal parts of the Kızılırmak Basin facing the Black Sea, the semi-arid climate type is dominant in the inner parts. The total catchment area is 78,180 km². Yamula, Hirfanli, Kesikköprü, Kapulukaya, Obruk, Boyabat, Altınkaya and Derbent Dams are located on Kizilirmak River (Minarecioglu and Citakoglu, 2019).

The annual total average precipitation of Kizilirmak Basin increases when going towards the north of the basin (in the direction of the Black Sea Region). It increases significantly from the Central Anatolia Region to the Black Sea Region and the daily maximum precipitation reach the highest values in the Black Sea Region.

The average total precipitation of Kizilirmak Basin is 444.3 mm. The annual average temperature of Kizilirmak Basin was found to be 10.5°C.

Streams running along steep and deep valleys in this part of the basin and having irregular flow regimes have sometimes caused significant damage to residential areas and agricultural areas in the limited plain areas on the valley floors. Landslides have also been experienced frequently due to weak vegetation and current geological conditions along the valleys that receive heavy rainfall(General Directorate of State Hydraulic Works, 2020).

Periodic floods occur in Kizilirmak Basin and its tributaries. The total of 249 floods occurred for the interval from 1956 to 2019 in the basin (Anonymous, 2019). It has been determined that the droughts experienced in the Kizilirmak Basin lasted longer in recent years. Especially in 12 and 60 month periods, this period is about 3-7 times longer than previous droughts. The basin is under threat of drought (Arslan et al., 2016). Figures 3.2 and 3.3 show the locations and the boundaries of the Kizilirmak and Yesilirmak Basins, respectively.

Figure 3.2. Kizilirmak Basin boundaries (General Directorate of State Hydraulic Works, 2020).

3.3.2. Yesilirmak Basin

Yesilirmak Basin is located between 40°- 38' north latitudes and 35°- 49' east longitudes. Yesilirmak Basin is the 14th basin of Turkey. It is located in the Black Sea Region. Yesilirmak Basin covers approximately 5% of Turkey's surface area and covers an area of 37,823 km^2, which is the third-largest precipitation area in Turkey.

Yesilirmak River is a river in northern Turkey. Its source is located north-east of Sivas and it pours into the Black Sea near Carsamba area. Yesilirmak's length is 519 km long. While passing through Tokat, Amasya and Samsun, it merges with various rivers. The river mainly consists of three junctions. Kelkit stream is the greatest river in the basin. Yesilirmak delta is one of the largest deltas on the Black Sea coast of Turkey. A very large part of the delta has been dried and turned into an agricultural area (Serancam and Dabanli, 2020). Yesilirmak has an irregular stream on which the Almus, Hasan Ugurlu and Suat Ugurlu Dams are built with various installed capacities.

The Black Sea temperate climate and Central Anatolia continental climate are seen in Yesilirmak Basin. The effects of the Black Sea climate are seen in the regions along the coastline. In these regions, summer is hot, and winter is mild and rainy. In land areas are under the influence of high mountains.

When the precipitation characteristics in the basin are examined, it is seen that the average annual precipitation is around 50 mm and this precipitation increases slightly (60-65mm) in the winter months. In the summer months, the lowest rainfall is seen as 26.5-24.6 mm in July and August.

Temperature is the most important element of climate elements. According to the data obtained from the stations in the basin, when the annual average temperature values are examined, it is seen that this value is around 12°C. In the parts of the basin close to the coast, the temperatures are relatively higher than in the inner parts. Average temperatures in the winter months characterizing the cold period are 1-3°C, and the average highest temperature in the summer months characterizing the hot period is 21.8°C.

Between 1908 and 2015, 40 floods were experienced in the Yeşilırmak basin. River floods (floods that spread over a wide area and occur over time as a result of long-term precipitation) are frequently seen in the Yeşilırmak basin. Sudden city floods, especially from Samsun and other city centers, are an important type of flood

in the Yesilirmak Basin. Such events are always associated with very heavy rainfall. Sudden urban floods occur as a result of heavy rainfall and insufficient infrastructure (Anonymous, 2015).

A drought trend is observed in the inner parts of the Yeşilırmak basin. The risk of drought is much higher in the interior compared to the coastal areas (Beden et al., 2020).

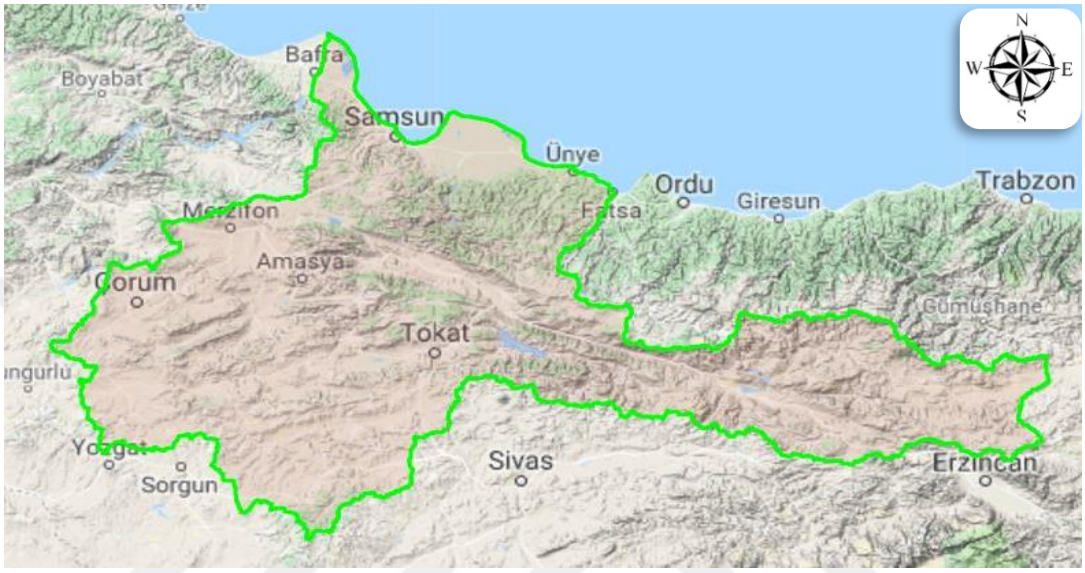

Figure 3.3. Yesilirmak Basin boundaries (General Directorate of State Hydraulic Works, 2020).

3.4. Datasets

Many various datasets are used in the AI of this thesis to perform homogenity tests and trend analysis and applying models. The data is divided into GCM data and historical data. The historical data consit of temperature and precipitation data which are obtained from TSMS and TSHW. The data interval is from 1970 to 2008. The volume of each reservoir has reflected the amount of precipitation during the year. This value is measured as million cubic meter unit (m^3). HEPP data include energy production in kWh, the total incoming water in million m^3. These data are obtained from TEGC and TETC. Energy Production represents the value of the electricity (energy) that the HEPP can produce in the dam. This value usually varies from one season to another and from one time to another.

The GCM data include precipitation and temperature data of RCP 8.5 and RCP 4.5 scenarios. The data interval is from 2018 to 2080. Precipitation data will be used in the trend analysis and validation step after each process. The trend analysis will show the trend direction for each basin. Temperature data will be used in the trend

analysis and validation step after each process. Energy Production and water flow are important factors for this study because these values can make the prediction more accurate and can help in estimating the energy production situation in the future. The water level data provided by TEGC and TETC were not suffiecient and therefore, this study does not include water as a parameter for energy forecasting process. Many studies that use different IPCC models are checked in order to estimate the effect of climate change on stream flows by many years.

3.4.1. Yesilirmak and Kizilirmak's HEPP

As mentioned before, Yesilirmak and Kizilirmak Basins are selected to predict the energy production of HEPPs and study the impact of climate change on it. Table 3.1 shows the installed capacities of HEPPs in the basins Yesilirmak and Kizilirmak with opening date for each HEPP. Figure 3.5 shows the locations of the available dams that will be used as case studies in this thesis. Three dams are located in Kizilirmak basin and another three dams are located in Yesilirmak Basin.

Table 3.1. The Hydroelectric Power Plants in the basins Yesilırmak and Kizilirmak.

Basin	HEPP name	Opening year	Installed Capacity (MW)
Yesilirmak	Almus Dam and HEPP	1966	27
	Hasan Ugurlu Dam and HEPP	1981	500
	Suat Ugurlu Dam and HEPP	1982	46
Kizilirmak	Hirfanli Dam and HEPP	1959	128
	Kesikkopru Dam and HEPP	1966	76
	Kapulukaya Dam and HEPP	1989	54

The oldest HEPP is Hirfanli. it's been established on 1959 as shown in Table 3.1. Also, the HEPP with the highest capacity is Hasan Ugurlu (500 MW). It is expected that HEPPs with small capacities and small lake volume will be less affected by climate change than HEPPs with larger capacities. In that case for example, the effect of climate change on Hasan Ugurlu HEPP will not be the same as that on on Almus HEPP.

Figure 3.4. The available dams to use as case study.

Geografically, Suat ugurlu HEPP and Hasan Ugurlu HEPP are very close from each other in location. Also, Kesikkopru and Hirfanli are very close in location as sown in Figure 3.4. In the next sub sections, the data and characterictics of each HEPP are explained with details. Beside of these details, the statistical analysis of historical Precipitation and temperature are estimated for each HEPP.

3.4.2. Almus Dam and HEPP

Almus Dam is located near the town of Almus 28 kilometers from Tokat city (40°24′27″N, 36°54′11″E) in the northen east of Turkey. It is an earthen embankment dam. The dam is constructed on the Yesilirmak River, which runs into the Black Sea. The purposes of Almus Dam were to used for flood control, irrigation and hydroelectricity. The HEPP established in 1966 with capacity of 27 megawatts. The plant is divided into three facilities; each facility has a 9-Megawatt capacity (General Directorate of State Hydraulic Works, 2018). Table 3.2 shows the characteristics of the Almus Dam and HEPP in meter and cubic meter units for levels and volumes, respectively.

Table 3.2. Almus Dam and HEPP Characteristics (General Directorate of State Hydraulic Works, 2018a).

Dam name	Almus
Province	Tokat
River	Yesilirmak
Minimum operating level (altitude)	767.37 meters
Maximum operating level (altitude)	804.5 meters
Water volume of minimum operating level	151.473 thousand m^3
Water volume of maximum operating level	1.006.730 thousand m^3
Water used for power generation	855.257 thousand m^3
Lake area	31 km^2
Height from the riverbed	78 meters
Power	27 MW
Annual production	99 Gwh

The annual energy production (AEP) is 99 GWh for Almus HEPP as shown in Table 3.2. The table also shows the maximum and minimum operating level which are 804.5 and 767.37 meters, respectively. The upstream lake area is 31 km^2 and the riverbed height is 78 meters. According to the historical data from TSMS, Some statistical parameters calculated for Annual mean Temperature, Annual Precipitation and AEP of Almus Dam and HEPP. Table 3.3 shows the statistical analysis results of the annual mean temperature, annual precipitation and AEP. The mean results are 12.42 degree, 436.33 mm and 89,296,043.47 Kwh, respectively.

Table 3.3. Statistical results of historical data for Almus Dam and HEPP.

Parameter	Annual mean Temperature	Annual Precipitation	AEP
Number of samples	48	48	51
Mean	12.42	436.33	89,296,043.47
Standard deviation	0.95	69.28	30,162,952.76
Coefficient of variation	0.08	0.16	0.34
Coefficient of skewness	0.62	0.14	-0.10

3.4.3. Hasan Ugurlu Dam and HEPP

Hasan Ugurlu is located on the River Yeşilırmak 25 km east of Samsun and 23 km south of Çarşamba town in Northern Turkey. It's a rock-fill dam for hydro power purposes. In past, it was named the Ayvacık Dam. The Dam Started operation in 1981. It generates 500 MW (4x125) of power giving an annual electricity production of 1,217 GWh. The change of the name came from story about Hasan Uğurlu. He was an engineer who died together with his wife following an accident while working at this dam's project. The second dam in the same area is called for his wife's name Suat

Uğurlu. It's far 24 km downstream of Hasan Ugurlu Dam (General Directorate of State Hydraulic Works, 2018b). Table 3.4 shows more characteristics details for the Hasan Ugurlu Dam and HEPP in meter, cubic meter units and mega-watt for levels, volumes and power production, respectively.

Table 3.4. Hasan Ugurlu Dam and HEPP Characteristics (General Directorate of State Hydraulic Works, 2018b).

Dam name	Hasan Ugurlu
Province	Samsun
River	Yesilirmak
Minimum operating level (altitude)	150 meters
Maximum operating level (altitude)	190 meters
Water volume of minimum operating level	382,298 thousand m^3
Water volume of maximum operating level	1,018,360 thousand m^3
Water used for power generation	636,062 thousand m^3
Lake area	23 km^2
Height from the riverbed	175 meters
Power	500 MW
Annual production	1217 Gwh

The upstream lake area is 23 km^2. The AEP is 1,217 GWh for Hasan Ugurlu HEPP as shown in table 3.4. Also, The table showed the maximum and minimum operating level which are 190 and 150 meters, respectively. According to the historical data from TSMS, Some statistical parameters calculated for Annual mean Temperature, Annual Precipitation and AEP of Hasan Ugurlu Dam and HEPP. Table 3.5 shows the statistical analysis results of the annual mean temperature, annual precipitation and AEP of Hasan Ugurlu Dam's area. The mean results are 14.36 degree, 697.63 mm and 1268,567,733 Kwh, respectively.

Table 3.5. Statistical results of historical data for Hasan Ugurlu Dam and HEPP.

Parameter	Annual mean Temperature	Annual Precipitation	AEP
Number of samples	48	48	40
Mean	14.36	697.63	1268,567,733
Standard deviation	0.63	105.15	415,310,731.81
Coefficient of variation	0.04	0.15	0.33
Coefficient of skewness	0.50	0.52	0.40

3.4.4. Suat Ugurlu Dam and HEPP

Suat Ugurlu Dam and HEPP is located on Yesilırmak in Carşamba district of Samsun. The power plant operated by (TEGC). Suat Ugurlu Dam and HEPP can meet all the electrical energy needs of 82,897 people in their daily lives (such as housing,

environmental lighting, industry, government offices and metro transportation) with an average electricity production of 301,082,425 kWh. The purpose of Suat Ugurlu Dam was to used for hydroelectricity and irrigation. The hydroelectricity power plant, established in 1982, has a capacity of 46 megawatts. (General Directorate of State Hydraulic Works, 2018c). Table 3.6 shows the characteristics of Suat Ugurlu Dam and HEPP in meter, cubic meter units and mega-watt for levels, volumes and power production, respectively.

Table 3.6. Suat Ugurlu Dam and HEPP Characteristics (General Directorate of State Hydraulic Works, 2018c).

Dam name	Suat Ugurlu
Province	Samsun
River	Yesilirmak
Minimum operating level (altitude)	58.5 meters
Maximum operating level (altitude)	61.5 meters
Water volume of minimum operating level	154,371 thousand m^3
Water volume of maximum operating level	182,461 thousand m^3
Water used for power generation	28,090 thousand m^3
Lake area	10 km^2
Height from the riverbed	51 meters
Power	46 MW
Annual production	273 Gwh

The AEP is 273 GWh for Suat Ugurlu HEPP as shown in table 3.6. Also, the table shows the maximum and minimum operating level which are 61.5 and 58.5 meters, respectively. The upstream lake area 10 km^2 and the height from the riverbed is 51 meters. According to the historical data from TSMS, Some statistical parameters calculated for Annual mean Temperature, Annual Precipitation and AEP of Suat Ugurlu Dam and HEPP. Table 3.7 shows the statistical analysis results of the annual mean temperature, annual precipitation and AEP of Suat Ugurlu Dam's area. The mean results are 14.36 degree, 697.63 mm and 316,064,295.9 Kwh, respectively.

Tablo 3.7. Statistical results of historical data for Suat Ugurlu Dam and HEPP.

Parameter	Annual mean Temperature	Annual Precipitation	AEP
Number of samples	48	48	34
Mean	14.36	697.63	316,064,295.9
Standard deviation	0.63	105.15	68,689,110.29
Coefficient of variation	0.04	0.15	0.22
Coefficient of skewness	0.50	0.52	-1.19

3.4.5. Hirfanli Dam and HEPP

Hirfanli Dam is located on the Kızılırmak river, between Kirsehir and Sereflikochisar, in Kirsehir province. This dam is a rock body fill type and is 78 meters high from the stream bed. The HEPP established in 1959 for energy generation and flood control purposes, with a power capacity of 128 MW provides 400 GWh electrical energy production per year (General Directorate of State Hydraulic Works, 2018d). Table 3.8 shows the characteristics of Hirfanlı Dam and HEPP in meter, cubic meter units and mega-watt for levels, volumes and power production, respectively.

Table 3.8. Hirfanli Dam and HEPP Characteristics (General Directorate of State Hydraulic Works, 2018d).

Dam name	Hirfanli
Province	Kirsehir
River	kizilirmak
Minimum operating level (altitude)	842 meters
Maximum operating level (altitude)	851 meters
Water volume of minimum operating level	3,705,300 thousand m^3
Water volume of maximum operating level	5,740,420 thousand m^3
Water used for power generation	2,035,120 thousand m^3
Lake area	263 km^2
Height from the riverbed	78 meters
Power	128 MW
Annual production	400 Gwh

The AEP is 400 GWh for Hirfanli HEPP. The upstream lake area is 263 km^2 and the height from the riverbed is 78 meters as shown in Table 3.8. According to the historical data from TSMS, Some statistical parameters calculated for Annual mean Temperature, Annual Precipitation and AEP of Hirfanli Dam and HEPP. Table 3.9 shows the statistical analysis results of the annual mean temperature, annual precipitation and AEP of Hirfanli Dam's area.

The mean results are 11.49 degree, 381 mm and 276,240,840.6 Kwh, respectively. Beside of that, the standard deviation values are 0.93, 77.06 and 117,430,336.75 for the annual mean temperature, annual precipitation and AEP, respectively.

Table 3.9. Statistical results of historical data for Hirfanli Dam and HEPP.

Parameter	Annual mean Temperature	Annual Precipitation	AEP
Number of samples	48	48	57
Mean	11.49	381	276,240,840.6
Standard deviation	0.93	77.06	117,430,336.75
Coefficient of variation	0.08	0.20	0.43
Coefficient of skewness	0.55	0.26	1.00

3.4.6. Kesikkopru Dam and HEPP

The operation of the Kesikköprü Dam has started in 1966 for irrigation and energy production on Kizilirmak in the Bala district of Ankara. The dam is a rock body fill type. The lake area is 6.50 km² at normal water level.

Kesikkopru HEPP generartes 250 GWh of electrical energy per year with its 76 MW power capacity (General Directorate of State Hydraulic Works (d), 2018). Table 3.10 shows the characteristics of Kesikkopru Dam and HEPP in meter and cubic meter units and mega-watt for levels, for levels, volumes and power production, respectively.

Tablo 3.10. Kesikkopru Dam and HEPP Characteristics (General Directorate of State Hydraulic Works, 2018e).

Dam name	Kesikkopru
Province	Ankara
River	kizilirmak
Minimum operating level (altitude)	772.48 meters
Maximum operating level (altitude)	785.55 meters
Water volume of minimum operating level	31,085 thousand m^3
Water volume of maximum operating level	88,053 thousand m^3
Water used for power generation	56,946 thousand m^3
Lake area	6.5 km^2
Height from the riverbed	49 meters
Power	76 MW
Annual production	250 Gwh

The lake area before the dam is 6.5 km^2. The AEP is 250 GWh for Kesikkopru HEPP as shown in table 3.10. Also, The table shows the maximum and minimum operating level which are 785.55 and 772.48 meters, respectively. According to the historical data from TSMS, Some statistical parameters calculated for Annual mean Temperature, Annual Precipitation and AEP of Kesikkopru Dam and HEPP. Table 3.11 shows the statistical analysis results of the annual mean temperature, annual precipitation and AEP of Kesikkopru Dam's area. The mean results are 10.41 degree, 456.44 mm and 173,406,405 Kwh, respectively.

Table 3.11. Statistical results of historical data for Kesikkopru Dam and HEPP

Parameter	Annual mean Temperature	Annual Precipitation	AEP
Number of samples	48	48	50
Mean	10.41	456.44	173,406,405
Standard deviation	0.96	90.18	71,470,548.7
Coefficient of variation	0.09	0.20	0.41
Coefficient of skewness	0.47	0.32	0.80

3.4.7. Kapulukaya Dam and HEPP

Kapulukaya Dam is built on Kizilirmak in Kirikkale and its operation has started in 1989 for drinking water supply and electricity generation purposes. The body volume of the dam is an earth body fill type. The lake area at normal water level is 20.70 km². The HEPP established in 1966, has a capacity of 54 megawatts which provides 190 GWh electrical energy production per year (General Directorate of State Hydraulic Works (e), 2018). Table 3.12 shows the characteristics of Kapulukaya Dam and HEPP in meter and cubic meter units for levels and volumes, respectively.

Table 3.12. Kapulukaya Dam and HEPP characteristics (General Directorate of State Hydraulic Works, 2018f).

Dam name	Kapulukaya
Province	Kirikkale
River	kizilirmak
Minimum operating level (altitude)	715 meters
Maximum operating level (altitude)	724 meters
Water volume of minimum operating level	145,388 thousand m^3
Water volume of maximum operating level	286,149 thousand m^3
Water used for power generation	140,761 thousand m^3
Lake area	21 km^2
Height from the riverbed	61 meters
Power	54 MW
Annual production	190 Gwh

The AEP is 190 GWh for Kapulukaya HEPP. Also, The table shows the maximum and minimum operating level which is 724 and 715 meters, respectively. The lake area before the dam is 21 km^2 and the height from the riverbed is 61 meters as shown in Table 3.12. According to the historical data from TSMS, Some statistical parameters calculated for Annual mean Temperature, Annual Precipitation and AEP of Kapulukaya Dam and HEPP. Table 3.13 shows the statistical analysis results of the annual mean temperature, annual precipitation and AEP of Kapulukaya Dam's area. The mean results are 10.75 degree, 414.23 mm and 146,828,250.4 Kwh, respectively.

Table 3.13. Statistical results of historical data for Kapulukaya Dam and HEPP

Parameter	Annual mean Temperature	Annual Precipitation	AEP
Number of samples	48	48	28
Mean	10.75	414.23	146,828,250.4
Standard deviation	0.89	69.55	61,347,653.61
Coefficient of variation	0.08	0.17	0.42
Coefficient of skewness	0.37	0.05	0.41

This chapter showed all the climate characteristic and topography of black Sea Regionof the basins (Kizilirmak and Yesilirmak). The historical data used to calculate the statistical parameters of Annual mean Temperature, Annual Precipitation and AEP. Datasets section focused on six HEPPS (Almus HEPP, Suat Ugurlu HEPP, Hasan Ugurlu HEPP, Hirfanli HEPP, Kesikkopru HEPP and Kapulukaya HEPP) which cover the study area with historical data more than 30 years. These HEPPs have various capacities and characterictics.

4. METHODS

This chapter discusses the methodology in this research study. These methods start with homogeneity tests and end with using Machine Learning (ML) techniques. GCM models, RCP, Homogeneity tests, Mann Kendall test, Rapidminer program and ML models are explained with details in this chapter and will be applied in the following chapter.

4.1. Global Circulation Model (GCM)

Climate is considered as one of the most challenging geophysical systems to simulate as a result of the wide range of time and spatial scales of relevant processes and the number of components and their complexity (Laprise R., 2008).

General circulation models (GCMs) provide the most accurate estimates for the climate change with time (Randall et al., 2007). These types of models are used and introduced for simulating the climate for present condition and future scenarios (Liu et al., 2013; Sun et al., 2010).

Generally, spatial resolution of GCMs is widely used for large scale applications (typically ~50,000 km^2) but their efficiency is very limited in the specific and regional studies. Downscaling solves the resolution issue. It works by converting climatic variables from large scale to regional scale which is needed in climate change impact studies. Beside of that, statistical downscaling is used in predicting hydrological impacts under climatic scenarios (Fu and Charles, 2011; Khan et al., 2006; Harpham and Wilby, 2005).

According to the data distribution center of IPCC, GCMs are classifying physical situation processes in the ocean, land surface and atmosphere, are the most advanced tools currently available for simulating the response of the global climate system to increasing greenhouse gas concentrations (IPCC, 2019b). GCMs are an important tool to understand, evaluate and predict the climate change impacts. These mathmetical coupled models combine many earth systems including the land surface, oceans, sea-ice and atmosphere and offer considerable potential for climate change studies and variability (Gharbia et al., 2016; Fowler et al. 2007).

Climate models are very proper tools available for researching and investigating the reactive of the climate system to many forces, for making climate forecasting on seasonal to decadal time scales and for estimating projections of future periods (Flato et al., 2013). Climate impact studies often depend on climate change projections at fine

spatial resolution. GCMs, which are the tools for obtaining future climate scenarios, work on a very coarse scale, so the output from GCMs require to be downscaled to estimate a finer spatial resolution. The GCM gives a clear quantitative projection of many atmospheric components at various scales (regional or global). Beside of that, it still has regional biases to be removed using bias correction or downscaling models (statistically or dynamically and temporally or spatially) (Maraun et al., 2010; Schmidli, 2006).

Many such GCMs were used by climate modeling researching groups from around the world to improve the development of the Intergovernmental Panel on Climate Change (IPCC)'s 5th Assessment Report (AR5) through a set of climate model experiments, which is known as the Coupled Model Intercomparison Project Phase 5 (CMIP5) (Taylor et al., 2012). CMIP5 experiments were designed to help simulate the possible effects of future climate change and to promote the understanding of the climate under the scenarios known as the Representative Concentration Pathways (RCPs) (Moss et al., 2010).

GCMs depict the climate using a three-dimensional (3-D) grid over the globe, typically having 10 to 20 vertical layers in the atmosphere and sometimes as many as 30 layers in the oceans and a horizontal resolution of between 250 and 600 kilometers. Moreover, various physical processes, such as those linked to clouds, also occur at smaller scales and cannot be properly modelled (IPCC, 2019b). Figure 4.1 shows more explanation for GCMs grid.

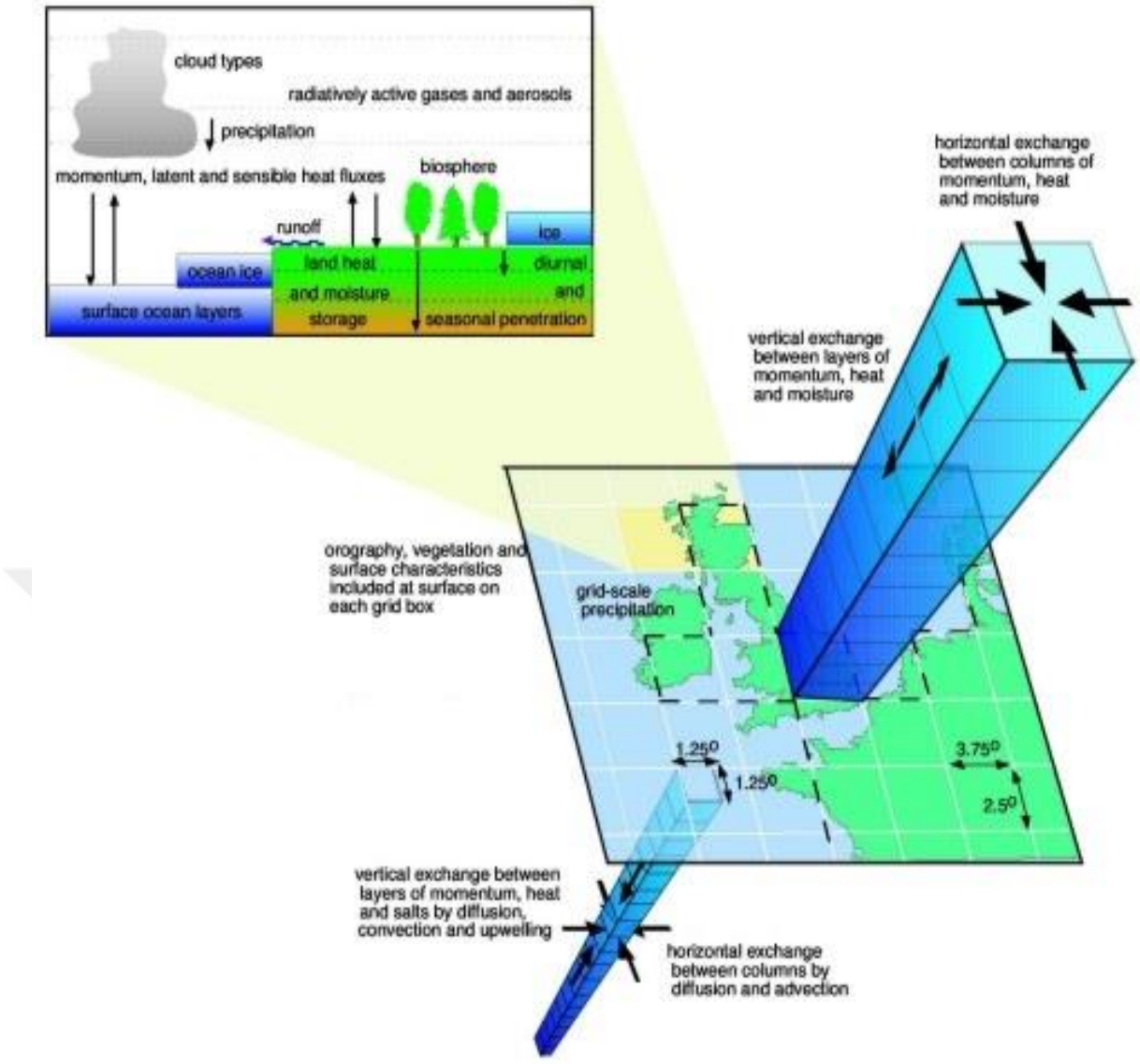

Figure 4.1. Explanation of GCMs grid (IPCC, 2019b).

The grid of the GCMs divides the world map as small cells horizontally and vertically as shown in Figure 4.1. These cells are divided to many sub cells base on horizontal exchange between columns with 3.75° and 2.5° cell to study the area more accurately.

4.1.1. HadGEM2 ES

HadGEM2 is one of the three GCMs whose precipitation and temperature data will be used for the energy prediction process. It's an overall Earth-System Model which was developed by Hadley Centre of UK Met Office as a second version. The standard component of this model contains thirty-eight levels extending to near forty km height. The horizontal resolution of HadGEM2 is 1.25° latitude and 1.875°

longitude (~112.5 km) (192 x 145 grid cells) (Demircan et al.,2017). This is similar to a surface resolution of about 139 km x 208 km at the Equator, reducing to 139 km x 120 km at 55 degrees of latitude. A vertically extended version, with sixty levels extending to eighty-five km height, is also used for investigating stratospheric processes and their influence on global climate (Collins et al., 2008). This model has a group of model specific configurations which includes various levels of mixture but in a physical certain framework (Coupled ocean-atmosphere configuration without or with vertical extension) (Demircan et al.,2017).

4.1.2. GFDL ESM 2M

GFDL-ESM-2M is a very complete system developed by National Oceanic and Atmospheric Administration (NOAA) Geophysical Fluid Dynamics Laboratory (GFDL) using numerical and dynamical models and computer simulations (Dunne et al., 2020). The resolution of this version is 24 level in the vertical and 2° latitude and 2.5° longitude (~220 km) in the horizontal (Demircan et al.,2017). ESM is a shortcut for Earth System Model which is constructed by GFDL (Winton et al., 2020).

4.1.3. MPI ESM MR

The third model in this study, MPI ESM MR is the comprehensive Earth-System Model developed by Max Plank Institute (MPI) for Meteorology (MR mixed resolution). The resolution of this version is 95 level in the vertical and 63 level in the horizontal (approximately 1.9° (~210 km) on a Gaussian grid) (Demircan et al.,2017). MPI-ESM couples the land surface, atmosphere and ocean by exchanging water, momentum, carbon dioxide and energy.

4.2. Representative Concentration Pathways (RCPs)

A group of scenarios known as RCPs have been adopted by climate researchers to supply a range of possible futures for the evolution of atmospheric composition. These RCPs have started to replace earlier scenario-based projections of atmospheric composition (Gharbia et al., 2016).

Scenarios which include time series of emissions and aerosols and chemically active gases, as well as land use/land cover (Moss et al., 2008). RCPs usually refer to the portion of the concentration pathway extending up to 2100, for which Integrated Assessment Models produced corresponding emission scenarios. Four RCPs (RCP 8.5, RCP 4.5, RCP 6.0 and RCP 2.6) produced from Integrated Assessment Models

were chosen from the published literature and are used in the 5th IPCC Assessment as a basis for the climate predictions. In RCP 4.5 intermediate stabilization pathway, the radiative forcing is stabilized at approximately 4.5 W m-2 after 2100. RCP 8.5 one high pathway for which radiative forcing reaches greater than 8.5 W m-2 by 2100 and continues to rise for some amount of time (IPCC, 2019b; van Vuuren et al., 2011). Table 4.1 shows the types of RCP which are used in this study and their parameters.

Table 4.1. Types of Representative Concentration Pathways (Rogelj et al., 2012).

Name of RCP's	Radiative Forcing	Time	Pathway shape	Concentration (ppm)	Emissions (Kyoto Protocol's greenhouse gases)
RCP 4.5	~4.5 W/m^2	at stabilization after 2100	Stabilization without overshoot	~650 CO2-eq	Decline from the mid-century
RCP 8.5	> 8.5 W/m^2	in 2100	Rising	> ~1370 CO2-eq	Rising continues until 2100.

4.3. Downscaling

A downscaling technique are required to overcome the scale incompatibility problem between the resolution required for regional scale impact assessment and the coarse resolution GCM outputs.

There are two downscaling techniques: statistical downscaling, which is done by relating GCM-resolution climate variables and local observation data empirically with a statistical relationship (Wilby et al., 1998; Bhuvandas et al., 2014).

The dynamical downscaling, in which a fine-resolution regional climate model (RCM) is embedded within a GCM to obtain local weather variables by the explicit solution of the process-based physical dynamics of the system (Jakob Themeßl et al., 2011; Fowler et al., 2007; Spak et al., 2007). The Both techniques have disadvantages and advantages, and their results are changeable based on the study area (Jang and Kavvas, 2015).

In statistical downscaling, there is an empirical statistical relationship between catchment scale hydroclimatic variables and GCM outputs (Benestad et al., 2008). The physics-based equations are used for the same purpose in dynamic downscaling (Fowler and Wilby, 2010).

4.4. Homogeneity test

Homogeneous rainfall records are often required in hydrologic design. Homogenization in climate change research means the removal of non-climatic changes. The most common statistical homogeneity tests are Standard Normal Homogeneity Test (SNHT) for a single break (Alexandersson, 1986), Pettit's Test (Pettitt, 1979), Von Neumann Ratio (Von Neumann, 1941) and Buishand's Test (Buishand, 1982).

4.4.1. Standard Normal Homogeneity Test (SNHT)

SNHT should be applied in series comparison with reference to obtain reliable break points. Furthermore, the limits of this test should be considered during the homogenization procedure.

The wrong application of homogenization procedures to climate data can then lead to unreliable climate analysis. SNHT provides a very accurate results by preventing corrections and incorrect estimates made as a result of misinterpretation of the inhomogeneous situation (Toreti et al., 2010). SNHT is calculated by the following equations:

$$T(k) = k\bar{z}_1^{-2} + (n-k)\bar{z}_2^{-2} \quad k = 1,\ldots..,n \tag{4.1}$$

$$\bar{z}_1 = \frac{1}{k}\sum_{i=1}^{k}(Y_i - \bar{Y})\Big/ s \tag{4.2}$$

$$\bar{z}_2 = \frac{1}{n-k}\sum_{i=k+1}^{n}(Y_i - \bar{Y})\Big/ s \tag{4.3}$$

$$T_0 = \max_{1\le k\le n} T_{(k)} \tag{4.4}$$

Table 4.2. Critical test values for SNHT based on the number of data entries at significance levels 1%

N	20	30	40	50	70	100
1%	9.56	10.45	11.01	11.38	11.89	12.32

Table 4.2 shows the critical values for limits based on the number of samples and significance level 1% for SNHT test.

4.4.2. Von Neumann Ratio Test

Von neumann ratio is a test that uses the ratio of mean square successive difference to the variance. The test statistic is shown as follows:

$$N = \frac{\sum_{i=1}^{n-1}(Y_i - Y_{i+1})^2}{\sum_{i=1}^{n}(Y_i - \bar{Y})^2} \quad (4.5)$$

If the result of the test is larger than the determined critical value, the data set is considered homogeneous. These critical values are given in Table 4.3 (Buishand ,1982).

Table 4.3. Critical test values for Von Neumann ratio test based on the number of data entries at significance levels 1%

N	20	30	40	50	70	100
1%	1.04	1.2	1.29	1.36	1.45	1.54

4.4.3. Buishand's Test

The test is used to detect any change in the mean by checking the cumulative deviation from the mean. According to Buishand (1982), It is based on the adjusted cumulative deviation from the mean. The Buishand range test is classified as a parametric test which assumes the test values are identically normally distributed and independent. The adjusted partial sum is defined as:

$$S_0^* = 0 \;\; ve \;\; S_k^* = \sum_{i=1}^{k}(Y_i - \bar{Y}) \qquad k = 1, \ldots . n \quad (4.6)$$

$$R = {\left(\max_{0 \le k \le n} S_k^* - \min_{0 \le k \le n} S_k^*\right)}/{S} \quad (4.7)$$

The ${R}/{\sqrt{n}}$ is then compared with the critical values which given by Buishand (1982).

When ${R}/{\sqrt{n}}$ is less than a critical ${R}/{\sqrt{n}}$ the null hypothesis is accepted.

When ${R}/{\sqrt{n}}$ is greater than a critical ${R}/{\sqrt{n}}$ the null hypothesis should be rejected (Alghazali and Alawadi, 2014).

Table 4.4. 1% critical values of f Buishand Range Test for Expression of R in n Function (Buishand, 1982).

N	20	30	40	50	70	100
1%	1.6	1.7	1.74	11,19	1.81	1.86

Table 4.4 shows the critical values for limits based on the number of samples and significance level 1% for Buishand's test.

4.4.4. Pettit's Test

Pettitt test, which is estimated to find the change point monthly or yearly, is applied to determine the change point in a time series and is classified as a non-parametric test (Pettitt, 1979).

$$X_k = 2\sum_{i=1}^{k} r_i - k(n+1) \quad \text{k=1,…, n} \tag{4.8}$$

$$X_E = \max_{1\le k\le n} |X_k| \tag{4.9}$$

Table 4.5. Critical test values for Pettitt test based on the number of data at significance levels 1%

N	20	30	40	50	70	100
1%	71	133	208	293	488	841

Table 4.5 shows the critical values for limits based on the number of samples and significance level 1% for Pettitt's test.

4.5. Trend Analysis

The main aim of trend analysis is to estimate and examine if a series of observations of a random variable is decreasing or increasing with time. Although, parametric trend tests are more effective, non-parametric trend tests are used as the researchers require the data be independent (Tabari et al., 2011).

The presence of a monotonic decreasing or increasing trend has to be estimated using the non-parametric Mann-Kendall test. Also, the regression analysis will be calculated to develop regression models. All parameters are subjected to statistical, Mann-Kendall and regression tests (Machina and Sharma, 2017). Turkey has started to concentrate on using trend analysis on precipitation and temperature patterns to apply many of non-parametric tests. Turkes et al. (1995) applied these tests for data interval between 1930 – 1992. After that, Turkes (1996) published wider studies related to the annual rainfall series. Kadioglu (1997) and Tayanc et al. (1997) also examined trends for different intervals.

In 2004, Kahya and Kalayci made a 31-year period trend analysis also for 26 basins in Turkey. In 2001, Kahya and Karabork used the available data to estimate the homogeneity. In this study, the non-parametric Mann–Kendall test is used in trend

detection of precipitation and temperature in Yesilirmak and Kizilirmak basins.

4.5.1. Mann – Kendall test (MK)

The Mann-Kendall test is determining monotonic trends and is based on ranks (Helsel and Hirsch, 2002). This is a test for correlation between sequences of pairs of values. The significance of the detected trends can be obtained at a different level of significance. The Mann-Kendall test has been suggested by the World Meteorological Organization (WMO) to estimate the existence of statistically significant trends in hydrologic and climate data time series. The MK test statistic and the sign function are calculated using the formula:

$$S = \sum_{i=1}^{n-1} \quad \sum_{j=i+1}^{n} \; sign\,(x_j - x_i) \tag{4.10}$$

x_i and x_j are the data values for time series i and j, in Equation 4.10, n is the number of data points and sign $(x_j - x_i)$ is the sign function in Equation 4.11 below:

$$sign\,(x_j - x_i) \begin{cases} +1 & x_j > x_i \\ 0 & x_j = x_i \\ -1 & x_j < x_i \end{cases} \tag{4.11}$$

Where n is the number of data, x is the data point at times I and j (j > i).

4.6. Machine Learning Models

This growing interest among researchers is stemmed from the fact that these learning machine models have excellent performance in the issues of pattern recognition and the modeling of linear and nonlinear relationships of multivariate dynamic systems. The Artificial Neural Network (ANN) is used widely in specific operations because of the prediction of higher accuracy and among several Artificial Intelligence (AI) built on soft computing methods. Therefore, ANN gives a flexible and fast passage for integration of data and the development of the model. (Hammid et al., 2018). Kankal et al. (2011) has examined studies related to energy predicting for Turkey and has found ANN, swarm optimization, genetic algorithm approach, harmony search algorithm and ARIMA methods. Until today, ANN models have been used by many researchers to predict energy production (Hamzacebi et al., 2017; Dmitrieva, 2015; Zhang et al., 1998). It was found that the ANN used in these studies gave better results than the conventional models.

As a result of very quick technology development, data mining and machine learning became one of the most important and effective methods in processing data sets. Machine learning (ML) are specific computer algorithm techniques that develop

through trials and experience (Lange and Sippel, 2020). ML is a subset branch of artificial intelligence. ML algorithms build a model based on a very sample of data to estimate a forecasting of decisions without any straight programing (Lange and Sippel, 2020). ML has been used in water resources management and HEPP prediction.

The energy power of HEPP forecasting studies in Turkey have started since 1960s, and as of 1984, econometric models have been applied for prediction purposes (Kankal et al., 2011).

4.6.1. Deep Learning Model

Deep Learning (DL) techniques are considered as a significant part of ML methods with fundamental rules of ANN. DL techniques have been used in analyzing, processing, calculating and detection tasks. DL is the outcome of developing ANN which makes prediction more accurate and gives positive results for long-term periods. DL can double layers of models to learn and support representation of data. The deep neural networks can increase the performance of load forecasting by making a high focus on parameter optimization (Gokgoz and Filiz, 2018).

4.6.2. Gradient Boosted Trees Model

Gradient boosting is one of the most powerful techniques for building predictive models. The idea of this technique initiated in the observations that boosting can be explained as a special algorithm (Optimization algorithm). This observation was made by Breiman (1997). Jerome H. Friedman (1999) developed these explicit regression gradients boosting algorithms.

4.6.3. Decision Tree Model

Decision Tree (DT) is one of non-parametric learning method for regression and classifying. The main purpose of DT is to start a pattern or model. This pattern predicts the value of the targeted variable by getting a new technique and simple decision rules resulted from the data features. DT method is an estimation model and is used for data collection. An upside-down tree is created from general to specific while the model training process (Sattari et al., 2012).

4.6.4. Generalized Linear Model

The generalized linear model (GLM) is a flexible generalization of ordinary linear regression that allows for the variables of response. The GLM popularizes linear

regression by permitting the linear model to be linked to the response variable through a link function and by permitting the magnitude of the difference or variance of each measurement to be a function of its forecasted value (Nelder and Wedderburn, 1972).

4.6.5. Random Forest Model

Random Forest (RF) is a ML technique which is very powerful and easy ensemble classifiers (Krusic et al., 2017). Breiman (2001) studied and developed this type of model based on decision trees. RF generate a multiple tree according to random bootstrapped samples of the training dataset (Breiman 2001). The concept of the technique is to run a random binary tree which uses a subset of the observations through bootstrapping techniques. The model is built from the data sampled from the original data (Catani et al. 2013). The RF forecasts the significance of variables by searching for the amount of forecasting error increases (Liaw and Wiener 2002; Catani et al. 2013).

4.7. RapidMiner Studio

RapidMiner Studio Program is used in the energy prediction step. It's a data science software platform which was developed for deep learning, machine learning and analysis purposes. It gives two options for modeling, Auto model or designing your own model. Also, it processes the operation based on Classification or Regression (Kotu and Deshpande, 2019).

Data Hasan Ugurlu

Add new data sets on the left. Details for the selected data are shown below. You can change the data with the following actions.

TRANSFORM | CLEANSE | GENERATE | PIVOT | MERGE | MODEL | CHARTS | CREATE PROCESS | HISTORY

date *Date / Time*	Production (KWh) *Number*	total incoming Water (... *Number*	INCOMING flow (M3 / S) *Number*	Precipitation (mm) *Number*	Temperature © *Number*
Jan 1, 1980	132993690	252.400	94.240	51.200	5.400
Feb 1, 1980	63958810	299.700	119.600	42.900	5.900
Mar 1, 1980	212921980	1058.200	395.100	81.300	7.600
Apr 1, 1980	197101730	1561.900	602.600	95.900	10.100
May 1, 1980	145207360	1667.600	622.600	92.400	14.100
Jun 1, 1980	82906820	368.600	142.200	29.500	19.300
Jul 1, 1980	121383880	175.400	65.500	4.100	22.600
Aug 1, 1980	114310440	169.500	63.300	33.500	22.900
Sep 1, 1980	6088200	147.200	56.800	67.800	18.400
Oct 1, 1980	10003730	223.100	83.300	56.500	15.800

Figure 4.2. Turbo Prep for preparing the data before applying the model.

Preparing data, classification and related test had to be estimated before applying the models as shown in Figure 4.2. In the energy prediction process, the test and the experimental percentage should be identified. Because of the restriction of the data, the experiment percentage is collected as 85% and the test percentage as 15% from the total number of data.

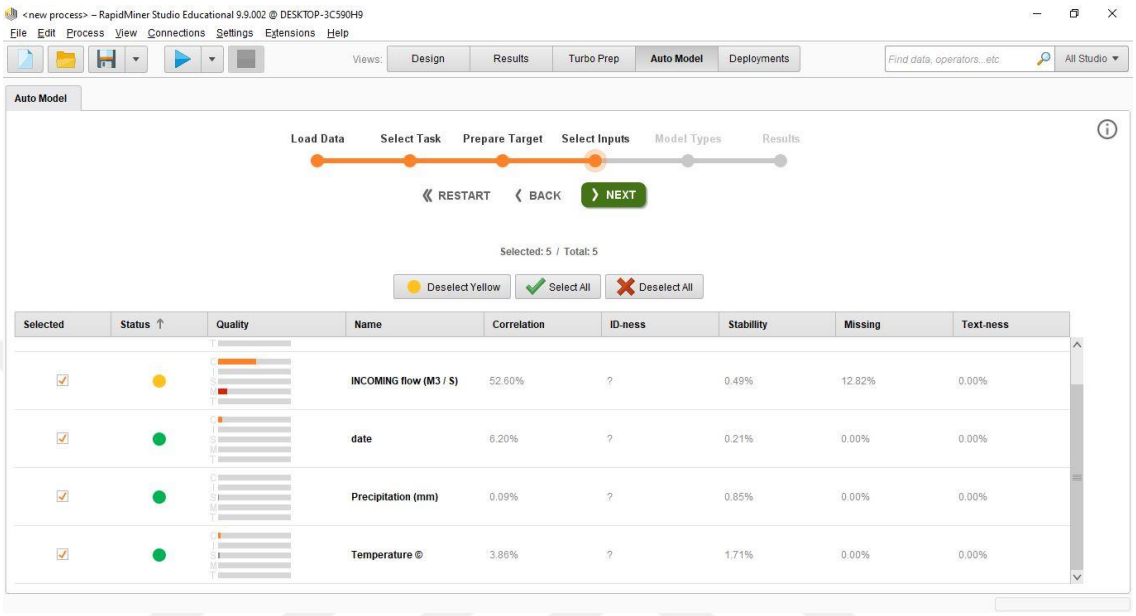

Figure 4.3. Auto model process to estimate the correlation and relative error and applying the model.

The auto model is used after preparing the data for estimating the correlation and relative error values. The data must be selected before applying the models as shown in Figure 4.3. One model will be used for energy production forecasting based on the correlation and relative error values. The model with the highest correlation and the lowest relative error among the six models is used for the energy production prediction process.

4.8. Standardization

Standardization or the standard score is the same proccess for converting any raw score by subtracting the mean from the raw score and then dividing the difference by the standard deviation. The below equation shows the estimation of the standard score (Z-Score).

$$z = \frac{x-\mu}{\sigma} \tag{4.12}$$

Where: μ is the mean and σ is the standard deviation.

Standardization processes were calculated automatically in RapidMiner

Program as check process before modeling (Spiegel and Stephens, 2008).

4.9. Validation assessment

Performance estimation is a very important process for any study. Correlation (R), Root Mean Squared Error (RMSE), Absolute Error (AE) and Relative Error (RE).

$$RMSE = \sqrt{\frac{\sum_{m=1}^{n}(X_p - X_o)^2}{n}} / \bar{X}_o \quad (4.13)$$

$$AE = \left|\sum_{m=1}^{n}(X_p - X_o)\right| \quad (4.14)$$

$$RE = \left|\sum_{m=1}^{n}(X_p - X_o)\right| / X_o \quad (4.15)$$

$$R = \frac{\sum(X_o - \bar{X}_o)(X_p - \bar{X}_p)}{\sqrt{\sum(X_o - \bar{X}_o)^2 \sum(X_p - \bar{X}_p)^2}} \quad (4.16)$$

n is the number of the data, X_p is the predicted data, X_o is observed data, $\bar{X}_p$ is the average of predicted data, $\bar{X}_o$ is the average of observed data.

5. APPLICATIONS AND RESULTS

GCMs are an important tool to understand and help to predict the impacts of climate change on the study area. These complicated numerical coupled models combine many earth systems including the atmosphere, oceans, land surface and sea-ice and variability and offer considerable potential for the study of climate change (Gharbia et al., 2016; Fowler et al. 2007).

This chapter discusses Homogeneity test and trend analysis using Mann Kendal test for the GCMs data of RCP 8.5 and RCP 4.5 scenarios and shows the difference of the trend between them. The trend analysis is applied for the annual mean temperature and the annual precipitation for the period from 2018 to 2080. These tests can help in the primary indication of the effects of climate change on many fields, including the field of hydropower.

5.1. Homogeneity test

In this section, the result of the homogenity tests is shown for each GCMs of using both RCP (RCP 8.5 and RCP 4.5). The tests are applied for the annual mean temperature and the annual precipitation for the interval from 2018 to 2080.

5.1.1. Annual Mean Temperature test

The four tests of homogeneity are estimated for the data of the six HEPP locations. Tables 5.1 to 5.6 show the four tests (Buishand's Test, Standard Normal Homogeneity Test, Pettit's Test, Von Neumann Ratio Test) which are applied for the six HEPP in Kizilirmak and Yesilirmak Basins for GCM data.

Table 5.1. The results of the temperature homogeneity tests of Almus HEPP.

GCM model	N	Standard Normal Homogeneity Test	Buishand's Test	Pettit's Test	Von Neumann Ratio Test	Result	Comment
HadGEM RCP 4.5	63	***23.99***	2.39	***40342***	1.15	2	Homogeneity doubt
MPI RCP 4.5	63	15.70	2.03	***37898***	1.91	1	Homogeneous
GFDL RCP 4.5	63	16.01	1.96	***38338***	1.66	1	Homogeneous
HadGEM RCP 8.5	63	***42.80***	***3.15***	***37338***	0.49	3	Homogeneously Flawed
MPI RCP 8.5	63	***34.61***	***2.93***	***39664***	0.67	3	Homogeneously Flawed
GFDL RCP 8.5	63	***31.73***	***2.71***	***43004***	0.78	3	Homogeneously Flawed

In Table 5.1, the results show that the only hemogenous data are for MPI RCP 4.5 and GFDL RCP 4.5 models. The other model results were either Homogeneity

doubt or Homogeneously Flawed. The boxes highlighted in yellow are the ones that failed the test.

Table 5.2. The results of the temperature homogeneity tests of Hasan Ugurlu HEPP.

GCM model	N	Standard Normal Homogeneity Test	Buishand's Test	Pettit's Test	Von Neumann Ratio Test	Result	Comment
HadGEM RCP 4.5	63	***22.43***	2.36	***40342***	1.18	2	Homogeneity doubt
MPI RCP 4.5	63	13.24	1.89	***37898***	1.87	1	Homogeneous
GFDL RCP 4.5	63	12.71	1.78	***38338***	1.77	1	Homogeneous
HadGEM RCP 8.5	63	***38.90***	***3.00***	***37338***	0.62	3	Homogeneously Flawed
MPI RCP 8.5	63	***32.23***	***2.81***	***39664***	0.70	3	Homogeneously Flawed
GFDL RCP 8.5	63	***27.11***	***2.51***	***43004***	1.04	3	Homogeneously Flawed

In Table 5.2, the results show that the only hemogenous data are for MPI RCP 4.5 and GFDL RCP 4.5 models. The other model results were either Homogeneity doubt or Homogeneously Flawed. The boxes highlighted in yellow are the ones that failed the test.

Table 5.3. The results of the temperature homogeneity tests of Suat Ugurlu HEPP.

GCM model	N	Standard Normal Homogeneity Test	Buishand's Test	Pettit's Test	Von Neumann Ratio Test	Result	Comment
HadGEM RCP 4.5	63	***19.18***	2.18	***40342***	1.29	2	Homogeneity doubt
MPI RCP 4.5	63	12.84	1.88	***37898***	1.93	1	Homogeneous
GFDL RCP 4.5	63	12.43	1.78	***38338***	1.72	1	Homogeneous
HadGEM RCP 8.5	63	***36.96***	***2.93***	***37338***	0.68	3	Homogeneously Flawed
MPI RCP 8.5	63	***32.42***	***2.84***	***39664***	0.70	3	Homogeneously Flawed
GFDL RCP 8.5	63	***25.95***	***2.45***	***43004***	1.04	3	Homogeneously Flawed

Table 5.3 shows the results of the homogeneity test of Suat Ugurlu HEPP. The boxes highlighted in yellow are the ones that failed the test. The only hemogenous data resulted in MPI RCP 4.5 and GFDL RCP 4.5 GCM data. The other model results are either Homogeneity doubt or Homogeneously Flawed.

Table 5.4. The results of the temperature homogeneity tests of Hirfanli HEPP.

GCM model	N	Standard Normal Homogeneity Test	Buishand's Test	Pettit's Test	Von Neumann Ratio Test	Result	Comment
HadGEM RCP 4.5	63	***25.45***	2.46	***40342***	1.06	2	Homogeneity doubt
MPI RCP 4.5	63	15.82	2.02	***37898***	1.85	1	Homogeneous
GFDL RCP 4.5	63	15.47	1.92	***38338***	1.72	1	Homogeneous
HadGEM RCP 8.5	63	***42.37***	***3.13***	***37338***	0.48	3	Homogeneously Flawed
MPI RCP 8.5	63	***35.10***	***2.96***	***39664***	0.65	3	Homogeneously Flawed
GFDL RCP 8.5	63	***32.85***	***2.76***	***43004***	0.75	3	Homogeneously Flawed

Table 5.4 shows the results of the homogeneity test of Hirfanli HEPP. The boxes highlighted in yellow are the ones that failed the test. The only hemogenous data resulted in MPI RCP 4.5 and GFDL RCP 4.5 GCM data. The other model results are either Homogeneity doubt or Homogeneously Flawed.

Table 5.5. The results of the temperature homogeneity tests of Kesikkopru HEPP.

GCM model	N	Standard Normal Homogeneity Test	Buishand's Test	Pettit's Test	Von Neumann Ratio Test	Result	Comment
HadGEM RCP 4.5	63	***24.56***	2.28	***40342***	1.15	2	Homogeneity doubt
MPI RCP 4.5	63	15.88	2.03	***37898***	1.89	1	Homogeneous
GFDL RCP 4.5	63	15.57	1.93	***38338***	1.70	1	Homogeneous
HadGEM RCP 8.5	63	***42.72***	***3.15***	***37338***	0.48	3	Homogeneously Flawed
MPI RCP 8.5	63	***34.94***	***2.95***	***39664***	0.66	3	Homogeneously Flawed
GFDL RCP 8.5	63	***32.71***	***2.75***	***43004***	0.75	3	Homogeneously Flawed

Table 5.5 shows the results of the homogeneity test of Kesikkopru HEPP. The boxes highlighted in yellow are the ones that failed the test. The only hemogenous data resulted in MPI RCP 4.5 and GFDL RCP 4.5 GCM data. The other model results are either Homogeneity doubt or Homogeneously Flawed.

Table 5.6. The results of the temperature homogeneity tests of Kapulukaya HEPP.

GCM model	N	Standard Normal Homogeneity Test	Buishand's Test	Pettit's Test	Von Neumann Ratio Test	Result	Comment
HadGEM RCP 4.5	63	***23.99***	2.39	***40342***	1.15	2	Homogeneity doubt
MPI RCP 4.5	63	15.70	2.03	***37898***	1.91	1	Homogeneous
GFDL RCP 4.5	63	16.01	1.96	***38338***	1.66	1	Homogeneous
HadGEM RCP 8.5	63	***42.80***	***3.15***	***37338***	0.49	3	Homogeneously Flawed
MPI RCP 8.5	63	***34.61***	***2.93***	***39664***	0.67	3	Homogeneously Flawed
GFDL RCP 8.5	63	***31.73***	***2.71***	***43004***	0.78	3	Homogeneously Flawed

Table 5.6 shows the results of the homogeneity test of annual mean temperature GCM data for Kapulukaya HEPP. The boxes highlighted in yellow are the ones that failed the test. The only hemogenous data resulted in MPI RCP 4.5 and GFDL RCP 4.5 GCM data. The other model results are either Homogeneity doubt or Homogeneously Flawed.

In all of the tests, the samples (N) are 63 as annual data for all GCMs models. The results of all homogeneity tests of annual mean temperature are the same for all GCMs. For RCP 4.5, the HadGEM model is Homogeneity doubt. However, MPI and GFDL models are Homogeneous. The results of all RCP 8.5 are Homogeneously Flawed for each model in all the HEPP.

5.1.2. Precipitation Homogeneity test

All GCMs precipitation data were used for these tests after the downscaling step, which is made by DMI. This section shows the homogeneity test results for the precipitation data. It's applied for each downscaled data from GCMs. using both RCPs (RCP 8.5 and RCP 4.5). Tables 5.7 to 5.12 show the four tests (Buishand's Test, Standard Normal Homogeneity Test, Pettit's Test, Von Neumann Ratio Test). Table 5.7 shows the results of the homogeneity test of annual precipitation GCM data for Almus HEPP. All the GCM were homogenous except MPI RCP 4.5 which resulted as homogeneity doubt.

Table 5.7. The results of the precipitation homogeneity tests for Almus HEPP.

GCM model	N	Standard Normal Homogeneity Test	Buishand's Test	Pettit's Test	Von Neumann Ratio Test	Result	Comment
HadGEM RCP 4.5	63	8.73	1.26	***40342***	1.71	1	Homogeneous
MPI RCP 4.5	63	1.73	0.76	***37898***	***2.62***	2	Homogeneity doubt
GFDL RCP 4.5	63	9.92	1.49	***38338***	1.93	1	Homogeneous
HadGEM RCP 8.5	63	2.73	0.67	***37338***	2.46	1	Homogeneous
MPI RCP 8.5	63	4.77	1.50	***39664***	2.29	1	Homogeneous
GFDL RCP 8.5	63	6.73	1.37	***43004***	1.81	1	Homogeneous

Table 5.8 shows the results of the homogeneity test for the annual precipitation GCM data for Hasan Ugurlu HEPP. The number of samples (N) is 63. All the GCM were homogenous with differences in the values of the four tests (SNHT, Buishand's Test, Pettit's Test and Von Neumann Ratio Test).

Table 5.8. The results of the precipitation homogeneity tests for Hasan Ugurlu HEPP.

GCM model	N	Standard Normal Homogeneity Test	Buishand's Test	Pettit's Test	Von Neumann Ratio Test	Result	Comment
HadGEM RCP 4.5	63	6.59	1.27	***40342***	1.89	1	Homogeneous
MPI RCP 4.5	63	1.46	0.88	***37898***	2.28	1	Homogeneous
GFDL RCP 4.5	63	6.92	1.47	***38338***	2.23	1	Homogeneous
HadGEM RCP 8.5	63	7.78	0.87	***37338***	2.17	1	Homogeneous
MPI RCP 8.5	63	5.35	1.31	***39664***	2.04	1	Homogeneous
GFDL RCP 8.5	63	3.48	1.14	***43004***	1.87	1	Homogeneous

Table 5.9 shows the results of the homogeneity test of the annual precipitation GCM data for Suat Ugurlu HEPP. All GCMs are homogenous with differences in the values of the four tests. The similarity in the results of Hasan Ugurlu HEPP and Suat Ugurlu HEPP is a normal result of the short distance between the two HEPP and the similarity of GCM data.

Table 5.9. The results of the precipitation homogeneity tests for Suat Ugurlu HEPP.

GCM model	N	Standard Normal Homogeneity Test	Buishand's Test	Pettit's Test	Von Neumann Ratio Test	Result	Comment
HadGEM RCP 4.5	63	2.56	1.00	***40342***	1.92	1	Homogeneous
MPI RCP 4.5	63	2.02	1.09	***37898***	2.18	1	Homogeneous
GFDL RCP 4.5	63	6.59	1.56	***38338***	2.00	1	Homogeneous
HadGEM RCP 8.5	63	3.47	0.74	***37338***	2.31	1	Homogeneous
MPI RCP 8.5	63	8.22	1.55	***39664***	1.83	1	Homogeneous
GFDL RCP 8.5	63	3.96	1.17	***43004***	2.00	1	Homogeneous

Table 5.10 shows the results of the homogeneity test of annual precipitation GCM data for Hirfanli HEPP. All GCM are homogenous with differences in the values of the four tests.

Table 5.10. The results of the precipitation homogeneity tests for Hirfanli HEPP.

GCM model	N	Standard Normal Homogeneity Test	Buishand's Test	Pettit's Test	Von Neumann Ratio Test	Result	Comment
HadGEM RCP 4.5	63	3.37	1.28	***40342***	1.90	1	Homogeneous
MPI RCP 4.5	63	2.90	0.92	***37898***	1.95	1	Homogeneous
GFDL RCP 4.5	63	7.69	1.36	***38338***	1.77	1	Homogeneous
HadGEM RCP 8.5	63	5.96	1.06	***37338***	2.24	1	Homogeneous
MPI RCP 8.5	63	4.44	1.25	***39664***	2.16	1	Homogeneous
GFDL RCP 8.5	63	10.41	1.62	***43004***	1.63	1	Homogeneous

Table 5.11 shows the results of the homogeneity test of the annual precipitation GCM data for Kesikkopru HEPP. All of the GCM were homogenous with differences in the values of the four tests.

Table 5.11. The results of the precipitation homogeneity tests for Kesikkopru HEPP.

GCM model	N	Standard Normal Homogeneity Test	Buishand's Test	Pettit's Test	Von Neumann Ratio Test	Result	Comment
HadGEM RCP 4.5	63	2.59	1.22	***40342***	2.07	1	Homogeneous
MPI RCP 4.5	63	2.27	0.72	***37898***	2.20	1	Homogeneous
GFDL RCP 4.5	63	10.57	1.57	***38338***	1.65	1	Homogeneous
HadGEM RCP 8.5	63	4.49	1.08	***37338***	2.09	1	Homogeneous
MPI RCP 8.5	63	5.06	1.47	***39664***	2.18	1	Homogeneous
GFDL RCP 8.5	63	9.50	1.57	***43004***	1.71	1	Homogeneous

Table 5.12 shows the results of the homogeneity test of annual precipitation

GCM data for Kapulukaya HEPP. All of the GCM were homogenous with differences in the values of the four tests.

Table 5.12. The results of the precipitation homogeneity tests for Kapulukaya HEPP.

GCM model	N	Standard Normal Homogeneity Test	Buishand's Test	Pettit's Test	Von Neumann Ratio Test	Result	Comment
HadGEM RCP 4.5	63	3.74	1.15	***40342***	2.20	1	Homogeneous
MPI RCP 4.5	63	2.44	0.95	***37898***	2.14	1	Homogeneous
GFDL RCP 4.5	63	4.70	1.50	***38338***	1.88	1	Homogeneous
HadGEM RCP 8.5	63	6.08	1.07	***37338***	2.13	1	Homogeneous
MPI RCP 8.5	63	4.11	1.22	***39664***	2.32	1	Homogeneous
GFDL RCP 8.5	63	6.62	1.33	***43004***	2.05	1	Homogeneous

In all of the tests, the samples (N) are 63 as annual data for all GCMs models. All the homogeneity tests of annual precipitation showed the same results for all GCMs (Homogeneous) except for MPI RCP 4.5 in Almus HEPP data (Homogeneity doubt). In General, the data of the study area for all GCMs scenarios are homogenous which means that the data could be used to get accurate results of predicting the energy production.

On the other hand, the results of annual mean temperature homogeneity showed Homogeneity doubt for HadGEM RCP 4.5, Homogeneous for MPI RCP 4.5 and GFDL RCP 4.5 and Homogeneously Flawed for all GCMs of RCP 8.5.

5.2. Mann-Kendall Test

In this section, the trend analysis is calculated for each downscaled data from GCMs using both RCPs (RCP 5.5 and RCP 4.5). The test is applied for the annual mean temperature and the annual precipitation for the interval from 2018 to 2080 for the GCMs data of RCP 4.5 and RCP 8.5 for Almus HEPP, Suat Ugurlu HEPP, Hasan Ugurlu HEPP, Hirfanli HEPP, Kesikkopru HEPP and Kapulukaya HEPP.

5.2.1. Mann-Kendall test for Temperature

The annual mean temperature data for the six HEPP is used for the period from 2018 to 2080 at each model to estimate the trend situation based on each GCM. Figure 5.1 shows the trend analysis of the annual mean temperature of Almus HEPP in each scenario.

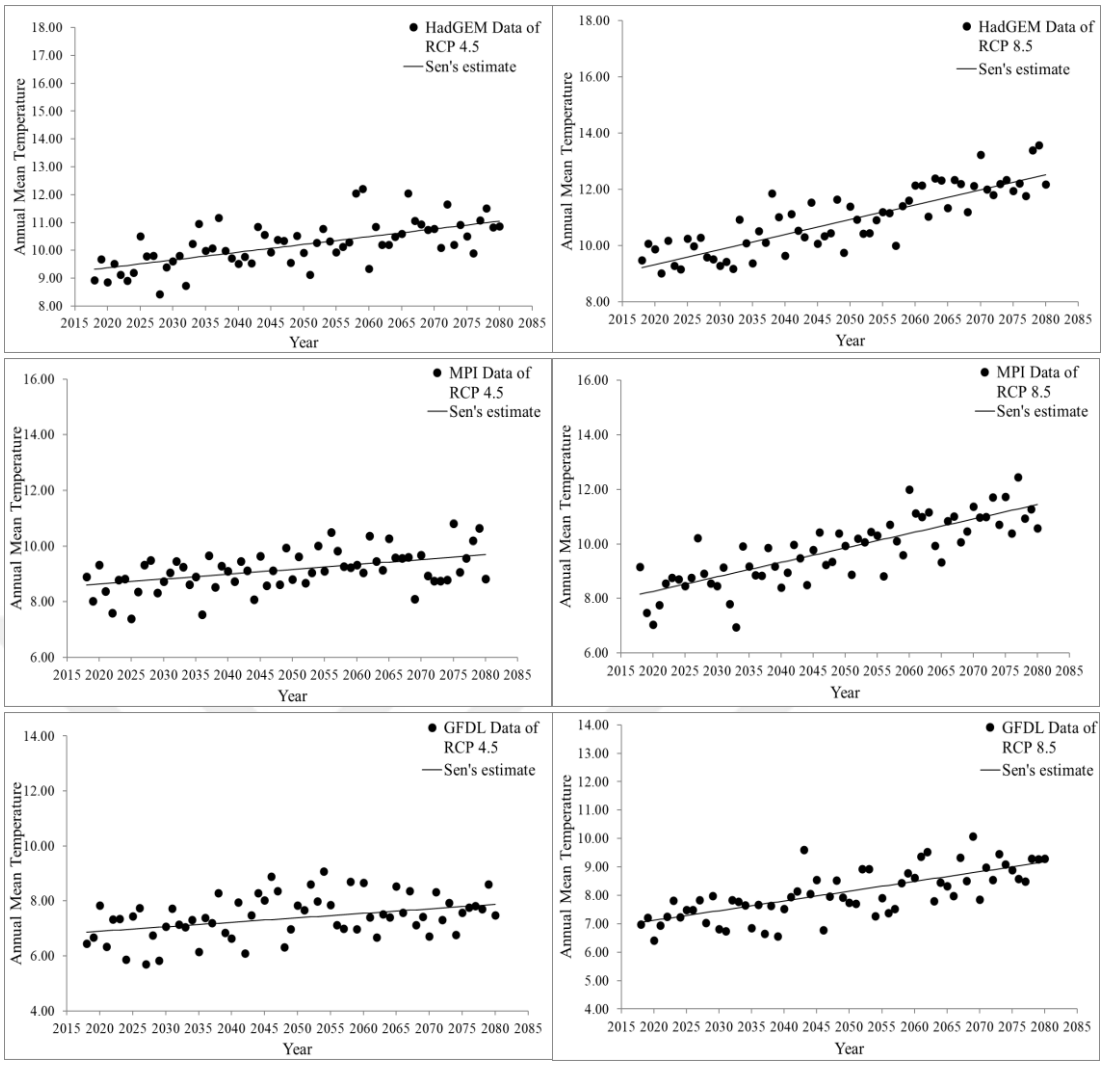

Figure 5.1. Trend results of the annual mean temperature of Almus HEPP for each GCM.

The trend direction is going up for each scenario of the GCMs for RCP 8.5 and RCP 4.5. For HadGEM, both GCMtrends of RCP 4.5 and RCP 8.5 of GCMs are positive. In RCP 8.5 the trends are more intensely positive than RCP 4.5 trends. In each model, the highest increase in the annual temperature is predicted in the worst scenarios the RCP 8.5, which is the worst scenario in comparison with RCP 4.5 scenarios.

Table 5.13 shows the Z value with positive values of each GCM and for both scenarios. The Z test results are 5.39, 7.51, 3.49, 7.24, 2.9 and 6.07 for HadGEM RCP 4.5, HadGEM RCP 8.5, MPI RCP 4.5, MPI RCP 8.5, GFDL RCP 4.5 and GFDL RCP 8.5, respectively. Also, the table shows the 1% and 5% values of T minimum and maximum.

Table 5.13. Mann-Kendall test of the annual mean temperature of Almus HEPP.

Model	First year	Last Year	n	Test Z	T	T_{min99}	T_{max99}	T_{min95}	T_{max95}
HadGEM RCP 4.5	2018	2080	63	5.39	0.028	0.018	0.037	0.020	0.035
HadGEM RCP 8.5	2018	2080	63	7.51	0.053	0.040	0.064	0.044	0.061
MPI RCP 4.5	2018	2080	63	3.49	0.018	0.005	0.031	0.008	0.028
MPI RCP 8.5	2018	2080	63	7.24	0.053	0.040	0.067	0.042	0.063
GFDL RCP 4.5	2018	2080	63	2.90	0.016	0.002	0.031	0.005	0.027
GFDL RCP 8.5	2018	2080	63	6.07	0.034	0.024	0.046	0.026	0.042

Figure 5.2 shows the trend analysis of annual mean temperature of Hasan Ugurlu HEPP for each scenario.

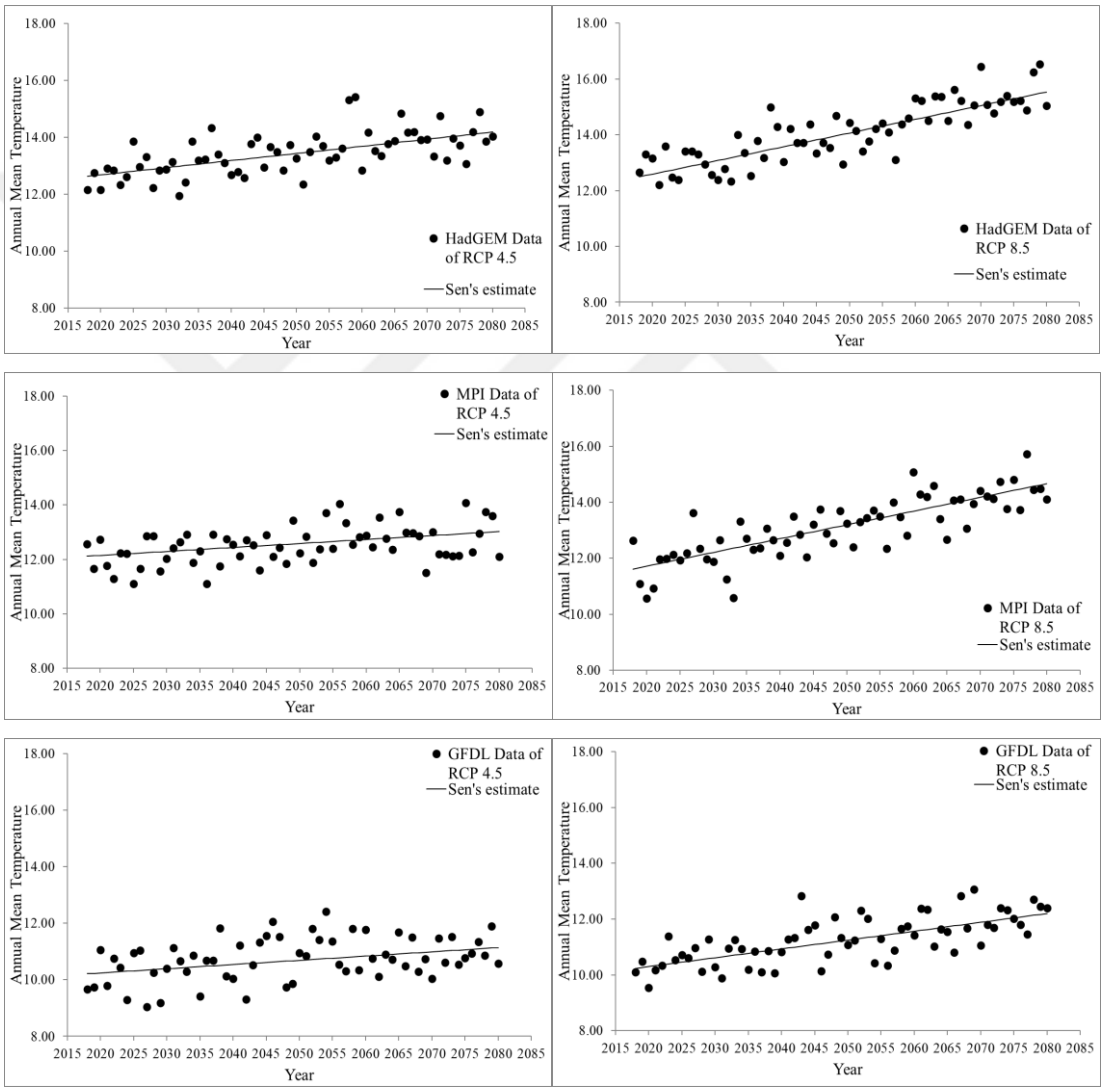

Figure 5.2. Trend results of the annual temperature of Hasan Ugurlu HEPP for each GCM.

The trend direction is positive for each scenario of the GCMs for RCP 8.5 and RCP 4.5. For all GCMs, both trends of RCPs 4.5 and 8.5 are positive. In each model, the highest increase in the annual temperature is predicted in the worst scenarios in the

RCP 8.5, which is the worst scenario in comparison with RCP 4.5 scenarios.

All the trends of GCMs are positive with high positivity in RCP 8.5 scenarios as shown in Table 5.14. The Z Test results are as following 5.37, 7.24, 3.02, 7.31, 2.64 and 5.94 for HadGEM RCP 4.5, HadGEM RCP 8.5, MPI RCP 4.5, MPI RCP 8.5, GFDL RCP 4.5 and GFDL RCP 8.5, respectively. Also, the table shows the 1% and 5% values of T minimum and maximum.

Table 5.14. Mann-Kendall test of the annual mean temperature of Hasan Ugurlu HEPP.

Model	First year	Last Year	n	Test Z	T	T_{min99}	T_{max99}	T_{min95}	T_{max95}
HadGEM RCP 4.5	2018	2080	63	5.37	0.025	0.015	0.035	0.018	0.033
HadGEM RCP 8.5	2018	2080	63	7.24	0.049	0.037	0.060	0.040	0.057
MPI RCP 4.5	2018	2080	63	3.02	0.015	0.002	0.028	0.005	0.025
MPI RCP 8.5	2018	2080	63	7.31	0.049	0.037	0.061	0.040	0.057
GFDL RCP 4.5	2018	2080	63	2.64	0.015	0.000	0.029	0.004	0.026
GFDL RCP 8.5	2018	2080	63	5.94	0.032	0.021	0.044	0.024	0.040

Figure 5.3 shows the trend analysis for the annual mean temperature of Suat Ugurlu HEPP in each scenario (RCP 8.5 and RCP 4.5).

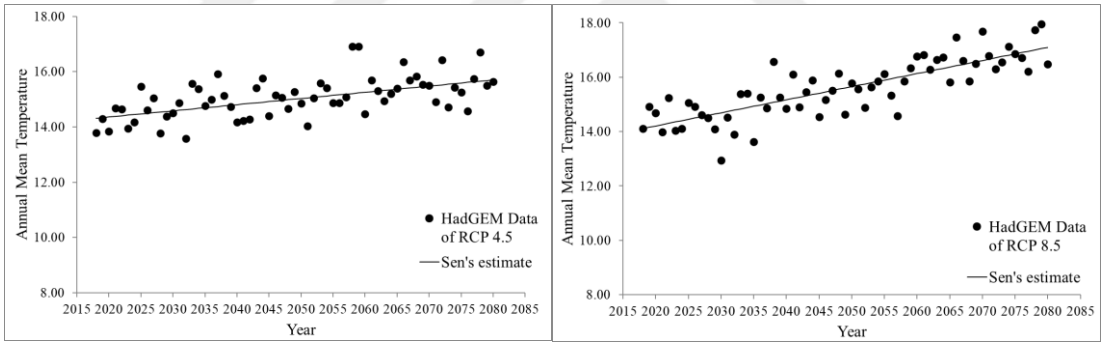

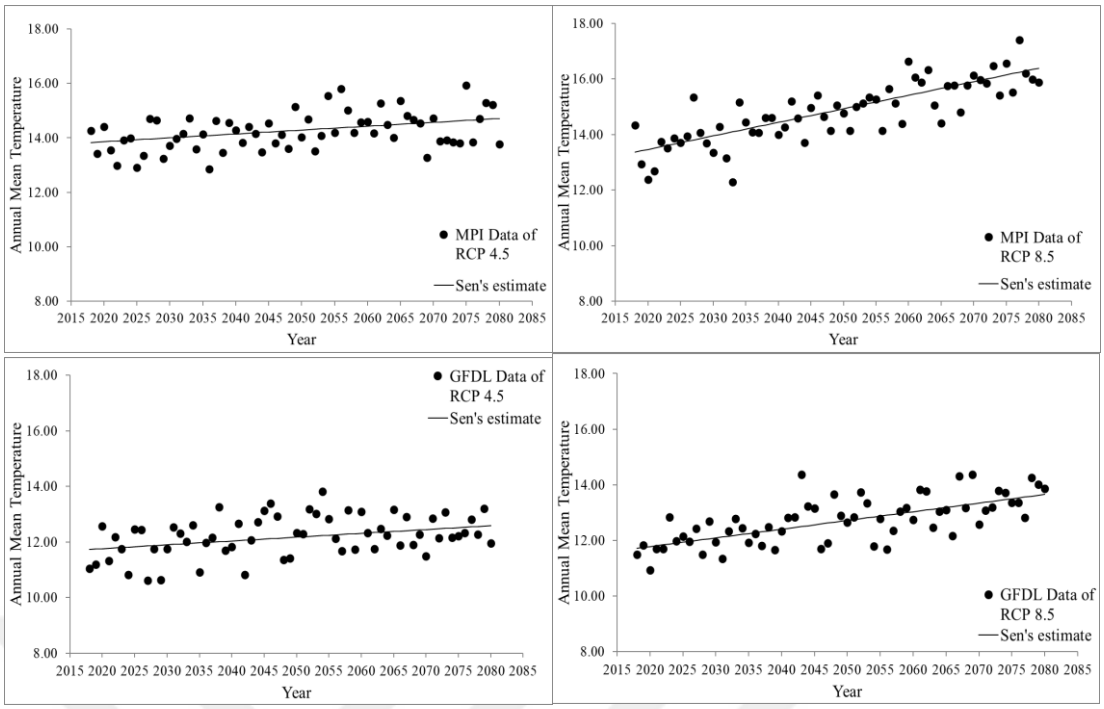

Figure 5.3. Trend results of the annual temperature of Suat Ugurlu HEPP for each GCM.

The trend direction is going up for each scenario of the GCMs for RCP 4.5 and 8.5. In each model, the highest increase in the annual temperature is predicted in the worst scenarios in the RCP 8.5, which is the worst scenario in comparison with RCP 4.5 scenarios. All the trends of GCMs are positive with high positivity in RCP 8.5 scenarios as shown in Table 5.15. As a result of the short geographic distance between Suat Ugurlu HEPP and Hasan Ugurlu HEPP (about 15.6 Km), the trend results are very close to each other. The Z Test results were as following 4.75, 7.19, 2.84, 7.31, 2.64 and 5.85 for HadGEM RCP 4.5, HadGEM RCP 8.5, MPI RCP 4.5, MPI RCP 8.5, GFDL RCP 4.5 and GFDL RCP 8.5, respectively. Also, the table shows the 1% and 5% values of T minimum and maximum.

Table 5.15. Mann-Kendall test of the annual mean temperature of Suat Ugurlu HEPP.

Model	First year	Last Year	n	Test Z	T	T_{min99}	T_{max99}	T_{min95}	T_{max95}
HadGEM RCP 4.5	2018	2080	63	4.75	0.022	0.012	0.034	0.015	0.031
HadGEM RCP 8.5	2018	2080	63	7.19	0.048	0.036	0.059	0.039	0.057
MPI RCP 4.5	2018	2080	63	2.84	0.014	0.001	0.027	0.004	0.025
MPI RCP 8.5	2018	2080	63	7.31	0.049	0.038	0.059	0.040	0.056
GFDL RCP 4.5	2018	2080	63	2.64	0.014	0.001	0.028	0.004	0.025
GFDL RCP 8.5	2018	2080	63	5.85	0.031	0.021	0.043	0.024	0.040

Figure 5.4 shows the trend analysis of the annual mean temperature of Hirfanli HEPP in each scenario (RCP 8.5 and 4.5).

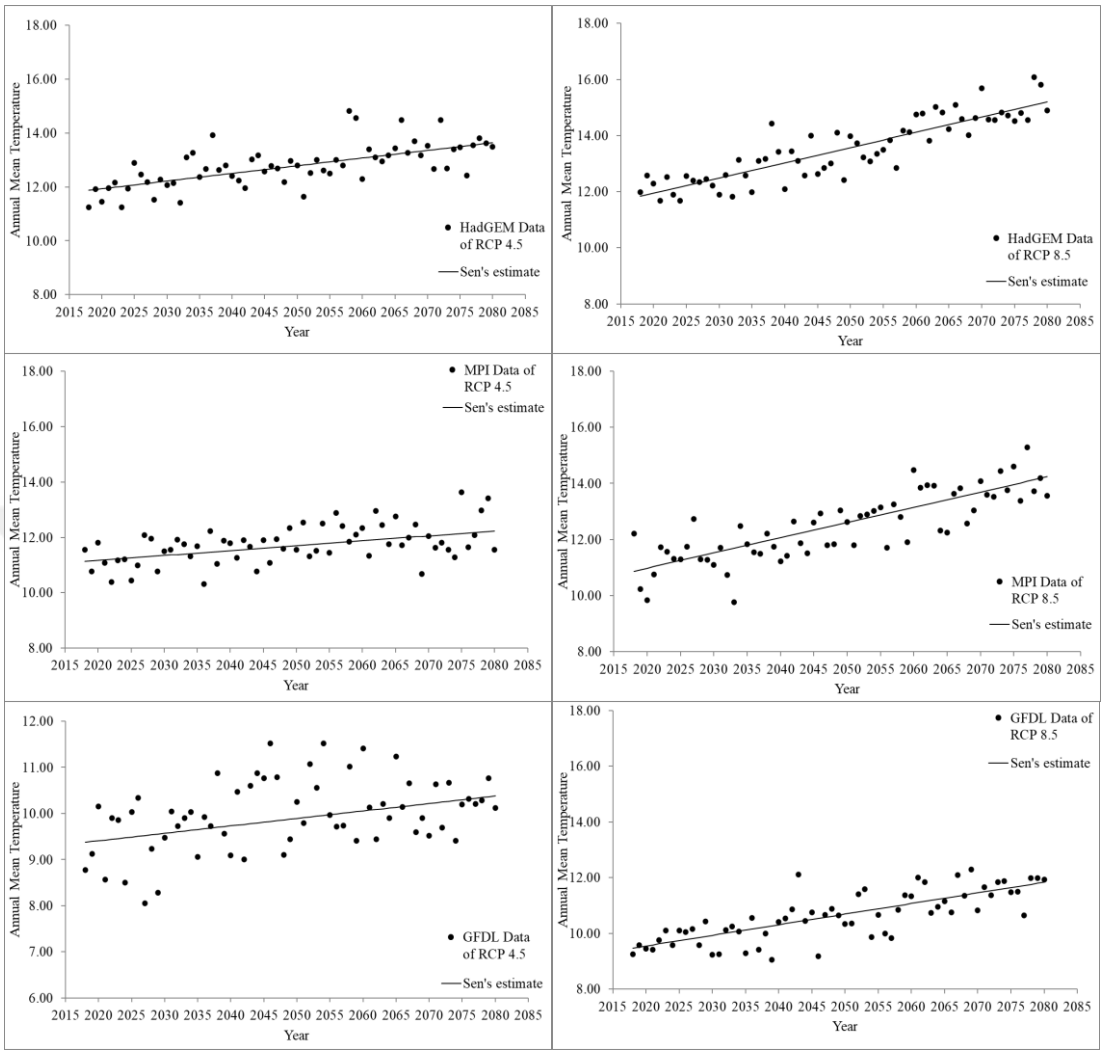

Figure 5.4. Trend results of the annual temperature of Hirfanli HEPP for each GCM.

The trends of RCP 8.5 and RCP 4.5 are positive in all GCMs. In RCP 8.5 the trends are more positive than RCP 4.5 trends for HadGEM and MPI. In each model, the highest increase in the annual temperature is predicted in the worst scenarios in the RCP 8.5, which is the worst scenario in comparison with RCP 4.5 scenarios.

Table 5.16 shows the Z value with positive values of each GCM and for both scenarios. The Z Test results are 6.07, 7.94, 3.78, 7.21, 2.88 and 6.71 for HadGEM RCP 4.5, MPI RCP 4.5, GFDL RCP 4.5, HadGEM RCP 8.5, MPI RCP 8.5and GFDL RCP 8.5, respectively. These values show that the increase of RCP 4.5 in HadGEM is more than the increase of RCP 4.5 in MPI and GFDL models. Also, the table shows the 1% and 5% values of T minimum and maximum.

Table 5.16. Mann-Kendall test of the annual mean temperature of Hirfanli HEPP.

Model	First year	Last Year	n	Test Z	T	T_{min99}	T_{max99}	T_{min95}	T_{max95}
HadGEM RCP 4.5	2018	2080	63	6.07	0.028	0.020	0.037	0.022	0.035
HadGEM RCP 8.5	2018	2080	63	7.94	0.054	0.043	0.066	0.046	0.062
MPI RCP 4.5	2018	2080	63	3.78	0.018	0.005	0.031	0.008	0.028
MPI RCP 8.5	2018	2080	63	7.21	0.054	0.040	0.068	0.043	0.064
GFDL RCP 4.5	2018	2080	63	2.88	0.016	0.002	0.030	0.005	0.026
GFDL RCP 8.5	2018	2080	63	6.71	0.038	0.029	0.048	0.031	0.045

Figure 5.5 shows the trend analysis of the annual mean temperature of Kesikkopru HEPP for RCP 8.5 and RCP 4.5 scenarios

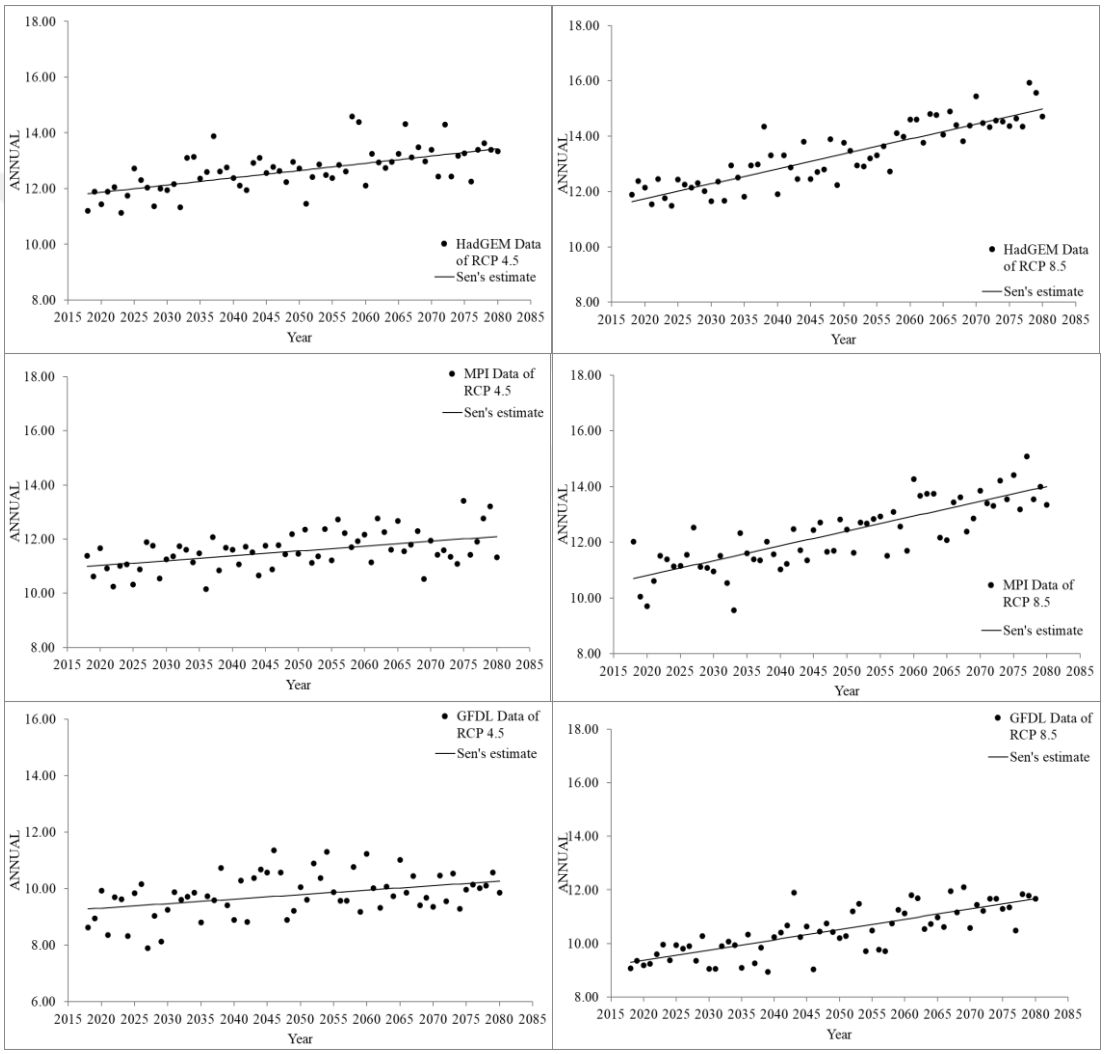

Figure 5.5. Trend results of the annual temperature of Kesikkopru HEPP for each GCM.

The trend direction is going up for each scenario of the GCMs for RCPs 4.5 and 8.5. However, in RCP 8.5, the trends are more positive than those of RCP 4.5. In each model, the highest increase in the annual temperature is predicted in the worst scenarios in the RCP 8.5, which is the worst scenario in comparison with RCP 4.5

scenarios. Table 5.17 shows the Z value with positive values of each GCM and for both scenarios. The Z Test results are 5.77, 7.85, 3.62, 7.24, 2.88, and 6.7 for HadGEM RCP 4.5, MPI RCP 4.5, GFDL RCP 4.5, HadGEM RCP 8.5, MPI RCP 8.5 and GFDL RCP 8.5, respectively. These values show that the increase of RCP 4.5 in HadGEM is more than the increase of RCP 4.5 in MPI and GFDL models.

Table 5.17. Mann-Kendall test of the annual mean temperature of Kesikkopru HEPP.

Model	First year	Last Year	n	Test Z	T	T_{min99}	T_{max99}	T_{min95}	T_{max95}
HadGEM RCP 4.5	2018	2080	63	5.77	0.026	0.017	0.036	0.020	0.033
HadGEM RCP 8.5	2018	2080	63	7.85	0.054	0.043	0.065	0.046	0.062
MPI RCP 4.5	2018	2080	63	3.62	0.018	0.005	0.031	0.008	0.028
MPI RCP 8.5	2018	2080	63	7.24	0.053	0.039	0.067	0.043	0.063
GFDL RCP 4.5	2018	2080	63	2.88	0.016	0.002	0.030	0.006	0.026
GFDL RCP 8.5	2018	2080	63	6.70	0.038	0.030	0.049	0.032	0.046

Figure 5.6 shows the trend analysis of the annual mean temperature of Kapulukaya HEPP for each scenario. The trend direction is going up for each scenario of the GCMs for RCP 8.5 and RCP 4.5. For HadGEM, both trends of RCP 4.5 and RCP 8.5 are positive. In RCP 8.5 the trends are more positive than RCP 4.5 trends. In each model, the highest increase in the annual temperature is predicted in the worst scenarios in the RCP 8.5, which is the worst scenario in comparison with RCP 4.5 scenarios.

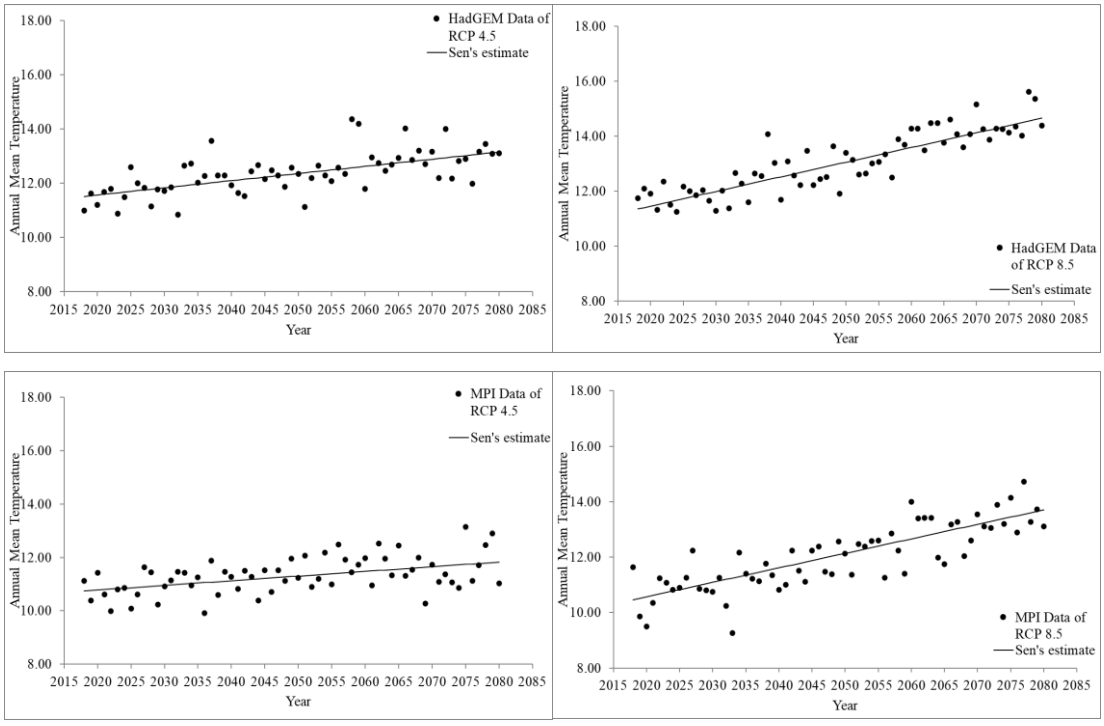

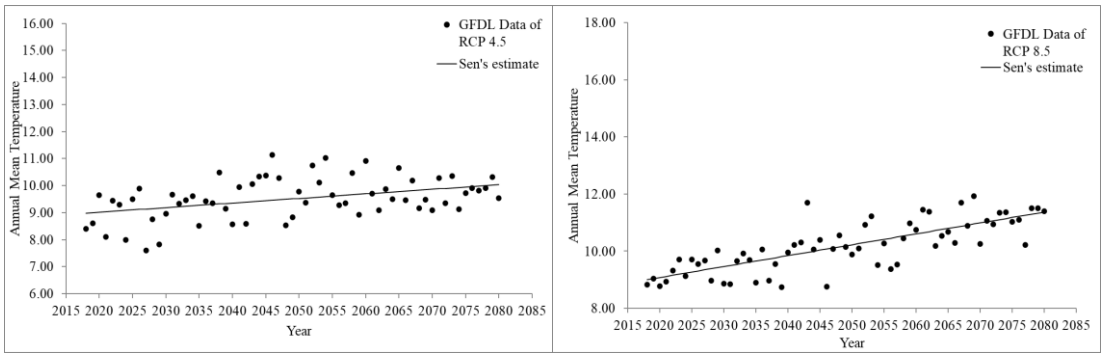

Figure 5.6. Trend results of the annual temperature of Kapulukaya HEPP for each GCM.

Table 5.18 shows the Z value with positive values of each GCM and for both scenarios. The Z Test results are 5.77, 7.82, 3.71, 7.31, 3.09, and 6.82 for HadGEM RCP 4.5, MPI RCP 4.5, GFDL RCP 4.5, HadGEM RCP 8.5, MPI RCP 8.5 and GFDL RCP 8.5, respectively. These values show that the increase of RCP 4.5 in HadGEM is more than the increase of RCP 4.5 in MPI and GFDL models. Also, the table shows the 1% and 5% values of T minimum and maximum.

Table 5.18. Mann-Kendall test of the annual mean temperature of Kapulukaya HEPP.

Model	First year	Last Year	n	Test Z	T	T_{min99}	T_{max99}	T_{min95}	T_{max95}
HadGEM RCP 4.5	2018	2080	63	5.77	0.026	0.018	0.036	0.020	0.033
HadGEM RCP 8.5	2018	2080	63	7.82	0.053	0.042	0.064	0.045	0.061
MPI RCP 4.5	2018	2080	63	3.71	0.017	0.005	0.031	0.008	0.028
MPI RCP 8.5	2018	2080	63	7.31	0.052	0.039	0.066	0.042	0.062
GFDL RCP 4.5	2018	2080	63	3.09	0.017	0.003	0.031	0.006	0.028
GFDL RCP 8.5	2018	2080	63	6.82	0.038	0.028	0.048	0.031	0.045

The results of the trend show increasing in the mean temperature GCMs data of RCP 4.5 and RCP 8.5 with time for Almus HEPP, Suat Ugurlu HEPP, Hasan Ugurlu HEPP, Hirfanli HEPP, Kesikkopru HEPP and Kapulukaya HEPP.

5.2.2. Precipitation Mann-Kendall test

Trend analyses are estimated for the annual precipitation of each GCMs (HadGEM, GFDL and MPI) for RCP 8.5 and RCP 4.5 in this section. The annual data is used for the period from 2018 to 2080 at each model.

Figure 5.7 shows the trend analysis of annual precipitation of Almus HEPP for RCP 8.5 and RCP 4.5 scenarios.

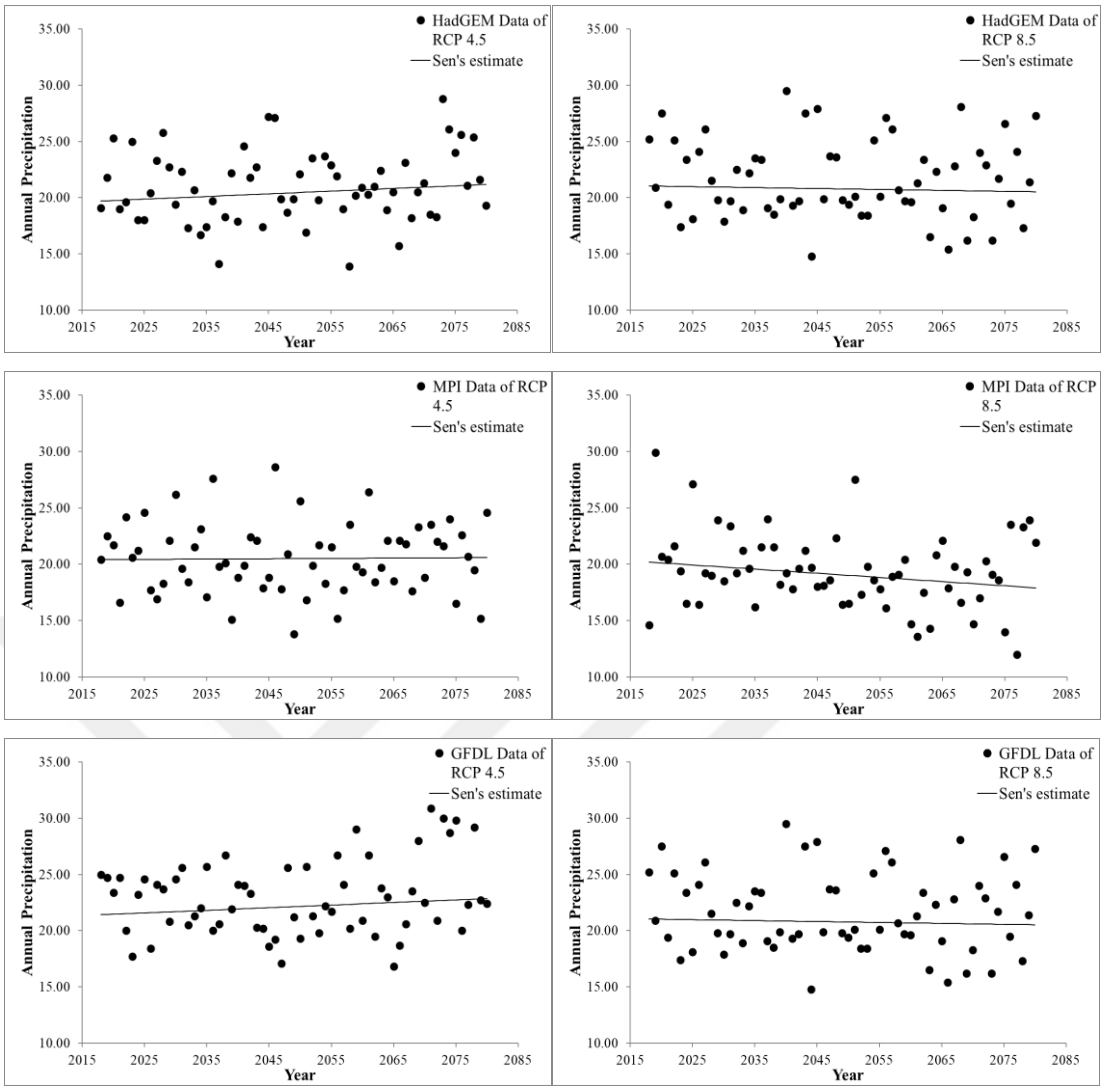

Figure 5.7. Trend results of Annual Precipitation of Almus HEPP for each GCM.

Positive trends are in the RCP 4.5 scenario of the GCMs as shown in Figure 5.7. On the other hand, negative trends are in RCP 8.5 scenarios. MPI model gives the most negative trend (-1.51). HadGEM have the highest positive trend (0.96) in comparison with other RCP 4.5 results.

Table 5.19 shows the Z value with positive values of each GCM and for both scenarios. The Z Test results are 0.96, -0.42, 0.17, -1.51, 0.83 and -1.09 for HadGEM RCP 4.5, MPI RCP 4.5, GFDL RCP 4.5, HadGEM RCP 8.5, MPI RCP 8.5and GFDL RCP 8.5, respectively. These values show that the increase of RCP 4.5 in HadGEM is more than the increase of RCP 4.5 in MPI and GFDL models. On the other hand, the decrease in scenario RCP8.5 in MPI model is more than the decrease of RCP 8.5 in HadGEM and GFDL models. Also, the table shows the 1% and 5% values of P minimum and maximum.

Table 5.19. Mann-Kendall test of the annual precipitation of Almus HEPP.

Model	First year	Last Year	n	Test Z	P	P_{min99}	P_{max99}	P_{min95}	P_{max95}
HadGEM RCP 4.5	2018	2080	63	0.96	0.024	-0.044	0.079	-0.026	0.065
HadGEM RCP 8.5	2018	2080	63	-0.42	-0.008	-0.080	0.057	-0.062	0.040
MPI RCP 4.5	2018	2080	63	0.17	0.003	-0.059	0.061	-0.041	0.048
MPI RCP 8.5	2018	2080	63	-1.51	-0.037	-0.103	0.027	-0.086	0.011
GFDL RCP 4.5	2018	2080	63	0.83	0.023	-0.043	0.092	-0.030	0.076
GFDL RCP 8.5	2018	2080	63	-1.09	-0.030	-0.093	0.032	-0.077	0.017

Figure 5.8 shows the trend analysis of annual precipitation of Hasan Ugurlu HEPP for each scenario.

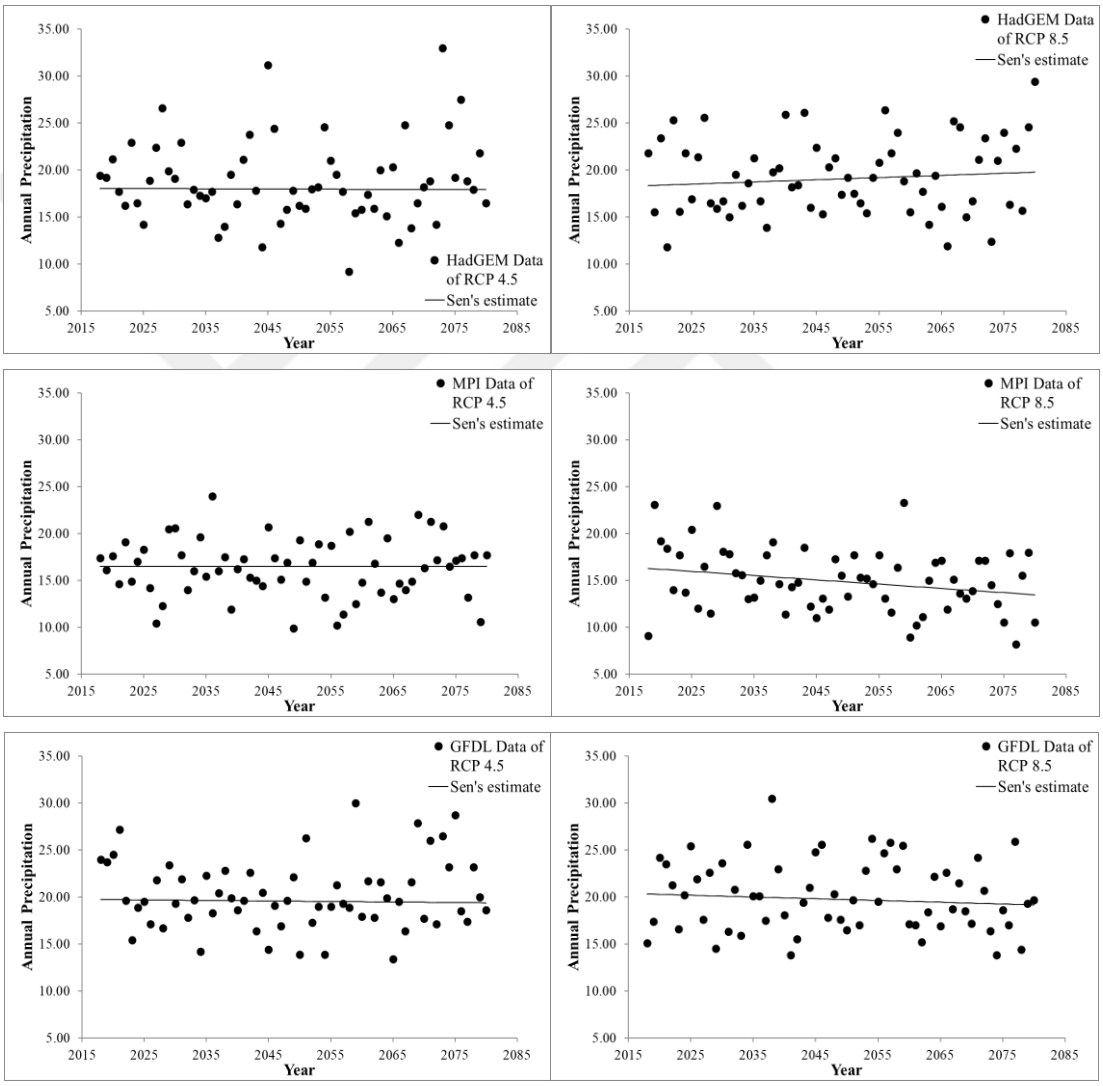

Figure 5.8. Trend results of Annual Precipitation of Hasan Ugurlu HEPP for each GCM.

A positive trend results in HadGEM model for RCP 8.5 scenario only. On the other hand, negative trends are for all other scenarios and models.

Table 5.20. Mann-Kendall test of the annual precipitation of Hasan Ugurlu HEPP.

Model	First year	Last Year	n	Test Z	P	P_{min99}	P_{max99}	P_{min95}	P_{max95}
HadGEM RCP 4.5	2018	2080	63	-0.12	-0.002	-0.077	0.067	-0.060	0.047
HadGEM RCP 8.5	2018	2080	63	0.71	0.023	-0.054	0.108	-0.038	0.090
MPI RCP 4.5	2018	2080	63	-0.04	0.000	-0.061	0.060	-0.044	0.045
MPI RCP 8.5	2018	2080	63	-2.00	-0.045	-0.114	0.016	-0.100	0.000
GFDL RCP 4.5	2018	2080	63	-0.21	-0.006	-0.066	0.070	-0.050	0.052
GFDL RCP 8.5	2018	2080	63	-0.68	-0.019	-0.099	0.050	-0.074	0.034

All GCMs show negative trends of each scenario. However, the trend of RCP 8.5 of HadGEM model showed a positive trend for Hasan Ugurlu HEPP. MPI model gave the most negative trend (-2.00) in comparison with other GCMs. MPI model for RCP 4.5 scenario resulted in a near zero negative trend (-0.04) as shown in Table 5.20. Figure 5.9 shows the trend analysis of the annual precipitation of Suat Ugurlu HEPP for RCP 4.5 and 8.5 scenarios.

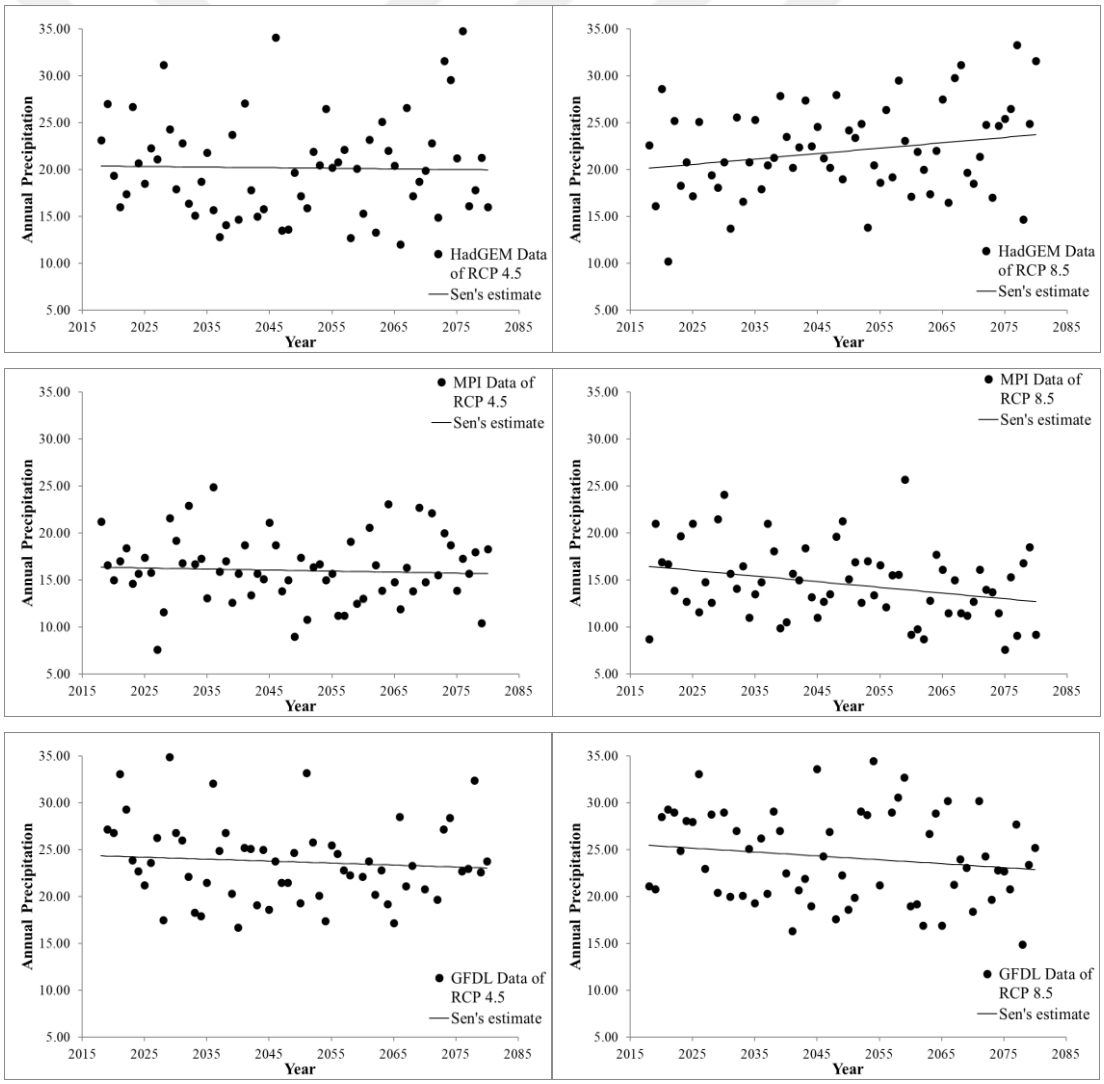

Figure 5.9. Trend results of the annual precipitation of Suat Ugurlu HEPP for each GCM.

A positive trend results in HadGEM model for RCP 4.5 scenario only. On the other hand, negative trends are for all other scenarios and models.

Table 5.21. Mann-Kendall test of the annual Precipitation of Suat Ugurlu HEPP.

Model	First year	Last Year	n	Test Z	P	P_{min99}	P_{max99}	P_{min95}	P_{max95}
HadGEM RCP 4.5	2018	2080	63	-0.12	-0.006	-0.101	0.100	-0.079	0.073
HadGEM RCP 8.5	2018	2080	63	1.45	0.058	-0.040	0.157	-0.020	0.135
MPI RCP 4.5	2018	2080	63	-0.52	-0.011	-0.077	0.056	-0.060	0.040
MPI RCP 8.5	2018	2080	63	-1.98	-0.060	-0.131	0.015	-0.114	0.000
GFDL RCP 4.5	2018	2080	63	-0.54	-0.021	-0.107	0.082	-0.080	0.058
GFDL RCP 8.5	2018	2080	63	-1.13	-0.042	-0.132	0.050	-0.106	0.030

As mentioned in section 5.2.1, as a result of the short geographic distance between Suat Ugurlu HEPP and Hasan Ugurlu HEPP (around 15.6 Km), the trends of the annual precipitation are very close to each other. All the GCMs showed negative trends of each scenario except the trend of RCP 8.5 of HadGEM model. It showed a positive trend (1.45) as shown in Figure 5.9 and Table 5.21. Figure 5.10 shows the trend analysis of the annual precipitation of Hirfanli HEPP for RCP 4.5 and RCP 8.5 scenarios.

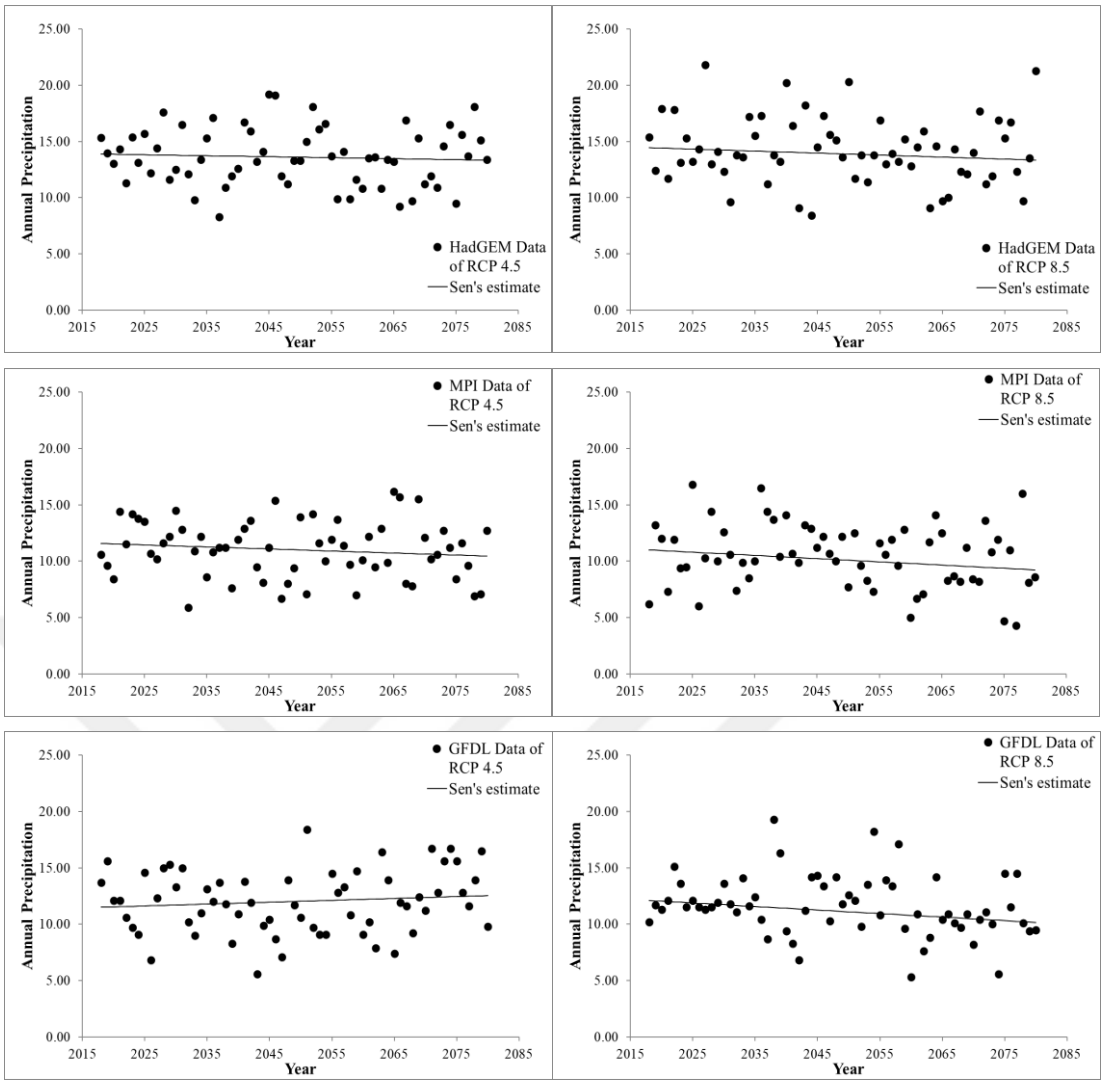

Figure 5.10. Trend results of the annual precipitation of Hirfanli HEPP for each GCM.

Negative trends are in all scenarios and models except GFDL RCP 4.5 which showed a positive trend (0.81). Table 5.22 shows the Z value with positive values of each GCM and for both scenarios.

Table 5.22. Mann-Kendall test of the annual precipitation of Hirfanli HEPP.

Model	First year	Last Year	n	Test Z	P	P_{min99}	P_{max99}	P_{min95}	P_{max95}
HadGEM RCP 4.5	2018	2080	63	-0.48	-0.009	-0.061	0.042	-0.048	0.029
HadGEM RCP 8.5	2018	2080	63	-0.85	-0.018	-0.075	0.037	-0.062	0.023
MPI RCP 4.5	2018	2080	63	-0.97	-0.018	-0.068	0.034	-0.054	0.021
MPI RCP 8.5	2018	2080	63	-1.32	-0.029	-0.082	0.028	-0.070	0.016
GFDL RCP 4.5	2018	2080	63	0.81	0.017	-0.039	0.072	-0.026	0.058
GFDL RCP 8.5	2018	2080	63	-2.11	-0.031	-0.074	0.010	-0.060	0.000

The Z Test results are -0.48, - 0.85, -0.97, -1.32, 0.81 and -2.11, for HadGEM

RCP 4.5, HadGEM RCP 8.5, MPI RCP 4.5, MPI RCP 8.5, GFDL RCP 4.5 and GFDL RCP 8.5, respectively. The trends of all GCMs of Hairfanli HEPP are negative except the trend of RCP 4.5 of GFDL model. The negative trends in RCP 4.5 scenarios are negatively lower than the negative of RCP 8.5 scenario. Also, the table shows the 1% and 5% values of P minimum and maximum. Figure 5.11 shows the trend analysis of the annual precipitation of Kesikkopru HEPP for RCP 8.5 and RCP 4.5 scenarios.

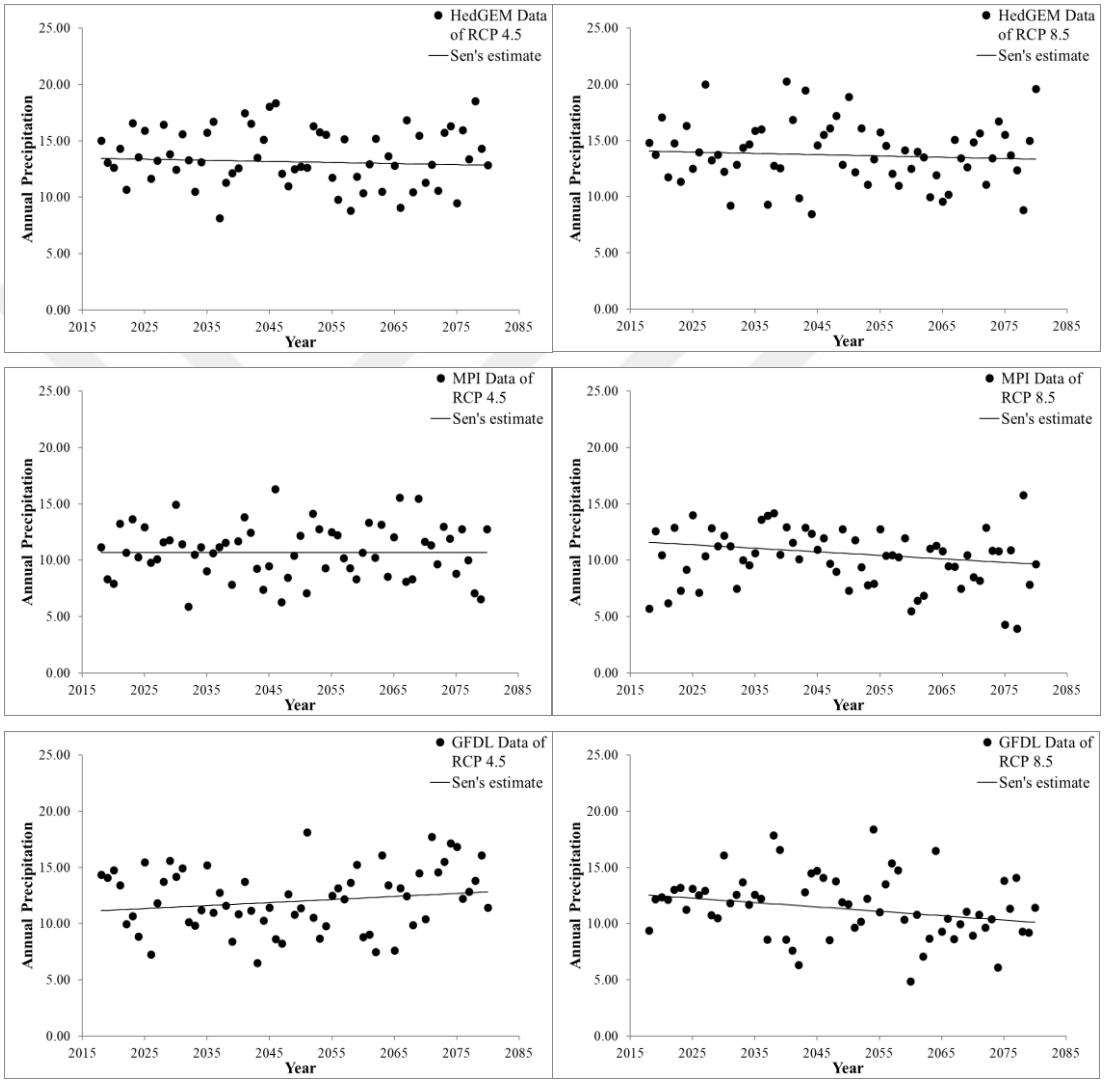

Figure 5.11. Trend results of the annual precipitation of Kesikkopru HEPP for each GCM.

Negative trends are in all scenarios and models except GFDL RCP 4.5 which showed a positive trend (1.10). Table 5.23 shows the Z value with positive values of each GCM and for both scenarios.

Table 5.23. Mann-Kendall test of the annual precipitation of Kesikkopru HEPP.

Model	First year	Last Year	n	Test Z	P	P_{min99}	P_{max99}	P_{min95}	P_{max95}
HadGEM RCP 4.5	2018	2080	63	-0.51	-0.010	-0.060	0.038	-0.049	0.026
HadGEM RCP 8.5	2018	2080	63	-0.65	-0.011	-0.067	0.038	-0.050	0.026
MPI RCP 4.5	2018	2080	63	-0.02	0.000	-0.050	0.046	-0.038	0.034
MPI RCP 8.5	2018	2080	63	-1.47	-0.031	-0.077	0.020	-0.068	0.009
GFDL RCP 4.5	2018	2080	63	1.10	0.027	-0.034	0.081	-0.022	0.067
GFDL RCP 8.5	2018	2080	63	-1.96	-0.039	-0.079	0.015	-0.070	0.000

The Z Test results are -0.51, -0.65, -0.02, -1.47, 1.1 and -1.96, for HadGEM RCP 4.5, MPI RCP 4.5, GFDL RCP 4.5, HadGEM RCP 8.5, MPI RCP 8.5 and GFDL RCP 8.5, respectively. As a result of the short distance between Hirfanli HEPP and Kesikkopru HEPP (around 16 Km), the trend results are close to each other. A positive trend (1.10) resulted in the trend of RCP 4.5 of GFDL model. On the other hand, all the GCMs trends resulted with negative trends. Also, the table shows the 1% and 5% values of P minimum and maximum.

Figure 5.12 shows the trend analysis of the annual precipitation of Kapulukaya HEPP for RCP 8.5 and RCP 4.5 scenarios.

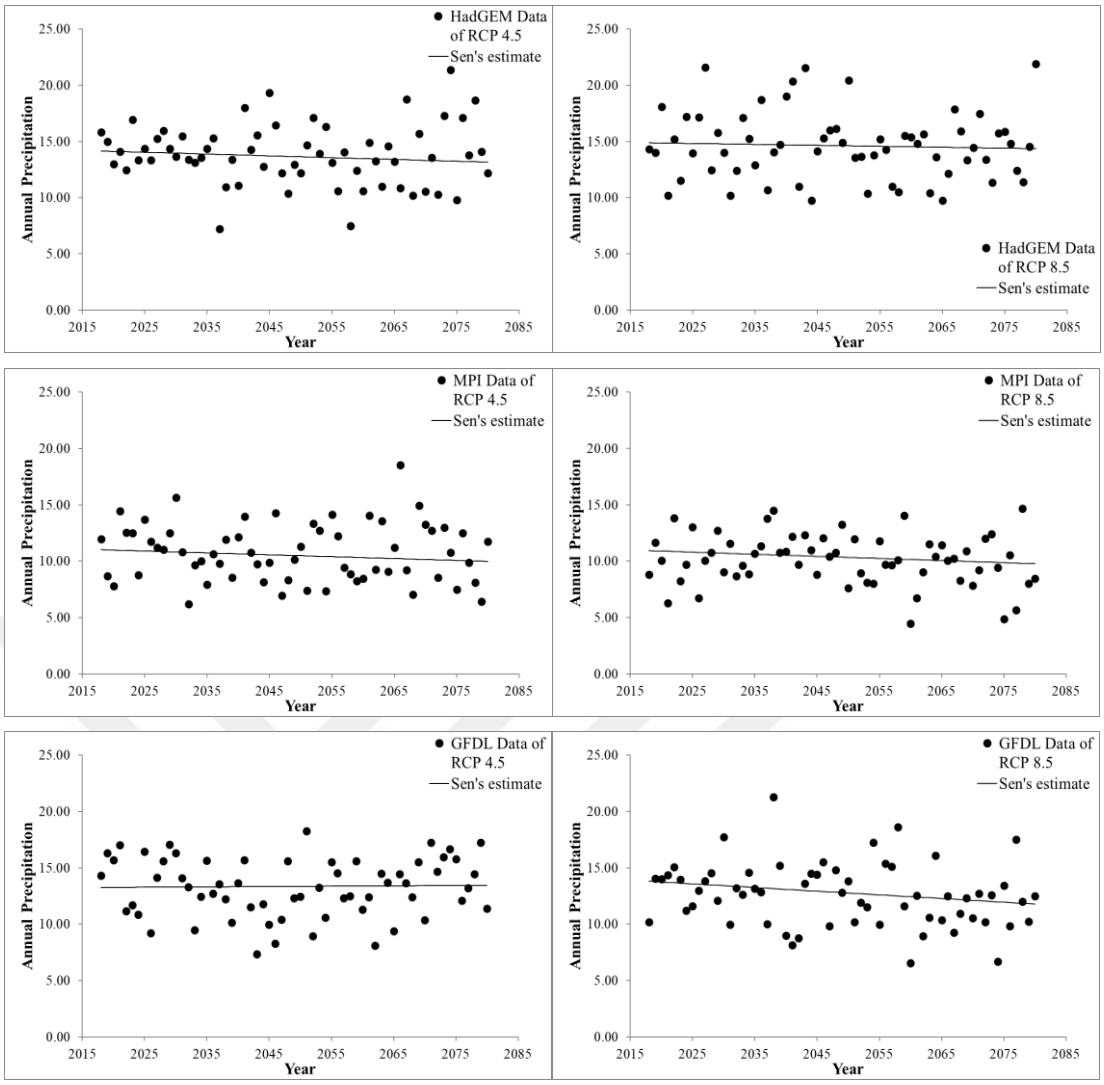

Figure 5.12. Trend results of the annual precipitation of Kapulukaya HEPP for each GCM.

Negative trends are for all scenarios and models except GFDL RCP 4.5 which showed a positive trend (0.15). Table 5.24 shows the Z value with positive values of each GCM and for both scenarios.

Table 5.24. Mann-Kendall test of the annual precipitation of Kapulukaya HEPP.

Model	First year	Last Year	n	Test Z	P	P_{min99}	P_{max99}	P_{min95}	P_{max95}
HadGEM RCP 4.5	2018	2080	63	-0.88	-0.016	-0.066	0.034	-0.054	0.021
HadGEM RCP 8.5	2018	2080	63	-0.34	-0.008	-0.064	0.044	-0.050	0.032
MPI RCP 4.5	2018	2080	63	-0.78	-0.017	-0.064	0.037	-0.055	0.023
MPI RCP 8.5	2018	2080	63	-1.03	-0.019	-0.061	0.026	-0.050	0.015
GFDL RCP 4.5	2018	2080	63	0.15	0.003	-0.047	0.058	-0.037	0.042
GFDL RCP 8.5	2018	2080	63	-1.80	-0.033	-0.080	0.017	-0.068	0.006

The Z Test results are -0.88, -0.34, -0.78, -1.03, 0.15 and -1.8 for HadGEM RCP 4.5, HadGEM RCP 8.5, MPI RCP 4.5, GFDL RCP 4.5, MPI RCP 8.5 and GFDL RCP 8.5, respectively. All the GCMs of Kapulukaya HEPP show negative trends except the

trend of RCP 4.5 of GFDL model like Hirfanli HEPP and Kesikkopru HEPP which resulted in a positive trend (0.15). According to the relationship between precipitation and temperature, when the mean temperature increases the amount of precipitation decreases with time. The results for the HEPs of the two basins are very logical because of climate change. Also, the table shows the 1% and 5% values of P minimum and maximum.

The results show various trends using the downscaled GCMs data of precipitaion for Almus HEPP, Suat Ugurlu HEPP, Hasan Ugurlu HEPP, Hirfanli HEPP, Kesikkopru HEPP and Kapulukaya HEPP. The results RCP 4.5 scenario have positively more than the results of RCP 8.5 scenario. The exception case is in HadGEM of RCP 8.5 in Hasan Ugurlu HEPP. It's increase slowly with time for the interval between 2018 to 2080.

5.3. Using Machine Learning Technique for Prediction

In this section, the main aim is to predict the hydroelectric power generation (the energy production) of GCMs using deep learning and machine learning algorithms in the main Hydroelectric Power Plants of Yesilirmak and Kizilirmak Basins (Almus HEPP, Suat Ugurlu HEPP, Hasan Uğurlu HEPP, Hirfanlı HEPP, Kesikköprü HEPP and Kapulukaya HEPP). This step will support reaching the purpose of this study to analyze the effect and impact of climate change on the HEPPs. The prediction period is between 2018 to 2080. The predicted period is divided into two-time intervals. The first is from 2018 to 2050 and the second is from 2051 to 2080. These deep learning and machine learning algorithms are Generalized Linear (GL), Random Forest (RF), Deep Learning (DL), Gradient boosted trees (GBT) and Decision Tree (DT). This historical data-based predicting analyses the future situations of energy production and the effectiveness of using Machine Learning (ML) models to understand the behavior of the system.

In this section, GBT, DL, RF, GL and DT are utilized to predict the hydropower production of the HEPPs. seven hundred and fifty-six monthly data (Precipitation, temperature and energy production) were used in each HEPP as the data range from these HEPPs to running these models. The temperature and precipitation data of the GCMs (GFDL, MPI and HadGEM) are used to predict the electricity production of the HEPPs for scenarios RCP 8.5 and RCP 4.5. The prediction is estimated using only one ML model after checking the most accurate model among them (DL, GBT, RF, GL

and DT). The checking process was applied based on the relative error and the correlation values. The criterion is to select a model for the predict process which has the highest correlation and the lowest relative error values.

5.3.1. Almus HEPP

Before any prediction process, the relative error (RE) and the correlation (R) values are calculated to decide which machine learning technique will be more accurate in energy production predicting. Figure 5.13 shows RE values between the applied models (DT, DL, GL, GBT and RF) for the historical data of Almus HEPP and the precipitation and temperature data of the GCMs. Figure 5.14 shows the correlation (R) values of the applied models for the same data for the Almus HEPP.

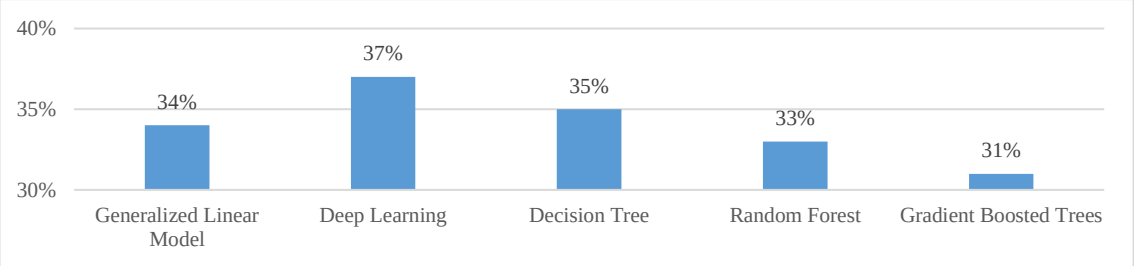

Figure 5.13. The Relative Error values between the applied models for the historical data of Almus HEPP.

Figure 5.14. The correlation values of the applied models for the historical data of Almus HEPP.

Figure 5.13 facilitates the selection process of the most accurate model between all machine learning models. The performance check process shows that the gradient boosted trees model (GBT) has the lowest relative error value in comparison with other models. In Figure 5.14, the results show the correlation values of 0.447, 0.401, 0.543, 0.483 and 0.717 for GL, DL, DT, RF and GBT models, respectively. GBT's correlation value is the highest value which means that the GBT model is the most suitable model for the data. The previous steps mean that GBT model is the most accurate and suitable model to apply predicting the energy production with the historical data of energy

production and GCMs data. Figures 5.15, 5.16, 5.17, 5.18, 5.19 and 5.20 show the predict of energy production during the time series of the selected model.

5.3.1.1. Energy prediction for 2018 to 2050 Interval

After testing the performance of the models, the most accurate model is selected to be used in the prediction process. The energy productions are predicted for the GCMs for each scenario of Almus HEPP using the GBT model. Figure 5.15 shows the predicted energy production using the GBT model during the 2018 to 2050 interval based on the GFDL model's data for both scenarios RCP 8.5 and RCP 4.5.

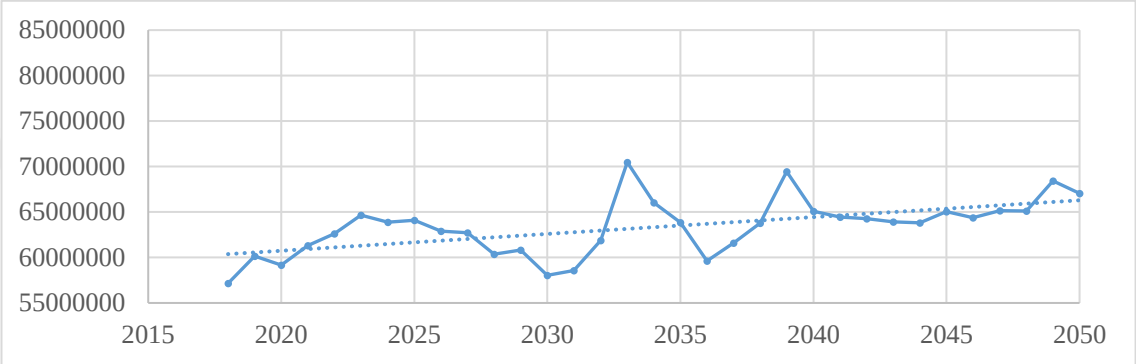

(a) GFDL 4.5

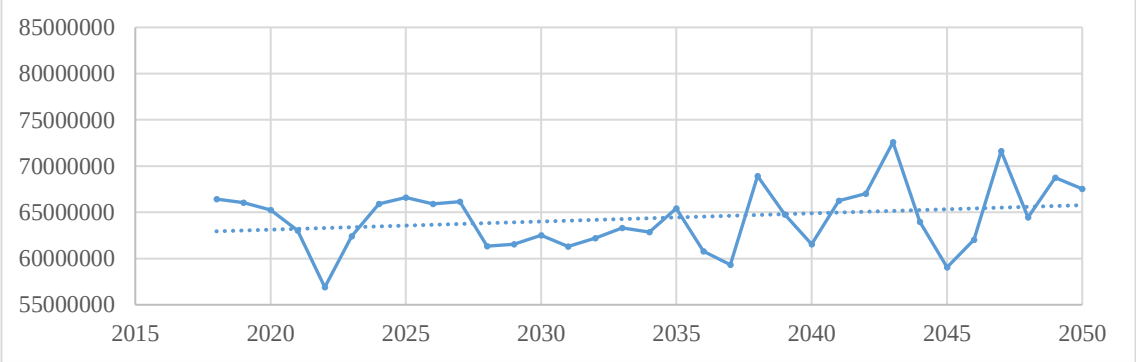

(b) GFDL 8.5

Figure 5.15. The prediction of annual electricity production (Kwh) for the 2018 – 2050 interval using (a): GFDL 4.5 and (b): GFDL 8.5 data.

As shown in Figure 5.15, the range of annual energy productions (AEPs) are between 56,000,000 Kwh and 73,000,000 Kwh. The lowest production values are in the years of 2018 and 2022 for GFDL 4.5 and GFDL 8.5 scenarios with values near 57,000,000 Kwh, respectively. On the other hand, the highest production values are in 2033 and 2043 for GFDL 4.5 and GFDL 8.5 scenarios, respectively.

Figure 5.16 shows the energy production predict during the same interval for HadGEM model for scenarios RCP 4.5 and RCP 8.5.

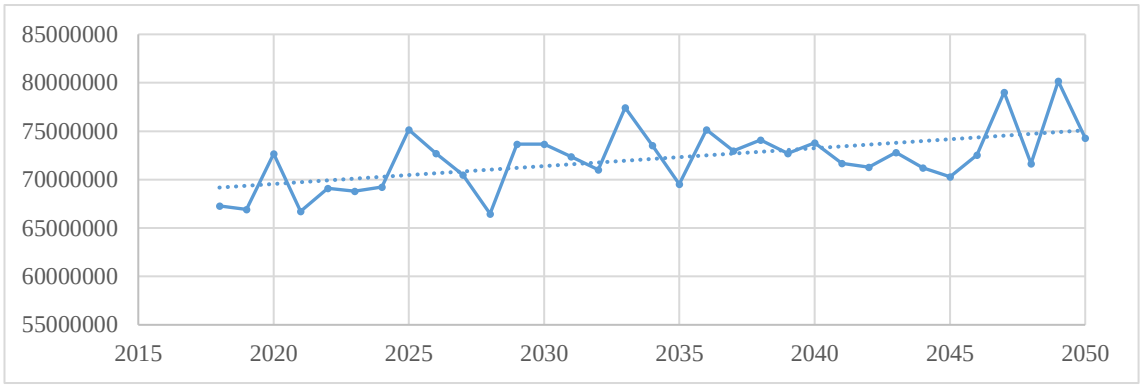

(a) HadGEM 4.5

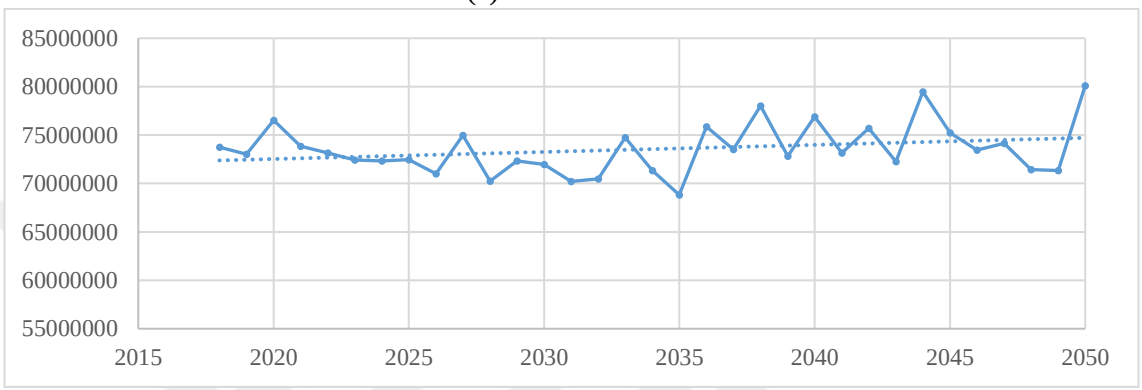

(b) HadGEM 8.5

Figure 5.16. The prediction of annual electricity production (Kwh) for the 2018 – 2050 interval using (a): HadGEM 4.5 and (b): HadGEM 8.5 data.

In Figure 5.16, the AEPs range between 65,000,000 Kwh and 80,000,000 Kwh. The highest production values were recorded in 2049 and 2050 for HadGEM 4.5 and HadGEM 8.5 scenarios, respectively. On the other hand, the lowest production values resulted in 2028 and 2035 for HadGEM 4.5 and HadGEM 8.5 scenarios with values near 66,000,000 and 69,000,000 Kwh, respectively.

Figure 5.17 shows the predicted energy production during the same interval for MPI model for scenarios RCP 8.5 and RCP 4.5.

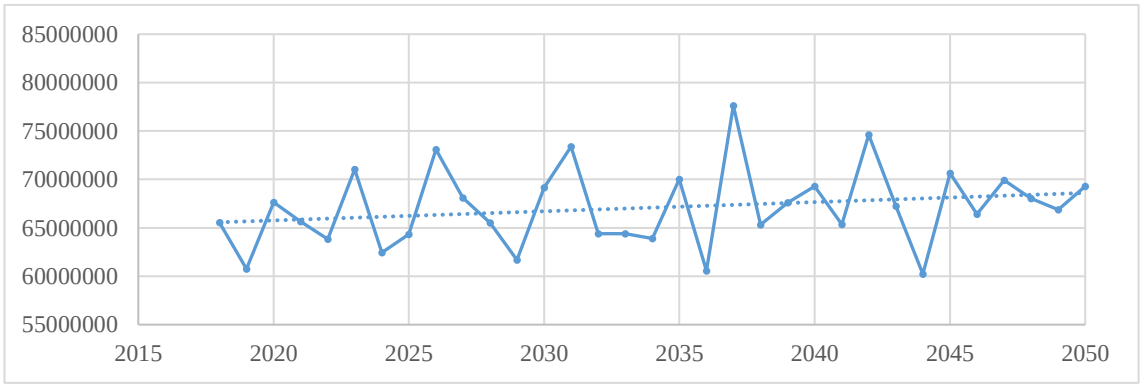

(a) MPI 4.5

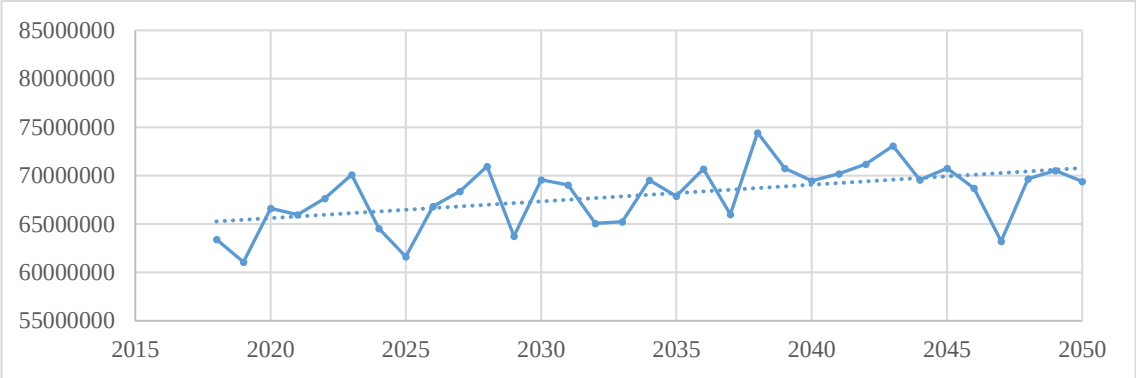

(b) MPI 8.5

Figure 5.17. The prediction of annual electricity production (Kwh) for the 2018 – 2050 interval using (a): MPI 4.5 and (b): MPI 8.5 data.

In Figure 5.17, the AEPs range between 60,000,000 Kwh and 78,000,000 Kwh. The lowest production values resulted in 2044 and 2019 for MPI 4.5 and MPI 8.5 scenarios with values near 60,000,000 Kwh, respectively. On the other hand, the highest production values resulted in 2037 and 2038 years for MPI 4.5 and MPI 8.5 scenarios, respectively.

The prediction of the energy production using GFDL model with 8.5 and 4.5 scenarios are shown in Figure 5.15. The results show a little difference between the two scenarios. This difference in the results of energy production range resulted in all RCP 8.5 scenarios, especially in GFDL 8.5 results.

5.3.1.2. Energy prediction for 2051 to 2080 Interval

Figures 5.18, 5.19 and 5.20 show the prediction of the AEP using the GBT model for three types of GCM in each scenario (RCP 4.5 and RCP 8.5) between 2051 and 2080.

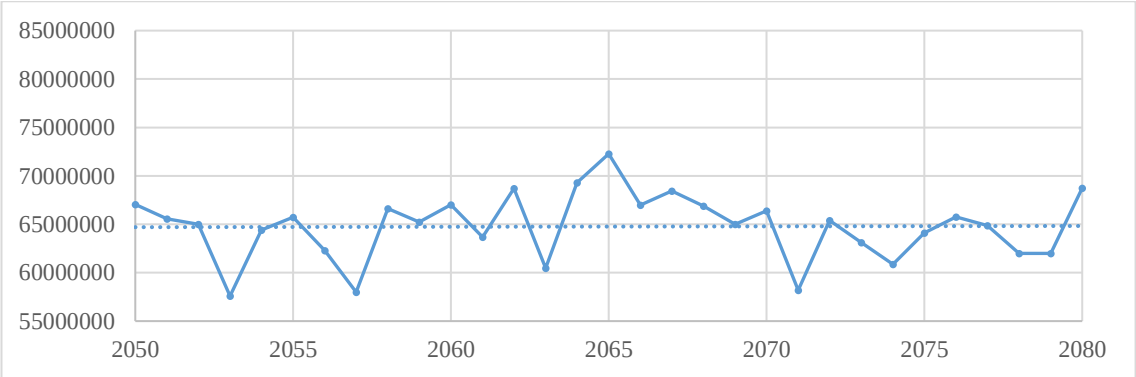

(a) GFDL 4.5

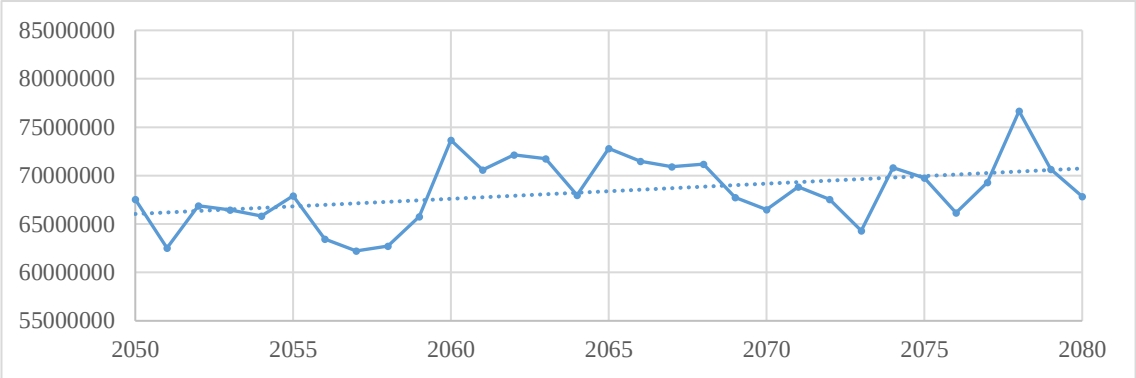

(b) GFDL 8.5

Figure 5.18. The prediction of annual electricity production (Kwh) for the 2051 – 2080 interval using (a): GFDL 4.5 and (b): GFDL 8.5 data.

In Figure 5.18, the AEPs range between 57,000,000 Kwh and 77,000,000 Kwh. The highest production values resulted in the years of 2065 and 2078for GFDL 4.5 and GFDL 8.5 scenarios with values near 72,200,000 and 76,600,000 Kwh, respectively. On the other hand, the lowest production values resulted in 2053 and 2057 for GFDL 4.5 and GFDL 8.5 scenarios, respectively.

Figure 5.19 shows the predicted energy production during the same interval for HadGEM model for scenarios RCP 8.5 and RCP 4.5.

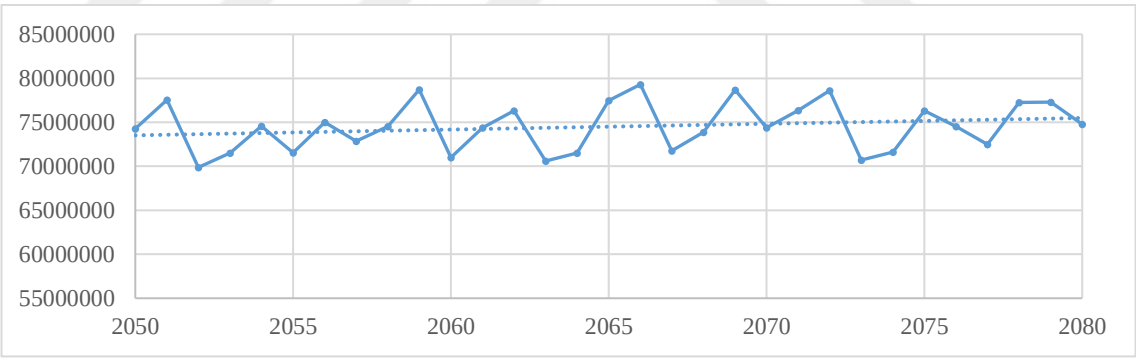

(a) HadGEM 4.5

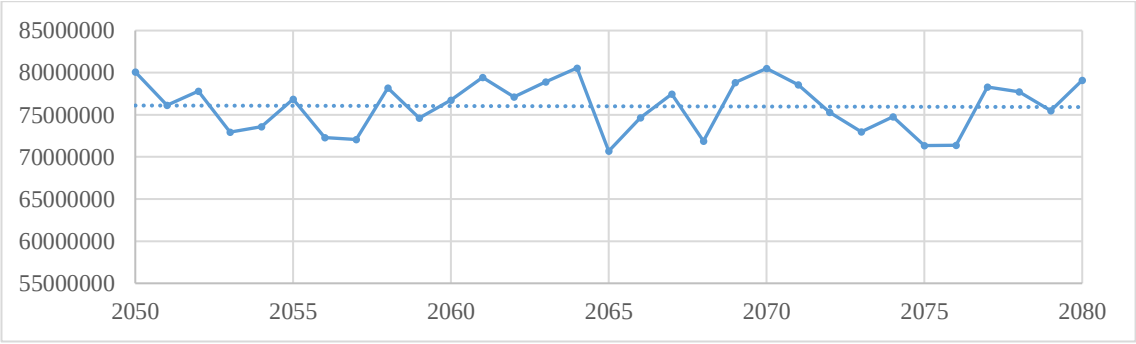

(b) HadGEM 8.5

Figure 5.19. The prediction of annual electricity production (Kwh) for the 2051 – 2080 interval using (a): HadGEM 4.5 and (b): HadGEM 8.5 data.

The prediction of the AEP using HadGEM model with 4.5 and 8.5 scenarios is shown in Figure 5.19. The AEPs range between 70,000,000 Kwh and 80,500,000 Kwh. The lowest production values resulted in the years of 2052 and 2065 for HadGEM 4.5 and HadGEM 8.5 scenarios with values near 70,700,000 for both scenarios. On the other hand, the highest production values resulted in many years for both scenarios with value near 80,000,000 Kwh. Figure 5.20 shows the predicted energy production during the same interval for MPI model for senarios RCP 4.5 and RCP 8.5.

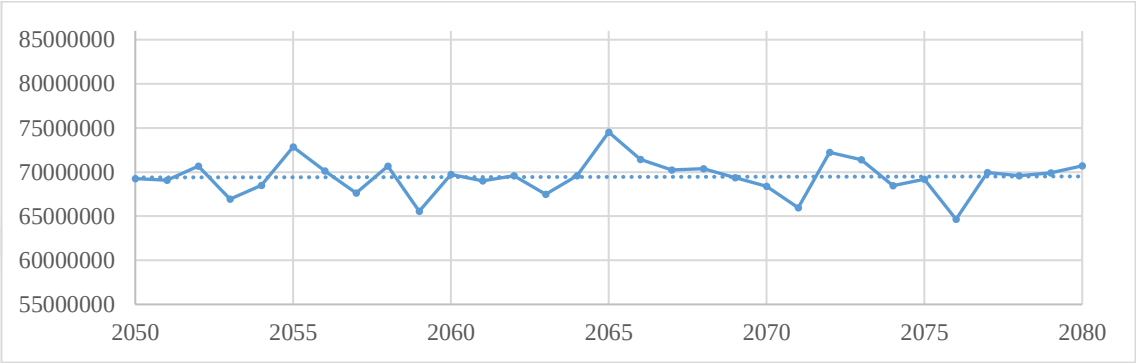

(a) MPI 4.5

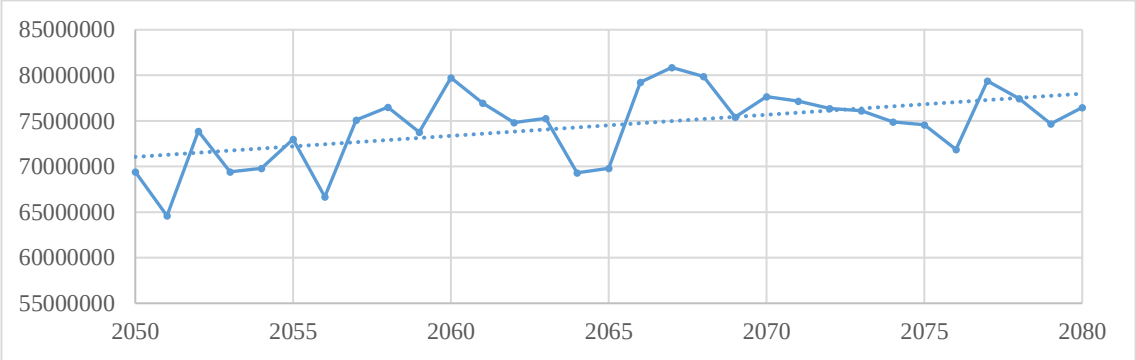

(b) MPI 8.5

Figure 5.20. The prediction of annual electricity production (Kwh) for the 2051 – 2080 interval using (a): MPI 4.5 and (b): MPI 8.5 data.

The prediction of the AEP using MPI model with 4.5 and 8.5 scenarios is shown in Figure 5.20. The AEPs range between 64,500,000 Kwh and 80,000,000 Kwh. The highest production values resulted in the years of 2065 and 2067 for MPI 4.5 and MPI 8.5 scenarios with values near 80,000,000 Kwh for both scenarios. On the other hand, the lowest production values resulted in the years of 2051 and 2076 for MPI 4.5 and MPI 8.5 scenarios, respectively.

5.3.2. Hasan Ugurlu HEPP

Figure 5.21 shows the relative error values among the applied models for the historical data of Hasan Ugurlu HEPP. Figure 5.22 shows R values of the applied

models for the historical data of Hasan Ugurlu HEPP.

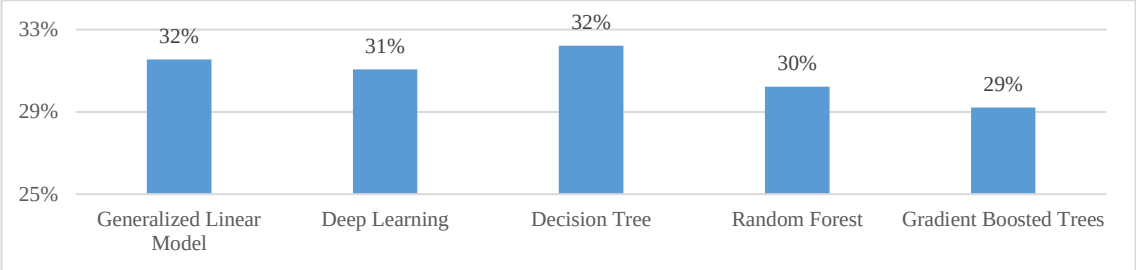

Figure 5.21. The Relative Error values among the applied models for the historical data of Hasan Ugurlu HEPP.

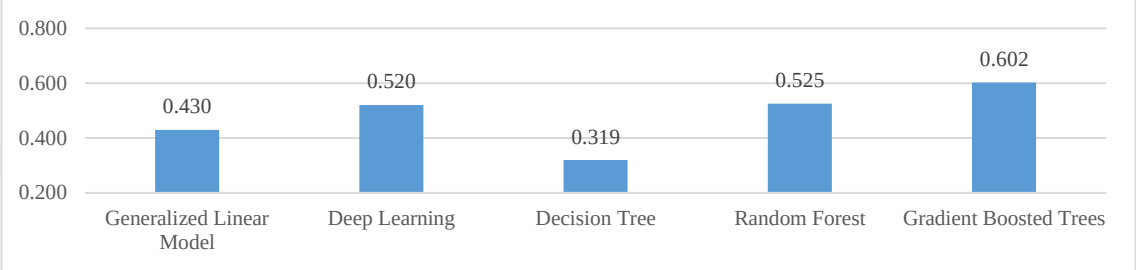

Figure 5.22. The correlation values of the applied models for the historical data of Hasan Ugurlu HEPP.

Figure 5.21 facilitate the process of selecting the most accurate model between all ML models. The GBT model is the most accurate model to apply predicting the energy production with GCMs data.

In Figure 5.22, the results show R values are 0.43, 0.52, 0.319, 0.525 and 0.602 for GL, DL, DT, RF and GBT models, respectively. GBT's correlation value is the highest value which means that the GBT model is the most suitable model for the data. As a result of R value of GBT model, the model is used in the prediction process for each GCM. Figures 5.23, 5.24, 5.25, 5.26, 5.27 and 5.28 show the prediction of energy production during the time series of the selected model.

5.3.2.1. Energy prediction for 2018 to 2050 Interval

Figure 5.23 shows the annual prediction energy production using the GBT model during the interval between 2018 to 2050 based on the GFDL model's data for both scenarios RCP 8.5 and RCP 4.5.

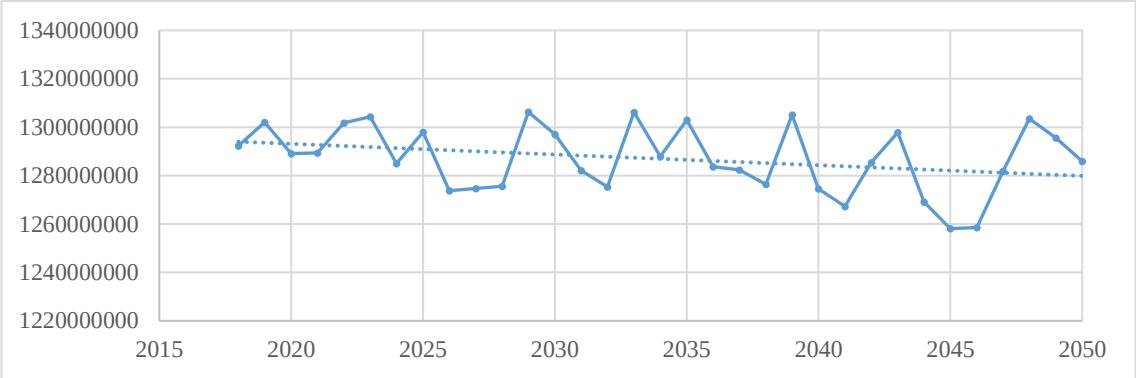

(a) GFDL 4.5

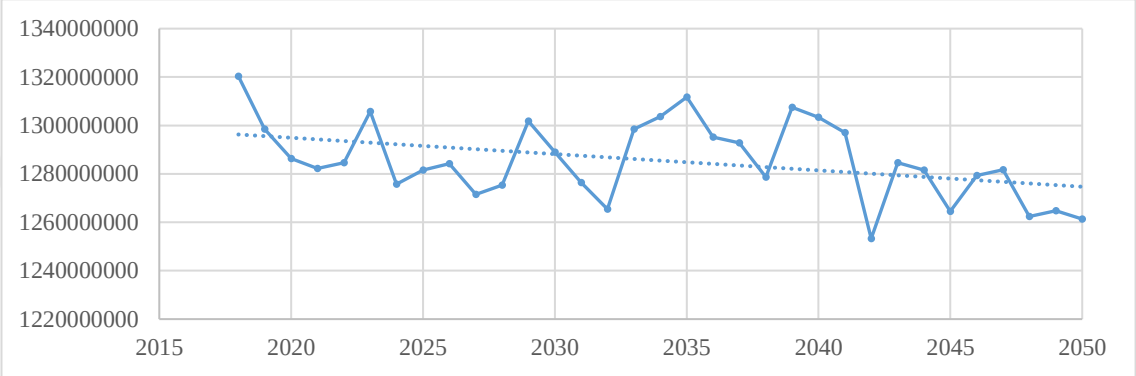

(b) GFDL 8.5

Figure 5.23. The prediction of annual electricity production (Kwh) for the 2018 – 2050 interval using (a): GFDL 4.5 and (b): GFDL 8.5 data.

In Figure 5.23, the AEPs range between 1250,000,000 Kwh and 1320,000,000 Kwh. The highest production values resulted in the years of 2029 and 2018 for GFDL 4.5 and GFDL 8.5 scenarios with values near 1300,000,000 and 1320,000,000 Kwh, respectively. On the other hand, the lowest production values resulted in the years of 2045 and 2042 for GFDL 4.5 and GFDL 8.5 scenarios, respectively.

Figure 5.24 shows the annual prediction energy production during the same interval for HadGEM model for scenarios RCP 8.5 and RCP 4.5.

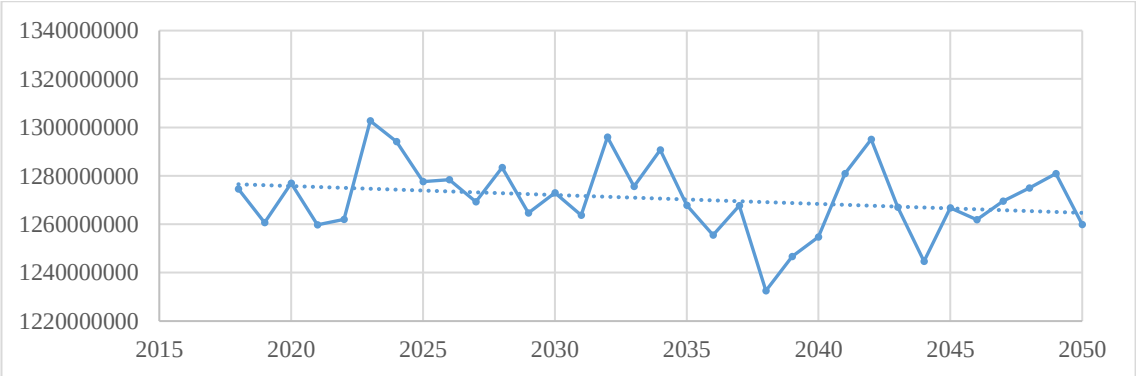

(a) HadGEM 4.5

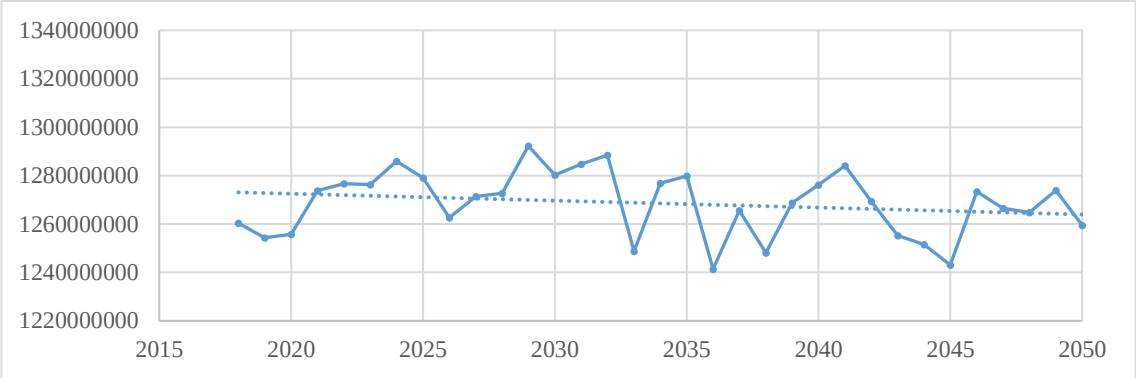

(b) HadGEM 8.5

Figure 5.24. The prediction of annual electricity production (Kwh) for the 2018 – 2050 interval using (a): HadGEM 4.5 and (b): HadGEM 8.5 data.

The prediction of the AEP using HadGEM model with 4.5 and 8.5 scenarios are shown in Figure 5.24. The AEPs range between 1230,000,000 Kwh and 1300,000,000 Kwh. The lowest production values resulted in the years of 2038 and 2036 for HadGEM 4.5 and HadGEM 8.5 scenarios, respectively.

Figure 5.25 shows the predicted energy production during the same interval for MPI model for scenarios RCP 8.5 and RCP 4.5.

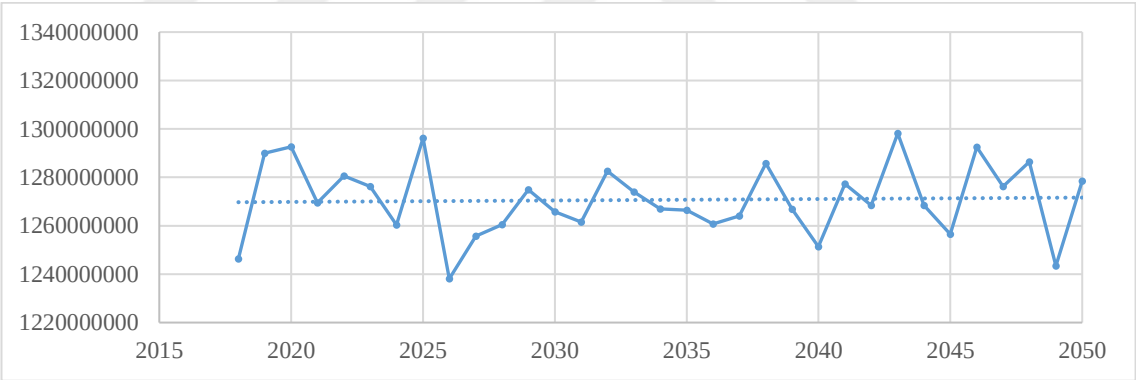

(a) MPI 4.5

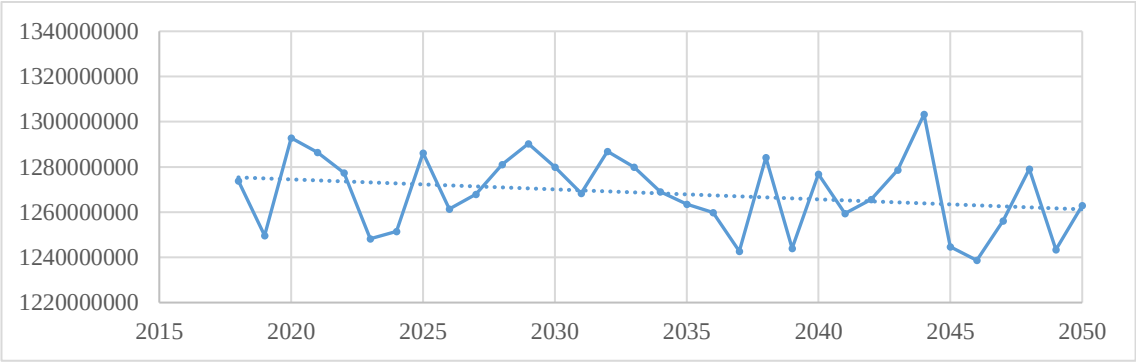

(b) MPI 8.5

Figure 5.25. The prediction of annual electricity production (Kwh) for the 2018 – 2050 interval using (a): MPI 4.5 and (b): MPI 8.5 data.

In scenario MPI 8.5, the energy production decreases with time. On the other hand, the energy production increases with time on MPI 4.5 scenario.

5.3.2.2. Energy prediction for 2051 to 2080 Interval

This section will focus on the AEP for the interval from 2018 to 2050. Figure 5.26 shows the predicted energy production using GBT based on the GFDL model's data for both senarios RCP 4.5 and 8.5.

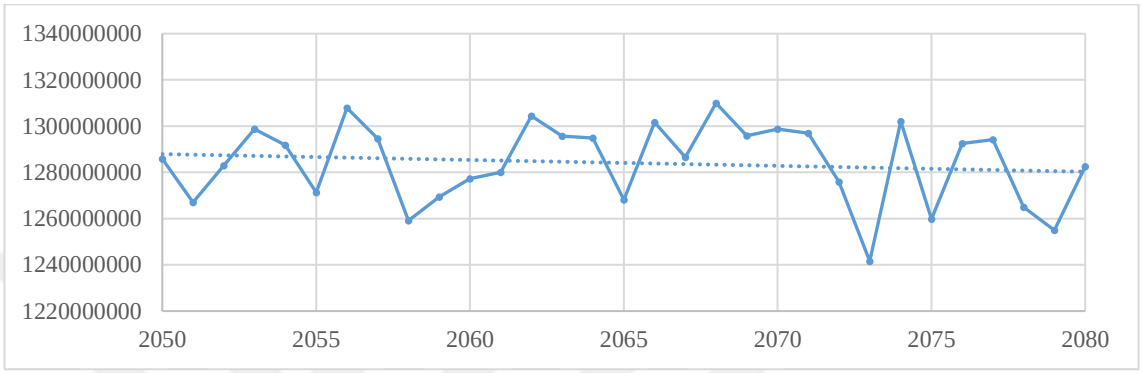

(a) GFDL 4.5

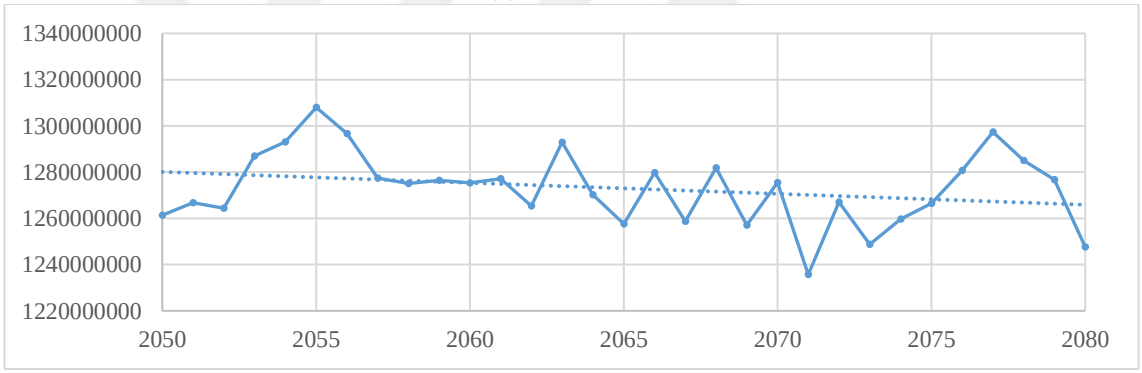

(b) GFDL 8.5

Figure 5.26. The prediction of annual electricity production (Kwh) for the 2051 – 2080 interval using (a): GFDL 4.5 and (b): GFDL 8.5 data.

In Figure 5.26, the AEPs range between 1230,000,000 Kwh and 1310,000,000 Kwh. The highest production values resulted in the years of 2068 and 2055 for GFDL 4.5 and GFDL 8.5 scenarios, respectively. On the other hand, the lowest production values resulted in the years of 2073 and 2071 for GFDL 4.5 and GFDL 8.5 scenarios, respectively.

Figure 5.27 shows the annual predicted energy production during the same interval for HadGEM model.

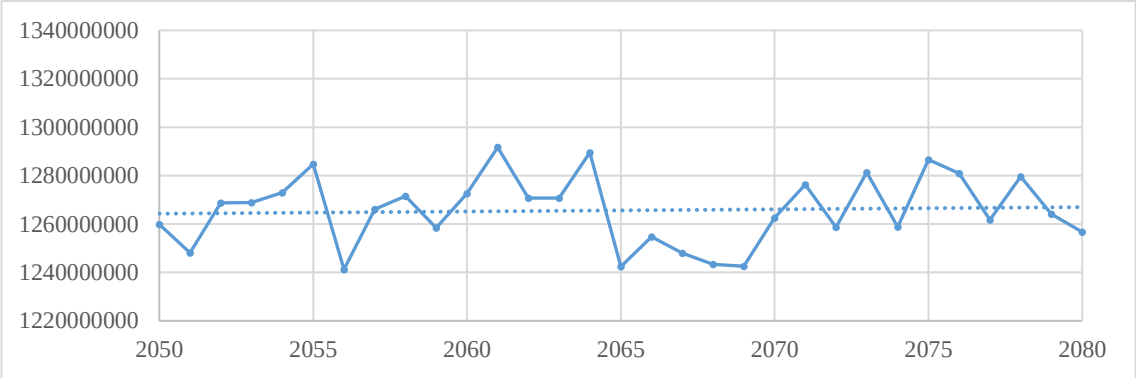

(a) HadGEM 4.5

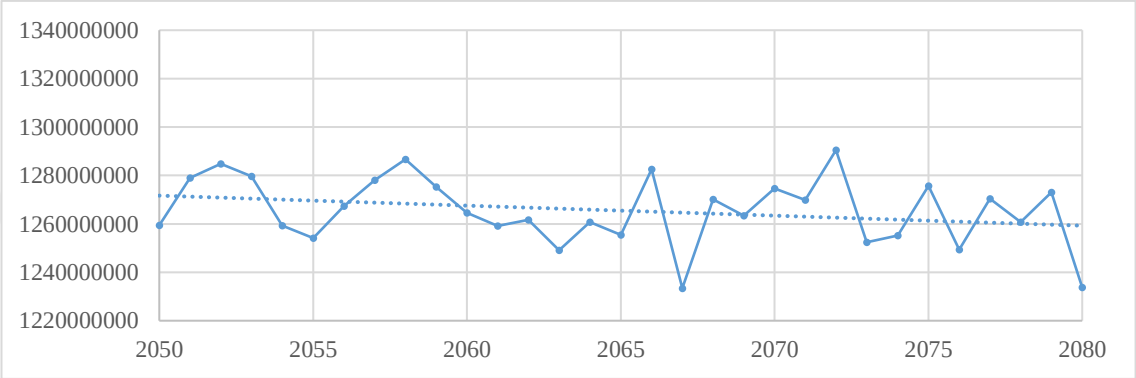

(b) HadGEM 8.5

Figure 5.27. The prediction of annual electricity production (Kwh) for the 2051 – 2080 interval using (a): HadGEM 4.5 and (b): HadGEM 8.5 data.

The prediction of the AEP using HadGEM model with 4.5 and 8.5 scenarios is shown in Figure 5.27. The AEPs range between 1230,000,000 Kwh and 1300,000,000 Kwh. The lowest production values resulted in the years of 2056 and 2067 for HadGEM 4.5 and HadGEM 8.5 scenarios, respectively.

Figure 5.28 shows the annual predicted energy production during the same interval for MPI model.

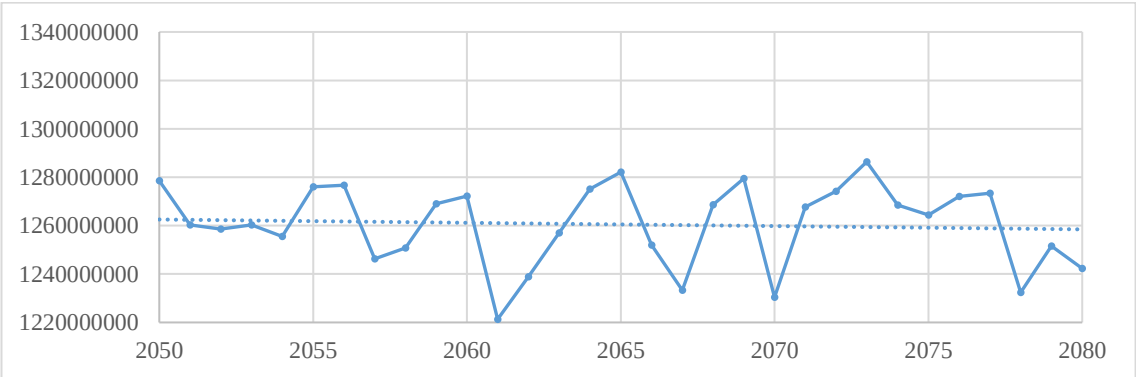

(a) MPI 4.5

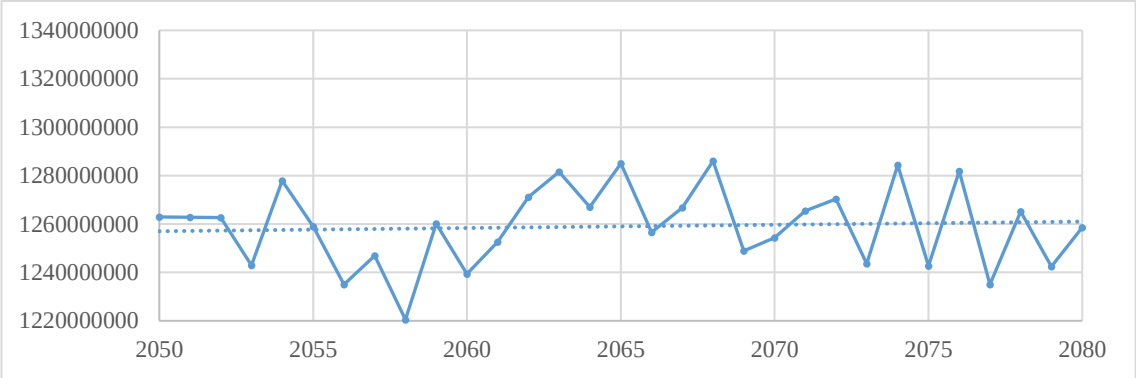

(b) MPI 8.5

Figure 5.28. The prediction of annual electricity production (Kwh) for the 2051 – 2080 interval using (a): MPI 4.5 and (b): MPI 8.5 data.

The AEPs range between 1220,000,000 Kwh and 1285,000,000 Kwh. The lowest production values resulted in the years of 2061 and 2058 for MPI 4.5 and MPI 8.5 scenarios, respectively. In scenario MPI 4.5, the energy production decreases with time. On the other hand, the energy production increases with time on MPI 8.5 scenario (The opposite situation of interval 2018-2050).

5.3.3. Suat Ugurlu HEPP

Figure 5.29 shows the relative error values among the applied models. Figure 5.30 shows the correlation values for the historical data of Suat Ugurlu HEPP.

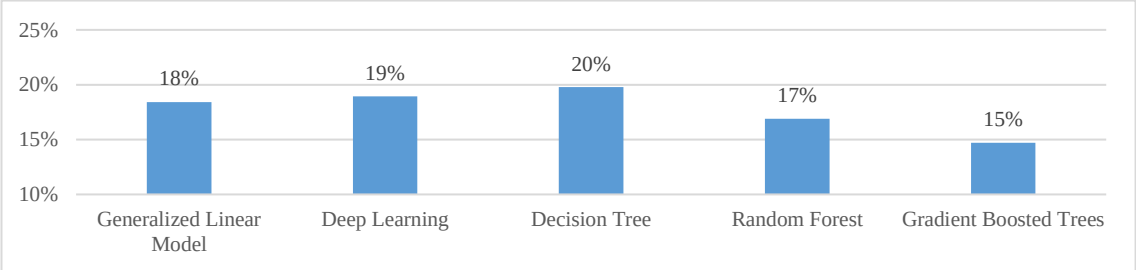

Figure 5.29. The Relative Error values among the applied models for the historical data of Suat Ugurlu HEPP.

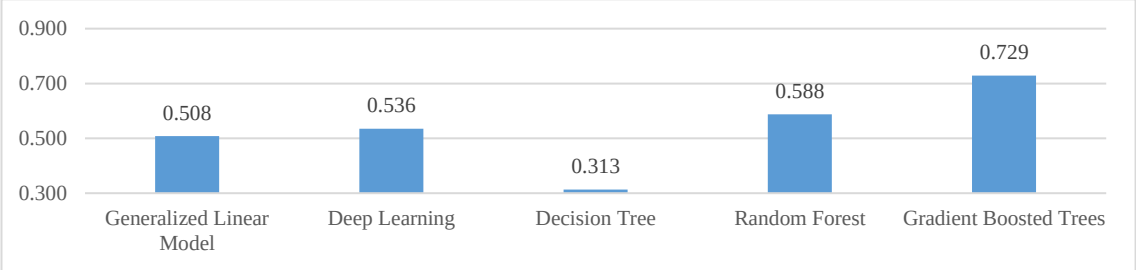

Figure 5.30. The correlation values of the applied models for the historical data of Suat Ugurlu HEPP.

Figure 5.29 helps in determining the most accurate model between all ML models. It shows that the GBT model has the lowest value in comparison with other models. This means that the GBT model is the most accurate model to apply predicting the energy production with GCMs data.

In Figure 5.30, the results show that the correlation value of the gradient boosted trees model equals 0.729, which means that the gradient boosted trees model is the most successful model for the data. As a result of the R value of the gradient boosted trees model, the model is used in the prediction process for each GCM. Figures 5.31, 5.32, 5.33, 5.34, 5.35 and 5.36 show the predicted energy production during the time series of the selected model.

5.3.3.1. Energy prediction for 2018 to 2050 Interval

After testing the performance, the most accurate model is selected to be used in the predicting process. Energy productions are predicted for the GCMs for each scenario using the GBT model. Figure 5.31 shows the annual predicted energy production using the gradient boosted trees model during the interval 2018 to 2050 based on the GFDL model's data for both scenarios RCP 8.5 and RCP 4.5.

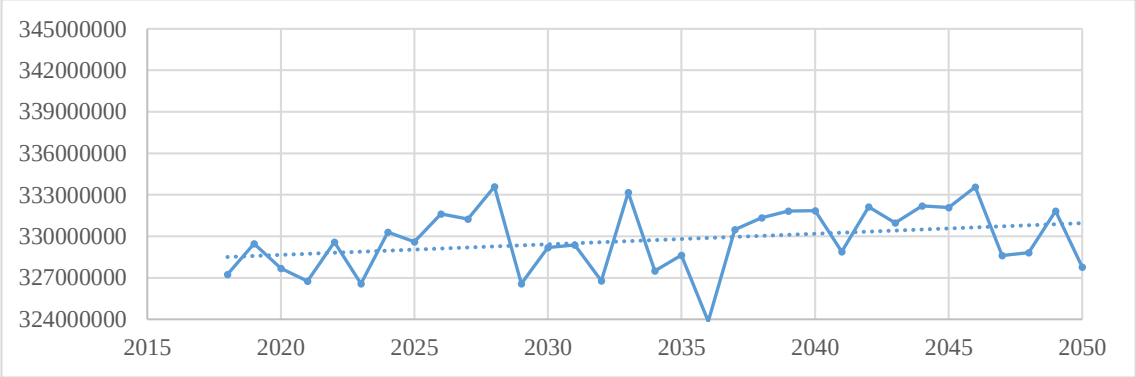

(a) GFDL 4.5

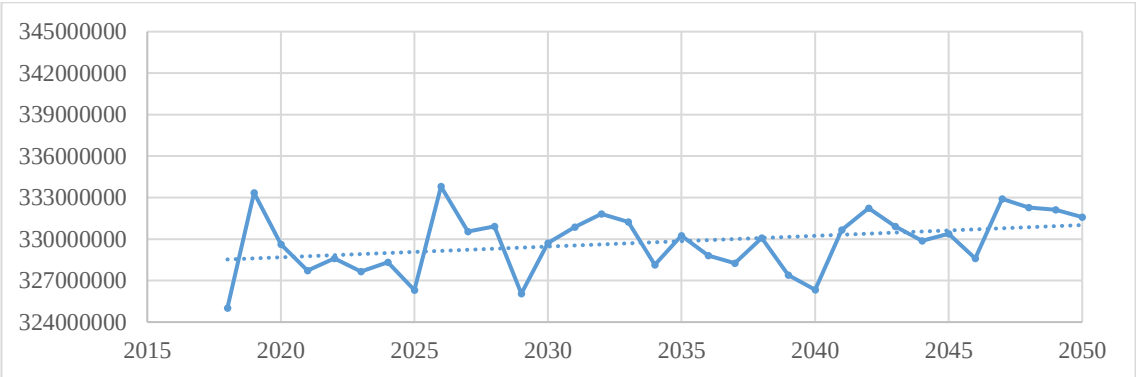

(b) GFDL 8.5

Figure 5.31. The prediction of annual electricity production (Kwh) for the 2018 – 2050 interval using (a): GFDL 4.5 and (b): GFDL 8.5 data.

In Figure 5.31, the AEPs range between 324,000,000 Kwh and 333,800,000 Kwh. The lowest production values resulted in the years of 2036 and 2018 years for GFDL 4.5 and GFDL 8.5 scenarios with values near 324,000,000 Kwh, respectively. On the other hand, the highest production values resulted in the years of 2028 and 2026 for GFDL 4.5 and GFDL 8.5 scenarios, respectively.

Figure 5.32 shows the predicted energy production during the same interval for HadGEM model for scenarios RCP 8.5 and RCP 4.5.

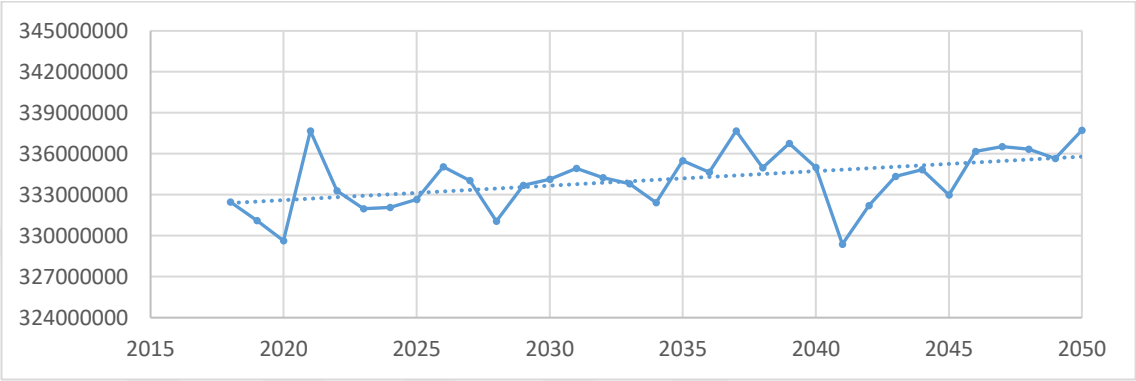

(a) HadGEM 4.5

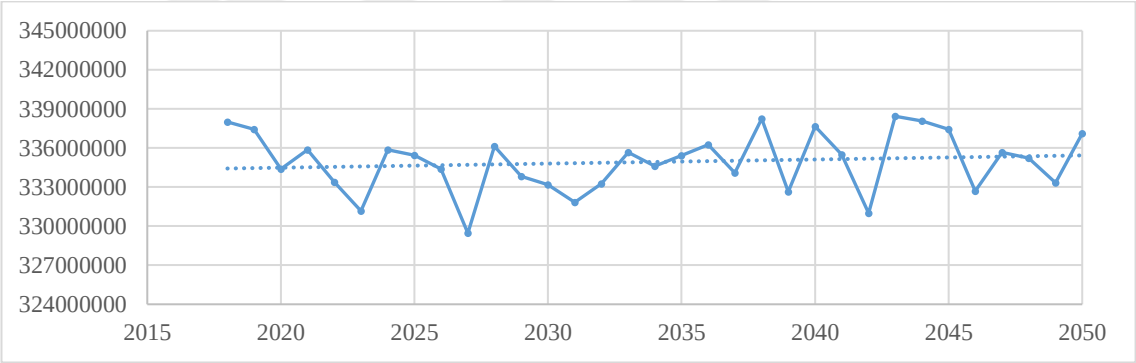

(b) HadGEM 8.5

Figure 5.32. The prediction of annual electricity production (Kwh) for the 2018 – 2050 interval using (a): HadGEM 4.5 and (b): HadGEM 8.5 data.

In Figure 5.32, the AEPs range between 329,000,000 Kwh and 339,000,000 Kwh. The highest production values resulted in the years of 2021 and 2043 for HadGEM scenarios, respectively. On the other hand, the lowest production values resulted in the years of 2027 and 2041 for HadGEM 4.5 and HadGEM 8.5 scenarios, respectively. Figure 5.33 shows the predicted energy production during the same interval for MPI model for scenarios RCP 8.5 and RCP 4.5.

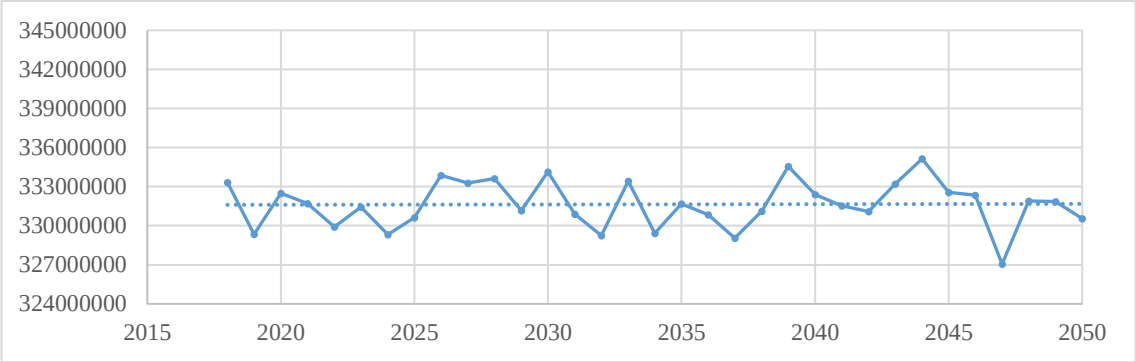

(a) MPI 4.5

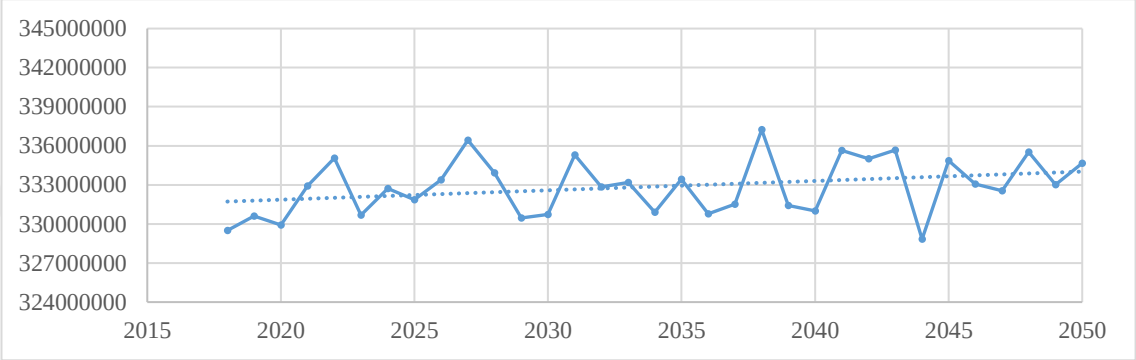

(b) MPI 8.5

Figure 5.33. The prediction of annual electricity production (Kwh) for the 2018 – 2050 interval using (a): MPI 4.5 and (b): MPI 8.5 data.

The prediction of the AEP using HadGEM model with 4.5 and 8.5 scenarios are shown in Figure 5.33. The AEPs range between 327,000,000 Kwh and 337,300,000 Kwh. The lowest production values resulted in the years of 2038 and 2036 for HadGEM 4.5 and HadGEM 8.5 scenarios, respectively.

5.3.3.2. Energy prediction for 2051 to 2080 Interval

Figure 5.34 shows the annual predicted energy production using the gradient boosted trees model during the interval 2018 to 2050 based on the GFDL model's data for both scenarios RCP 4.5 and RCP 8.5.

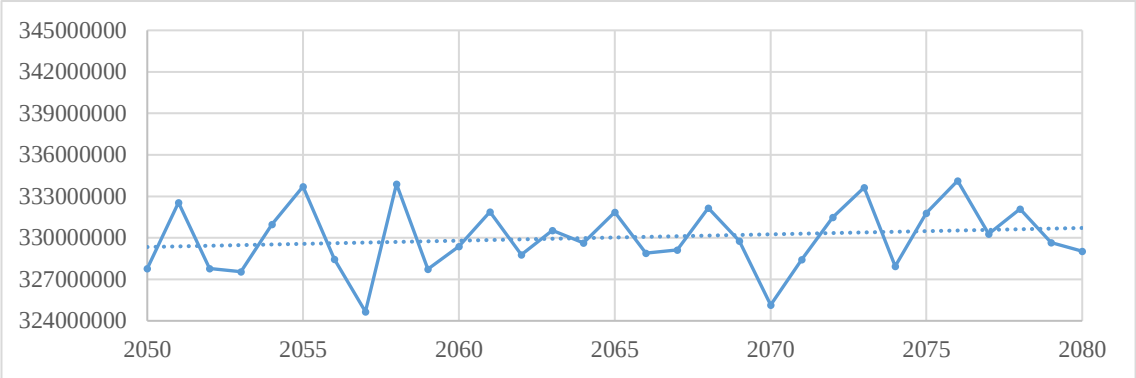

(a) GFDL 4.5

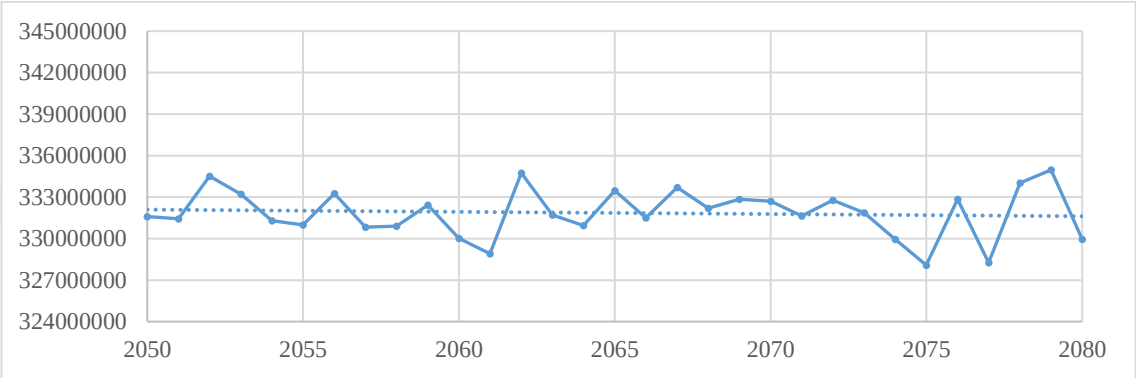

(b) GFDL 8.5

Figure 5.34. The prediction of annual electricity production (Kwh) for the 2051 – 2080 interval using (a): GFDL 4.5 and (b): GFDL 8.5 data.

In Figure 5.34, the AEPs range between 324,000,000 Kwh and 335,000,000 Kwh. The highest production values resulted in the years of 2058 and 2062 for GFDL 4.5 and GFDL 8.5 scenarios, respectively. On the other hand, the lowest production values resulted in the years of 2057 and 2075 for GFDL 4.5 and GFDL 8.5 scenarios, respectively.

Figure 5.35 shows the annual predicted energy production during the same interval for the HadGEM model.

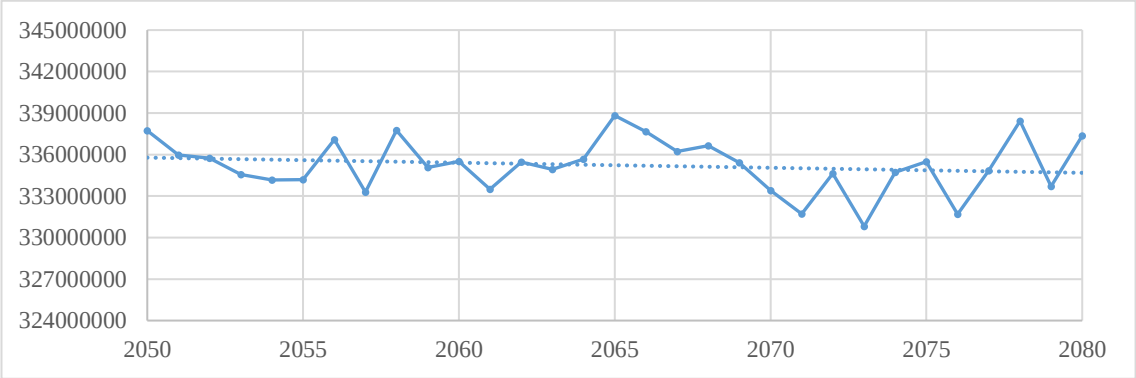

(a) HadGEM 4.5

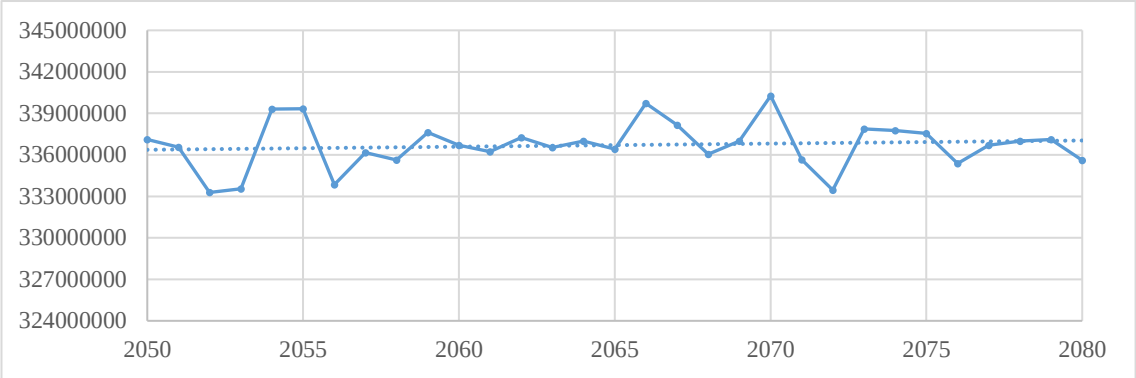

(b) HadGEM 8.5

Figure 5.35. The prediction of annual electricity production (Kwh) for the 2051 – 2080 interval using (a): HadGEM 4.5 and (b): HadGEM 8.5 data.

The prediction of the AEP using HadGEM model with 4.5 and 8.5 scenarios are shown in Figure 5.35. The AEPs range between 330,000,000 Kwh and 340,000,000 Kwh. The highest production values resulted in the years of 2065 and 2070 for HadGEM 4.5 and HadGEM 8.5 scenarios, respectively.

Figure 5.36 shows the predicted energy production during the same interval for MPI model for scenarios RCP 8.5 and RCP 4.5.

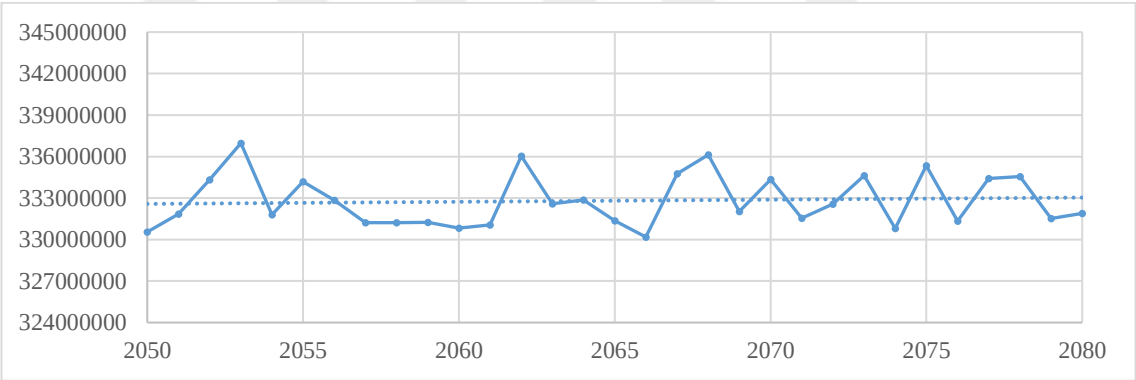

(a) MPI 4.5

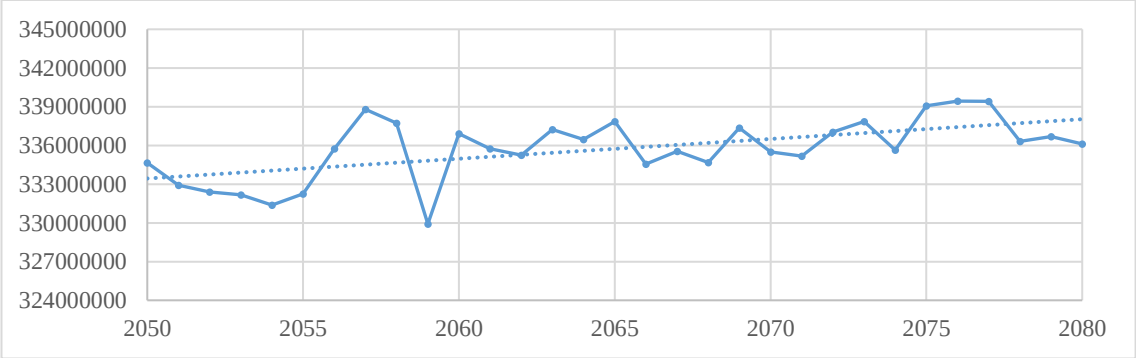

(b) MPI 8.5

Figure 5.36. The prediction of annual electricity production (Kwh) for the 2051 – 2080 interval using (a): MPI 4.5 and (b): MPI 8.5 data.

The prediction of the AEP using the MPI model with 8.5 and 4.5 scenarios is shown in Figure 5.36. The AEPs range between 330,000,000 Kwh and 339,000,000 Kwh. The highest production values resulted in the years of 2053 and 2057 for MPI 4.5 and MPI 8.5 scenarios with values near 337,000,000 and 339,000,000 Kwh, respectively. On the other hand, the lowest production values resulted in the years of 2066 and 2059 for MPI 4.5 and MPI 8.5 scenarios, respectively.

5.3.4. Hirfanli HEPP

Figure 5.37 shows the relative error values among the applied models for the historical data of Hirfanli HEPP. Figure 5.38 shows the R values of the applied models for the historical data of Hirfanli HEPP.

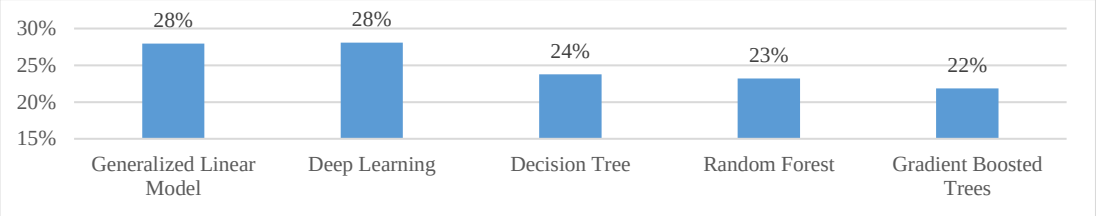

Figure 5.37. The Relative Error values among the applied models for the historical data of Hirfanli HEPP.

Figure 5.38. The correlation values of the applied models for the historical data of Hirfanli HEPP.

Figure 5.37 helps in selecting the most accurate model between all ML models. It shows again that the GBT model has the lowest value in comparison with other models. The GBT model is the most accurate model to apply in predicting the energy production with GCMs data.

In Figure 5.38, the results show that R value of the GBT model equals 0.76, which means that the GBT model is the most suitable model for the data. As a result of the correlation value of the GBT model, the model is used in the prediction process for each GCM. Figures 5.39, 5.40, 5.41, 5.42, 5.43 and 5.44 show the predict of the AEP during the time series of the selected model.

5.3.4.1. Energy prediction for 2018 to 2050 Interval

Figure 5.39 shows the predicted energy production using the gradient boosted trees model during the interval 2018 to 2050 based on the GFDL model's data for both scenarios RCP 8.5 and RCP 4.5.

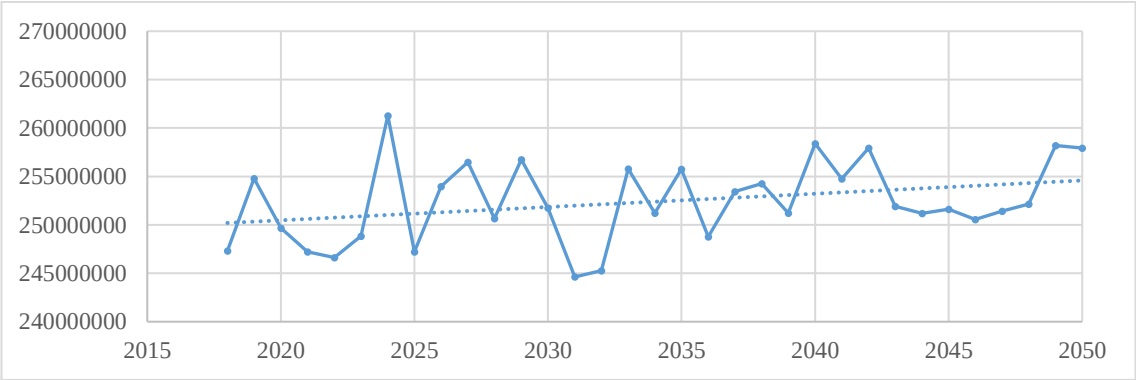

(a) GFDL 4.5

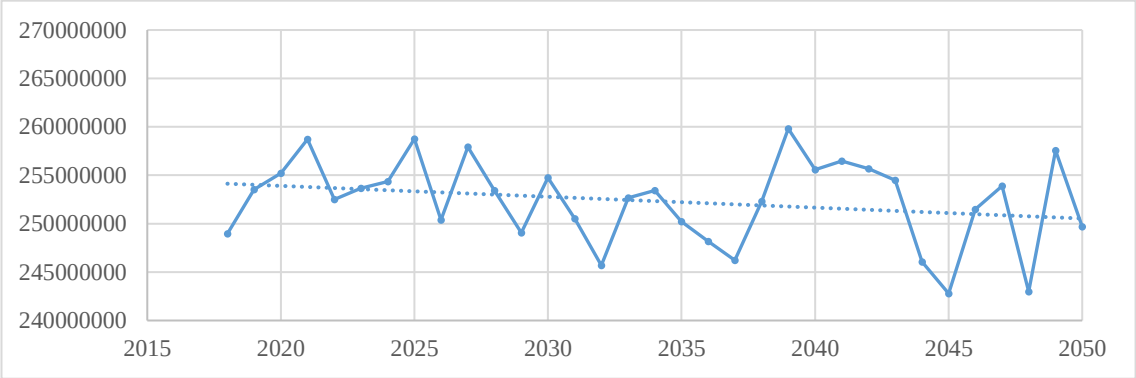

(b) GFDL 8.5

Figure 5.39. The prediction of annual electricity production (Kwh) for the 2018 – 2050 interval using (a): GFDL 4.5 and (b): GFDL 8.5 data.

In Figure 5.39, the AEPs range between 242,000,000 Kwh and 261,000,000 Kwh. The lowest production values resulted in the years of 2031 and 2045 for the GFDL 4.5 and GFDL 8.5 scenarios with values near 245,000,000 and 242,000,000 Kwh, respectively. On the other hand, the highest production values resulted in the years of 2024 and 2039 for the GFDL 4.5 and GFDL 8.5 scenarios, respectively.

Figure 5.40 shows the predicted energy production during the same interval for HadGEM model for scenarios RCP 8.5 and RCP 4.5.

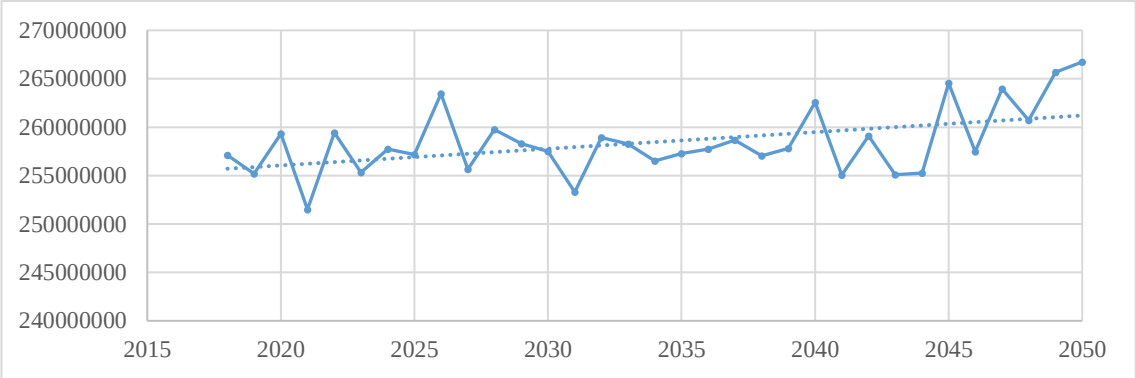

(a) HadGEM 4.5

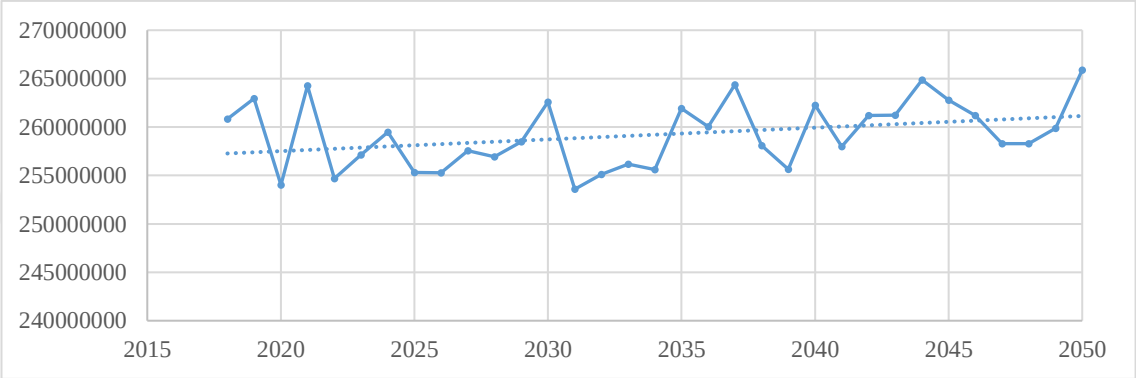

(b) HadGEM 8.5

Figure 5.40. The prediction of annual electricity production (Kwh) for the 2018 – 2050 interval using (a): HadGEM 4.5 and (b): HadGEM 8.5 data.

The prediction of the AEP using the HadGEM model with 8.5 and 4.5 scenarios is shown in Figure 5.40. The AEPs range between 251,000,000 Kwh and 266,700,000 Kwh. The lowest production values resulted in the years of 2021 and 2031 for the HadGEM 4.5 and HadGEM 8.5 scenarios with values near 251,000,000 and 253,500,000 Kwh, respectively. On the other hand, the highest production values resulted in many years for both scenarios with value near 266,000,000 Kwh.

Figure 5.41 shows the predicted energy production during the same interval for MPI model for scenarios RCP 8.5 and RCP 4.5.

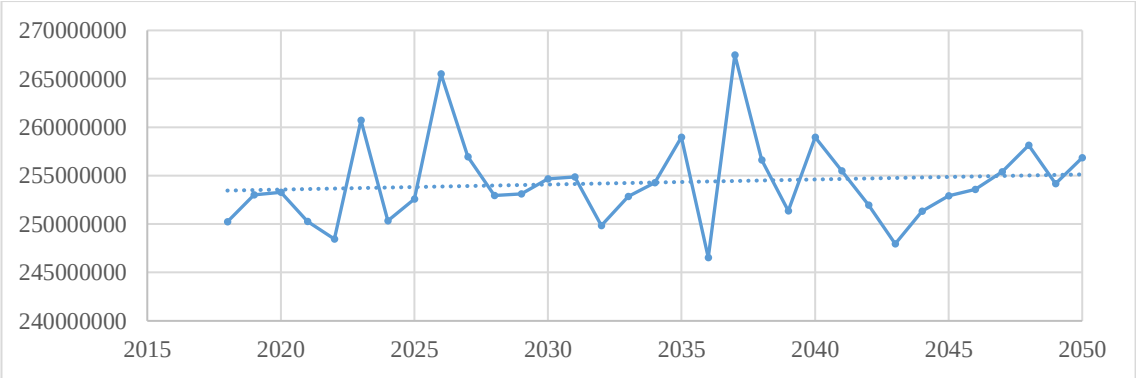

(a) MPI 4.5

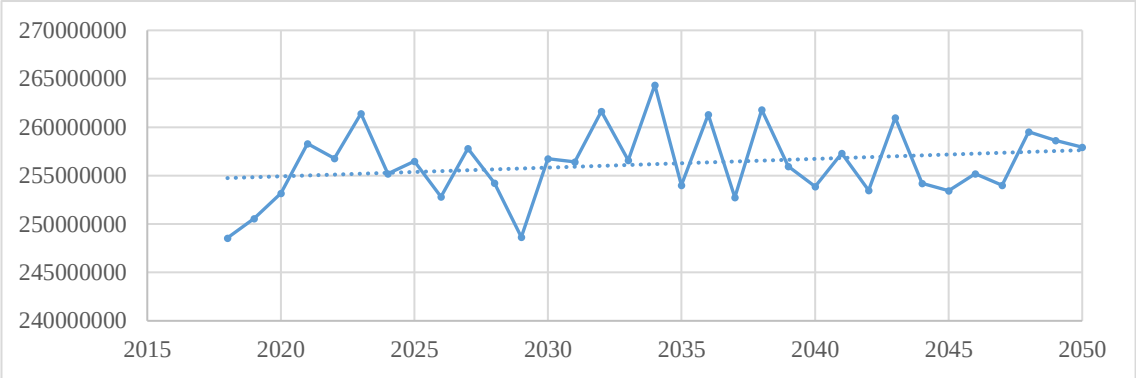

(b) MPI 8.5

Figure 5.41. The prediction of annual electricity production (Kwh) for the 2018 – 2050 interval using (a): MPI 4.5 and (b): MPI 8.5 data.

The annual prediction of the energy production using the MPI model with 4.5 and 8.5 scenarios is shown in Figure 5.41. The AEPs range between 246,500,000 Kwh and 267,500,000 Kwh. The highest production values resulted in the years of 2034 and 2037 for the MPI 4.5 and MPI 8.5 scenarios with values near 267,000,000 and 264,000,000 Kwh, respectively. On the other hand, the lowest production values resulted in 2036 and 2029 for MPI 4.5 and MPI 8.5 scenarios, respectively.

5.3.4.2. Energy prediction for 2051 to 2080 Interval

Figure 5.42 shows the predicted energy production using the gradient boosted trees model during the interval 2018 to 2050 based on the GFDL model's data for both scenarios RCP 8.5 and RCP 4.5.

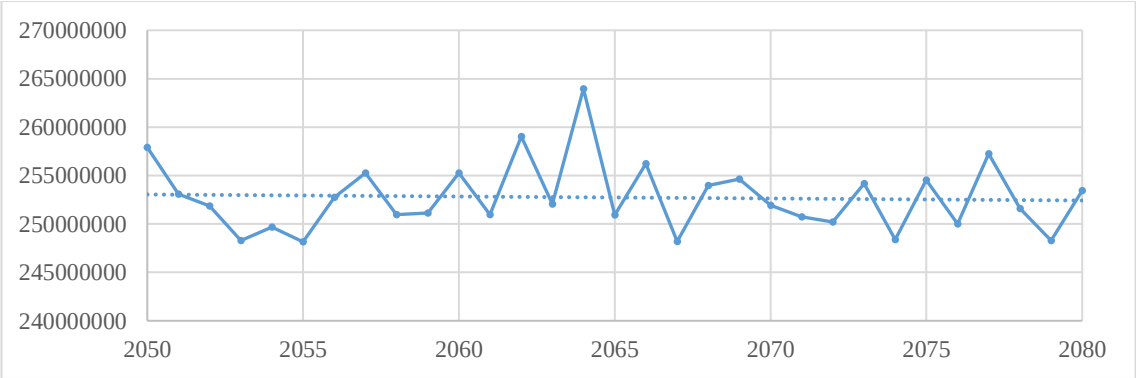

(a) GFDL 4.5

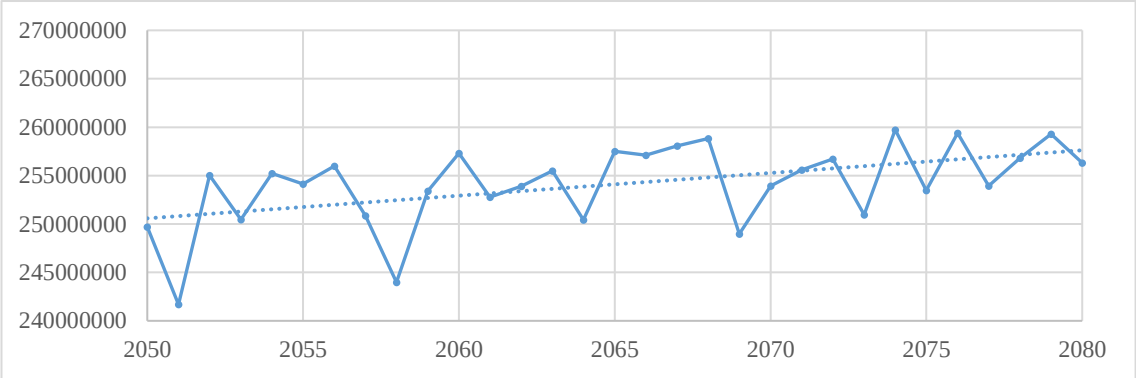

(b) GFDL 8.5

Figure 5.42. The prediction of annual electricity production (Kwh) for the 2051 – 2050 interval using (a): GFDL 4.5 and (b): GFDL 8.5 data.

In Figure 5.42, the AEPs range between 240,000,000 Kwh and 264,000,000 Kwh. The highest production values resulted in the years of 2064 and 2074 for the GFDL 4.5 and GFDL 8.5 scenarios, respectively. On the other hand, the lowest production values resulted in 2067 and 2051 for the GFDL 4.5 and GFDL 8.5 scenarios, respectively.

Figure 5.43 shows the annual predicted energy production during the same interval for the HadGEM model.

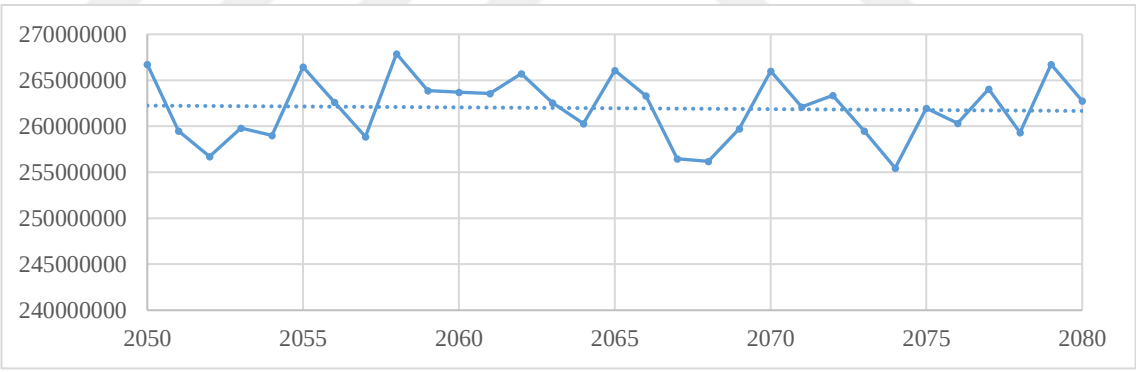

(a) HadGEM 4.5

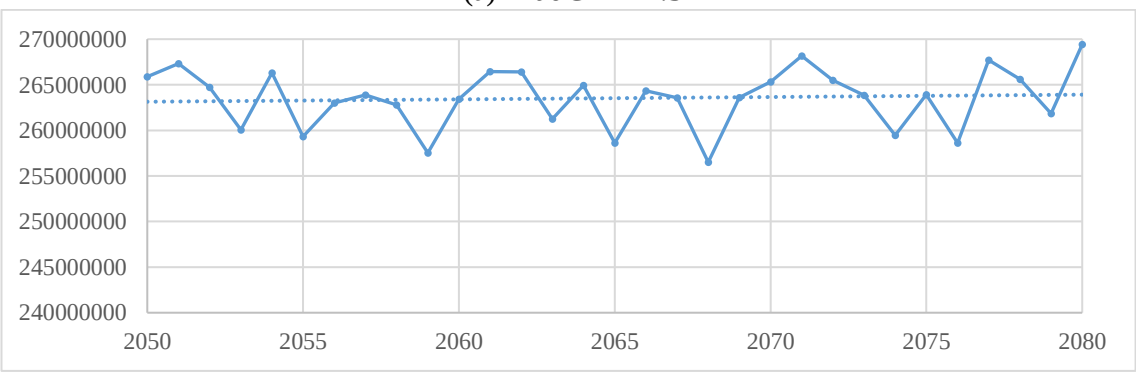

(b) HadGEM 8.5

Figure 5.43. The prediction of annual electricity production (Kwh) for the 2051 – 2080 interval using (a): HadGEM 4.5 and (b): HadGEM 8.5 data.

In Figure 5.43, the AEPs range between 255,000,000 Kwh and 270,000,000 Kwh. The highest production values resulted in the years of 2058 and 2080 for the HadGEM 4.5 and HadGEM 8.5 scenarios, respectively. On the other hand, the lowest production values resulted in 2074 and 2068 for the HadGEM 4.5 and HadGEM 8.5 scenarios, respectively. Figure 5.44 shows the predicted energy production during the same interval for MPI model for scenarios RCP 8.5 and RCP 4.5.

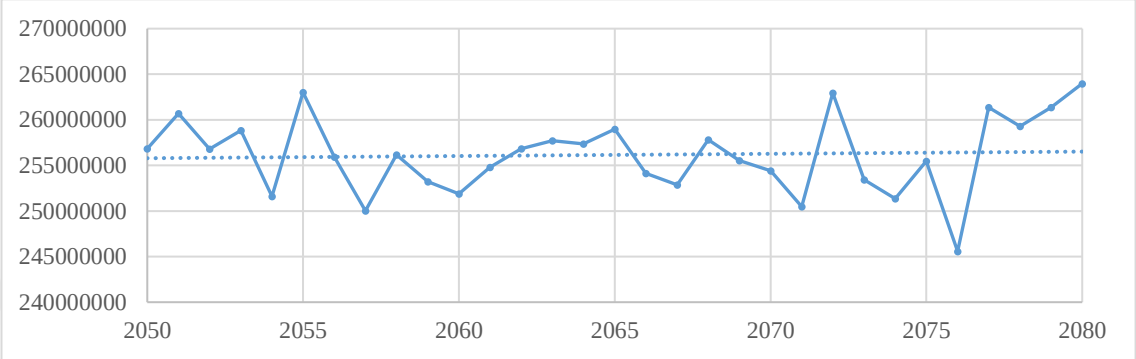

(a) MPI 4.5

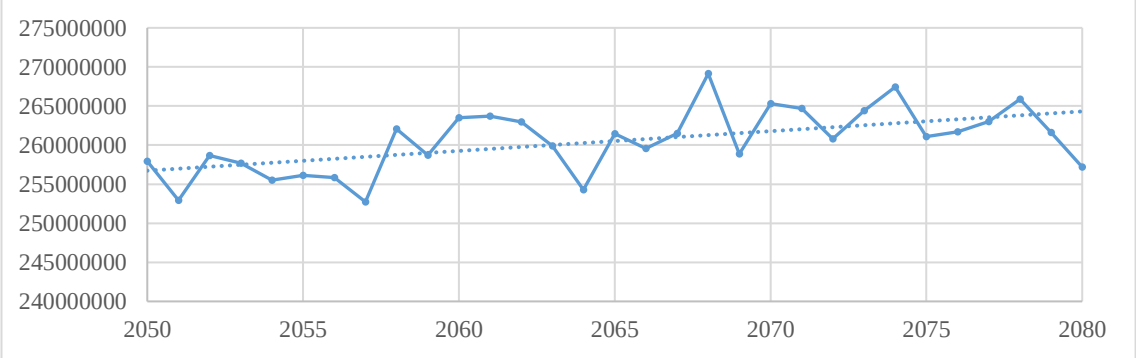

(b) MPI 8.5

Figure 5.44. The prediction of annual electricity production (Kwh) for the 2051 – 2080 interval using (a): MPI 4.5 and (b): MPI 8.5 data.

The prediction of the energy production using the MPI model with 8.5 and 4.5 scenarios is shown in Figure 5.44. The AEPs range between 245,000,000 Kwh and 270,000,000 Kwh. The highest production values resulted in the years of 2080 and 2068 for the MPI 4.5 and MPI 8.5 scenarios with values near 264,000,000 and 270,000,000 Kwh, respectively. On the other hand, the lowest production values resulted in 2057 and 2076 for the MPI 4.5 and MPI 8.5 scenarios, respectively.

5.3.5. Kesikkopru HEPP

Figure 5.45 shows the relative error values among the applied models for the historical data of Kesikkopru HEPP. Figure 5.46 shows the R values of the applied

models for the historical data of Kesikkopru HEPP.

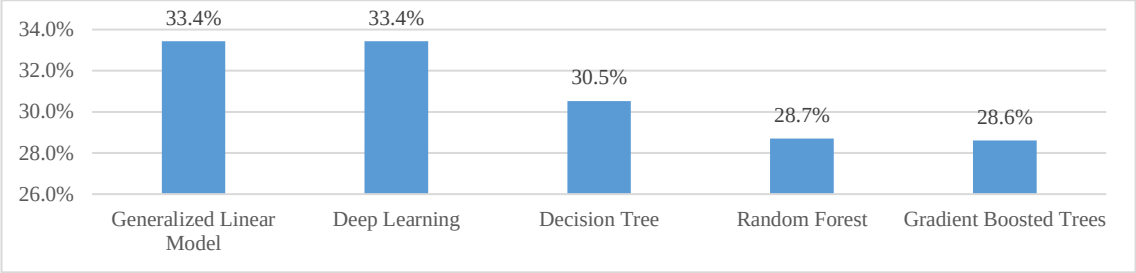

Figure 5.45. The Relative Error values among the applied models for the historical data of Kesikkopru HEPP.

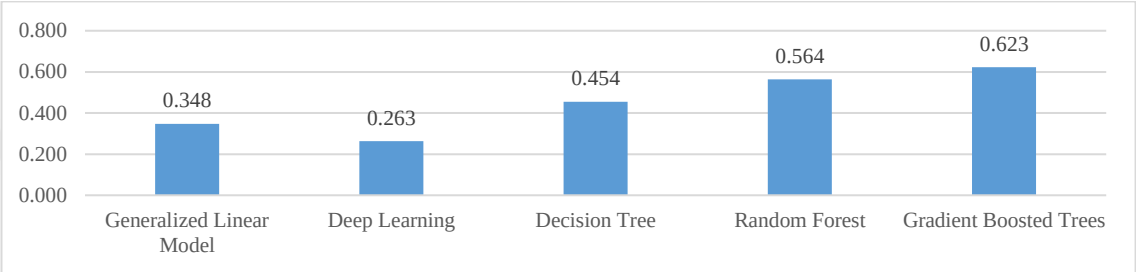

Figure 5.46. The correlation values of the applied models for the historical data of Kesikkopru HEPP.

Figure 5.45 is used in determining the most accurate model among all ML models. It shows that GBT model has the lowest value in comparison with other models. This means that the GBT model is the most accurate model to apply predicting the energy production with GCMs data.

In Figure 5.46, the results show that the correlation value of the GBT model equals 0.623, which means that the gradient boosted trees model is the most suitable model for the data. As a result of the correlation value of the gradient boosted trees model, the model is used in the prediction process for each GCM.

Figures 5.47, 5.48, 5.49, 5.50, 5.51 and 5.52 show the predict of the energy production during the time series of the selected model.

5.3.5.1. Energy prediction for 2018 to 2050 Interval

Figure 5.47 shows the predicted energy production using the gradient boosted trees model during the interval 2018 to 2050 based on the GFDL model's data for both scenarios RCP 8.5 and RCP 4.5.

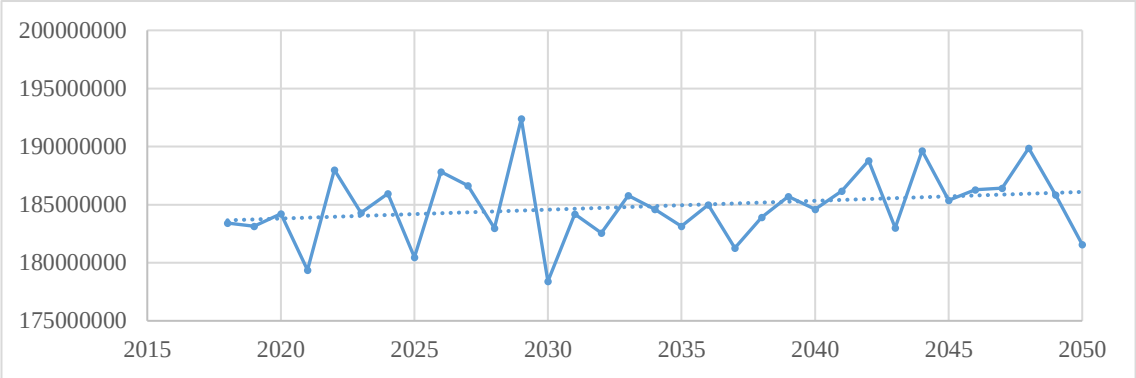

(a) GFDL 4.5

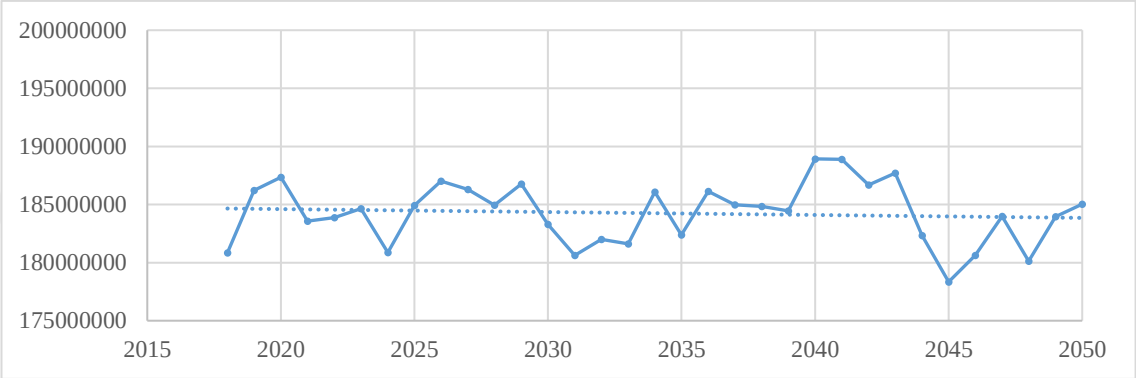

(b) GFDL 8.5

Figure 5.47. The prediction of annual electricity production (Kwh) for the 2018 – 2050 interval using (a): GFDL 4.5 and (b): GFDL 8.5 data.

In Figure 5.47, the AEPs range between 178,000,000 Kwh and 192,000,000 Kwh. The lowest production values resulted in the years of 2030 and 2045 for the GFDL 4.5 and GFDL 8.5 scenarios with values near 178,000,000 Kwh for both scenarios. On the other hand, the highest production values resulted in 2029 and 2040 for GFDL 4.5 and GFDL 8.5 scenarios, respectively.

Figure 5.48 shows the predicted energy production during the same interval for the HadGEM model for scenarios RCP 8.5 and RCP 4.5.

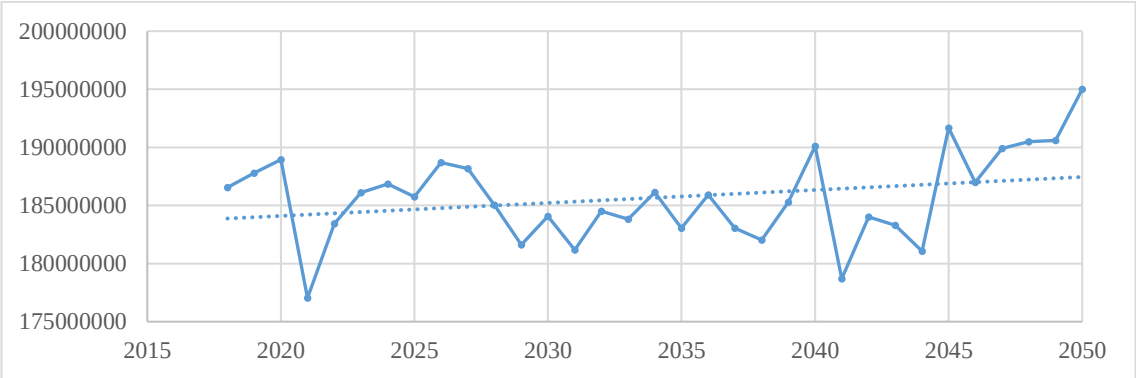

(a) HadGEM 4.5

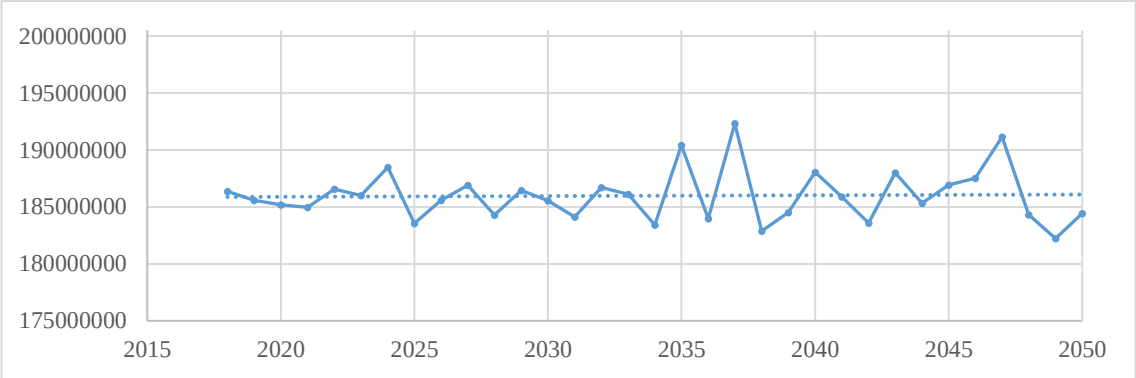

(b) HadGEM 8.5

Figure 5.48. The prediction of annual electricity production (Kwh) for the 2018 – 2050 interval using (a): HadGEM 4.5 and (b): HadGEM 8.5 data.

The prediction of the AEP using HadGEM model with 4.5 and 8.5 scenarios are shown in Figure 5.48. The AEPs range between 177,000,000 Kwh and 195,000,000 Kwh. The highest annual production values resulted in the years of 2050 and 2037 for the HadGEM 4.5 and HadGEM 8.5 scenarios with values near 195,000,000 and 192,000,000 Kwh, respectively. On the other hand, the lowest annual production values resulted in 2021 and 2047 for the HadGEM 4.5 and HadGEM 8.5 scenarios with values near 177,000,000 and 182,000,000 Kwh, respectively.

Figure 5.49 shows the predicted energy production during the same interval for the MPI model for scenarios RCP 8.5 and RCP 4.5.

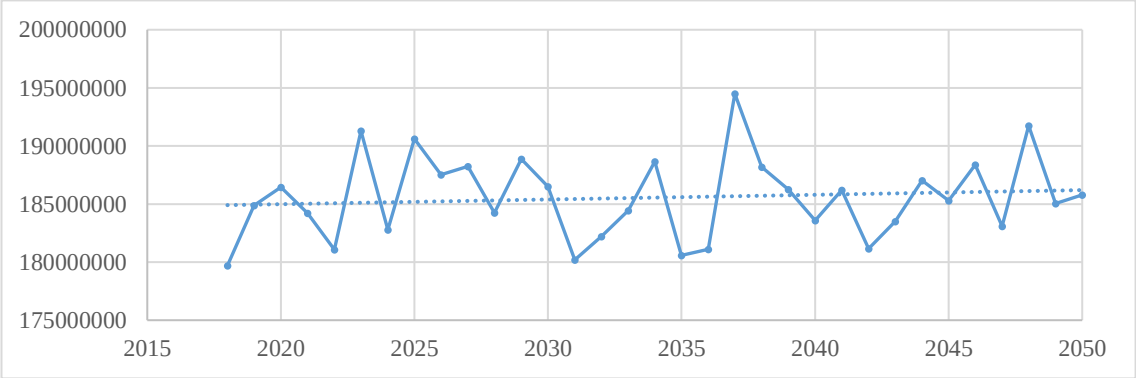

(a) MPI 4.5

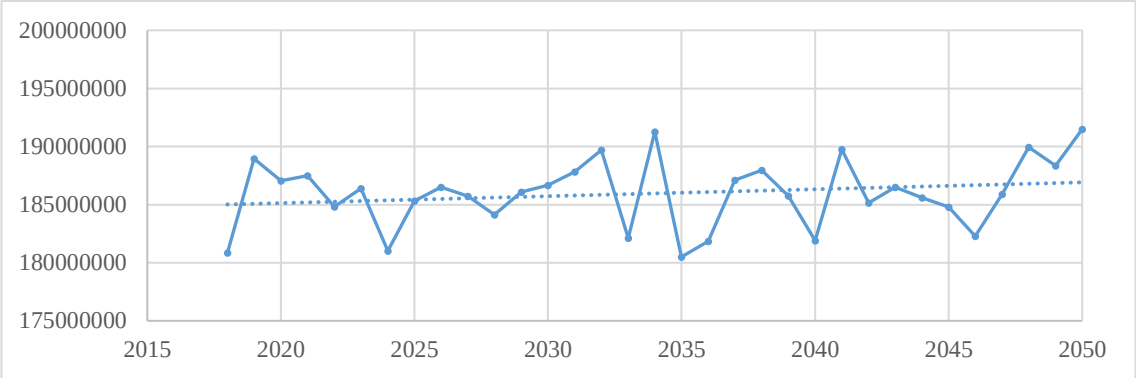

(b) MPI 8.5

Figure 5.49. The prediction of annual electricity production (Kwh) for the 2018 – 2050 interval using (a): MPI 4.5 and (b): MPI 8.5 data.

The prediction of the AEP using the MPI model with 4.5 and 8.5 scenarios is shown in Figure 5.49. The AEPs range between 179,600,000 Kwh and 195,000,000 Kwh. The highest production values resulted in the years of 2037 and 2050 for the MPI 4.5 and MPI 8.5 scenarios with values near 195,000,000 and 194,500,000 Kwh, respectively. On the other hand, the lowest production values resulted in 2031 and 2035 for the MPI 4.5 and MPI 8.5 scenarios, respectively.

5.3.5.2. Energy prediction for 2051 to 2080 Interval

Figure 5.50 shows the predicted energy production using the gradient boosted trees model during the interval 2018 to 2050 based on the GFDL model's data for both scenarios RCP 8.5 and RCP 4.5.

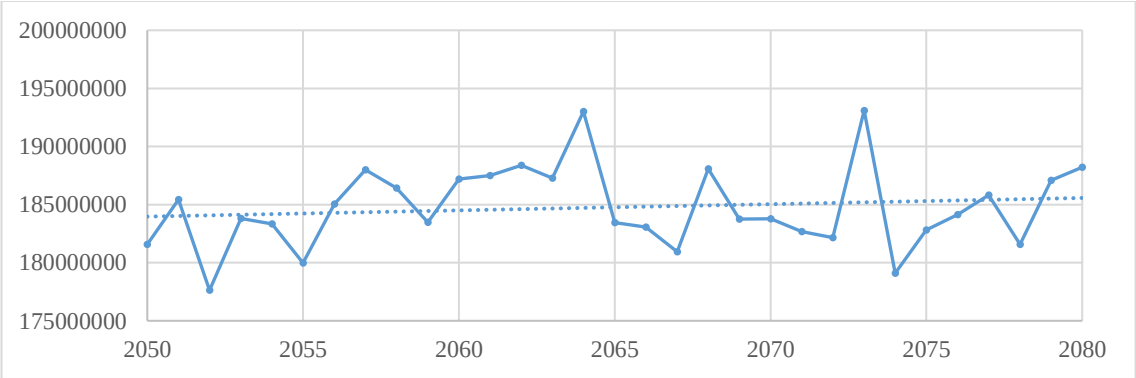

(a) GFDL 4.5

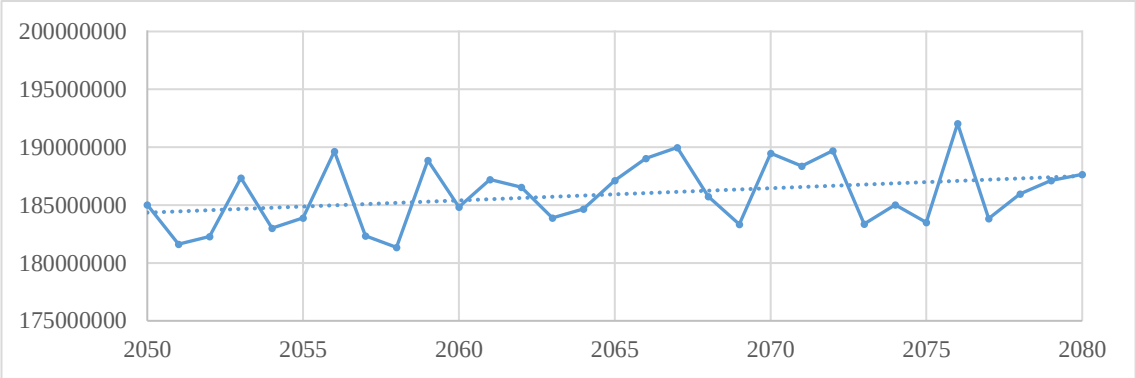

(b) GFDL 8.5

Figure 5.50. The prediction of annual electricity production (Kwh) for the 2051 – 2080 interval using (a): GFDL 4.5 and (b): GFDL 8.5 data.

In Figure 5.50, the AEPs range between 177,500,000 Kwh and 193,000,000 Kwh. The highest production values resulted in the years of 2073 and 2076 for the GFDL 4.5 and GFDL 8.5 scenarios, respectively. On the other hand, the lowest production values resulted in 2052 and 2058 for the GFDL 4.5 and GFDL 8.5 scenarios, respectively.

Figure 5.51 shows the annual predicted energy production during the same interval for the HadGEM model.

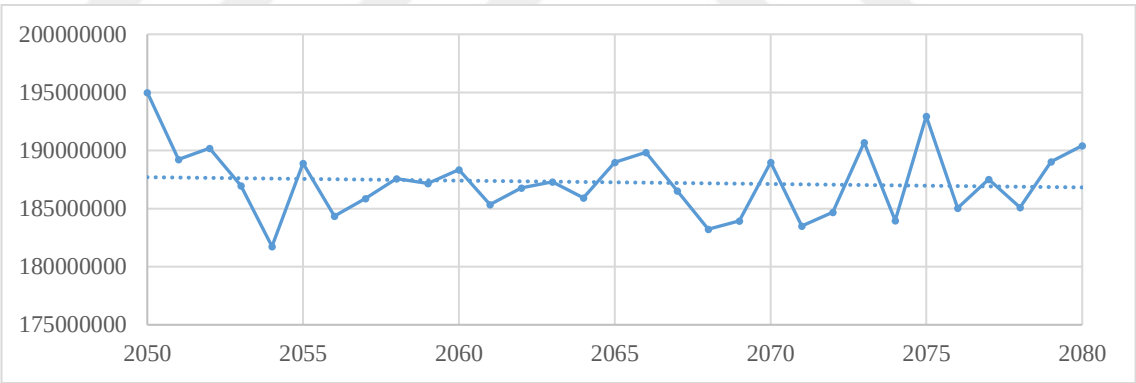

(a) HadGEM 4.5

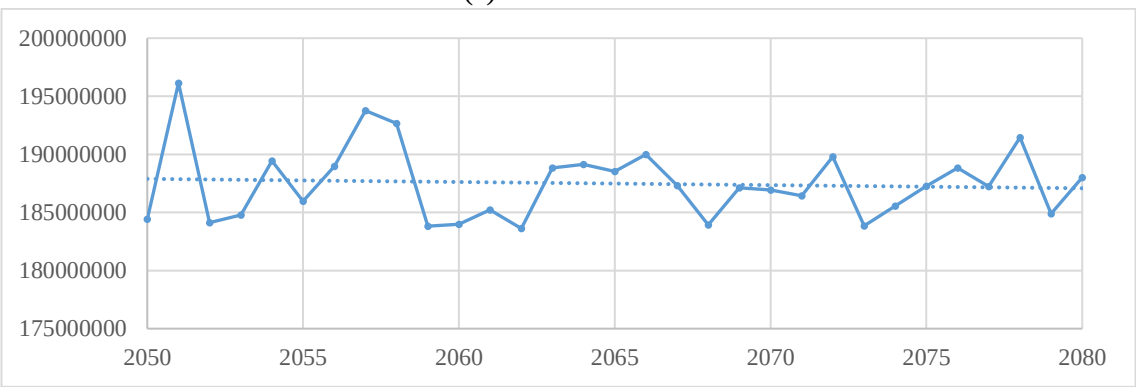

(b) HadGEM 8.5

Figure 5.51. The prediction of annual electricity production (Kwh) for the 2051 – 2080 interval using (a): HadGEM 4.5 and (b): HadGEM 8.5 data.

The prediction of the AEP using the HadGEM model with 4.5 and 8.5 scenarios is shown in Figure 5.51. The AEPs range between 181,700,000 Kwh and 196,000,000 Kwh. The lowest production values resulted in the years of 2054 and 2062 for the HadGEM 4.5 and HadGEM 8.5 scenarios. On the other hand, the highest production values resulted in many years for both scenarios with values near 195,000,000 and 196,000,000 Kwh, respectively.

Figure 5.52 shows the predicted energy production during the same interval for the MPI model for scenarios RCP 8.5 and RCP 4.5.

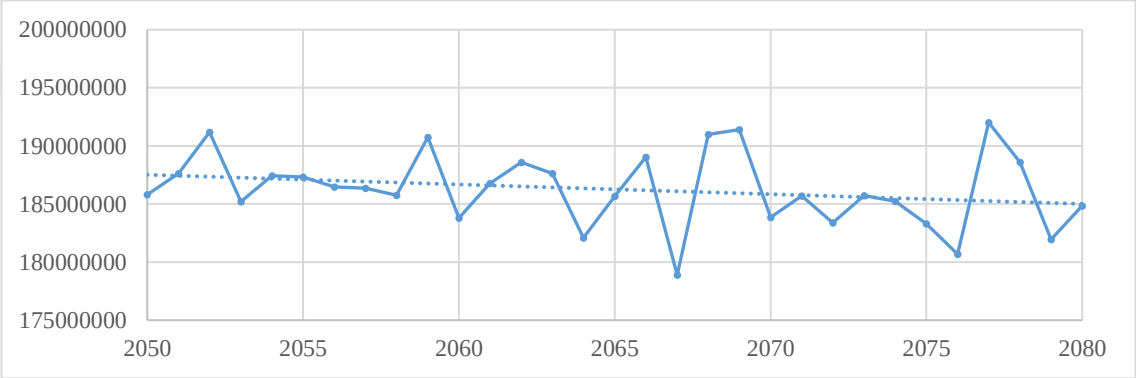

(a) MPI 4.5

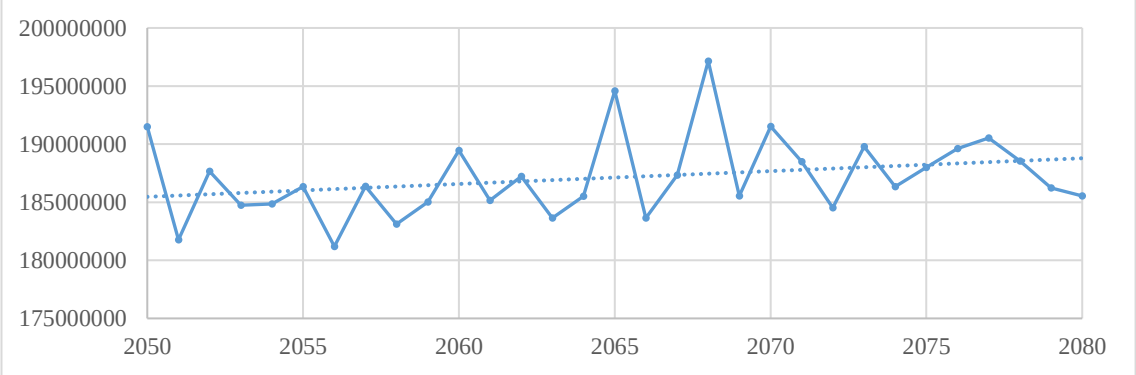

(b) MPI 8.5

Figure 5.52. The prediction of annual electricity production (Kwh) for the 2051 – 2080 interval using (a): MPI 4.5 and (b): MPI 8.5 data.

The prediction of the AEP using the MPI model with 4.5 and 8.5 scenarios is shown in Figure 5.52. The AEPs range between 178,800,000 Kwh and 197,100,000 Kwh. The highest production values resulted in the years of 2077 and 2068 for the MPI 4.5 and MPI 8.5 scenarios with values near 192,000,000 and 197,100,000 Kwh, respectively. On the other hand, the lowest production values resulted in 2067 and

2056 for the MPI 4.5 and MPI 8.5 scenarios, respectively.

5.3.6. Kapulukaya HEPP

Figure 5.53 shows the relative error values among the applied models for the historical data of Kapulukaya HEPP. Figure 5.54 shows R values of the applied models for the historical data of Kapulukaya HEPP.

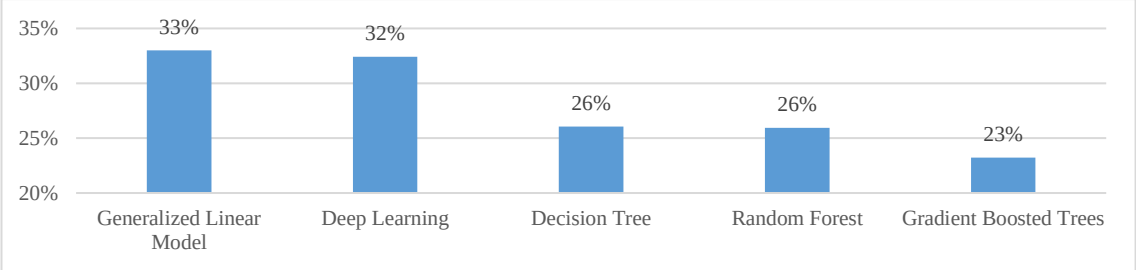

Figure 5.53. The Relative Error values among the applied models for the historical data of Kapulukaya HEPP.

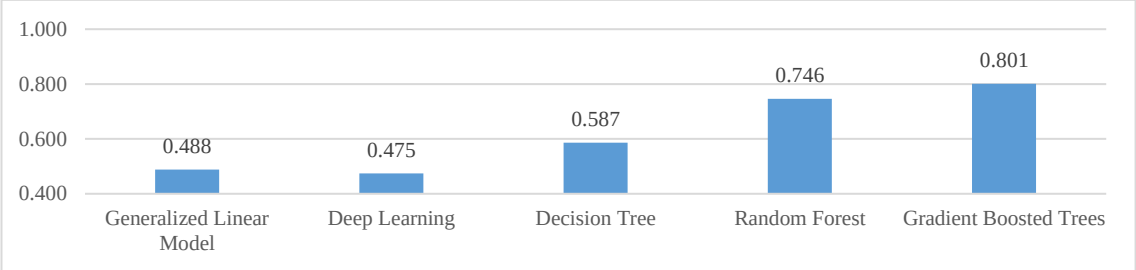

Figure 5.54. The correlation values of the applied models for the historical data of Kapulukaya HEPP.

Figure 5.53 facilitate selecting the most accurate model among all ML models. GBT model has the lowest value in comparison with other models. This means that the GBT model is the most accurate model to apply in predicting the energy production with GCMs data.

In Figure 5.54, the results show that the correlation value of the GBT model equals 0.801, which means that GBT model is the most suitable model for the data. As a result of the correlation value of the GBT model, the model is used in the prediction process for each GCM. Figures 5.55, 5.56, 5.57, 5.58, 5.59 and 5.60 show the predict of the energy production during the time series of the selected model.

5.3.6.1. Energy prediction for 2018 to 2050 Interval

Figure 5.55 shows the predicted energy production using the GBT model during the interval 2018 to 2050 based on the GFDL model's data for both scenarios RCP 8.5 and RCP 4.5.

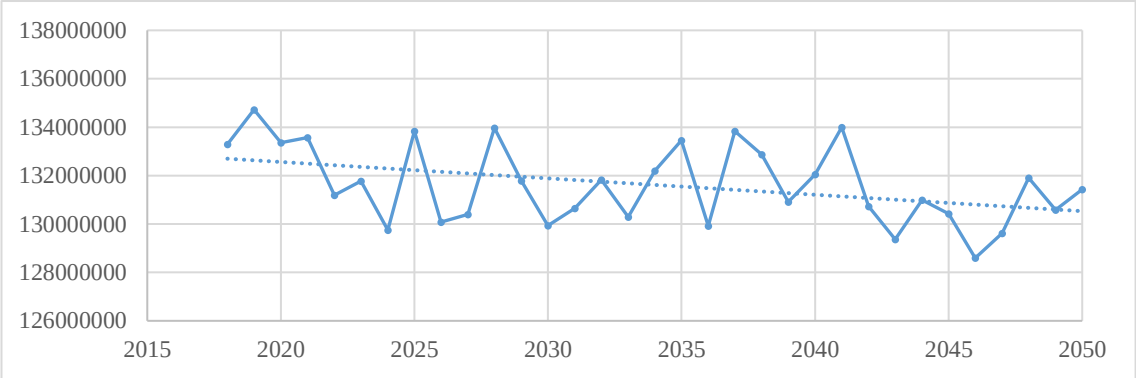

(a) GFDL 4.5

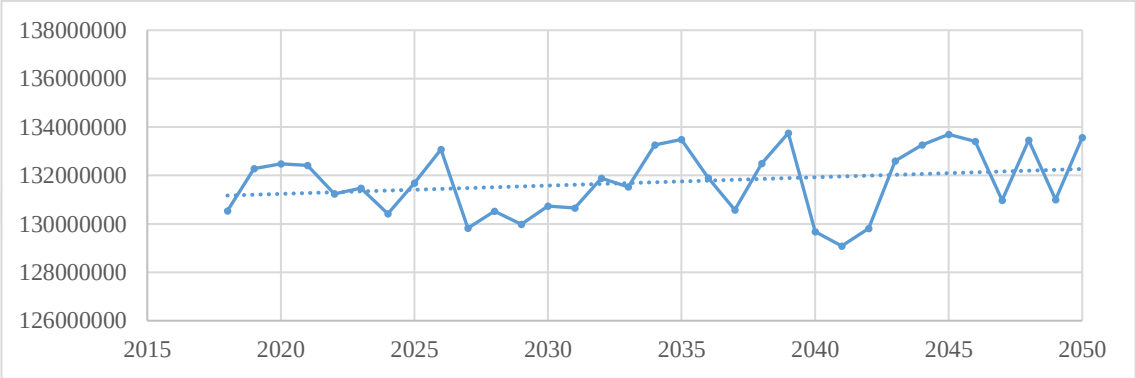

(b) GFDL 8.5

Figure 5.55. The prediction of annual electricity production (Kwh) for the 2018 – 2050 interval using (a): GFDL 4.5 and (b): GFDL 8.5 data.

In Figure 5.55, the AEPs range between 128,500,000 Kwh and 134,700,000 Kwh. The highest production values resulted in the years of 2019 and 2039 for the GFDL 4.5 and GFDL 8.5 scenarios, respectively. On the other hand, the lowest production values resulted in 2046 and 2041 for the GFDL 4.5 and GFDL 8.5 scenarios, respectively.

Figure 5.56 shows the annual predicted energy production during the same interval for the HadGEM model.

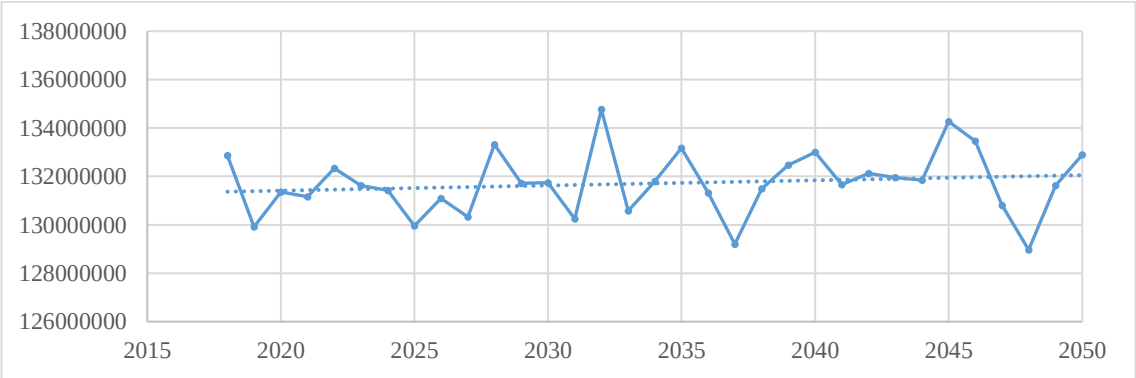

(a) HadGEM 4.5

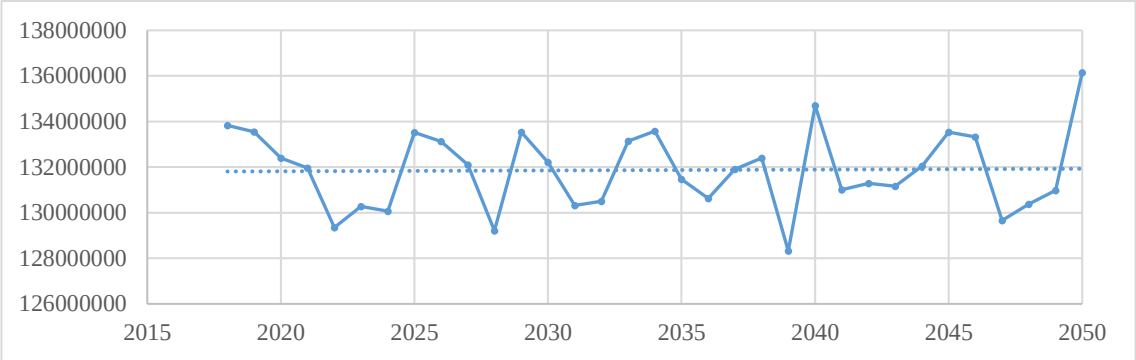

(b) HadGEM 8.5

Figure 5.56. The prediction of annual electricity production (Kwh) for the 2018 – 2050 interval using (a): HadGEM 4.5 and (b): HadGEM 8.5 data.

The prediction of the AEP using HadGEM model with 4.5 and 8.5 scenarios are shown in Figure 5.56. The AEPs range between 128,000,000 Kwh and 136,000,000 Kwh. The highest production values resulted in the years of 2032 and 2050 for the HadGEM 4.5 and HadGEM 8.5 scenarios, respectively. Figure 5.57 shows the predicted energy production during the same interval for the MPI model for scenarios RCP 8.5 and RCP 4.5.

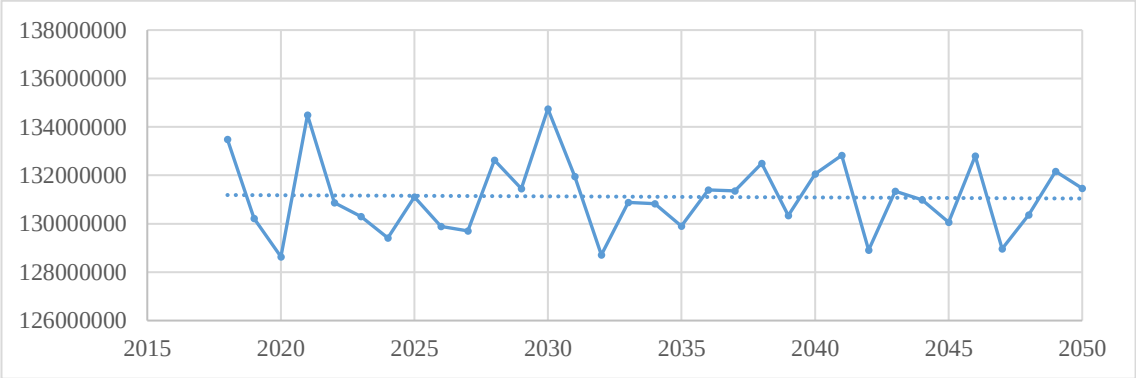

(a) MPI 4.5

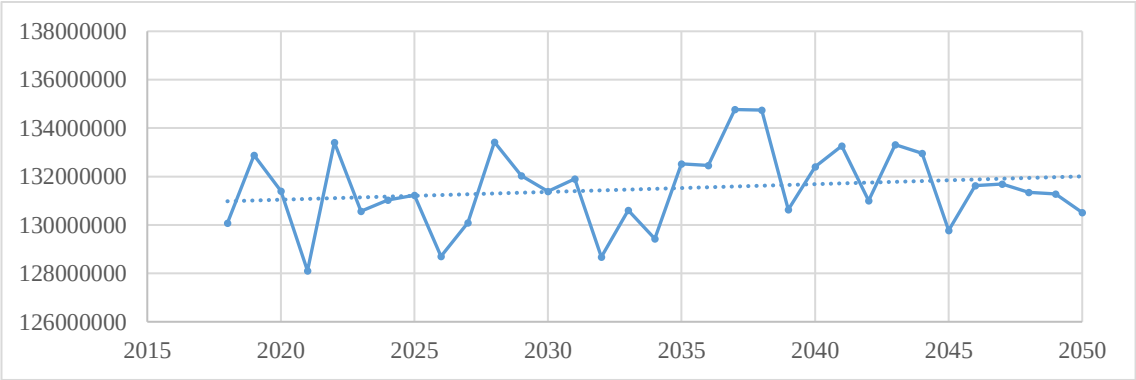

(b) MPI 8.5

Figure 5.57. The prediction of annual electricity production (Kwh) for the 2018 – 2050 interval using (a): MPI 4.5 and (b): MPI 8.5 data.

The prediction of the AEP using the MPI model with 4.5 and 8.5 scenarios is shown in Figure 5.57. The AEPs range between 128,000,000 Kwh and 134,700,000 Kwh. The highest production values resulted in the years of 2030 and 2037 for MPI 4.5 and MPI 8.5 scenarios with values near 134,700,000 Kwh for both scenarios. On the other hand, the lowest production values resulted in 2020 and 2021 for MPI 4.5 and MPI 8.5 scenarios, respectively.

5.3.6.2. Energy prediction for 2051 to 2080 Interval

Figure 5.58 shows the predicted energy production using the gradient boosted trees model during the interval 2018 to 2050 based on the GFDL model's data for both scenarios RCP 8.5 and RCP 4.5.

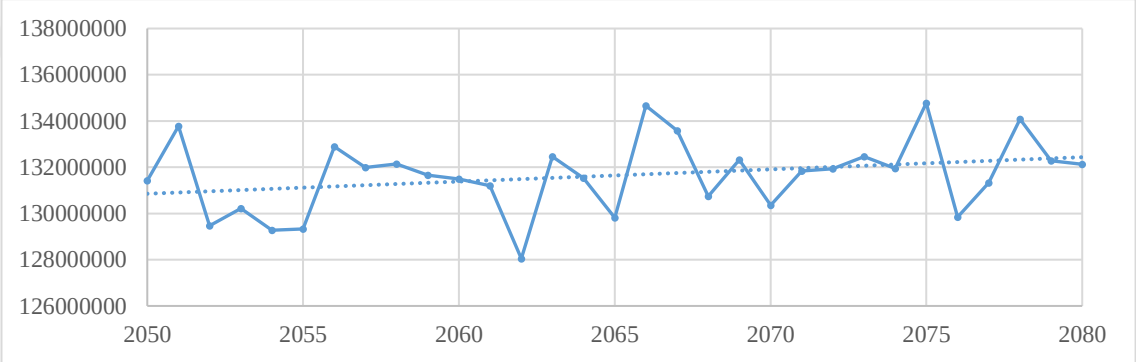

(a) GFDL 4.5

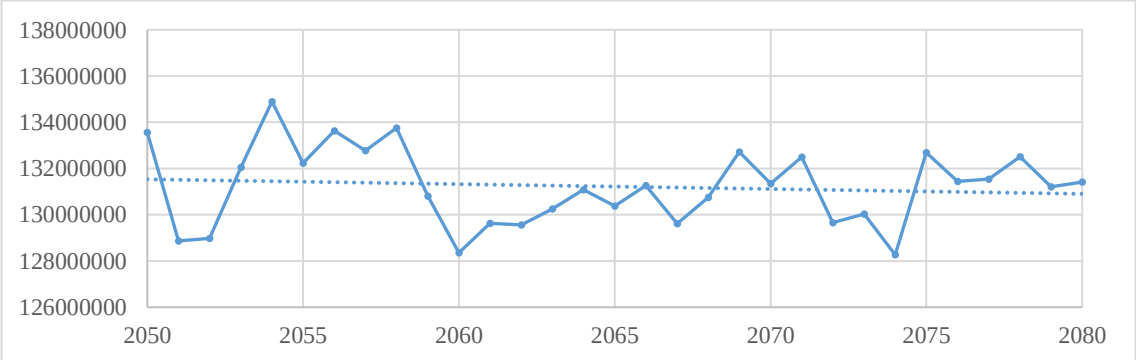

(b) GFDL 8.5

Figure 5.58. The prediction of annual electricity production (Kwh) for the 2051 – 2080 interval using (a): GFDL 4.5 and (b): GFDL 8.5 data.

In Figure 5.58, the AEPs range between 128,000,000 Kwh and 134,800,000 Kwh. The lowest production values resulted in the years of 2062 and 2074 for the GFDL 4.5 and GFDL 8.5 scenarios with values near 128,000,000 Kwh, respectively. On the other hand, the highest production values resulted in 2075 and 2054 for the GFDL 4.5 and GFDL 8.5 scenarios, respectively.

Figure 5.59 shows the predicted energy production during the same interval for the HadGEM model for scenarios RCP 8.5 and RCP 4.5.

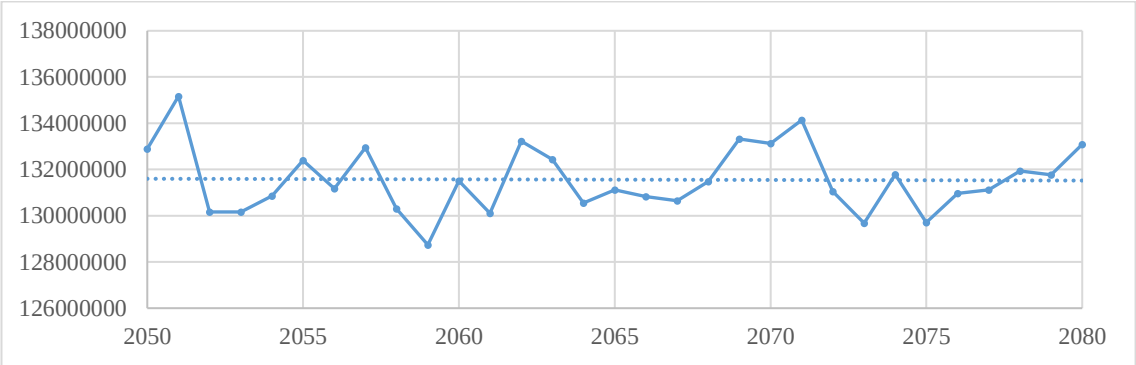

(a) HadGEM 4.5

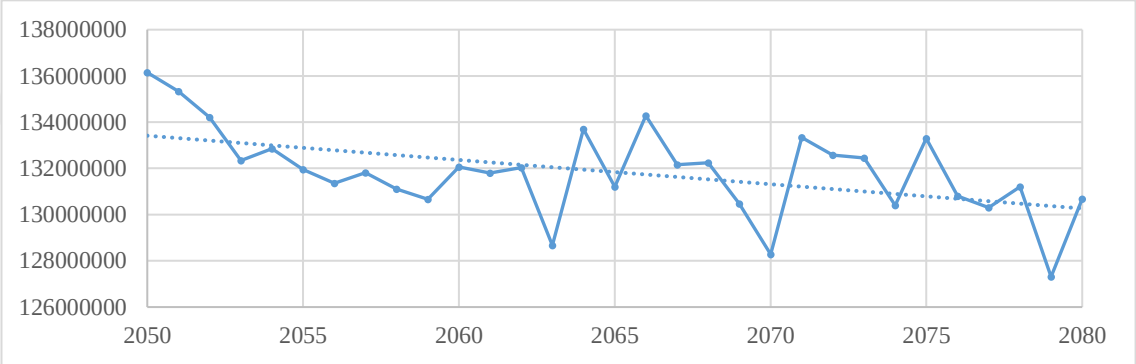

(b) HadGEM 8.5

Figure 5.59. The prediction of annual electricity production (Kwh) for the 2051 – 2080 interval using (a): HadGEM 4.5 and (b): HadGEM 8.5 data.

In Figure 5.59, the AEPs range between 127,300,000 Kwh and 136,000,000 Kwh. The highest production values resulted in the years of 2051 and 2050 for the HadGEM 4.5 and HadGEM 8.5 scenarios, respectively. On the other hand, the lowest production values resulted in 2059 and 2079 for the HadGEM 4.5 and HadGEM 8.5 scenarios, respectively.

Figure 5.60 shows the predicted energy production during the same interval for the MPI model for scenarios RCP 8.5 and RCP 4.5.

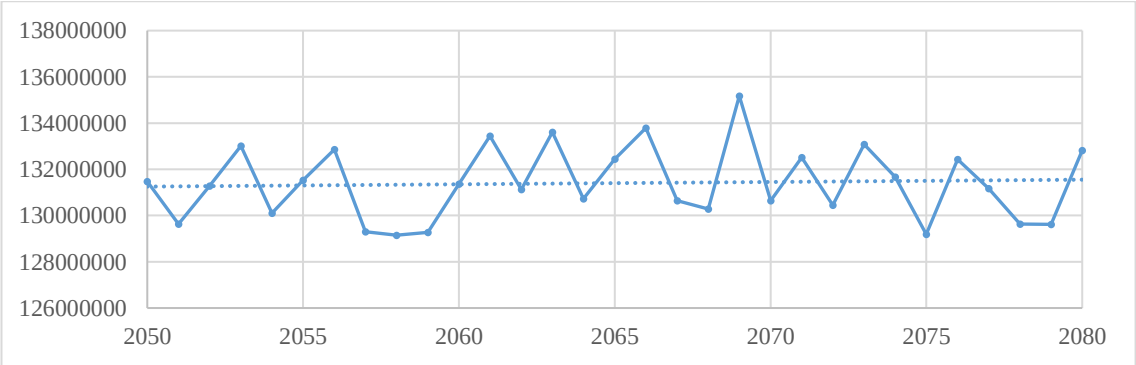

(a) MPI 4.5

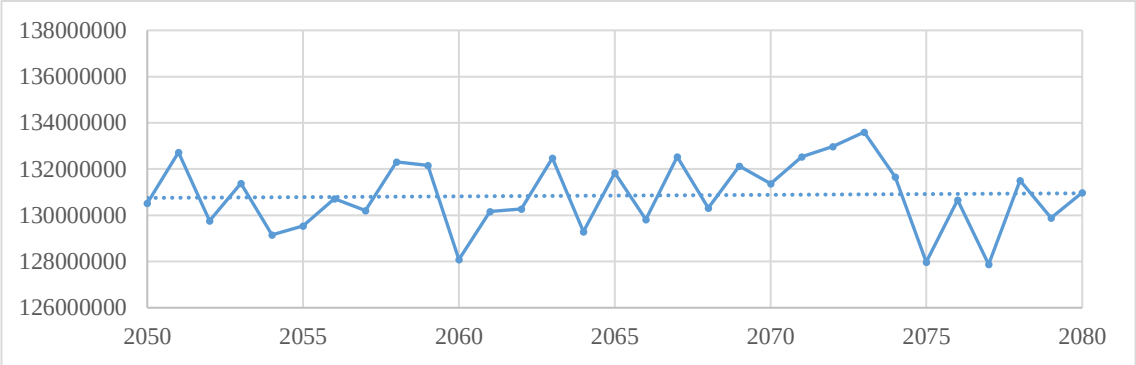

(b) MPI 8.5

Figure 5.60. The prediction of annual electricity production (Kwh) for the 2051 – 2080 interval using (a): MPI 4.5 and (b): MPI 8.5 data.

The prediction of the AEP using the MPI model with 8.5 and 4.5 scenarios is shown in Figure 5.60. The AEPs range between 128,000,000 Kwh and 135,000,000 Kwh. The highest production values resulted in the years of 2069 and 2073 for MPI 4.5 and MPI 8.5 scenarios with values near 135,100,00 and 134,000,000 Kwh, respectively. On the other hand, the lowest production values resulted in 2075 and 2077 for the MPI 4.5 and MPI 8.5 scenarios, respectively.

5.4. Summary

This chapter discussed the results of the three main rephrase processes which are Homogeneity test, Mann Kandell test and Machine Learning Techniques for predicting the energy production. The results were shown for two intervals, from 2018 to 2050 and from 2051 to 2080. The simulation processes applied for six HEPP. Three HEPPs were from Yesilirmak Basin (Almus HEPP, Suat Ugurlu HEPP and Hasan Ugurlu HEPP) and Three HEPPs were from Kizilirmak Basin (Hirfanli HEPP, Kesikkopru HEPP and Kapulukaya HEPP). In every HEPP, the range of the AEPs were very close to each other. The results showed various increasing and decreasing based on the GCM and the RCP. Chapter 6 will present in detail the differences between the results.

6. ANALYSIS AND DISCUSSIONS

This chapter focuses on the annual results for the full interval from 2018 to 2080. It gives more comparisons between the models and the scenarios 4.5 and 8.5 to understand the impact of climate change on the HEPPs of the studied basins.

6.1. Almus HEPP

This section is focused on the annual results of the Almus HEPP and the differences between historical data and GCM results of energy production. Figures 6.1, 6.2 and 6.3 show the AEP of the GFDL, HadGEM and MPI models for scenario RCP 4.5. The three figures show an increasing in energy production with time, but the increase of the HadGEM model is more than that of the MPI and GFDL models as shown in the figures.

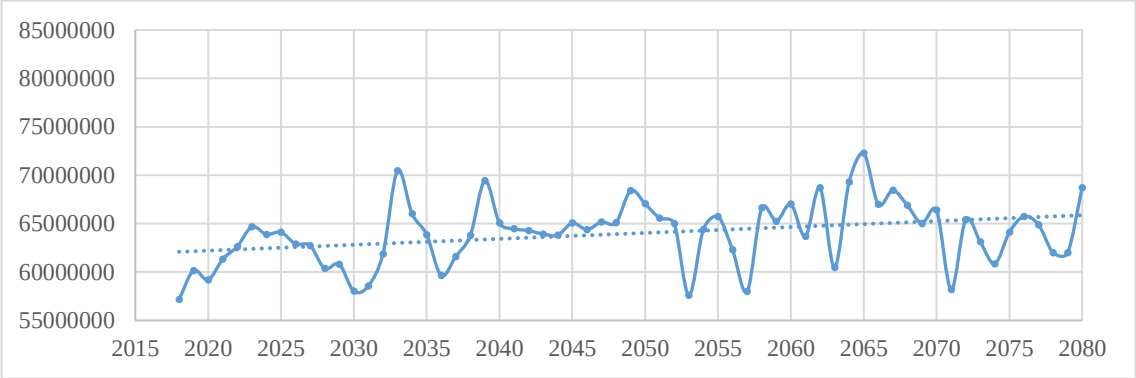

Figure 6.1. The annual production of electricity (Kwh) results of Almus HEPP using GFDL 4.5 model.

Despite some decreases in a few years, the energy production increases for the interval 2018 to 2080. The range of the annual energy is between 57,000,000 to 72,000,000 Kwh as shown in Figure 6.1.

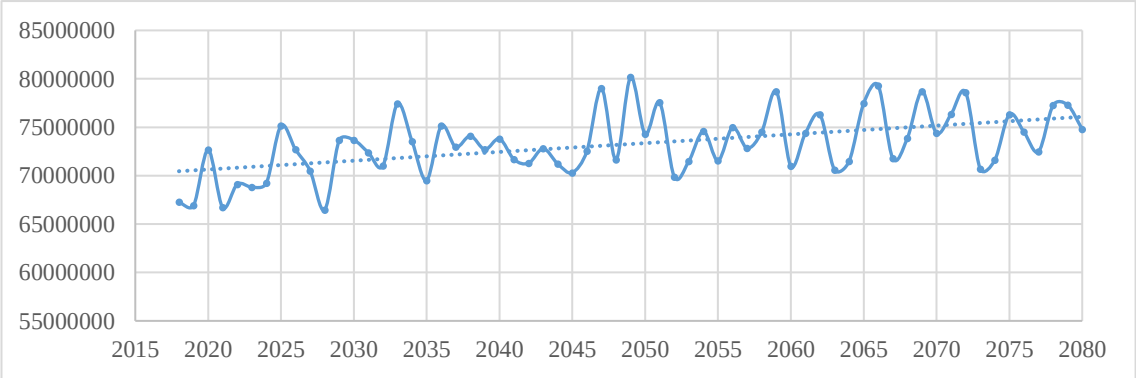

Figure 6.2. The annual production of electricity (Kwh) results of Almus HEPP using HadGEM 4.5 model.

The energy production increases using the HadGEM temperature and precipitation data for the interval from 2018 to 2080 with a range from 66,900,000 to 80,000,000 Kwh as shown in Figure 6.2.

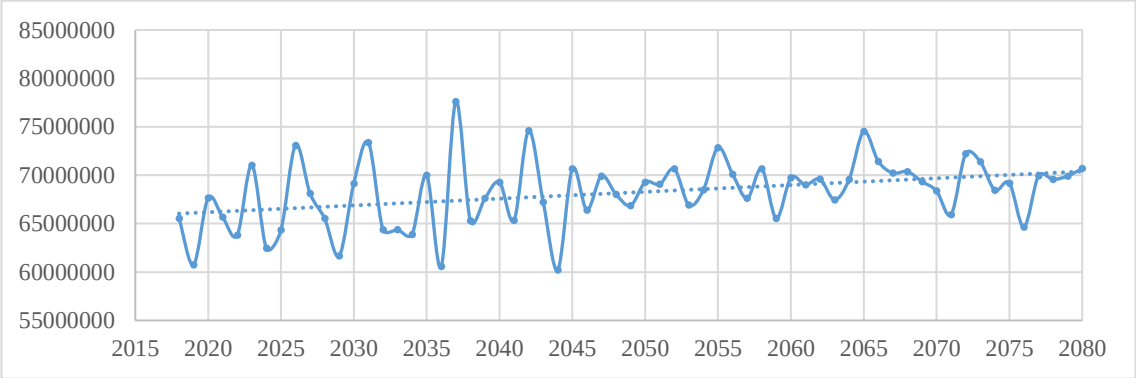

Figure 6.3. The annual production of electricity (Kwh) results of Almus HEPP using MPI 4.5 model.

The energy production increases for the interval from 2018 to 2080 with a range from 60,000,000 to 77,000,000 Kwh as shown in Figure 6.3.

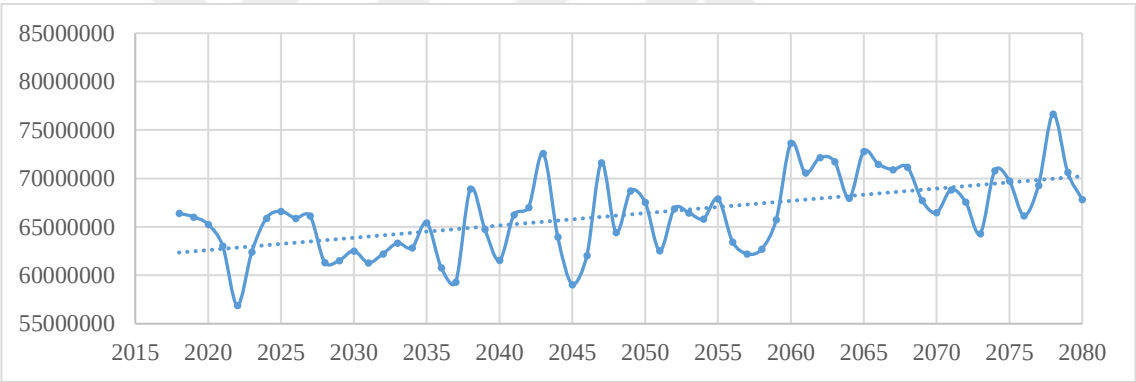

Figure 6.4. The annual production of electricity (Kwh) results of Almus HEPP using GFDL 8.5 model.

The prediction of the AEP increases using the GFDL precipitation and temperature data for 8.5 scenario as shown in Figure 6.4. The range of the AEPs are between 56,900,000 Kwh and 76,600,000 Kwh.

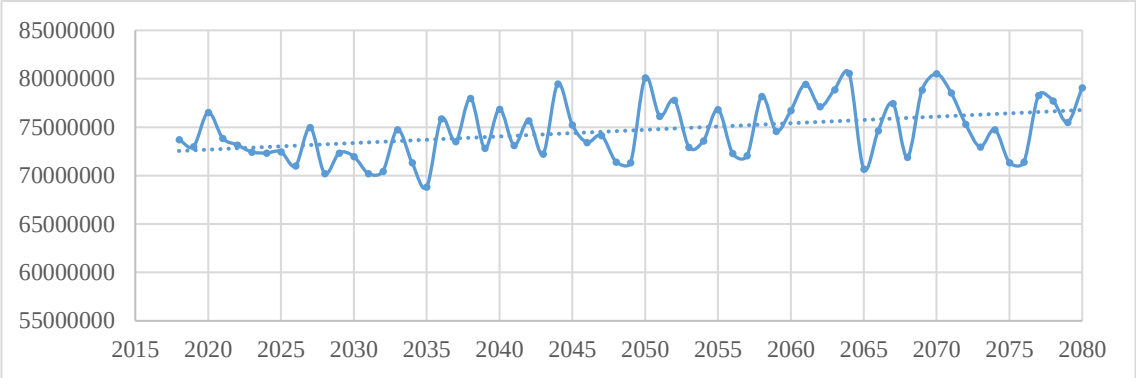

Figure 6.5. The annual production of electricity (Kwh) results of Almus HEPP using HadGEM 8.5 model.

The prediction of the AEP increases using the HadGEM precipitation and temperature data for 8.5 scenario as shown in Figure 6.5. The range of the AEPs are between 68,000,000 Kwh and 80,500,000 Kwh.

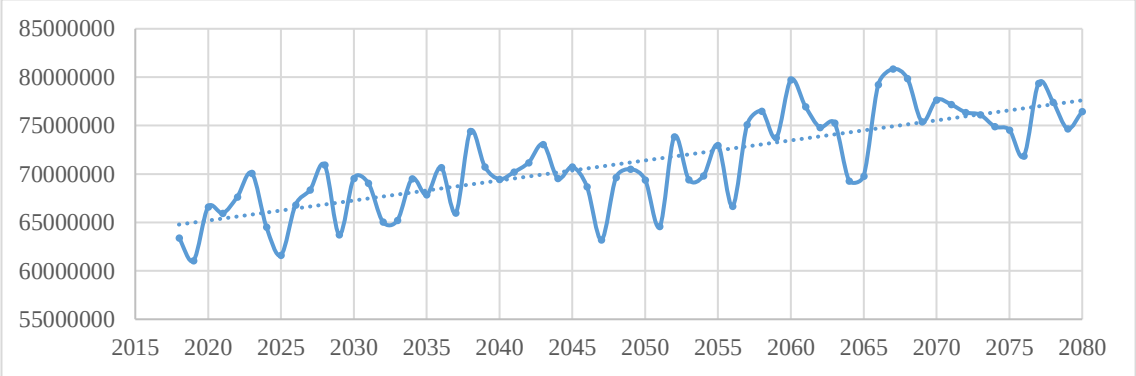

Figure 6.6. The annual production of electricity (Kwh) results of Almus HEPP using MPI 8.5 model.

The prediction of the AEP increases using the MPI precipitation and temperature data for 8.5 scenario as shown in Figure 6.6. The AEP range is between 61,000,000 Kwh and 80,800,000 Kwh.

Table 6.1. The mean annual production of historical data and predicted energy production of Almus HEPP

GCM	Historical Data	2018 - 2050	2051-2080	Percentage of change for 2018 to 2050 results	Percentage of change for 2051 to 2080 results
GFDL 4.5	89,296,043.5	63,328,643.4	64,685,436.2	-29.1%	-27.6%
GFDL 8.5		64,358,033.8	68,413,924.8	-27.9%	-23.4%
HadGEM 4.5		72,133,914.4	74,508,308.1	-19.2%	-16.6%
HadGEM 8.5		73,546,854.3	75,877,618.5	-17.6%	-15.0%
MPI 4.5		67,087,275.5	69,454,007.7	-24.9%	-22.2%
MPI 8.5		68,021,430.3	74,689,133.4	-23.8%	-16.4%

The differences between the mean annual predicted production and the historical production were estimated as shown in Table 6.1. Despite the increase of the predicted energy production in all GCMs and scenarios of the intervals (From 2018 to 2050 and from 2051 to 2080), it decreased based on the historical data with various percentages from 17.6% to 29.1% for interval between 2018 to 2050 and from 15% to 27.6% for interval between 2051 to 2080. The table showed that the mean annual predicted production of RCP 8.5 scenario results higher than the mean values of RCP 4.5 scenarios. The table showed that the mean annual predicted production of 2018 to 2050 interval results lower than the mean values of mean annual predicted production of 2051 to 2080.

The prediction of AEP was estimated for 8.5 and 4.5 scenarios using GCMs as shown in Figures 6.1, 6.2, 6.3, 6.4, 6.5 and 6.6. All the GCMs results show that the highest values of energy production were in the sudden raining season in Almus's location (July and August) and the lowest energy production were in the month of April as shown in Figure 6.7. The trendlines of predicted energy are very close to the near range that indicates the prediction of energy productions is very close based on the prediction of temperature and precipitation values.

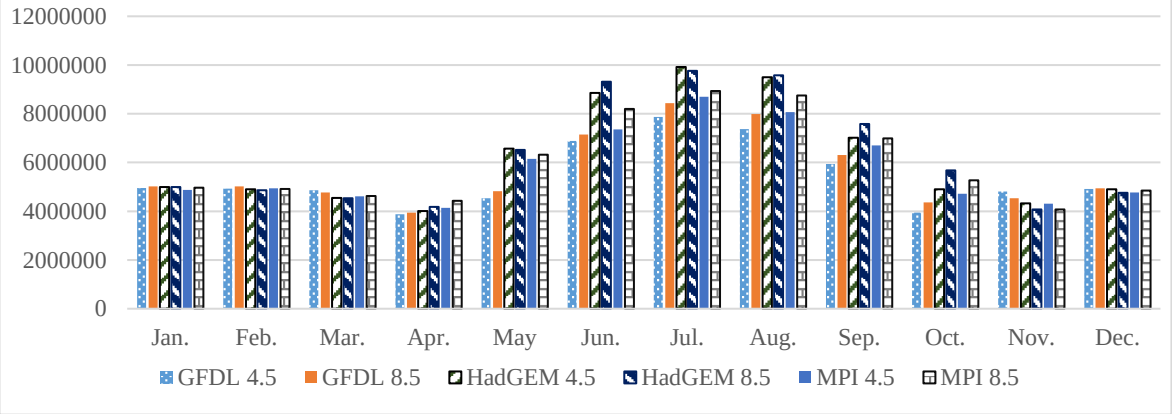

Figure 6.7. The mean monthly production of GCM predicted energy production of Almus HEPP.

The energy production in the GFDL 4.5 has increased slower than the GFDL 8.5 as shown in Figures 6.1 and 6.4. The range of values in the HadGEM 8.5 and HadGEM 4.5 are very near to each other as shown in Figures 6.2 and 6.5. HadGEM results show a higher value than the other GCMs in the peak raining season (July and August). Although all the GCMs showed an increased trend of energy production, this trend was different between the models.

In Figures 6.3 and 6.6, The prediction of energy production using the MPI model shows that the values decrease with time for the 4.5 scenario in comparison to the 8.5 scenario. In RCP 4.5, the results show a lower trend increase in comparison to the results of RCP 8.5. This means that the trend of the 4.5 scenario is lower than the trend of the 8.5 scenario. Although there are differences between temperature and precipitation data for GCMs for Almus HEPP, the reults of the prediction of electricity are very near to each other.

6.2. Hasan Ugurlu HEPP

The energy production of Hasan Ugurlu HEPP had been predicted in the previous chapter and this section designates to show the results and the differences between the historical data and GCM results of energy production. Figures 6.8, 6.9 and 6.10 show the AEP of the GFDL, HadGEM and MPI models for scenarios RCP 4.5. The three figures show decreasing in energy production with same behaviour.

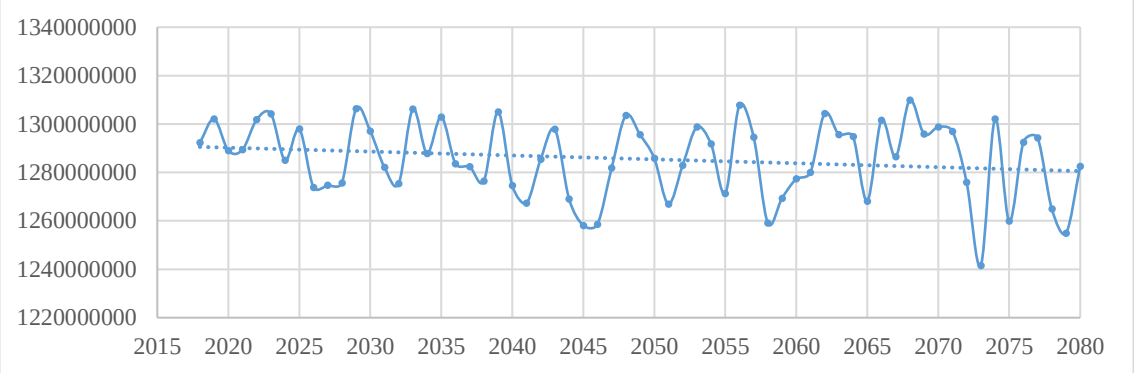

Figure 6.8. The annual production of electricity (Kwh) results of Hasan Ugurlu HEPP using GFDL 4.5 model.

The energy production curve shows a decrease with time for the interval from 2018 to 2080. The annual energy range is between 1240,000,000 to 1310,000,000 Kwh as shown in Figure 6.8.

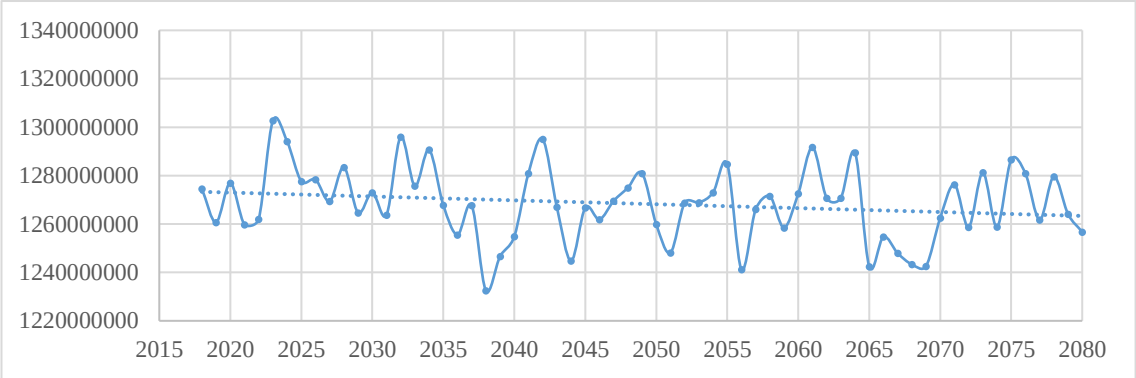

Figure 6.9. The annual production of electricity (Kwh) results of Hasan Ugurlu HEPP using HadGEM 4.5 model.

The energy production increases with time using the HadGEM temperature and precipitation data for the interval from 2018 to 2080 with a range between 1232,000,000 to 1302,000,000 Kwh as shown in Figure 6.9.

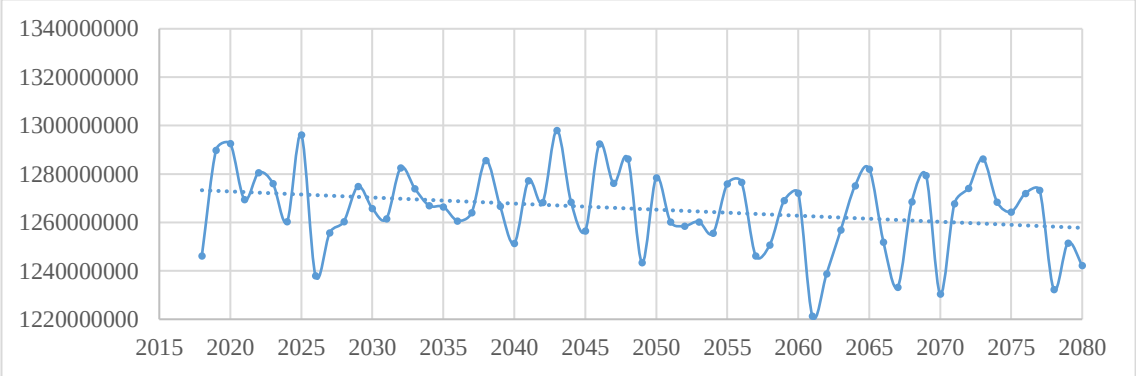

Figure 6.10. The annual production of electricity (Kwh) results of Hasan Ugurlu HEPP using MPI 4.5 model.

The energy production increases using the MPI 4.5 Data of precipitation and temperature of the interval from 2018 to 2080 with a range between 1221,000,000 to 1300,000,000 Kwh as shown in Figure 6.10. Figures 6.11, 6.12, and 6.13 show the AEP of the GFDL, HadGEM and MPI models for scenarios RCP 8.5.

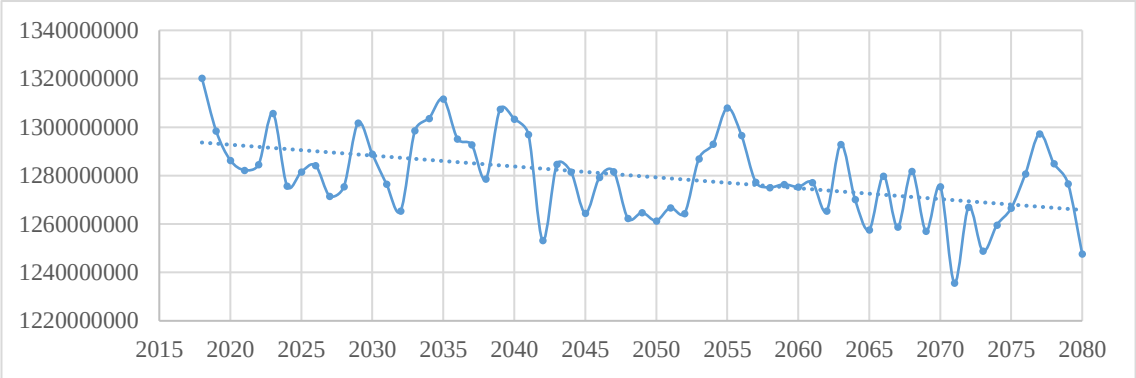

Figure 6.11. The annual production of electricity (Kwh) results of Hasan Ugurlu HEPP using GFDL 8.5 model.

The prediction of the AEP decreases using the GFDL precipitation and temperature data for the 8.5 scenario as shown in Figure 6.11. The AEPs range is between 1235,000,000 and 1320,000,000 Kwh.

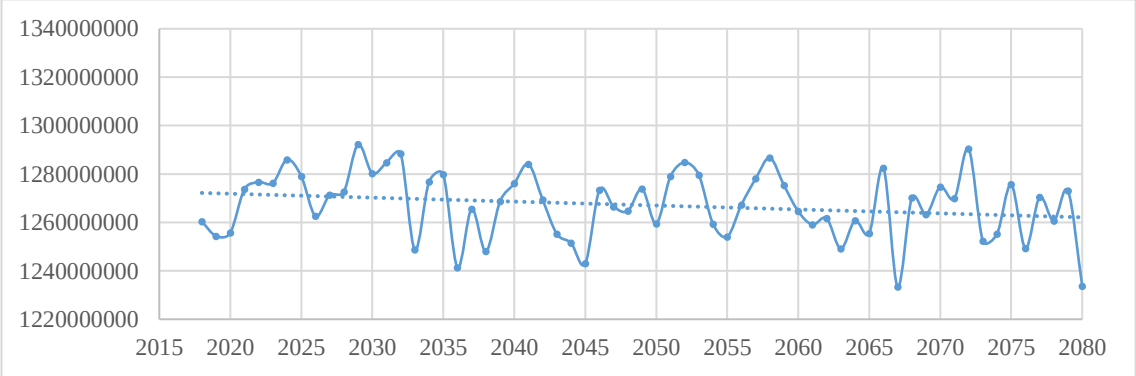

Figure 6.12. The annual production of electricity (Kwh) results of Hasan Ugurlu HEPP using HadGEM 8.5 model.

The prediction of the AEP decreases using the HadGEM precipitation and temperature data for the 8.5 scenario as shown in Figure 6.12. The AEPs range is between 1233,000,000 and 1292,000,000 Kwh.

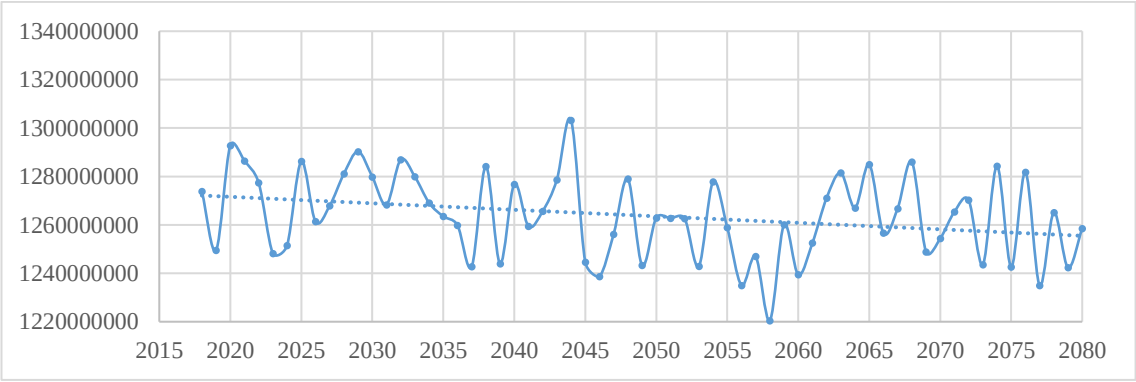

Figure 6.13. The annual production of electricity (Kwh) results of Hasan Ugurlu HEPP using MPI 8.5 model.

The prediction of the energy production decreases using the MPI precipitation and temperature data for the 8.5 scenario as shown in Figure 6.13. The AEPs range is between 1220,000,000 and 1303,000,000 Kwh.

Table 6.2. The mean annual production of the historical data and predicted energy production of Hasan Ugutlu HEPP

GCM	Historical Data	2018 - 2050	2051-2080	Percentage of change for 2018 to 2050 results	Percentage of change for 2051 to 2080 results
GFDL 4.5	1,268,567,732.9	1,286,932,381.9	1,284,035,114.6	1.4%	1.2%
GFDL 8.5		1,285,482,820.2	1,273,388,623.1	1.3%	0.4%
HadGEM 4.5		1,270,610,683.6	1,265,807,663.9	0.2%	-0.2%
HadGEM 8.5		1,268,515,121.6	1,265,665,916.5	0%	-0.2%
MPI 4.5		1,270,678,775.2	1,259,888,420.1	0.2%	-0.7%
MPI 8.5		1,268,304,120.3	1,258,875,363.7	0%	-0.8%

The differences between the mean annual predicted production and the historical production of Hasan Ugurlu's Data were estimated as shown in Table 6.2. The predicted energy production in all GCMs resulted based on the historical data with various percentages from 0% to 1.4% for interval between 2018 to 2050 and from -0.8% to 1.2% for interval between 2051 to 2080. The table showed that the mean annual predicted production of RCP 4.5 scenario results higher than the mean values of RCP 8.5 scenarios. Beside of that, the table showed that the mean annual predicted production of 2018 to 2050 interval results higher than the mean values of mean annual predicted production of 2051 to 2080.

Figure 6.14 shows the mean monthly production of GCM predicted energy production of Hasan Ugurlu HEPP.

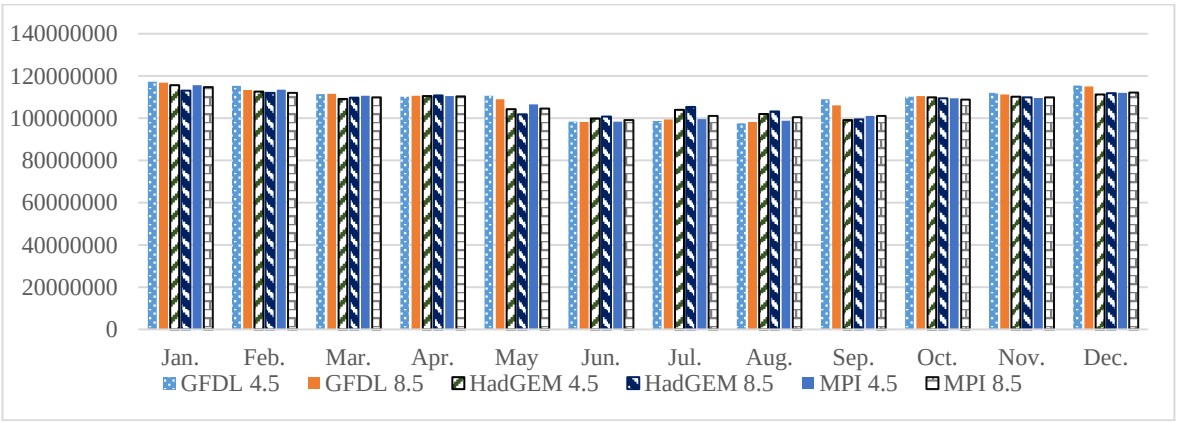

Figure 6.14. The mean monthly production of GCM predicted energy production of Hasan Ugurlu HEPP.

The annual prediction of the energy production was estimated for the 4.5 and 8.5 scenarios using GCMs as shown in Figures 6.8, 6.9, 6.10, 6.11, 6.12 and 6.13. All the GCMs results show that the peak values of energy production were in the winter season (Janurary and February), and the lowest values were in the month of June as shown in Figure 6.14. The trendlines are very close to the same range which indicates that the prediction of energy productions is very close based on the prediction of temperature and precipitation values. All prediction results using GCM data showed for a decrease of energy production with time. The energy production in the GFDL 8.5 has decreased faster than the GFDL 4.5 as shown in Figures 6.8 and 6.11. The range of values in the HadGEM 8.5 and HadGEM 4.5 are very near to each other as shown in figures 6.9 and 6.12. In Figures 6.10 and 6.13, The prediction of energy production using the MPI model shows that the values decrease with time for the RCP 8.5 and RCP 4.5 scenarios.

6.3. Suat Ugurlu HEPP

Section 6.3 focuses on the annual results of Suat Ugurlu HEPP and the differences between historical data and GCM results of energy production. Figures 6.15, 6.16 and 6.17 show the AEP of GFDL, HadGEM and MPI models for the scenario RCP 4.5. The three figures show an increase with time for the energy production but the increase of the HadGEM model is more than that of the MPI and GFDL models as shown in the below figures.

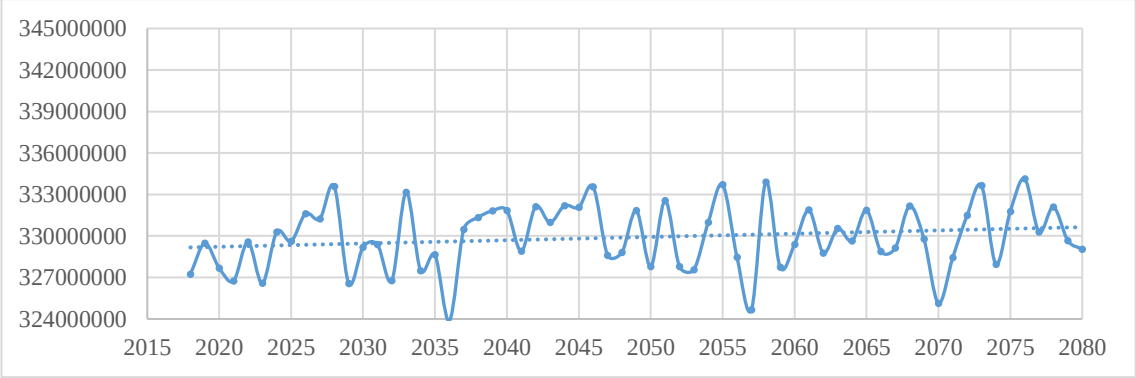

Figure 6.15. The annual production of electricity (Kwh) results of Suat Ugurlu HEPP using GFDL 4.5 model.

The AEP increases with time for the interval from 2018 to 2080. The range of the annual energy is between 324,000,000 to 333,800,000 Kwh as shown in Figure 6.15.

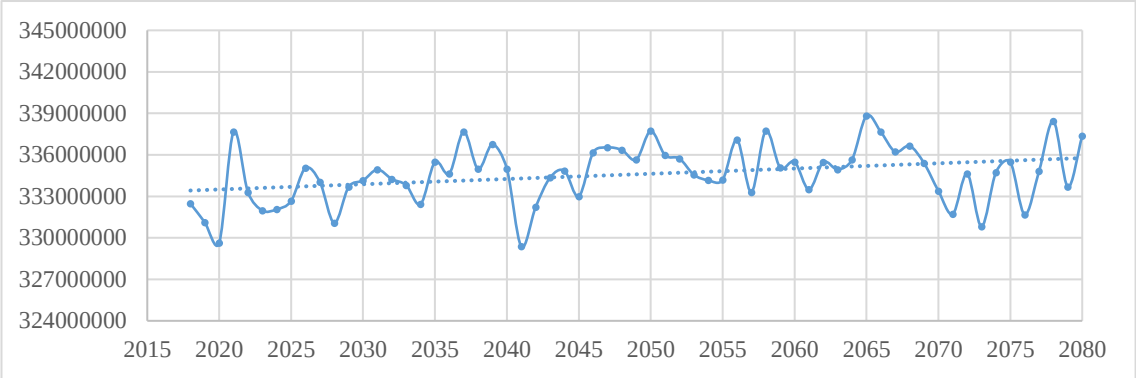

Figure 6.16. The annual production of electricity (Kwh) results of Suat Ugurlu HEPP using HadGEM 4.5 model.

The energy production increases with time using the HadGEM temperature and precipitation data for the interval from 2018 to 2080 with a range between 329,300,000 to 339,000,000 Kwh as shown in Figure 6.16.

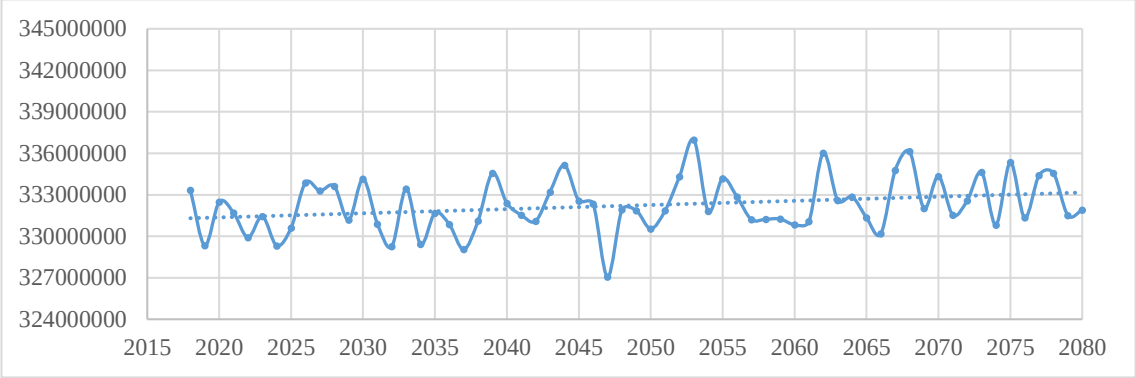

Figure 6.17. The annual production of electricity (Kwh) results of Suat Ugurlu HEPP using MPI 4.5 model.

The energy production increases with time for the interval from 2018 to 2080 with a range between 327,000,000 to 336,900,000 Kwh as shown in Figure 6.17.

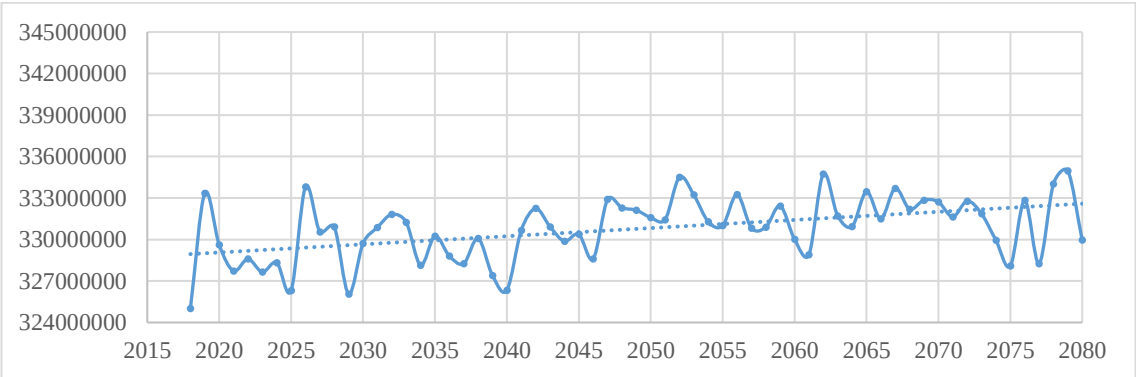

Figure 6.18. The annual production of electricity (Kwh) results of Suat Ugurlu HEPP using GFDL 8.5 model.

The prediction of the AEP increases with time using the HadGEM precipitation and temperature data for the 8.5 scenario as shown in Figure 6.18. The range of the AEPs are between 325,000,000 and 334,900,000 Kwh.

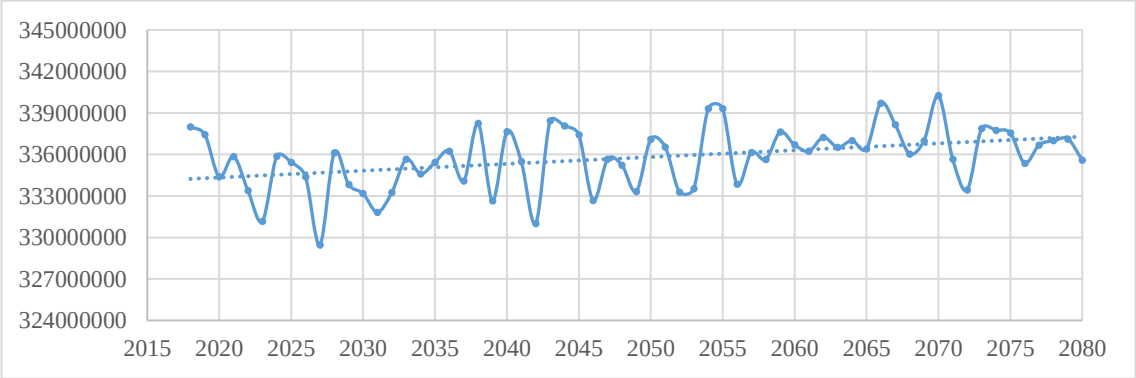

Figure 6.19. The annual production of electricity (Kwh) results of Suat Ugurlu HEPP using HadGEM 8.5 model.

The range of the AEPs increases using the MPI precipitation and temperature data for the 8.5 scenario between 329,500,000 Kwh and 340,200,000 Kwh as shown in Figure 6.19.

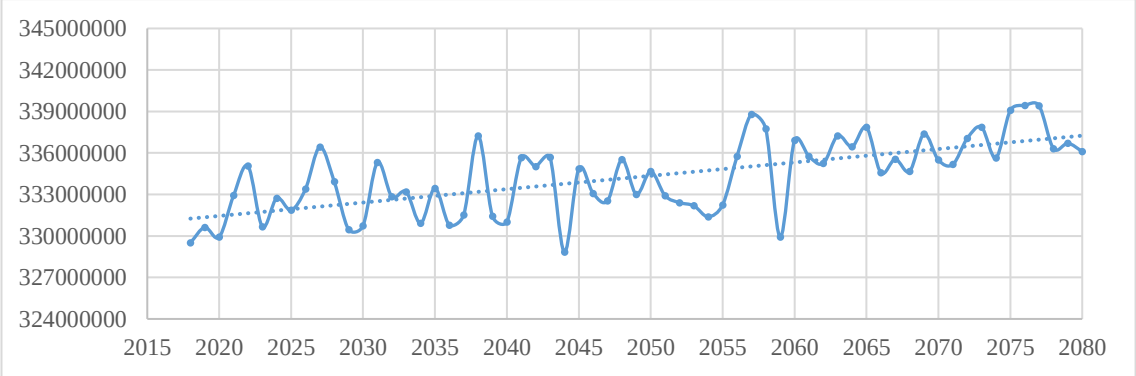

Figure 6.20. The annual production of electricity (Kwh) results of Suat Ugurlu HEPP using MPI 8.5 model.

The prediction of the AEP increases with time using the MPI precipitation and temperature data for 8.5 scenario as shown in Figure 6.20. The AEPs range is between 328,800,000 and 339,400,000 Kwh.

Table 6.3. The mean annual of the historical data and predicted energy production of Suat Ugutlu HEPP

GCM	Historical Data	2018 - 2050	2051-2080	Percentage of change for 2018 to 2050 results	Percentage of change for 2051 to 2080 results
GFDL 4.5	316,064,295.9	329,728,152.1	330,099,797.8	4.3%	4.4%
GFDL 8.5		329,771,504.4	331,865,362.2	4.3%	5.0%
HadGEM 4.5		334,091,139.9	335,147,090.3	5.7%	6.0%
HadGEM 8.5		334,926,653.5	336,687,959.2	6.0%	6.5%
MPI 4.5		331,641,733.2	332,882,772.6	4.9%	5.3%
MPI 8.5		332,869,665.0	335,772,431.9	5.3%	6.2%

The differences between the mean annual predicted production and the historical production were estimated as shown in Table 6.3. The table shows an increase in the predicted energy production in all GCMs and in all scenarios of the predicted intervals (From 2018 to 2050 and from 2051 to 2080), it increased based on the historical data with various percentages from 4.3% to 6% for interval between 2018 to 2050 and from 4.4% to 6.5% for interval between 2051 to 2080. The table showed that the mean annual predicted production of RCP 8.5 scenario results higher than the mean values of RCP 4.5 scenarios (Except the GDFL model in the interval between 2018 to 2050). Beside of that, the table showed that the mean annual predicted production of 2018 to 2050 interval results lower than the mean values of mean annual predicted production of 2051 to 2080.

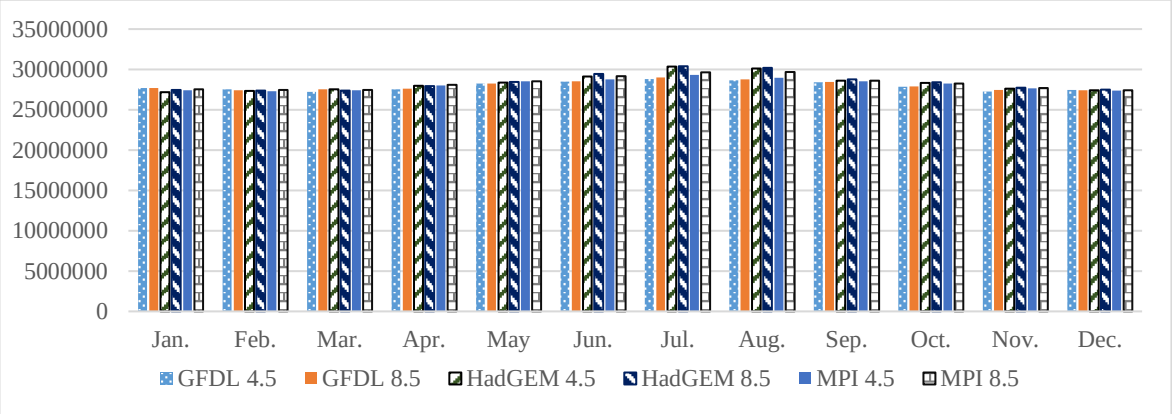

Figure 6.21. The mean monthly production of GCM predicted energy production of Suat Ugurlu HEPP.

The annual prediction of the energy production was estimated for the 4.5 and 8.5 scenarios using GCMs as shown in Figures 6.15, 6.16, 6.17, 6.18, 6.19 and 6.20. All the GCMs results show that the highest values of energy production were in the sudden raining season (July and August) and the lowest values were in the month of January as shown in Figure 6.21. The energy production in the GFDL 8.5 has increased faster

than the GFDL 4.5 as shown in Figures 6.15 and 6.18. HadGEM results show a higher value than the other GCMs in the sudden raining season (July and August). Although all the GCMs showed an increased trend of energy production, this trend was different between the models.

6.4. Hirfanli HEPP

This section focuses on the annual results of Hirfanli HEPP and the differences of historical data and GCM results of energy production. Figures 6.22, 6.23 and 6.24 show the AEP of GFDL, HadGEM and MPI models for scenarios RCP 4.5. The three figures show increase with time for the energy production but the increase of HadGEM model is more than MPI and GFDL models as shown in the below figures.

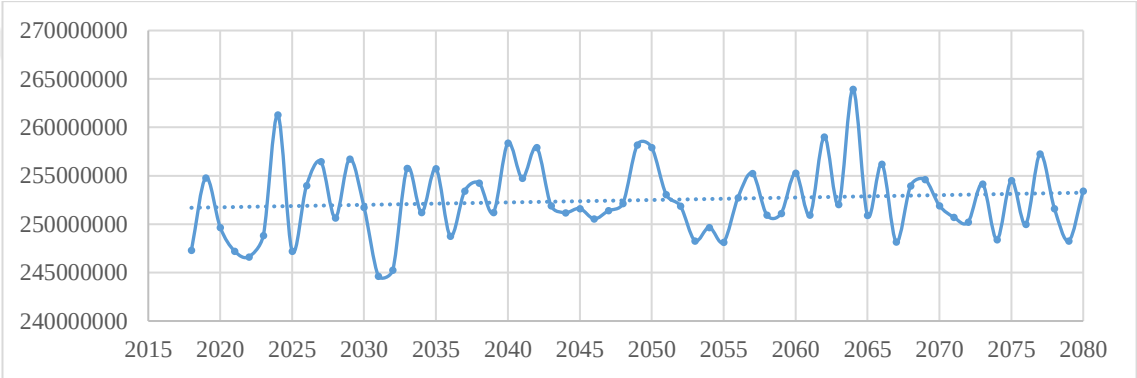

Figure 6.22. The annual production of electricity (Kwh) results of Hirfanli HEPP using GFDL 4.5 model.

The energy production increases with time for the interval from 2018 to 2080. The range of the annual energy starts between 245,000,000 to 264,000,000 Kwh as shown in Figure 6.22.

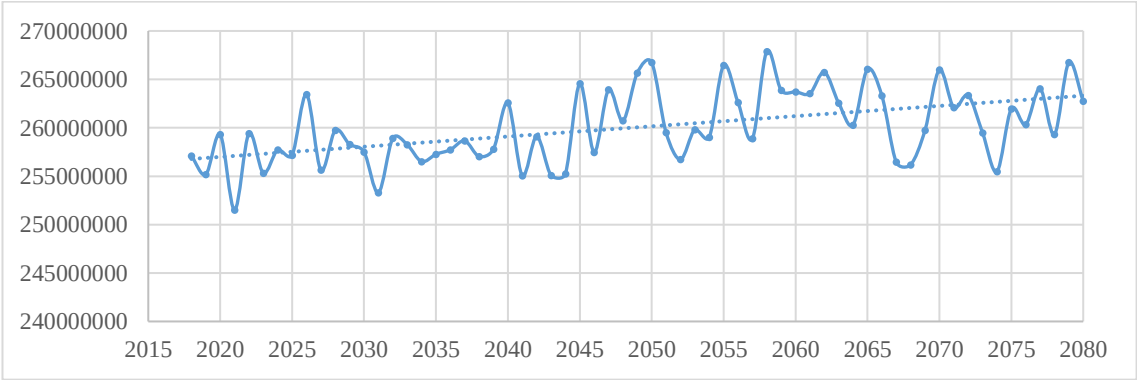

Figure 6.23. The annual production of electricity (Kwh) results of Hirfanli HEPP using HadGEM 4.5 model.

The energy production increases with time using HadGEM temperature and precipitation data for the interval from 2018 to 2080 with range between 251,500,000 to 267,900,000 Kwh as shown in Figure 6.23.

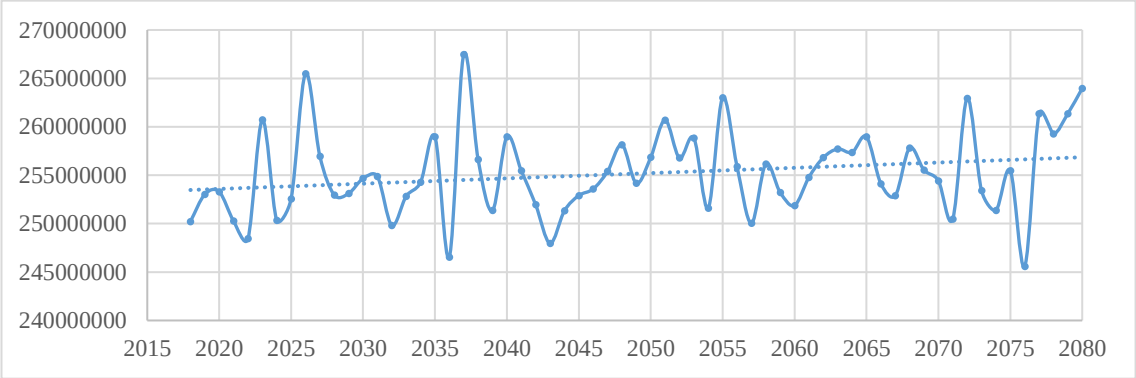

Figure 6.24. The annual production of electricity (Kwh) results of Hirfanli HEPP using MPI 4.5 model.

The energy production increases with time for the interval from 2018 to 2080 with range between 245,000,000 to 267,500,000 Kwh as shown in Figure 6.24.

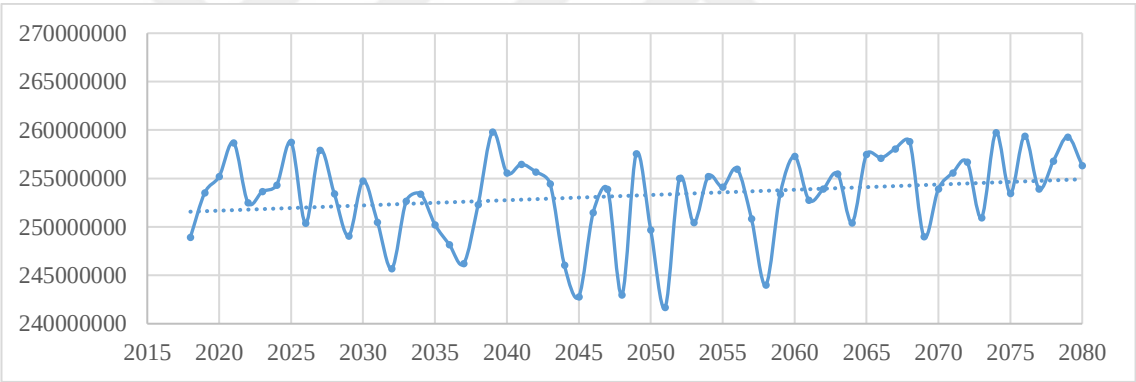

Figure 6.25. The annual production of electricity (Kwh) results of Hirfanli HEPP using GFDL 8.5 model.

The prediction of the AEP increases with time using GFDL precipitation and temperature data for 8.5 scenario as shown in Figure 6.25. The range of the AEPs are between 241,600,000 Kwh and 260,000,000 Kwh.

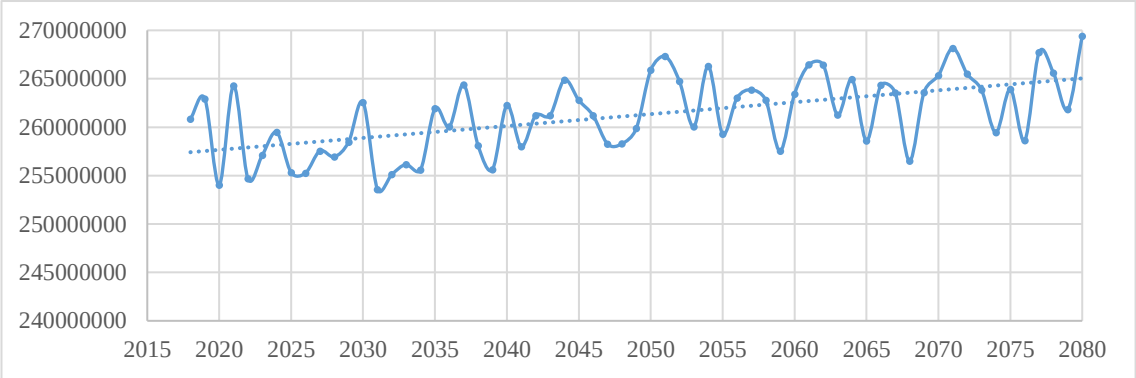

Figure 6.26. The annual production of electricity (Kwh) results of Hirfanli HEPP using HadGEM 8.5 model.

The prediction of the AEP increases with time using HadGEM precipitation and temperature data for 8.5 scenario as shown in Figure 6.26. The range of the AEPs are between 253,500,000 Kwh and 269,500,000 Kwh.

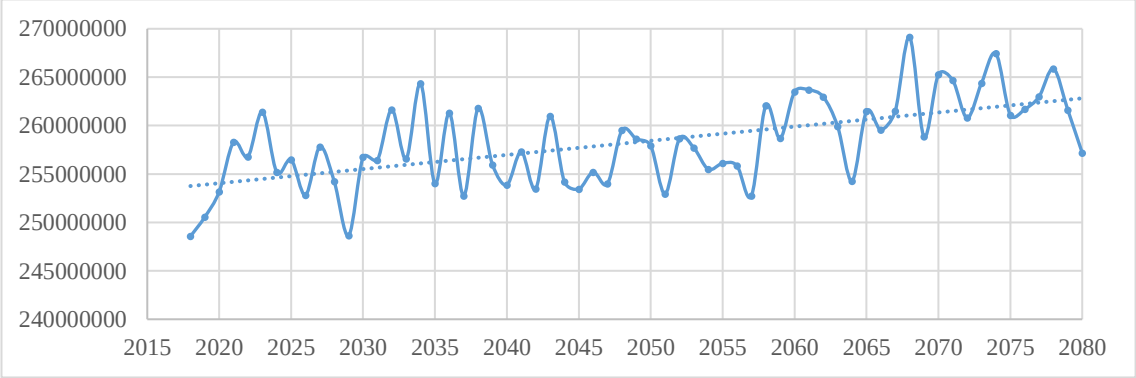

Figure 6.27. The annual production of electricity (Kwh) results of Hirfanli HEPP using MPI 8.5 model.

The prediction of the AEP increases with time using MPI precipitation and temperature data for 8.5 scenario as shown in Figure 6.27. The range of the AEPs are between 248,500,000 Kwh and 269,100,000 Kwh.

Table 6.4. The mean annual of historical data and predicted energy production of Hirfanli HEPP

GCM	Historical Data	2018 - 2050	2051-2080	Percentage of change for 2018 to 2050 results	Percentage of change for 2051 to 2080 results
GFDL 4.5	264,993,650.3	252,394,032.6	252,563,029.1	-4.8%	-4.7%
GFDL 8.5		252,331,093.0	254,245,073.2	-4.8%	-4.1%
HadGEM 4.5		258,457,395.6	261,799,319.7	-2.5%	-1.2%
HadGEM 8.5		259,207,675.5	263,447,935.2	-2.2%	-0.6%
MPI 4.5		254,291,668.0	256,129,007.0	-4.0%	-3.3%
MPI 8.5		256,185,270.0	260,605,583.2	-3.3%	-1.7%

The differences between the mean annual predicted production and the historical production were estimated as shown in Table 6.4. Despite the increase of the predicted energy production in all GCMs and scenarios of the intervals (From 2018 to 2050 and from 2051 to 2080), it decreased based on the historical data with various percentages from 2.2% to 4.8% for interval between 2018 to 2050 and from 0.6% to 4.7% for interval between 2051 to 2080. The table showed that the mean annual predicted production of RCP 8.5 scenario results higher than the mean values of RCP 4.5 scenarios (Except the GDFL model in the interval between 2018 to 2050). Beside of that, the table showed that the mean annual predicted production of 2018 to 2050 interval results lower than the mean values of mean annual predicted production of 2051 to 2080.

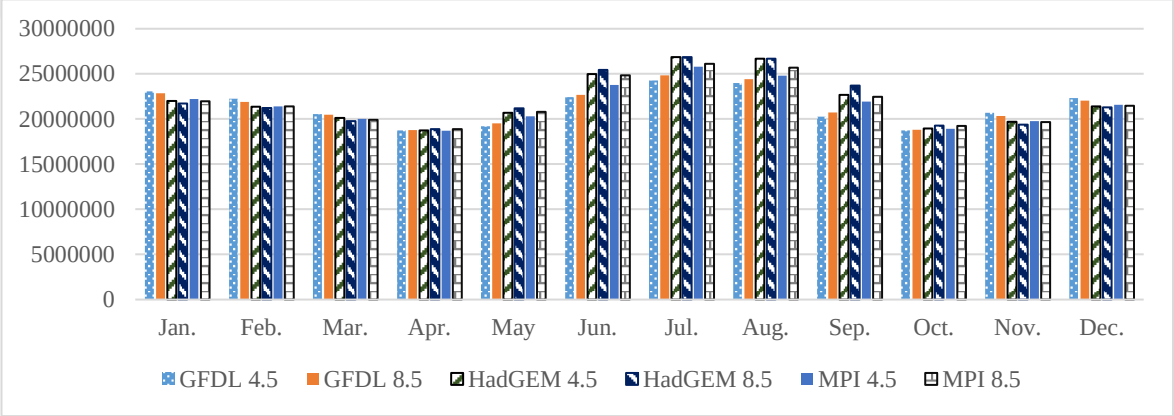

Figure 6.28. The mean monthly production of GCM predicted energy production of Hirfanli HEPP.

The prediction of AEP was estimated for 8.5 and 4.5 scenarios using GCMs as shown in Figures 6.22, 6.23, 6.24, 6.25, 6.26 and 6.27. All GCMs results show that the highest values of energy production were in the sudden raining season (July and August) and the lowest values were in the month of April as shown in Figure 6.28.

The energy production in GFDL 4.5 and GFDL 8.5 has increased in the same level as shown in figures 6.22 and 6.25. The range of values in the HadGEM 8.5 and HadGEM 4.5 are very close to each other as shown in figures 6.23 and 6.26. HadGEM results show a higher value than the other GCMs in the sudden raining season (July and August). Although all the GCMs showed an increased trend of energy production, this tren d was different between the models.

In Figures 6.24 and 6.27, The prediction of energy production using MPI model

shows that the values increase for the 8.5 scenario in comparison to the 4.5 scenario.

6.5. Kesikkopru HEPP

This section focuses on the annual results of Kesikkopru HEPP and the differences of historical data and GCM results of energy production. Figures 6.28, 6.29 and 6.30 show the AEP of GFDL, HadGEM and MPI models for scenarios RCP 4.5. The three figures show increase with time for the energy production but the increase of HadGEM model is more than MPI and GFDL models as shown in the below figures.

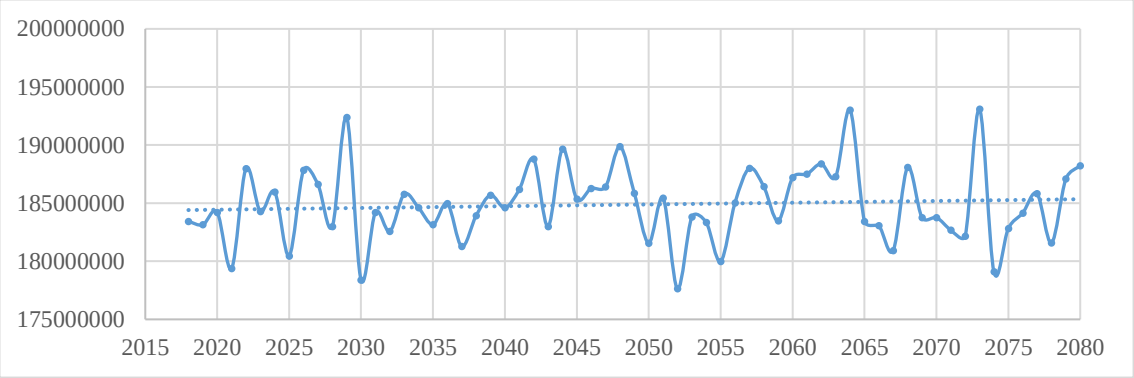

Figure 6.29. The annual production of electricity (Kwh) results of Kesikkopru HEPP using GFDL 4.5 model.

Despite of some dereases in few years, the energy production increases with time for the interval from 2018 to 2080. The range of the annual energy starts between 177,600,000 to 193,100,000 Kwh as shown in Figure 6.29.

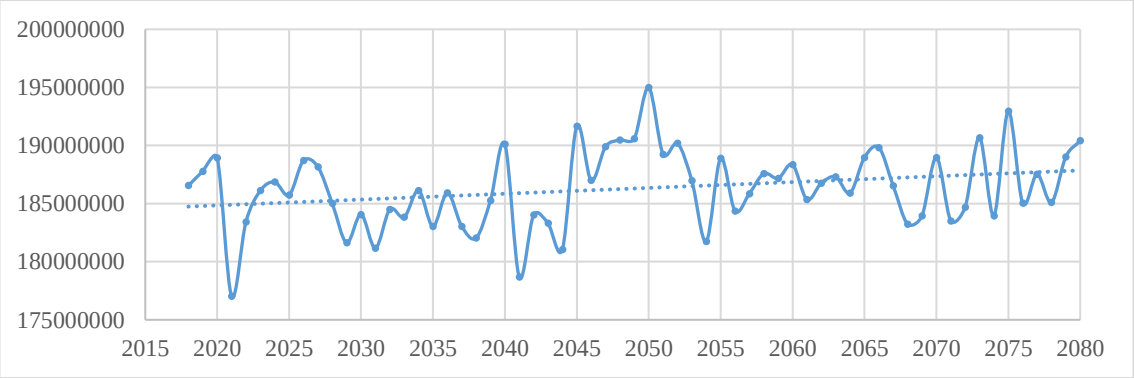

Figure 6.30. The annual production of electricity (Kwh) results of Kesikkopru HEPP using HadGEM 4.5 model.

The energy production increases with time using HadGEM temperature and precipitation data for the interval from 2018 to 2080 with range between 177,000,000 to 195,000,000 Kwh as shown in Figure 6.30.

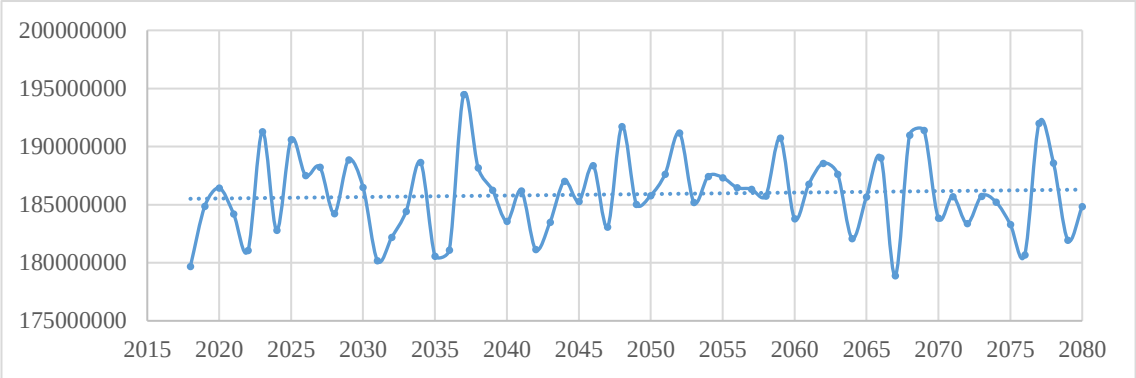

Figure 6.31. The annual production of electricity (Kwh) results of Kesikkopru HEPP using MPI 4.5 model.

The energy production increases with time for the interval from 2018 to 2080 with range between 60,000,000 to 77,000,000 Kwh as shown in Figure 6.31.

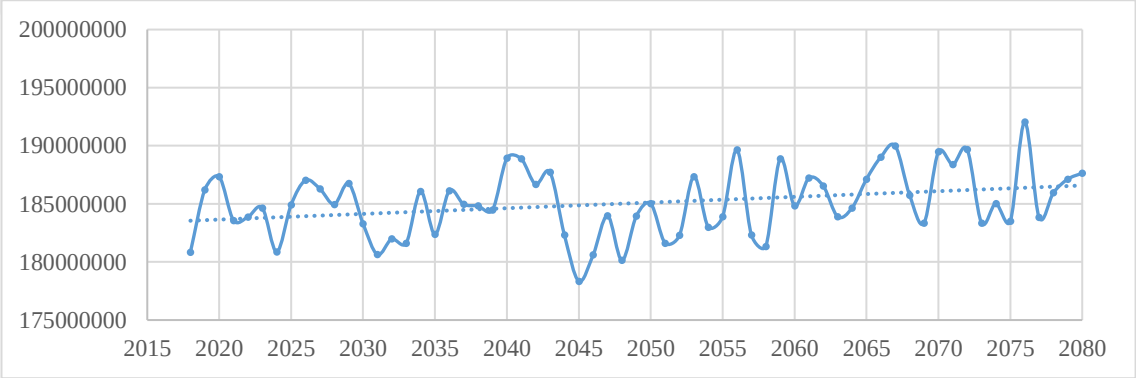

Figure 6.32. The annual production of electricity (Kwh) results of Kesikkopru HEPP using GFDL 8.5 model.

The prediction of the AEP increases with time using the GFDL precipitation and temperature data for 8.5 scenario as shown in Figure 6.32. The range of the AEPs are between 178,400,000 Kwh and 192,000,000 Kwh.

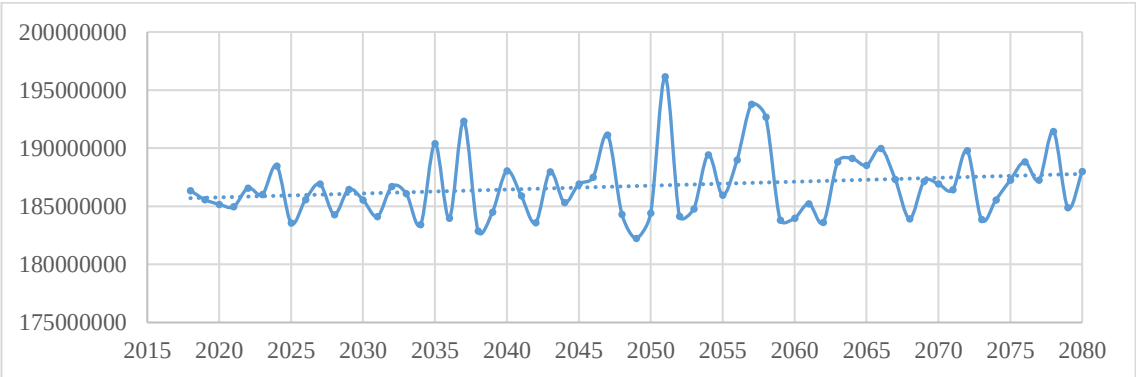

Figure 6.33. The annual production of electricity (Kwh) results of Kesikkopru HEPP using HadGEM 8.5 model.

The prediction of the AEP increases with time using HadGEM precipitation and

temperature data for 8.5 scenario as shown in Figure 6.33. The range of the AEPs are between 182,200,000 Kwh and 196,100,000 Kwh.

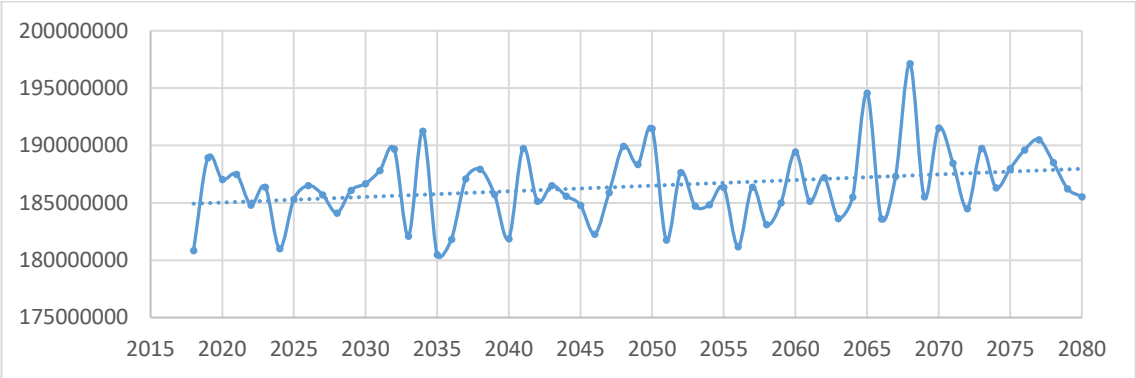

Figure 6.34. The annual production of electricity (Kwh) results of Kesikkopru HEPP using MPI 8.5 model.

The prediction of the AEP increases with time using MPI precipitation and temperature data for 8.5 scenario as shown in Figure 6.34. The range of the AEPs are between 180,000,000 Kwh and 197,150,000 Kwh.

Table 6.5. The mean annual of Hitorical data and predicted energy production of Kesikkopru HEPP

GCM	Historical Data	2018 - 2050	2051-2080	Percentage of change for 2018 to 2050 results	Percentage of change for 2051 to 2080 results
GFDL 4.5	173,406,404.5	184,872,262.4	184,875,541.3	6.6%	6.6%
GFDL 8.5		184,251,201.1	185,961,291.2	6.3%	7.2%
HadGEM 4.5		185,663,854.0	187,004,448.1	7.1%	7.8%
HadGEM 8.5		185,980,732.2	187,588,698.3	7.3%	8.2%
MPI 4.5		185,551,610.5	186,276,343.9	7.0%	7.4%
MPI 8.5		185,964,752.2	186,978,948.3	7.2%	7.8%

The differences between the mean anual predicted production and the historical production were estimated as shown in Table 6.5. As a result of the increasing of the predicted energy production in all GCMs and scenarios of the predicted intervals (From 2018 to 2050 and from 2051 to 2080), it increased based on the historical data with various percentages from 6.3% to 7.3% for interval between 2018 to 2050 and from 6.6% to 8.2% for interval between 2051 to 2080. The table showed that the mean anual predicted production of RCP 8.5 results are higher than the mean values of RCP 4.5 scenarios (Except the GDFL model in the interval between 2018 to 2050). Beside of that, the table showed that the mean annual predicted production of 2018 to 2050 interval results lower than the mean values of mean annual predicted production of 2051 to 2080 (Except the GDFL model result of RCP 4.5).

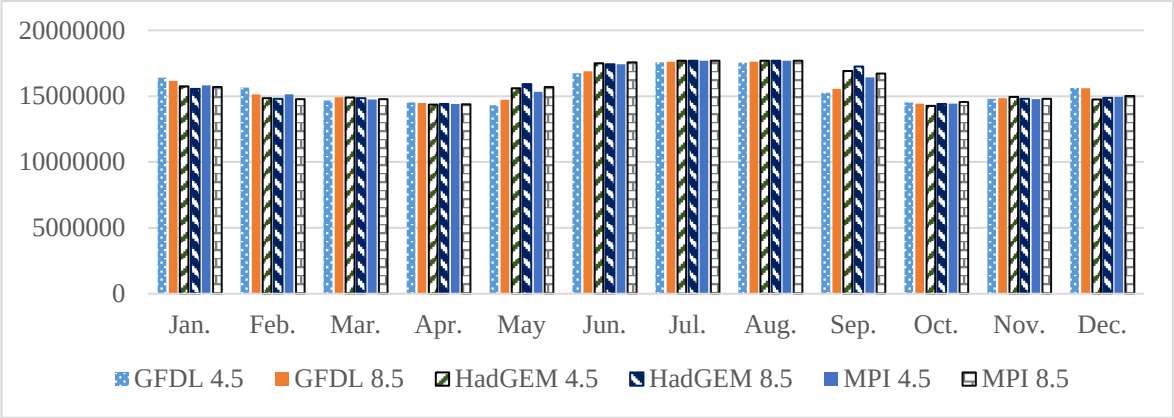

Figure 6.35. The mean monthly production of GCM predicted energy production of Kesikkopru HEPP.

The prediction of AEP was estimated for 8.5 and 4.5 scenarios using GCMs as shown in Figures 6.29, 6.30, 6.31, 6.32, 6.33 and 6.34. All GCMs results show that the highest values of energy production were in the sudden raining season (July and August) and the lowest values were in the month of April as shown in Figure 6.35. The trendlines are very close to the same range which indicates that the prediction of energy productions is very close based on the prediction of temperature and precipitation values.

The energy production in the GFDL 4.5 has decreased slower than the GFDL 8.5 as shown in figures 6.29 and 6.32. The range of values in the HadGEM 4.5 and HadGEM 8.5 are very near to each other as shown in figures 6.30 and 6.33.

In Figures 6.31 and 6.34, The prediction of energy production using MPI model shows that the values decrease with time for the 4.5 scenario in comparison to the 8.5 scenario. Although there are differences between temperature and precipitation data for GCMs, the prediction productions of electricity results are very near to each other.

6.6. Kapulukaya HEPP

This section focuses on the annual results of Kapulukayas HEPP and the differences of historical data and GCM results of energy production. Figures 6.36, 6.37 and 6.38 show the AEP of GFDL, HadGEM and MPI models for scenarios RCP 4.5.

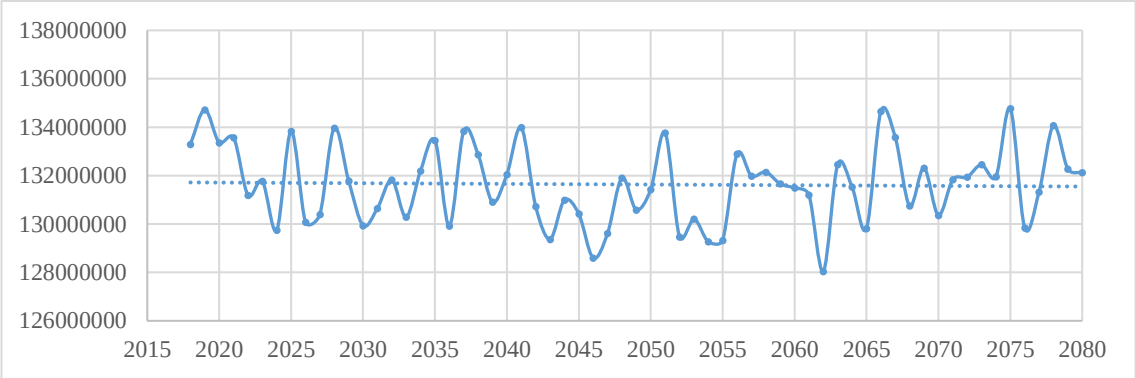

Figure 6.36. The annual production of electricity (Kwh) results of Kapulukaya HEPP using GFDL 4.5 model.

The energy production lightly decreases for the interval from 2018 to 2080. The range of the annual energy is between 128,000,000 to 134,700,000 Kwh as shown in Figure 6.36.

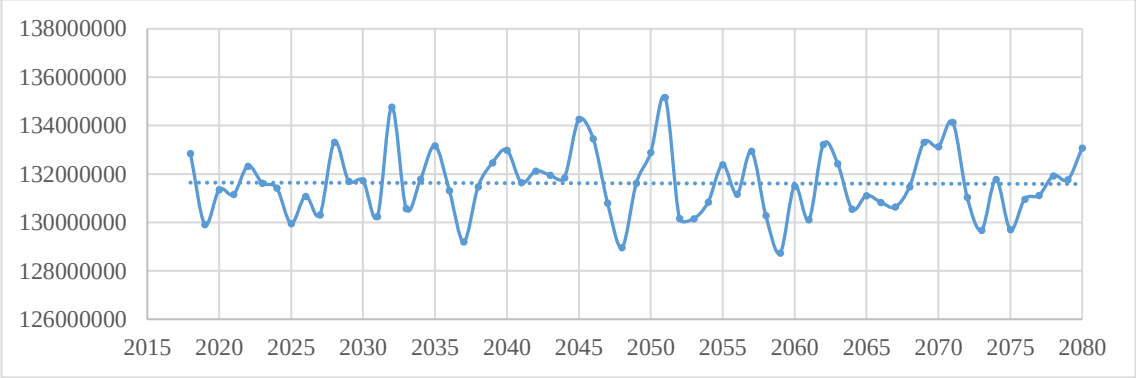

Figure 6.37. The annual production of electricity (Kwh) results of Kapulukaya HEPP using HadGEM 4.5 model.

The energy production results using HadGEM temperature and precipitation data is steady trend for the interval between 2018 to 2080 with range between 128,700,000 to 135,150,000 Kwh as shown in Figure 6.37.

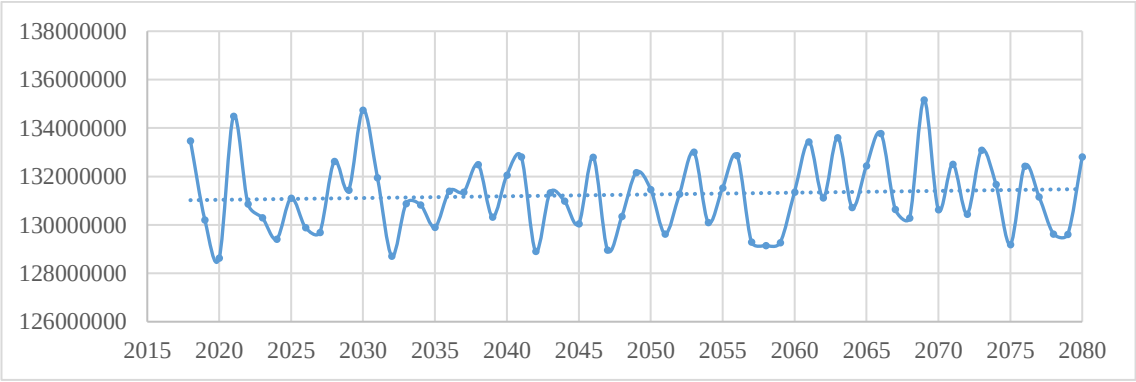

Figure 6.38. The annual production of electricity (Kwh) results of Kapulukaya HEPP using MPI 4.5 model.

The energy production increases for the interval from 2018 to 2080 with range between 128,630,000 to 135,170,000 Kwh as shown in Figure 6.38.

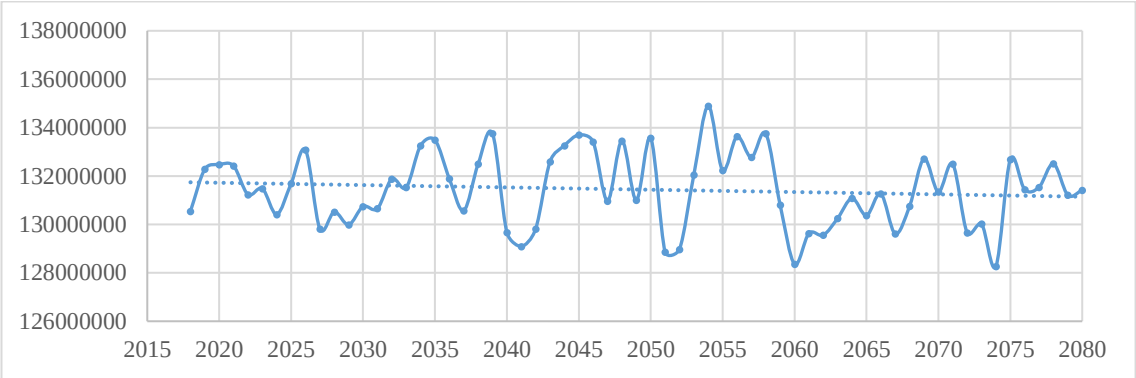

Figure 6.39. The annual production of electricity (Kwh) results of Kapulukaya HEPP using GFDL 8.5 model.

The prediction of the AEP decreases with time using the GFDL precipitation and temperature data for 8.5 scenario as shown in Figure 6.39. The range of the AEPs are between 128,270,000 Kwh and 134,900,000 Kwh.

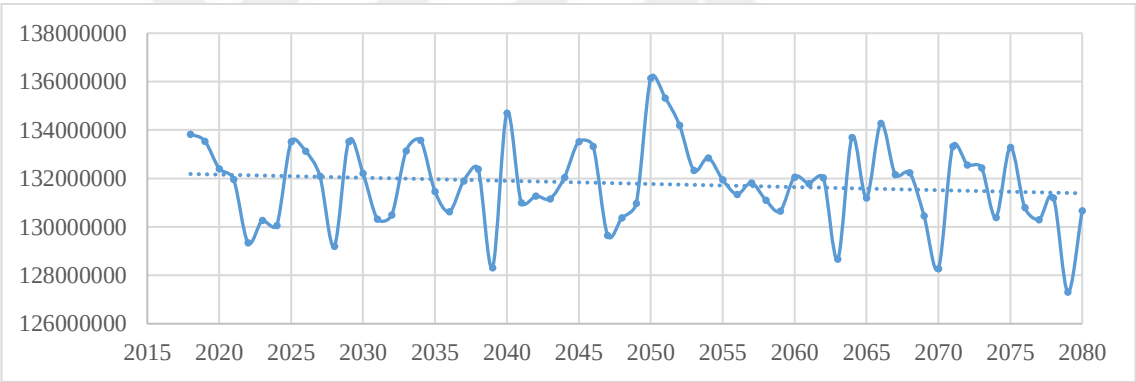

Figure 6.40. The annual production of electricity (Kwh) results of Kapulukaya HEPP using HadGEM 8.5 model.

The prediction of the AEP decreases with time using HadGEM precipitation and temperature data for 8.5 scenario as shown in Figure 6.40. The range of the AEPs are resulted between 127,300,000 Kwh and 136,150,000 Kwh.

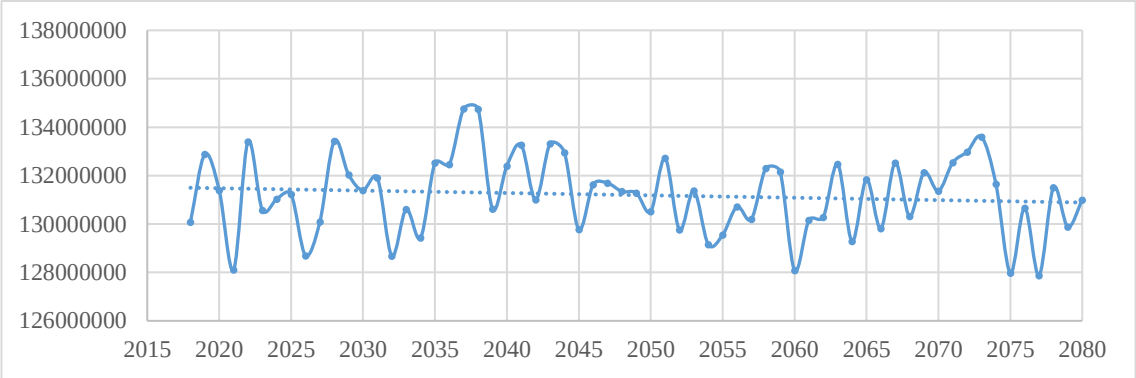

Figure 6.41. The annual production of electricity (Kwh) results of Kapulukaya HEPP using MPI 8.5 model.

The prediction of the AEP decreases with time using MPI precipitation and temperature data for 8.5 scenario as shown in Figure 6.41. The range of the AEPs are resulted between 127,900,000 Kwh and 134,800,000 Kwh.

Table 6.6. The mean annual of Hitorical data and predicted energy production of Kapulukaya HEPP

GCM	Historical Data	2018 - 2050	2051-2080	Percentage of change for 2018 to 2050 results	Percentage of change for 2051 to 2080 results
GFDL 4.5	146,828,250.4	131,615,126.2	131,651,854.8	-10.4%	-10.3%
GFDL 8.5		131,719,115.5	131,139,671.9	-10.3%	-10.7%
HadGEM 4.5		131,710,772.7	131,515,412.2	-10.3%	-10.4%
HadGEM 8.5		131,868,360.0	131,695,479.6	-10.2%	-10.3%
MPI 4.5		131,113,496.7	131,399,438.8	-10.7%	-10.5%
MPI 8.5		131,492,692.9	130,862,565.7	-10.4%	-10.9%

The differences between the mean anual predicted production and the historical production were estimated as shown in Table 6.6. Despite the increase of the predicted energy production in all GCMs and scenarios of the intervals (From 2018 to 2050 and from 2051 to 2080), it decreased based on the historical data with various percentages from 10.2% to 10.7% for interval between 2018 to 2050 and from 10.3% to 10.9% for interval between 2051 to 2080. The table showed that the mean annual predicted production of RCP 8.5 scenario results higher than the mean values of RCP 4.5 scenarios.

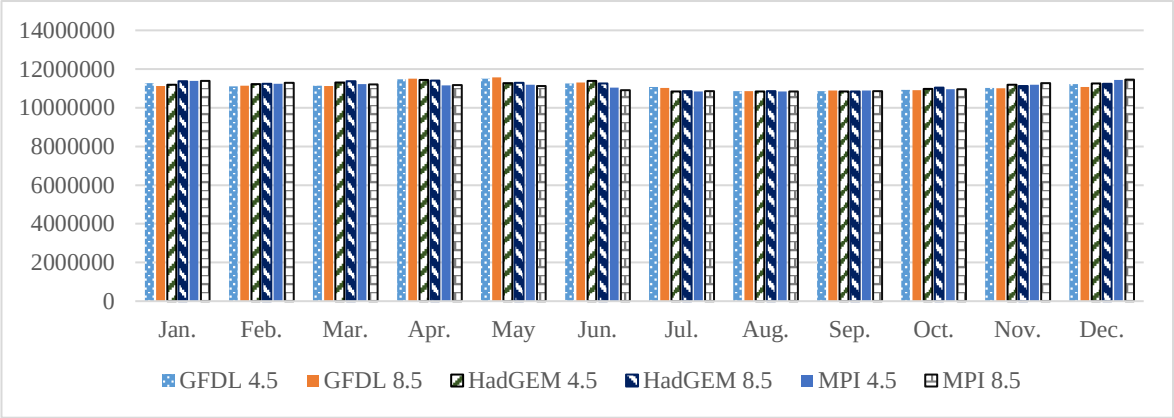

Figure 6.42. The mean monthly production of GCM predicted energy production of Kapulukaya HEPP.

The prediction of AEP was estimated for 8.5 and 4.5 scenarios using GCMs as shown in Figures 6.36, 6.37, 6.38, 6.39, 6.40 and 6.41. All GCMs results show that the highest values of energy production were in months April and May and the lowest values were in the month of August as shown in Figure 6.42.

The energy production in the GFDL 8.5 has decreased faster than the GFDL 4.5 as shown in figures 6.36 and 6.39. The range of values in the HadGEM 8.5 and HadGEM 4.5 are very close to each other as shown in figures 6.37 and 6.40. Despite of that, the trend of HadGEM 8.5 showed decreasing trend and neutral for HadGEM 4.5.

This chapter focuses on the annual prediction results of each HEPP. The figures show the prediction of energy production of each GCM. The mean anual predicted production is estimated for the GCMs data and Historical data as shown in tables 6.1, 6.2, 6.3, 6.4, 6.5 and 6.6. The differences between the mean anual predicted production and the historical production.

7. CONCLUSION AND RECOMMENDATIONS

This chapter will conclude all the previous works step by step directly. In the previous chapters, the procedures of this study were started by making searching for the literature reviews as first step. Secondly, the trends (homogeneity test Mann-Kendall test) were estimated for the GCMs data of temperature and precipitation for each scenario (RCP 8.5 and 4.5). The GCMs data after downscaling were sorted according to the study area and got all the data of the dam's locations. The performance validation step is used after any calculation process to get more accurate result.

This research study presents the use of machine learning techniques for power production, for which, there is clearly a gap in the literature. There is already lack in the studies that estimate the effect of climate change on hydropower plants in Turkey in general and especially in the Black Sea Basin. Furthermore, the hydropower studies in Turkey do not use the latest machine learning techniques. These techniques produce more accurate results for predicting the hydropower's production. This research also evaluates the impact of climate change on hydropower production in the Yesilirmak and Kizilirmak Basins. This evaluation can be used to analyse the climate situation in the next years and the possibilities of droughts and floods.

The study focused on two basins (Yesilirmak and Kizilirmak Basins) which included six main HEPPs (Almus HEPP, Suat Ugurlu HEPP, Hasan Uğurlu HEPP, Hirfanlı HEPP, Kesikköprü HEPP and Kapulukaya HEPP). This step supported reaching the purpose of this study to analyze the effect and impact of climate change on the HEPPs. The predict step was calculated based on RE and R values between the Mechine learning techniques. Five models were used to predict the energy production of HEPPs (Deep Learning (DL), Decision Tree (DT), Generalized Linear (GL), Random Forest (RF) and Gradient boosted trees (GBT)) using monthly hydroelectric power generation data from 1971 to 2018.

According to the temperature and precipitation values of the GCMs, the study presented the results of deploying Machine Learning Techniques in predicting the energy amount which will be produced by Hydroelectric Power Plants (from 2018 to 2080) in Yesilirmak and Kizilirmak Basins, Turkey.

Before predicting step, the study showed the differences between the five models and the quality of results in each model. The correlation and relative error values verified that GBT model gives more accurate results to the six main HEPPs. For RE,

the percantages of GBT were 31%, 29%, 15%, 22%, 28.6% and 23% for Almus, Hasan Ugurlu, Suat Ugurlu, Hirfanli, Kesikkopru and Kapulukaya, respectively. On the other hand, the results of R of GBT were 0.717, 0.602, 0.729, 0.76, 0.623 and 0.801 for Almus, Hasan Ugurlu, Suat Ugurlu, Hirfanli, Kesikkopru and Kapulukaya, respectively. According to that, the GBT model was used for predicting the production of electricity.

The results of all homogeneity tests of annual mean temperature are the same for all GCMs. For RCP 4.5, the HadGEM model is Homogeneity doubt. However, MPI and GFDL models are Homogeneous. The results of all RCP 8.5 are Homogeneously Flawed for each model in all the HEPP.

On the other hand, all the homogeneity tests of annual precipitation showed the same results for all GCMs (Homogeneous) except for MPI RCP 4.5 in Almus HEPP data (Homogeneity doubt). In General, the data of the study area for all GCMs scenarios are homogenous which means that the data could be used to get accurate results of predicting the energy production.

Mann Kendall test of temperature GCMs data showed positive trends for all HEPPs with time for the interval between 2018 and 2080. These reustls are very comfortable for Black Sea region with some previous studies like Ulke and Ozkoca (2018) and Tokgoz and Partal (2020). They estimated the trend analyses of temperature and precipitation of Black Sea region. On the other hand, Mann kendall test of precipitation GCMs data showed different results based on RCP. The most of RCP have negative trends for all HEPPs with time for the interval between 2018 and 2080 except some RCP models (Except all models with RCP 4.5 of Amus, HadGEM RCP 8.5 of Hasan ugurlu and Suat Ugurlu HEPPs, GFDL RCP 4.5 of Hirfanli, Kesikkopru and Kapulukaya HEPPs). They resulted with light negative trends.

In Almus HEPP, the predicted energy production has increased in all GCMs and in all scenarios of the interval 2018-2080. However, the mean predicted energy production has decreased based on the historical data with various percentages from 15% to 29.1%. The results showed that the mean annual predicted production values for RCP 8.5 scenarios are higher than those forRCP 4.5 scenarios. Although the results of Almus HEPP showed increase with time in predicting but it shows decreasing base on the historical data of energy production which is clear in Table 6.1. Alrayess and Ulke Keskin (2021) predicted the energy production of Almus HEPP using the same machine learning techniques. The study used the same criteria and the results showed

the time series of the predicted energy production using GCMs data of Precipitation and Temperature.

Despite the decrease of the predicted energy production in all GCMs and in all scenarios of the interval 2018-2080 in Hasan Ugurlu HEPP, the predicted energy production has unsimilarity results based on the historical data with various percentages. For GFDL GCM, the percentage of change is positive for both scenarios (RCP 8.5 and RCP 4.5). On the other hand, the percentage of change is negative for MPI GCM.

In Suat Ugurlu HEPP, the predicted energy production has increased in all GCMs and in all scenarios of the interval 2018-2080. Despite the precipitation decrease and the temperature increase of GFDL 8.5, the results show high values of energy production, more than GFDL 4.5 during the same period. Nevertheless, the results show a little difference between the two scenarios. However, the predicted energy production has increased based on the historical data with various percentages from 4.4% to 5.2%. The results showed that the mean annual predicted production values for RCP 8.5 scenarios are little higher than those for RCP 4.5 scenarios.

Despite the increase of the predicted energy production in all GCMs and in all scenarios of the interval 2018-2080 in Hirfanli HEPP, the predicted energy production has decreased based on the historical data with various percentages from 1.4% to 4.7%. The results showed that the mean annual predicted production values for RCP 8.5 scenarios are higher than those for RCP 4.5 scenarios.

In Kesikkopru HEPP, the predicted energy production has increased in all GCMs and in all scenarios of the interval 2018-2080. However, the predicted energy production has increased based on the historical data with various percentages from 6.6% to 7.7%. The results showed that the mean annual predicted production values for RCP 8.5 scenarios are higher than those forRCP 4.5 scenarios.

In Kapulukaya HEPP, despite the increase of the predicted energy production in all GCMs and in all scenarios of the interval 2018-2080, The predicted energy production decreased based on the historical data with various percentages from 10.2% to 10.6%. The results showed that the mean annual predicted production values are very near to each other for RCP 8.5 and RCP 4.5 scenarios.

The mean monthly production of historical data and GCM predicted energy

production of Almus, Hirfanli and Kesikkopru HEPPs are the same change of each month (Same behavior of change) which mean the predicted values of the mean monthly production will not have any change with time. Little differences appear in the mean monthly production of historical data and GCM predicted energy production of Suat Ugurlu, Hasan Ugurlu, and Kapulukaya in some months during the year.

This thesis examines the Yesilirmak and Kizilirmak Basins, but perhaps, because of this study, the need for a detailed study of the whole basins in Turkey will increase. The lack of data source and non-availability affected on the accuracy of predicting for the energy production like the water level and the historical data range of the energy production.

The thesis makes a clear indication about the hydropower production with time using two RCP scenarios and three GCMs in predicting to understand the behavior of the system. The results show that there are small differences between the models which means that the predictions are going in similar directions at all these models. All of GCMs give a very close results between each other so it's very hard to decide which GCM can provide the most accurate future prediction of energy production. The study showed that may the predicted for HEPPs which are located near to the coastal area have a little affect from the climate change. On the other hand, the predicted for HEPPs which are located internally to the anatolian side may not affect from the climate change.

REFERENCES

Akpinar, E. (2005). The Place of River Type Power Plants in Turkey. Hydroelectric Production. *Erzincan Journal of Education*. 7(2). 1-24.

Alexandersson, H. (1986). A homogeneity test applied to precipitation data. International *Journal of Climatology*. 6. 661-675.

Alghazali, N. and D. Alawadi (2014). Fitting Statistical Distributions of Monthly Rainfall for Some Iraqi Stations. *Civil and Environmental Research*. 6(6). 40-46.

Alrayess, H., S. Gharbia, N. Beden, and A. Ulke Keskin (2018, October). "Using Machine Learning Techniques and Deep Learning in Forecasting The Hydroelectric Power Generation in Almus Dam, Turkey". 5th International Symposium on Dam Safety, Istanbul, Turkey.

Alrayess, H. and A. Ulke Keskin (2021). Forecasting the hydroelectric power generation of GCMs using machine learning techniques and deep learning (Almus Dam, Turkey). *Geofizika*. 38(1). 1-14.

Beheshti, M., A. Heidari and B. Saghafian (2019). Susceptibility of Hydropower Generation to Climate Change: Karun III Dam Case Study. *Water*. 11(5) 1-17.

Benestad, R., I. Hanssen-Bauer and D. Chen (2008). *Empirical Statistical Downscaling.* World Scientific Publishing Company, Singapore. 228.

Beyene, T., D. P. Lettenmaier and P. Kabat (2010). Hydrological impacts of climate change on the Nile River basin: Implications of the 2007 IPCC climate scenarios. *Climate Change*. 100. 3–4.

Bhuvandas N., P. V. Timbadiya, P. L. Patel, & P. D. Porey. (2014). Review of Downscaling Methods in Climate Change and Their Role in Hydrological Studies. *International Journal of Geological and Environmental Engineering*. 8, 10.

Blackshear, B., T. Crocker, E. Drucker, J. Filoon, J. Knelman and M. Skiles (2011). *Hydropower vulnerability and climate change, a framework for modelling the future hydroelectric resources.* Middlebury: Environmental Studies, Middlebury College.

Black, E., D. Brayshaw and C. Rambeau (2010). Past, present and future precipitation in the Middle East: insights from models and observations. *Philos Trans R Soc A*. 368. 5173–5184.

Bonsor, K. 2019. *How Hydropower Plants Work. HowStuffWorks*. https://science.howstuffworks.com/environmental/energy/hydropower-plant1.htm (Accessed Sep 25 2021).

Bozkurt, D. and O. L. Sen (2011). Precipitation in the Anatolian Peninsula: sensitivity to increased SSTs in the surrounding seas. *Clim Dyn*. 36(3–4). 711–726.

Bozkurt, D., U. Turuncoglu, O. L. Sen, B. Onol and H. N. Dalfes (2012). Downscaled simulations of the ECHAM5, CCSM3 and HadCM3global models for the eastern Mediterranean– Black Sea region: evaluation of the reference period. *Clim Dyn*. 39(1–2). 207–225.

Bozkurt, D. and O. L. Sen (2013). Climate change impacts in the Euphrates–Tigris Basin based on different model and scenario simulations. *J Hydrol*. 480. 149–161.

Breiman, L. (2001). Random forests. *Mach Learn*. (45). 5–32. Doi:10.1023/A:1010933404324

Breiman, L. (1997). *Arcing The Edge, Technical Report 486*. Statistics Department, University of California, Berkeley.

Buishand, T.A. (1982). Some methods for testing the homogeneity of rainfall records. *Journal of Hydrology*. 58. 11-27.

Busuioc, A. and H. V. Storch (1996). Changes in the winter precipitation in Romania and its relation to the large-scale circulation. *Tellus.* 48 (A). 538-552.

Catani, F., D. Lagomarsino, S. Segoni and V. Tofani (2013). Landslide susceptibility estimation by random forests technique: sensitivity and scaling issues. *Nat Hazards Earth Syst Sci.* 13. 2815–2831. Doi: 10.5194/nhess-13-2815-2013

Chiang, J. L., H. Ch. Yang, Y. R. Chen and M. H. Lee (2013). Potential Impact of Climate Change on Hydropower Generation in Southern Taiwan. *Energy Procedia*. 40. 34 – 37.

Cografyaharita, 2017. *Turkey Hydroelectric Power Plants Map.* http://cografyaharita.com/haritalarim/4eturkiye-hidroelektrik-santralleri-haritasib-2017.png (Accessed 09.06.2021).

Collins, W. J., N. Bellouin, M. Doutriaux-Boucher, N. Gedney, T. Hinton, C. D. Jones, S. Liddicoat, G. Martin, F. O'Connor, J. Rae, C. Senior, I.Totterdell, S. Woodward, T. Reichler and J. Kim (2008). *Evaluation of the HadGEM2 model. Met Office Hadley Centre Technical Note no. HCTN 74.* http://www.metoffice.gov.uk/publications/HCTN/index.html

Demir, I. (2011, April). "Regional Climate Model Projections", ECHAM5-B1. 27- 29 April, *5th Atmospheric Science Symposium Proceedings Book*, ITU, Istanbul – Turkey.

Demircan, M., H. Gurkan, O. Eskioglu, H. Arabaci and M. Coskun (2017). Climate Change Projections for Turkey: Three Models and Two Scenarios. *Turkish Journal of Water Science and Management*. 1(1). 22-43.

Dmitrieva, K. (2015). *Forecasting of a hydropower plant energy production*. Ostfold University College, Master's Thesis in Computer Science, Halden, Norway, 69.

Dunne, J. P., L. W. Horowitz, A. J. Adcroft, P. Ginoux, I. M. Held, J. G. John, et al. (2020). The GFDL Earth SystemModel Version 4.1 (GFDL-ESM 4.1): Overall coupled model description andsimulation characteristics. *Journal of Advances in Modeling Earth Systems* .12. e2019MS002015.

Elias, K. and K. Miegel (2018). Assessment of the impact of climate change on future hydropower production from Koka Reservoir under two representative concentration pathways (RCP) emission scenarios. *Int J Energ Water Res.* 2. 49–62.

Enerji Atlas, 2020. *Distribution of HEPPs in Turkey*. https://www.enerjiatlasi.com/hes-haritasi/turkiye (Accessed 25.09.2021).

Flato, G., J. Marotzke, B. Abiodun, P. Braconnot, S.C. Chou, W. Collins, P. Cox, F. Driouech, S. Emori, V. Eyring, C. Forest, P. Gleckler, E. Guilyardi, C. Jakob, V. Kattsov, C. Reason and M. Rummukainen (2013). *Evaluation of Climate Models. In: Climate Change 2013: The Physical Science Basis. Contribution of Working Group I to the Fifth Assessment Report of the Intergovernmental Panel on Climate Change* [Stocker, T.F., D. Qin, G.-K. Plattner, M. Tignor, S.K. Allen, J. Boschung, A. Nauels, Y. Xia, V. Bex and P.M. Midgley (eds.)]. UK: Cambridge University Press.

Friedman, J. H. (1999). Greedy Function Approximation: A Gradient Boosting Machine.

Forrest, K., B. Tarroja, F. Chiang, A. Aghakouchak and S. Samuelsen (2018). Assessing climate change impacts on California hydropower generation and ancillary services provision. *Climatic Change*. 151. 395–412.

Fowler, H., S. Blenkinsop and C. Tebaldi (2007). Linking climate change modelling to impacts studies: recent advances in downscaling techniques for hydrological modelling. *Int J Climatol.* 27. 1547–1578.

Fowler, H. J. and R. L. Wilby (2010). Detecting changes in seasonal precipitation extremes using regional climate model projections: implications for managing fluvial flood risk. *Water Resour. Res.* 46. 1-17.

Fu, G. and S. P. Charles (2011, June). "Statistical downscaling of daily rainfall for southeastern Australia". *In Proceedings of the Symposium JH02 Held during IUGG2011*, 28 June–7 July 2011; IAHS Publ 344; IAHS Press: Wallingford, 69–74, Melbourn, Australia,.

Gao, X. and F. Giorgi (2008). Increased aridity in the Mediterranean region under greenhouse gas forcing estimated from high resolution simulations with a regional climate model. Global Planet. *Change*. 62. 195–209.

General Directorate of State Hydraulic Works, 2020. *Observation Stations Management System*. http://rasatlar.dsi.gov.tr/ (Accessed 09.02.2020).

General Directorate of State Hydraulic Works, 2018a. *Almus Dam details*, http://web.archive.org/web/20180225190623/http://www2.dsi.gov.tr/baraj/detay.cfm?BarajID=21 (Accessed 19.08.2018).

General Directorate of State Hydraulic Works, 2018b. *Hasan Ugurlu Dam details*,. http://web.archive.org/web/20180225190623/http://www2.dsi.gov.tr/baraj/detay.cfm?BarajID=21 (Accessed 19.08.2018).

General Directorate of State Hydraulic Works, 2018c. *Suat Ugurlu Dam details.* http://web.archive.org/web/20180225190623/http://www2.dsi.gov.tr/baraj/detay.cfm?BarajID=21 (Accessed 19.08.2018).

General Directorate of State Hydraulic Works, 2018d. *Hirfanli Dam details.* http://web.archive.org/web/20180225190623/http://www2.dsi.gov.tr/baraj/detay.cfm?BarajID=21 (Accessed 19.08.2018).

General Directorate of State Hydraulic Works, 2018e. *Kesikkopru Dam details.* http://web.archive.org/web/20180225190623/http://www2.dsi.gov.tr/baraj/detay.cfm?BarajID=21 (Accessed 19.08.2018).

General Directorate of State Hydraulic Works, 2018f. *Kapulukaya Dam details.* http://web.archive.org/web/20180225190623/http://www2.dsi.gov.tr/baraj/detay.cfm?BarajID=21 (Accessed 19.08.2018).

Gharbia, S. S., L. Gill, P. Johnston and F. Pilla (2016). Multi-GCM ensembles performance for climate projection on a GIS platform. Model. *Earth Syst. Environ.* 2(102). 2-21, DOI 10.1007/s40808-016-0154-2.

Gokgoz, F. and F. Filiz (2018). Deep Learning for Renewable Power Forecasting: An Approach Using LSTM Neural Networks. *International Journal of Energy and Power Engineering.* 12(6). 412-416.

Guclu, Y. S. (2020). Improved visualization for trend analysis by comparing with classical MannKendall test and ITA. *Journal of Hydrology.* 584. 1-9.

Hammid, A. T., M. H. Bin Sulaiman and A. N. Abdalla (2018). Prediction of small hydropower plant power production in Himreen Lake dam (HLD) using artificial neural network. *Alexandria Engineering Journal*. 57. 211-221.

Hamududu, B. and A. Killingtveit (2012). Assessing Climate Change Impacts on Global Hydropower. *Energires.* 5. 305 – 322. Doi:10.3390/en5020305

Hamzacebi, C., H. A. Es and R. Cakmak (2017). Forecasting of Turkey's monthly electricity demand by seasonal artificial neural network. *Neural Computing and Applications.* 1-15.

Harpham, C. and R. L. Wilby (2005). Multi-site downscaling of heavy daily precipitation occurrence and amounts. *J. Hydrol.* 312. 235–255.

Harrison, G. P. and H. W. Whittington (2002). Susceptibility of the Batoka Gorge hydroelectric scheme to climate change. *Journal of Hydrology*. 264. 230–241.

Helsel, D. R. and R. M. Hirsch (2002). *Statistical Methods in Water Resources Techniques of Water Resources Investigations*. U.S. Geological Survey.

Huang, H. and Z. Yan (2009). Present Situation and Future Prospect of Hydropower in China. *Renewable and Sustainable Energy Reviews.* 13(6). 1652-1656.

Huangpeng, Q., W. Huang and F. Gholinia (2021). Forecast of the hydropower generation under influence of climate change based on RCPs and Developed Crow Search Optimization Algorithm. *Energy Reports.* 7. 385-397.

IPCC (The Intergovernmental Panel on Climate Change). (2012) Renewable Energy Sources and Climate Change Mitigation Special Report of the Intergovernmental Panel on Climate Change, Cambridge University Press, ISBN 978-1-107-60710-1

IPCC (The Intergovernmental Panel on Climate Change). 2007a. Climate Change 2007: The Physical Science Basis. Contribution of Working Group I to the Fourth Assessment Report of the Intergovernmental Panel on Climate Change; IPCC: Geneva, Belgium.

IPCC (The Intergovernmental Panel on Climate Change). 2019b. *What is a GCM?.* http://www.ipcc-data.org/guidelines/pages/gcm_guide.html (Accessed 09 June 2019).

Iseri, E., and D. Guney (2017). Assessing Turkey's Climate Change Commitments: The Case of Turkey's Energy Policy. *PERCEPTIONS: Journal of International Affairs.* 22(2). 107-130.

Iimi, A. (2007). *Estimating Global Climate Change Impacts on Hydropower Projects: Applicationsin India*, Sri Lanka and Vietnam. World Bank Publications.

Jakob Themeßl, M., A. Gobiet, and A. Leuprecht. (2011), Empirical-statistical downscaling and error correction of daily precipitation from regional climate models. *International Journal of Climatology*. 31. 1530-1544.

Jang, S. and M. L. Kavvas (2015). Downscaling global climate simulations to regional scales: statistical downscaling versus dynamical downscaling. *J. Hydrol. Eng.* 20(1). https://doi.org/10.1061/(ASCE)HE.1943-5584.0000939.

Jong, P. D., C. A. S., Tanajura, A. S. Sánchez, R. Dargaville, A. Kiperstok and E. A. Torres, (2018). Hydroelectric production from Brazil's São Francisco River could cease due to climate change and inter-annual variability. *Sci. Total Environ.* 634. 1540–1553.

Kadioglu, M. (1997). Trends in Surface Air Temperature Data Over Turkey. *International Journal of Climatology*. 17. 511-520.

Kahya, E. and S. Kalayci (2004). Trend analysis of streamflow in Turkey. *Journal of Hydrology*. 289. 128-144.

Kahya, E. and Cagatay Karabork, M. (2001). The analysis of El Nino and La Nina signals in streamflows of Turkey. *International Journal of Climatology: A Journal of the Royal Meteorological Society,* 21(10), 1231-1250.

Kankal, M., A. Akpinar, M. I. Komurcu and T. S. Ozsahin (2011). Modeling and forecasting of Turkey's energy consumption using socio-economic and demographic variables. *Applied Energy*. 88(5). 1927-1939.

Kang, B., Y. D. Kim, J. M. Lee and S. J. Kim (2015). Hydro-environmental Runoff Projection under GCM Scenario Downscaled by Artificial Neural Network in the Namgang Dam Watershed, Korea. *KSCE Journal of Civil Engineering*. 19(2). 434-445.

Karabork, M., E. Kahya and A. U. Komuscu (2007). Analysis of Turkish precipitation data: homogeneity and the Southern Oscillation forcings on frequency distributions. *Hydrological Processes: An International Journal.* 21(23). 3203-3210.

Khan, M. S., P. Coulibaly and Y. Dibike (2006). Uncertainty analysis of statistical downscaling methods. *J. Hydrol.* 319. 357–382.

Kotu, V., B. Deshpande (2019). Data science concepts and Practice, 2nd edition. Morgan Kaufmann Publishers.

Krusic, J., M. Marjanovic, M. S. Petrovic, B. Abolmasov, K. Andrejev and S. Miladinovic (2017). Comparison of expert, deterministic and Machine Learning approach for landslide susceptibility assessment in Ljubovija Municipality, Serbia. *Geofizika*. 34. 251- 273. https://doi.org/10.15233/gfz.2017.34.15

Lange H., S. Sippel. (2020). Machine Learning Applications in Hydrology. In: Levia D.F., Carlyle-Moses D.E., Iida S., Michalzik B., Nanko K., Tischer A. (eds) Forest-Water Interactions. Ecological Studies (Analysis and Synthesis), vol 240. Springer, Cham.

Laprise, R. (2008). Regional climate modelling. *Journal of Computational Physics*. 227(7). 3641–3666.

Li, J., Z. Wang, X. Wu, Sh. Guo and X. Chen (2020). Flash droughts in the Pearl River Basin, China: Observed characteristics and future changes. *Science of The Total Environment.* 707. 1-15.

Liu, W., G. Fu, G. Liu, X. Song and R. Ouyang (2013). Projection of future rainfall for the North China Plain using two statistical downscaling models and its hydrological implications. *Stoch. Environ. Res. Risk Assess.* 27. 1783–1797.

Liaw, A. and M. Wiener (2002). Classification and regression by random forest. *R News.* 2. 18–22.

Madani, K. and J. R. Lund (2009). *Modeling California's high-elevation hydropower systems in energy units*. Water Resources Research. 45. no. 9. Article IDW09413.

Machina, M. B. and S. Sharma (2017). Assessment of Climate Change Impact on Hydropower Generation: A Case Study of Nigeria. *International Journal of Engineering Technology Science and Research*. 4(8). 753-762.

Maraun, D., F. Wetterhall, A. M. Ireson, R. E. Chandler, E. J. Kendon, M. Widmann, S. Brienen, H. W. Rust, T. Sauter, M. Themessl, V. K. C. Venema, K. P. Chun, C. M. Goodess, R. G. Jones, C. Onof, M. Vrac and I. Thiele-Eich (2010). Precipitation downscaling under climate change: recent developments to bridge the gap between dynamical models and the end user. *Rev. Geophys*. 48. 1-34.

Minarecioglu, N., H. Çıtakoglu (2019). Trend Analysis of Monthly Average Flows of Kizilirmak Basin. *Journal of Anatolian Environmental and Animal Sciences.* 4 (3). 454-459.

Minville, M., F. Brissette, S. Krau and R. Leconte (2009). Adaptation to Climate Change in the Management of a CanadianWater-Resources System Exploited for Hydropower. *Water Resour. Manag.* 23. 2965–2986.

Mishra, S. K., J. Hayse, V. Thomas, E. Yan, R. B. Kayastha, K. LaGory, K. McDonald, N. Steiner (2018). An integrated assessment approach for estimating the economic impacts of climate change on River systems: An application to hydropower and fisheries in a Himalayan River, Trishuli. *Environ. Sci. Policy*. 87. 102–111.

Moss, R. H., J. A. Edmonds, K. A. Hibbard, M. R. Manning, S. K. Rose, D. P. van Vuuren, T. R. Carter, S. Emori, M. Kainuma, T. Kram, G. A. Meehl, J.F. B. Mitchell, N. Nakicenovic, K. Riahi, S. J. Smith, R. J. Stouffer, A. M. Thomson, J. P. Weyant and T. J. Wilbanks (2010). The next generation of scenarios for climate change research and assessment. *Nature.* 463(7282). 747–756.

Moss, R., M., Babiker, S., Brinkman, E., Calvo, T., Carter, J., Edmonds, I., Elgizouli, S., Emori, L., Erda, K., Hibbard, R., Jones, M., Kainuma, J., Kelleher, J. F., Lamarque, M., Manning, B., Matthews, J., Meehl, L., Meyer, J., Mitchell, N., Nakicenovic, B., O'Neill, R., Pichs, K., Riahi, S., Rose, P., Runci, R., Stouffer, D., van Vuuren, J., Weyant, T., Wilbanks, J. P., van Ypersele and M. Zurek (2008). *Towards new scenarios for analysis of emissions, climate change, impacts and response strategies. IPCC Expert Meeting Report*. 19-21 September, Noordwijkerhout, Netherlands, 132-137, Intergovernmental Panel on Climate Change (IPCC), Geneva, Switzerland.

Nelder, J. A. and R. W. M. Wedderburn (1972). Generalized Linear Models. *Journal of the Royal Statistical Society, Series A (General)*. 135(3). 370-384.

Onol, B. and F. H. M. Semazzi (2009). Regionalization of climate change simulations over the eastern Mediterranean. *Journal of Climate*. 22(8). 1944–1961.

Onol, B. (2012). Effects of Coastal Topography on Climate: High-Resolution Simulation with a Regional Climate Model. *Clim. Research.* 52. 159–174.

Onol, B. and Y. S. Unal (2012). Assessment of climate change simulations over climate zones of Turkey. *Reg Environ Change.* 14. 1921-1935.

Onol, B., D. Bozkurt, U. U. Turuncoglu, O. L. Sen and H.N. Dalfes (2013). Evaluation of the twenty-first century RCM simulations driven by multiple GCMs over the Eastern Mediterranean–Black Sea region, Springer-Verlag, Berlin, Heidelberg, *Clim Dyn.* 42. 1949–1965.

Ozdogan, M. (2011). Climate change impacts on snow water availability in the Euphrates–Tigris basin. *Hydrol Earth Syst Sci*. 15. 2789–2803.

Partal, T. and E. Kahya (2006). Trend analysis in Turkish precipitation data. *Hydrol. Process.* 20. 2011–2026.

Pettitt, A. N.(1979). A Non-Parametric Approach to the Change-Point Problem. *Applied Statistics.* 2. 126 -135.

Pokhrel, Y., M. Burbano, J. Roush, H. Kang, V. Sridhar, D. W. Hyndman (2018). A Review of the Integrated Effects of Changing Climate, Land Use, and Dams on Mekong River Hydrology. *Water*.10. 266.

Pottinger, L. (2009). *Africa: The wrong climate for big dams.* World Rivers Review.

Rogelj, J., M. Meinshausen and R. Knutti (2012). Global warming under old and new scenarios using IPCC climate sensitivity range estimates. *Nature Clim Change*. 2. 248–253.

Randall, D. A., R. A. Wood, S. Bony, R. Colman, T. Fichefet, J. Fyfe, V. Kattsov, A. Pitman, J. Shukla, J. Srinivasan, R. J. Stouffer, A. Sumi and K. E. Taylor (2007). Climate Models and Their Evaluation. *In Climate Change 2007: The Physical Science Basis. Contribution of Working Group I to the Fourth Assessment Report of the Intergovernmental Panel on Climate Change*. UK: Cambridge University Press.

Sattari, M. T., A. S. Anli, H. Apaydin and S. Kodal (2012). Decision trees to determine the possible drought periods in Ankara. *Atmosfera.* 25(1). 65-83.

Schaeffer, R., A. S. Szklo, A. F. Lucena, B. S. Borba, L. P. Nogueira, F. P. Fleming, A. Troccoli, M. Harrison. and M. S. Boulahya (2012). Energy sector vulnerability to climate change: A review. *Energy*. 38. 1-12.

Schmidli, J., C. Frei and P. L. Vidale (2006). Downscaling from GCM precipitation: A benchmark for dynamical and statistical downscaling methods. *Int. J. Climatol.* 26(5). 679-689. DOI: 10.1002/joc.1287.

Sekkeli, M. and F. Kececioglu (2011). Investigation of The Hydropower Plants in Turkey: A Case Study on Kahramanmaras. KSU Engineering Sciences Journal. 14(2). 19-26.

Serancam, U. and I Dabanli (2020). Innovative flow risk assessment with climate change perspective in Yesilirmak Basin. *Fresenius Environmental Bulletin*. 29(1). 514-521.

Sen, O. L., A. Unal, D. Bozkurt and T. Kindap (2011). Temporal changes in the Euphrates and Tigris discharges and teleconnections. *Environ Res Lett.* 6. 1-9.

Sharma, R. H. and N. M. Shakya (2006). Hydrological changes and its impact on water resources of Bagmati Basin. Nepal. *J of Hydrology*. 327. 315–322.

Shrestha, S., M. Khatiwada, M. S. Babel and K. Parajuli (2014). Impact of Climate Change on River Flow and Hydropower Production in Kulekhani Hydropower Project of Nepal. *Environ. Proces.* 1. 231-250.

SNCT (2016). Sixth National Communication of Turkey under the UNFCCC (SNCT). Ankara: The Ministry of Environment and Urbanisation, Turkey.

Solaun, K. and E. Creda (2017). The Impact of Climate Change on the Generation of Hydroelectric Power—A Case Study in Southern Spain. *Energies*. 10. 1-19.

Spak, S., T. Holloway, B. Lynn and R. Goldberg (2007). A comparison of statistical and dynamical downscaling for surface temperature in North America. *J. Geophys. Res.-Atmos.* 112(D08101). 1-10. https://doi.org/10.1029/2005JD006712.

Spiegel, M. R. and L. J. Stephens (2008). *Schaum's Outlines Statistics* (Fourth ed.), McGraw Hill.

Sun, Y. and Y. Ding (2010). A projection of future changes in summer precipitation and monsoon in East Asia. *Sci. China Ser.* 53. 284–300.

Tabari, H., S. Marofi, A. Aeini, P. H. Talaee and K. Mohammadi (2011). Trend analysis of reference evapotranspiration in the western half of Iran. *Agricultural and Forest Meteorology*. 151. 128-136.

Tarhule, A. and M. Woo (1998). Changes in Rainfall Characteristics in Northern Nigeria. *International Journal of Climatology*. 18. 1261 -1271.

Tayanc, M., M. Karaca and O. Yenigun (1997). Annual and Seasonal Air Temperature Trend Patterns of Climate Change and Urbanization Effects in Relation with Air Pollutants in Turkey. *Journal of Geophys. Res.* 102. 1909 -1919.

Taylor, K. E., R. J. Stouffer and G. A. Meehl (2012). An overview of CMIP5 and the experiment design. Bull. *Am. Meteorol. Soc.* 93(4). 485–498. Doi:10.1175/BAMS-D-11-00094.1.

The Turkish Ministry of Energy and Natural Resources, 2019a. *Info bank- Energy-Hydraulics.* https://enerji.gov.tr/bilgi-merkezi-enerji-hidrolik-en (Accessed 15.09.2021).

The Turkish Ministry of Energy and Natural Resources, 2019b. *Info bank - Climate Change and International Negotiations.* https://enerji.gov.tr/infobank-climate-change-and-international (Accessed 15.09.2021).

The Turkish State of Meteorological Services, 2020. *State of the Turkey's Climate in 2020.* https://www.mgm.gov.tr/eng/Yearly-Climate/State_of_the_Climate_in_Turkey_in_2020.pdf (Accessed 19.09.2021).

Tokgoz, S., T. Partal (2020). Trend Analysis with Innovative Sen and Mann-Kendall methods of Annual Precipitation and Temperature data in the Black Sea Region. *Journal of the Institute of Science and Technology*. 10(2). 1107-1118.

Toreti, A., E. Xoplaki, D. Maraun, F. G. Kuglitsch, H. Wanner and J. Luterbacher (2010). Characterisation of extreme winter precipitation in Mediterranean coastal sites and associated anomalous atmospheric circulation patterns. *Nat. Hazards Earth Syst. Sci.* 10. 1037–1050.

Turkes, M. (1996). Spatial and Temporal Analysis of Annual Rainfall Variations in Turkey. *International Journal of Climatology*. 16. 1057 – 1076.

Turkes, M., U. M. Sumer and G. Kilic (1995).Variations and Trends in Annual Mean Air Temperatures in Turkey with Respect to Climatic Variability. *International Journal of Climatology*. 15. 557-569.

Ulke, A., T. Ozkoca (2018). Trend Analyses of Temperature Data of Sinop, Ordu and Samsun Provinces. *Gumushane University Journal of Science and Technology*. 8(2). 455-463.

Van Belle, G. and J. P. Hughes (1984). Nonparametric tests for trend in water quality. *Water Resources Research.* 20(1). 127–136.

van Vuuren, D.P., J. Edmonds, M. Kainuma, et al. (2011). The representative concentration pathways: an overview. *Climatic Change*. 109. 5. https://doi.org/10.1007/s10584-011-0148-z

Viollet P. L. (2017). From the water wheel to turbines and hydroelectricity. Technological evolution and revolutions. *Comptes Rendus Mecanique*. 345. 570 – 580.

Von Neumann, J. (1941). Distribution of the Ratio of the Mean Square Successive Difference to the Variance. *Ann. Math. Statist.* 12. 367 – 395.

Wilby, R. L., T. M. L. Wigley, D. Conway, P. D. Jones, B. C. Hewitson, J. Main and D. S. Wilks (1998). Statistical downscaling of general circulation model output: a comparison of methods. *Water Resour. Res.* 34(11). 2995–3008. https://doi.org/10.1029/98WR02577.

Winton, M., Adcroft, A., Dunne, J. P., Held, I. M., Shevliakova, E., Zhao, M., et al. (2020). Climate sensitivity of GFDL's CM4.0. *Journal of Advances in Modeling Earth Systems.* 12. e2019MS001838.

World Energy Council, 2018. *Hydropower.* https://www.worldenergy.org/data/resources/resource/hydropower/ (Accessed 05.02.2019).

Yacoub, E. and G. Tayfur (2020). Spatial and temporal of variation of meteorological drought and precipitation trend analysis over whole Mauritania. *Journal of African Earth Sciences.* 163. 1-12.

Yamba, F. D., H. Walimwipi, S. Jain, B. Cuamba and C. Mzezewa (2011). Climate change/variability implications on hydroelectricity generation in the Zambezi River Basin. *Mitigation and Adaptation Strategies for Global Change*. 16(6). 617–628.

Yildiz, D. and H. Ozguler, 2017. *Storing Water in Dam Reservoirs: Why is it Necessary?. World Water Diplomacy & Science News.*

Yilmaz, M. and F. Tosunoglu (2019). Trend assessment of annual instantaneous maximum flows in Turkey. *Hydrological Sciences Journal*. 64(7). 820-834.

Yuksel, I. (2008). Hydropower in Turkey for a clean and sustainable energy future. *Renewable and Sustainable Energy Reviews*. 12. 1622 – 1640, doi: 10.1016/j.rser.2007.01.024

Yuksek, O., M. I. Komurcu, I. Yuksel and K. Kaygusuz (2006). The role of hydropower in meeting Turkey's electric energy demand. *Energy Policy*. 34(17). 3093–3103.

Zhang, G. P., B. E. Patuwoand M. Y. Hu (1998). Forecasting With Artificial Neural Networks: The State Of The Art. *International Journal of Forecasting*. 14(1). 35-62.

CURRICULUM VITAE

Hesham ALRAYESS is a civil engineer with a master's degree in civil engineering (Infrastructures) from Islamic University of Gaza, Palestine. His work experience as a project engineer, water engineer and urban planning engineer. His major areas of interests are: Water networks, dams and reservoirs capacity estimation, drought analysis, hydraulic laboratory researchers, trend analysis, hydropower generation, climate change, water, water resources, environment and wastewater treatment plants.

ORCID ID: 0000-0001-6983-145X

Published Studies:

1. Hesham ALRAYESS, Asli Ulke KESKIN. (2021). Forecasting the hydroelectric power generation of GCMs using machine learning techniques and deep learning (Almus Dam, Turkey). Geofizika, 38, DOI: https://doi.org/10.15233/gfz.2021.38.4

2. Alrayess, H, Ülke, A, Gharbia, S. (2018). Comparison of Different Techniques about Reservoir Capacity Calculation at Sami Soydam Sandalcık Dam. Celal Bayar University Journal of Science, 14 (1), 23-29. DOI: 10.18466/cbayarfbe.309272.

3. Beden, N, **Alrayess, H,** Ulke Keskin, A. Flood Hydrology of Kurtun Stream, 1. International Technological sciences and Design Symposium (ITESDES). 27-29-June-2018, Giresun, Turkey.

4. Hesham Alrayess, Salem Gharbia, Neslihan Beden, Asli Ulke Keskin. Using Machine Learning Techniques and Deep Learning in Forecasting The Hydroelectric Power Generation in Almus Dam, Turkey. 5th International Symposium on Dam Safety, 27-31 October 2018, Istanbul, Turkey.

5. Neslihan Beden, Vahdettin Demir, **Hesham Alrayess,** Asli Ulke Keskin. Comparison Of 2d Hydraulic Models For Flood Simulation On The Mert River Turkey. 5th International Symposium on Dam Safety, 27-31 October 2018, Istanbul, Turkey.

6. Mohamad Mehyo, **Hesham Alrayess.** Numerical Simulation of a Two-Dimensional Laminar Flow in a Tank with Heat Transfer, 2nd International Students Science Congress 4-5 May 2018, Izmir, Turkey.

7. Neslihan Beden, **Hesham Alrayess**, Asli Ulke. (2018). A Chronological Research of Samsun City Floods, Journal of New Results in Science (JNRS), 7(2), 22-34.

8. U. Zeybekoglu, **H. Alrayess,** A. Ulke Keskin. Meteorological Drought Analysis in Sinop, Turkey. 13th International Congress on Advances in Civil Engineering, 12-14 September-2018, Izmir, Turkey.

9. H. Alrayess, U. Zeybekoglu and A. Ulke, "Different design techniques in determining reservoir capacity" European Water 60: 107-115, December 2017.

10. H. Alrayess, and A. Ulke, "Evaluation and development of spatial decision support system" European Water 60: 33-40, December 2017.

11. Neslihan BEDEN, **Hesham ALRAYESS** and Asli ULKE, A Research of Samsun City Floods with Infrastructure Problems, ISMSIT 2017, International Symposium on Multidisciplinary Studies and Innovative Technologies, 2-4, November 2017.

12. A, ÜLKE, V., DEMİR, U. Zeybekoğlu, **H. Al-Rayess**, C. SARAÇ. (2017). Trend Analysıs Annual Analysıs Maxımum Flows, 9. Hydrology Congress, 4-6 October 2017, Dicle University, Diyarbakır.

13. Hesham ALRAYESS, Utku ZEYBEKOGLU, Asli ULKE and Salem GHARBIA,"Reservoir Capacity Calculation Using Different Techniques: Sami Soydam Sandalcık Dam", 1896, ICOCEE 2017 2nd International Conference On Civil And Environmental Engineering, 8–10 May 2017, Cappadocia, Nevsehir, Turkey. (Abstract).

Awards and Scholarships

1. Turkish Scholarship (Türkiye Burslari -2015)

2. Erasmus + K.A 1 scholarship 2017 -2018